Deformation, erosion and sedimentation in collisional orogens: case studies from eastern Tibet and southwestern China

by

Christopher Terrance Studnicki-Gizbert

Submitted to the Department of Earth, Atmospheric and Planetary Sciences
in partial fulfillment of the requirements for the degree of

Doctor of Philosophy

at the

MASSACHUSETTS INSTITUTE OF TECHNOLOGY

September 2006

Author .....
Department of Earth, Atmospheric and Planetary Sciences
August 11, 2006

Certified by .....
B. Clark Burchfiel
Schlumberger Professor of Geology
Thesis Supervisor

Accepted by .....
Maria Zuber
Chair

Deformation, erosion and sedimentation in collisional orogens: case studies from eastern Tibet and southwestern China

by

Christopher Terrance Studnicki-Gizbert

Submitted to the Department of Earth, Atmospheric and Planetary Sciences
on August 11, 2006, in partial fulfillment of the
requirements for the degree of
Doctor of Philosophy

Abstract

This dissertation addresses aspects of the tectonics of regions adjacent to the eastern Himalayan syntaxis. The first chapter describes the Tertiary Gonjo basin, includes structural and sedimentologic observations, and interprets these as a record of limited upper crustal shortening during and immediately after early Tertiary ($\sim$ 40 Ma) time. The record of Cenozoic shortening of the upper crust cannot account for the gradient of crustal thicknesses from eastern Tibet southeast into Yunnan province. The second chapter provides a review of the regional geology of western Yunnan and the detailed structural geology of the region around the first bend of the Jinsha (Yangzi) river. Structures record a long history of multiple deformation generations, including early Mesozoic metamorphism and cooling, west-directed transport along thrusts and nappes in late Mesozoic time, limited Tertiary shortening and transtensional deformation from Pliocene to present time. The third chapter provides a synoptic view of the active tectonics around the eastern Himalayan syntaxis and integrates geologic mapping, slip-rate estimates, remote sensing, seismicity and geodesy. Fault slip rates are inferred by modeling the elastic deformation near major faults and the motions of a small number of crustal blocks. Elastic block modeling explains geodetic velocities but fails to capture many important aspects of the geologic record, especially poorly localized strain within and near the margins of the Lanping-Simao belt. The final chapter describes the Pliocene to present structural and geomorphic evolution of the Yulong mountains and the interactions of active upper-crustal transtensional deformation, weak lower or middle crust, and geomorphic processes (specifically river incision). The exposure of deep structural levels and high rock uplift rates of the Yulong mountains are explained as the result of erosion processes that balance rock uplift rates, a closed network of normal faults that accommodate differential rock uplift rates, and weak middle crust that flows in response to topographically imposed pressure gradients.

Thesis Supervisor: B. Clark Burchfiel
Title: Schlumberger Professor of Geology

The south peak of Yulong Xueshan looms over the city of Lijiang. Active normal faults associated with the uplift of this range ruptured in a 1997 magnitude 7 earthquake, levelling most of the city, but sparing most of the buildings built in the traditional Naxi style, including some dating from before the 12th century.

Dedicated to my father, the trilobite, and to my mother, for whom many of the biggest debates of continental tectonics are perfectly obvious.

Acknowledgments

While graduate studies can often feel like an extremely alienating and isolated existence, as I sit here tapping away on the final revisions and copy edits to this thesis, I cannot help but think of the many, many people whose kindness and generosity have provided invaluable aid throughout the entire process. What follows is a regrettably incomplete list of acknowledgements.

I originally became interested in geology when I found myself in Yellowknife, in the Northwest Territories of Canada looking for a summer job. Diamonds had just been discovered, and I was picked up by Gary Vivian, Doug Bryan and Matt Johnson more or less off the street, despite thinking that pretty much all grey, hard rocks were granite. Eventually I learned enough geology to join geological mapping projects for the Government of the Northwest Territories and the Geological Survey of Canada. More than any schooling, these Arctic field seasons working under some of the best field geologists anywhere trained me as a field geologist. Among these, I have to make special mention of: Carolyn Relf, Kate MacLachlan and Simon Hanmer; Jim Ryan, who taught me everything I know about how to interpret fabrics; and Hamish Sandeman, for an unforgettable field season in Committee Bay. Around this time, I studied geology at Carleton University, and have to acknowledge the inspiration and encouragement of Sharon Carr and Richard Brown, for which I might have to blame for ending up at MIT studying continental tectonics.

During my six years at MIT, I was unreasonably fortunate to work alongside a group of graduate students who comprised some of the brightest, most inspiring and generous colleagues imaginable. I could fill pages with names and anecdotes of help, encouragement and conversations containing invaluable seeds of insight. I would especially like to single out Sinan Akciz and Lindsay Schoenbohm, each of whom thought they were Clark Burchfiel's last graduate student, both of whom provided insight, criticism, discussion, support and friendship many times. Ben Crosby, possibly the wisest and most inspirational colleague and friend. Blair Schoene, a man of prodigious work ethic, amazing sense of humor and calmness, who opened my eyes to the virtues of cheap American beer and alternate uses for a fume hood. Brendan Meade and Eric Hetland may have managed to get some understanding of continental deformation into my thick head. Nick Austin, Sinan Akciz, Joel Johnson and Brandon MacElroy provided careful and thorough edits of various parts of this dissertation, and helped save me from at least some egregious errors and infelicities. Apart from the graduate student community, I have to thank Vicki MacKenna and Carol Sprague of the EAPS Education Office for their patience and willingness to come to my rescue many times when I made a hash of meeting MIT deadlines and countless administrative headaches of my own creation. Joe Hankins may have put his job on the line forgiving (many) hundreds of dollars of overdue library fines.

It was a great privilege to work alongside my advisor during my time at MIT. Clark Burchfiel is a unique and inspirational scientist, of perhaps unequalled intellectual honesty and generosity. I cannot thank him enough for giving me complete and total freedom to pursue any line of inquiry that proposed itself to me. This unfettered freedom included the freedom to hit more than a few dead ends, all of which, needless

to say, contained invaluable lessons. I must also thank the members of my thesis committee and other members of the EAPS faculty for their part in creating a rich, exciting and rigorous intellectual environment. Among these, I should like to take the opportunity to thank Kip Hodges and Kelin Whipple for advice, encouragement, and critical edits of various parts of this dissertation. John Geissman generously donated considerable amounts of his time to helping me along as well as valuable time and space in his lab in Albuquerque. Beyond one of the most careful and diligent editors one could hope for, I count him as a great friend. Without the generosity and help of my graduate student colleagues and thesis committee members, there is no doubt in my mind that this dissertation would never have happened. Having said that, many flaws remain, and I take sole ownership of those.

Outside of the confines of the Green building, I am most thankful for having the unreasonable fortune of being part of an amazing and supportive community of friends and family. A year into my studies at MIT, and well into some serious experiments in sleep deprivation and general misery, Ico San Martini invited me over for dinner, and thus began my association with the members of the Bishop Allen Drive collective. When life got a little hairy in Cambridge, I could always count on the BAD coop to provide a strong dose of humanity, perspective, laughter and good food. Ico, Zan, Melitta, Jeff, Sam, Paulina, Luke, Elke, Kai, Ben, Ona, Garth, Pete, Pete, Downing, Clay ... I cannot thank you enough. Finally, in the final and most trying year (and then some), Jessica Gath was a bright light in what often seemed to be dark times, never doubted that I would somehow manage to get it all done even as I insisted otherwise, and fairly carried me over some of the roughest patches, drawing on a seemingly inexhaustible spring of love and patience.

Contents

List of Figures

List of Tables

Chapter 1

Introduction

Of all the mountain belts in the world, the Tibet-Himalaya orogen holds the pre-eminent place as a natural laboratory for continental tectonics. It represents the canonical example of the effects of a continent-continent collision zone and geologists studying older collisional orogens invariably point to the modern, active India-Asia collision zone as an analog or as the source of inspiration. Physical models of continental deformation are developed and tested against observations of this orogen. As the largest area of high elevation on the Earth's surface, the Tibet-Himalayan orogen influences global climate, and it is the natural place to investigate recent hypotheses of the close coupling of climate and continental deformation. What is striking, then, is that despite its importance, our understanding of the India-Asia collision is not only incomplete, but is in many respects much less constrained even than other areas whose interpretation is inspired by the Tibet-Himalayan orogen. The simple physical challenges of working in the Himalaya account for some of this, but the limited access of western workers to the Tibetan plateau until comparatively recent times is also a major factor. Geological maps exist for Tibet, but these are not widely available, are mostly the products of reconnaissance geological surveys, and even first-order aspects of the stratigraphy, geochronology and structural geology are continually being

revised.

The Tibetan plateau, and its associated mountain belts (the Himalaya, the Tien Shan, the Longmen Shan, the Sanjiang Shan, the Kunlun Shan, the Qilian Shan, among others) have long been recognized as being the products of the collision of the Indian continent with Eurasia (*Molnar and Tapponnier* (1978), but this interpretation goes back at least to *Argand* (1924)). Beyond this uncontroversial interpretation, however, models for the growth and evolution of Tibet are rather varied, and the subject of considerable debate. This debate is often characterized in terms of two end-member member conceptions of how continental crust deforms in general, underscoring again the pre-eminent place of the India-Asia collision in continental tectonics. The first model emphasizes the apparent weakness of the Eurasian continent and suggests that the deformation of Eurasia – and by implication, continental crust generally – is best described as diffuse and continuous. The second characterizes the deformation of Eurasia in terms of the plate tectonics-like motion of a few rigid blocks bounded by narrow, lithospheric penetrating faults. The thin viscous sheet numerical model of *England and Houseman* (1988) is an often cited example of the first end-member; whereas analogue models using plasticine indented by a rigid die stands in for the latter conception (*Tapponnier et al.* (1982)). Either concept is readily transformed into a straw-man: Tibet is "clearly not" a viscous fluid, since the upper crust obviously deforms along seismic faults; just as obviously, strike-slip faulting alone cannot produce the >65km thick crust and high elevations that are the defining feature of the plateau. This fails to recognize that the original models highlighted important first-order aspects of the deformation (the high topography and crustal thicknesses on the one hand, the role of significant terrane motion and transfer of rotation and shortening on the other), and that the original proponents have since developed more nuanced descriptions of the evolution of the Tibet-Himalaya orogen (eg. compare *Tapponnier et al.* (2001) with *Tapponnier et al.* (1982)).

Ultimately, for Tibet to usefully inform our understanding of crustal deformation generally, we need to address the major outstanding issues regarding the geological evolution of the plateau specifically. A short list of these includes: When was the Tibetan crust thickened, and what mechanisms can be invoked to explain the thickening? Related to that is whether and how we can distinguish pre-Cenozoic deformation from the effects of collision? The present, active deformation is reasonably well-known, but how far can the present, active tectonics be extrapolated into the past? To what extent do the early stages of Cenozoic tectonics resemble the present tectonic regime? More generally, what is the relationship between upper crustal deformation and crustal thickening, both at present and in the past?

Certainly, this thesis should in no way be taken as representing the complete set of answers to these questions. Instead, these issues motivate a series of case studies, each almost entirely based on field mapping and observation, that provide contributions to understanding the tectonic evolution of the Tibetan crust specifically and continental crust generally. Above all, Tibet, and particularly eastern Tibet, represents an incredible natural laboratory for testing ideas and challenging assumptions about continental deformation. In what follows, I outline some of the major aspects of Tibetan tectonics and how work in the thesis chapters relates to these.

1.1 Pre-Cenozoic deformation

Even before the collision of India with the Eurasian continent occurred in the early Cenozoic (*Rowley* (1996)), the southern margin of Eurasia was the site of a number of terrane accretion events. Tibet, southern China and Indochina are a collage of distinct geological provinces (fig. 1-1) bounded by sutures of mainly Mesozoic age (*Sengor and Natalin* (1996); *Sengor et al.* (1984); *Metcalfe* (1998)), some of which represent continental fragments rifted off Gondwanaland and translated across the Tethyan

ocean, others which represent para-autochthonous arcs (eg. the Yidun arc), backarc basins or marginal seas (eg. Songpan-Ganzi). Most of the major boundaries between these are Mesozoic sutures, though the exact age and location of these sutures remains a subject of debate. After the accretion of the Lhasa block along the Bangong-Nujiang suture in late Jurassic – Cretaceous time, the southern Eurasian margin remained an active margin, and was the site of an Andean style continental arc.

Broadly, the consequences of this pre-Cenozoic history for the Cenozoic evolution of Tibet are two-fold. First, the long and protracted history of terrane accretion and associated magmatism and deformation is likely at least partially responsible for the apparent weakness of the Eurasian crust. This either motivates models of the India-Asia collision where India is characterized as a rigid, strong indentor, and Eurasian crust behaving either as a weak fluid (eg. *Kerr* (2004)) or interpretations that emphasize deformation along pre-existing zones of weakness (*Sengor et al.* (1984)). Secondly, the effects of pervasive pre-Cenozoic deformation must be disentangled from younger, Cenozoic deformation in order to assess the contribution of Cenozoic India-Asia collision to upper crustal deformation and crustal thickening.

These issues are highlighted by work described in chapters 2 and 3 of the dissertation. Chapter 2 describes geologic mapping of the Gonjo basin and adjacent rocks. Because these rocks are early Tertiary (Eocene-Oligocene) in age, the field relations expressed in these rocks provide a means of identifying Cenozoic deformation, and evidence is described for the existence of at least two pre-Cenozoic episodes of shortening, one of which post-dated deposition of Triassic strata. This presents a major problem for attempts to quantify Cenozoic shortening and thus its possible contribution to crustal thickening in this area. Structures affecting Gonjo basin rocks are clearly Cenozoic in age, but most of the rocks in this region are Triassic or older in age. These rocks have potentially suffered both Mesozoic and early Cenozoic shortening, and the lack of cross-cutting relations, re-folded folds or overprinting of

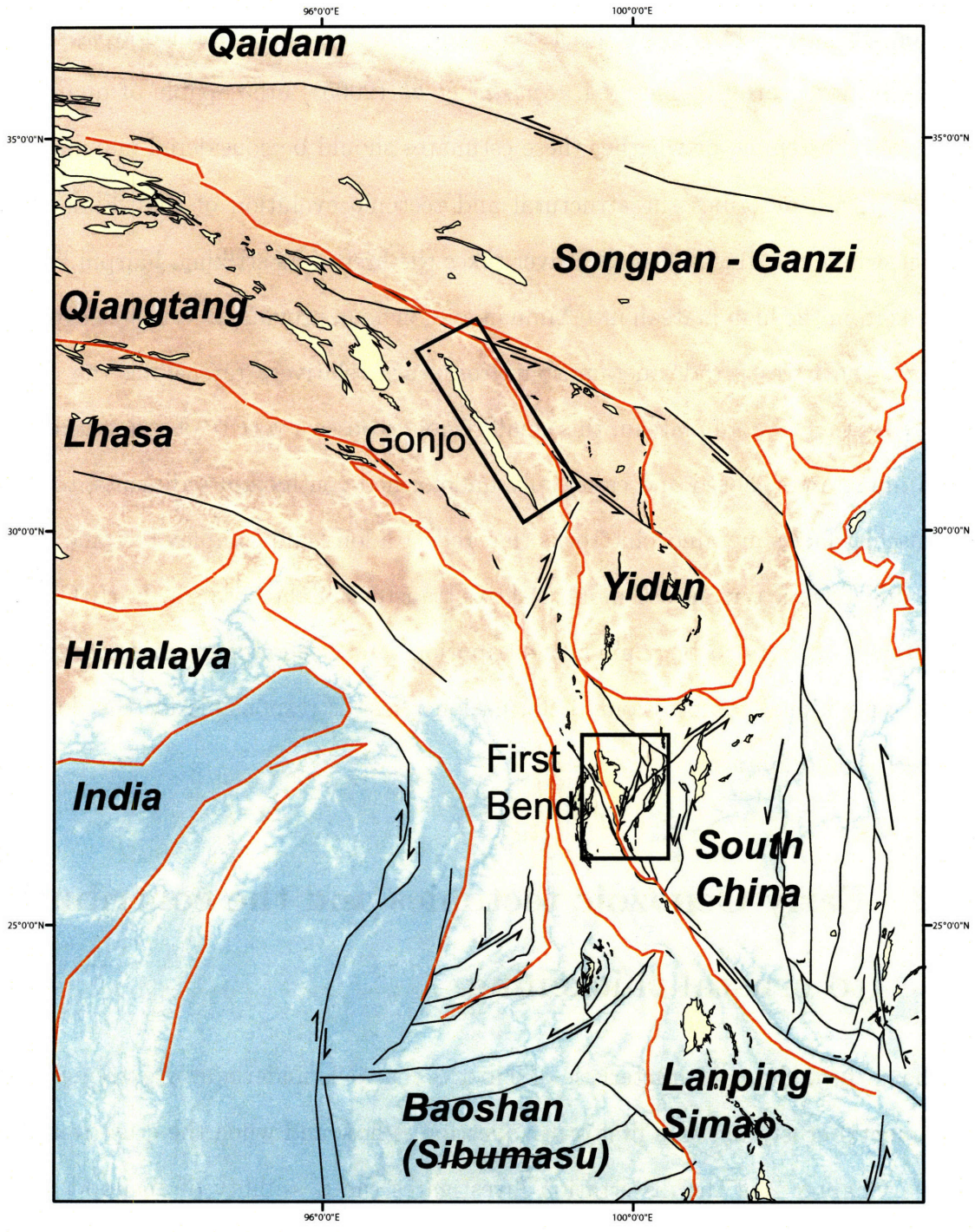

Figure 1-1: The eastern margin of the Tibetan plateau, showing the outlines of major geological units. Also shown is the distribution of early Cenozoic sedimentary basins and major active faults. Boxes show the region around the Gonjo basin and the "First Bend" region.

fabrics rules out obvious ways of disentangling the two post-Triassic episodes of deformation (fig. 1-2). This raises questions about whether retrodeformed cross-sections published for nearby regions (eg. *Spurlin et al.* (2005)) are capable of quantifying Cenozoic shortening, or whether these estimates should be considered maxima.

Chapter 3 describes the structural and tectonic evolution of the "First Bend" region, where the Jinsha (Yangzi) river takes the first of its striking, hairpin loops as it flows from the high plateau into Yunnan and Sichuan provinces. Whereas exposures of even the lowest grade metamorphic rocks are relatively rare along the eastern margin of the Tibetan plateau, this small region exposes a variety of structural levels, from unmetamorphosed and essentially undeformed continental sediments, to upper greenschist facies metamorphic rocks that reflect a long and complex tectonic history spanning Triassic terrane assembly to active transtensional tectonism. Early Cenozoic shortening appears to be a minor contribution, and a heretofore unrecognized late Mesozoic regional compressional deformation phase is responsible for the dominant structures and fabrics.

1.2 Early Cenozoic tectonics and the contribution to crustal thickening

Perhaps the defining characteristic of Tibet is that it is underlain by extremely thick continental crust, and so a first order question is how and when the crust was thickened. Chapter 2 of the dissertation investigates the possibility of an upper crustal record of crustal thickening processes during the early stages of India-Asia collision recorded by sedimentary rocks and structures of the Gonjo basin. Rocks of the Gonjo basin are folded into a broad syncline, and basin bounding reverse faults are demonstrated to have little throw associated with them. That is, rocks of the basin itself have suffered little shortening. The basin, however, is underlain by crust that exceeds

65km in thickness, which therefore raises the question of how this thickening was accomplished. If crustal thicknening was balanced by upper crustal shortening, this shortening had to have been accommodated on structures away from the basin. As noted above, however, pre-Cenozoic shortening can not be straightforwardly distinguished from Cenozoic deformation where structures do not directly affect Cenozoic rocks. Some of the crustal thickening of this area likely predated the India-Asia collision, consistent with suggestions by *Kapp et al.* (2005). The sedimentary record of aridity preserved in the Gonjo basin rocks at least suggests the possibility of nearby high topography at the time those rocks were deposited.

Alternative models of the evolution of the eastern margin of the plateau have suggested that much of the crustal thickening of the eastern margin of the Tibetan plateau as well as into southwestern China occurred without upper crustal shortening (*Clark and Royden* (2000); *Royden et al.* (1997)). While the possibility of Cenozoic reactivation of shortening structures that do not directly involve Cenozoic rocks cannot be ruled out, exposures of Cenozoic continental sedimentary rocks associated with compressional structures analogous to those exposed in the Gonjo basin are widely distributed from the latitude of the Gonjo basin south into southwest China. (Some of these are described in chapter 3 where they are exposed in the First Bend region). Unequivocally Cenozoic structures are generally parallel to the trends of fold axes and faults that do not directly affect Cenozoic rocks. Although it is unclear how much this structural grain reflects Cenozoic deformation away from the limited exposures of Cenozoic rocks, the strikes of faults and folds are strongly oblique to the gradient of surface elevations and crustal thickness. That is, although the Cenozoic basins of the eastern margin of the plateau do not completely constrain the amount of Cenozoic shortening, just the spatial pattern alone of that deformation is not obviously and straightforwardly related to variations in crustal thickness of the eastern plateau.

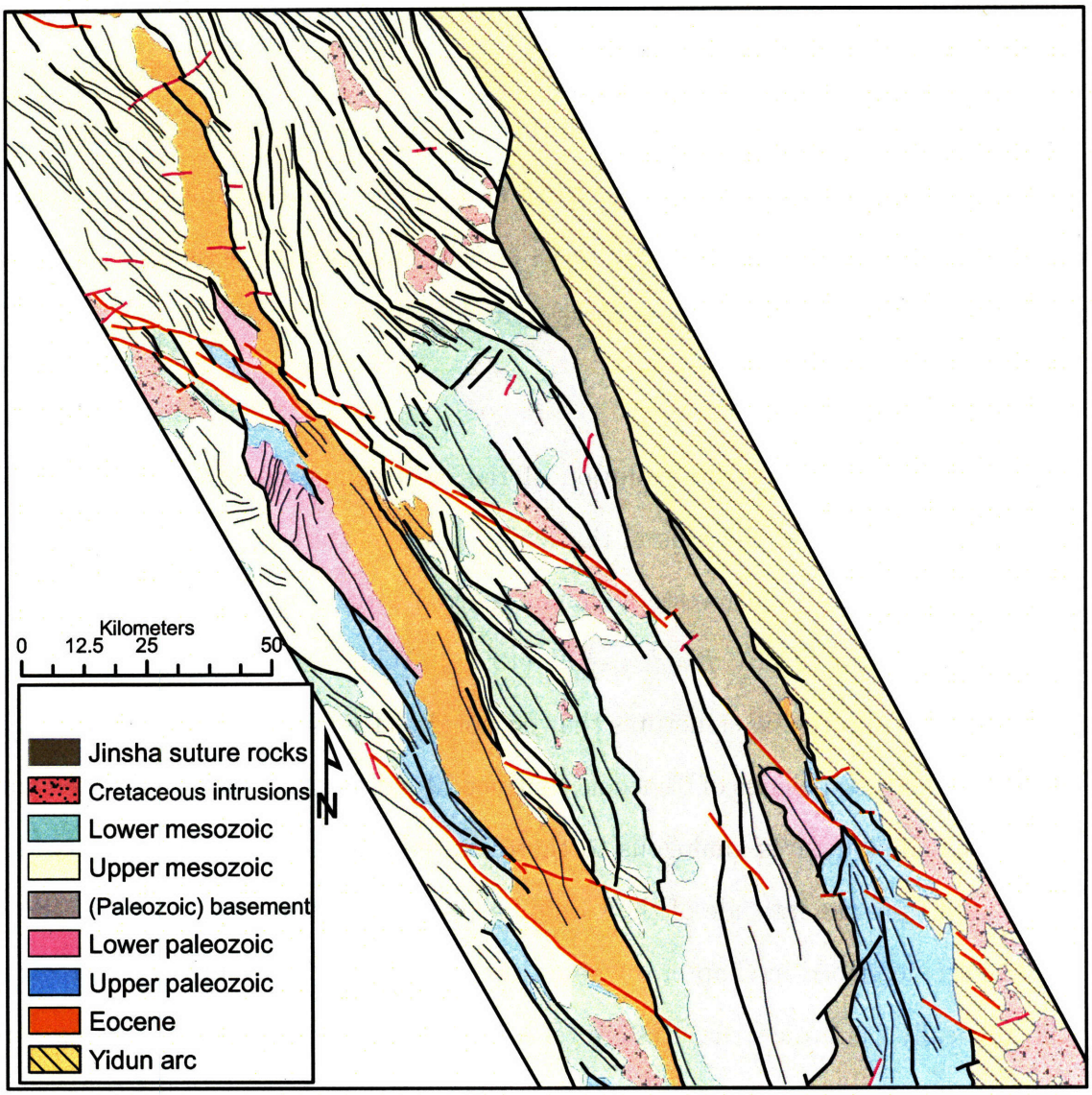

Figure 1-2: The early Cenozoic Gonjo basin and nearby structures. Thin lines are the traces of fold axes; thick black lines are reverse faults; red lines are late strike-slip faults

1.3 Active deformation

To a first order, active tectonism in eastern Tibet is characterized by clockwise rotation of a crustal fragment bounded by the left-lateral Ganzi, Xianshuihe, Xiaojiang, Dien Bien Phu and related faults about the eastern Himalayan syntaxis. This first order picture is well-established from modelling of seismic moment release (*Holt et al.* (2000, 1991), geologic mapping *Wang et al.* (1998); *Wang and Burchfiel* (2000) and geodetic data (*Shen et al.* (2005); *Chen et al.* (2000); *King et al.* (1997); *Zhang et al.* (2004)). Beyond this simple picture are additional complexities: within the larger rotating blocks are smaller, differentially rotating fragments (*Wang et al.* (1998)); normal faulting and extensional strain is at least as important as strike-slip faulting in many places; strain is commonly poorly localized, partitioned into many minor faults or not associated with obvious faults at all (*Burchfiel* (2004); *Burchfiel et al.* (submitted)).

Chapter 4 synthesizes seismologic, geologic and geodetic perspectives of the active deformation of this area. A survey of inferred geologic slip rates for active faults in this area shows considerable uncertainty and inconsistency. Whereas east-west extension is a clear and robust feature of the geodetic velocity field and is reflected in the patterns of seismic moment release, most geologic work in this area has failed to recognize the importance of extension. Importantly, geologic maps showing the distribution of active faults highlight some of the challenges of interpreting geodetic data. Apparently smoothly-varying geodetic velocities in the central Tibetan plateau have been interpreted as requiring continuous and "fluid-like" deformation of the upper crust (*Zhang et al.* (2004)), but most of the apparent smoothness of geodetic velocity gradients can be ascribed to interseismic locking of faults. Recent work by *Meade* (submitted) has shown that the same data which have been interpreted as reflecting continuous deformation are better described by a model consisting of a small number of fault-bounded elastic blocks. In chapter 4, it is shown that geodetic

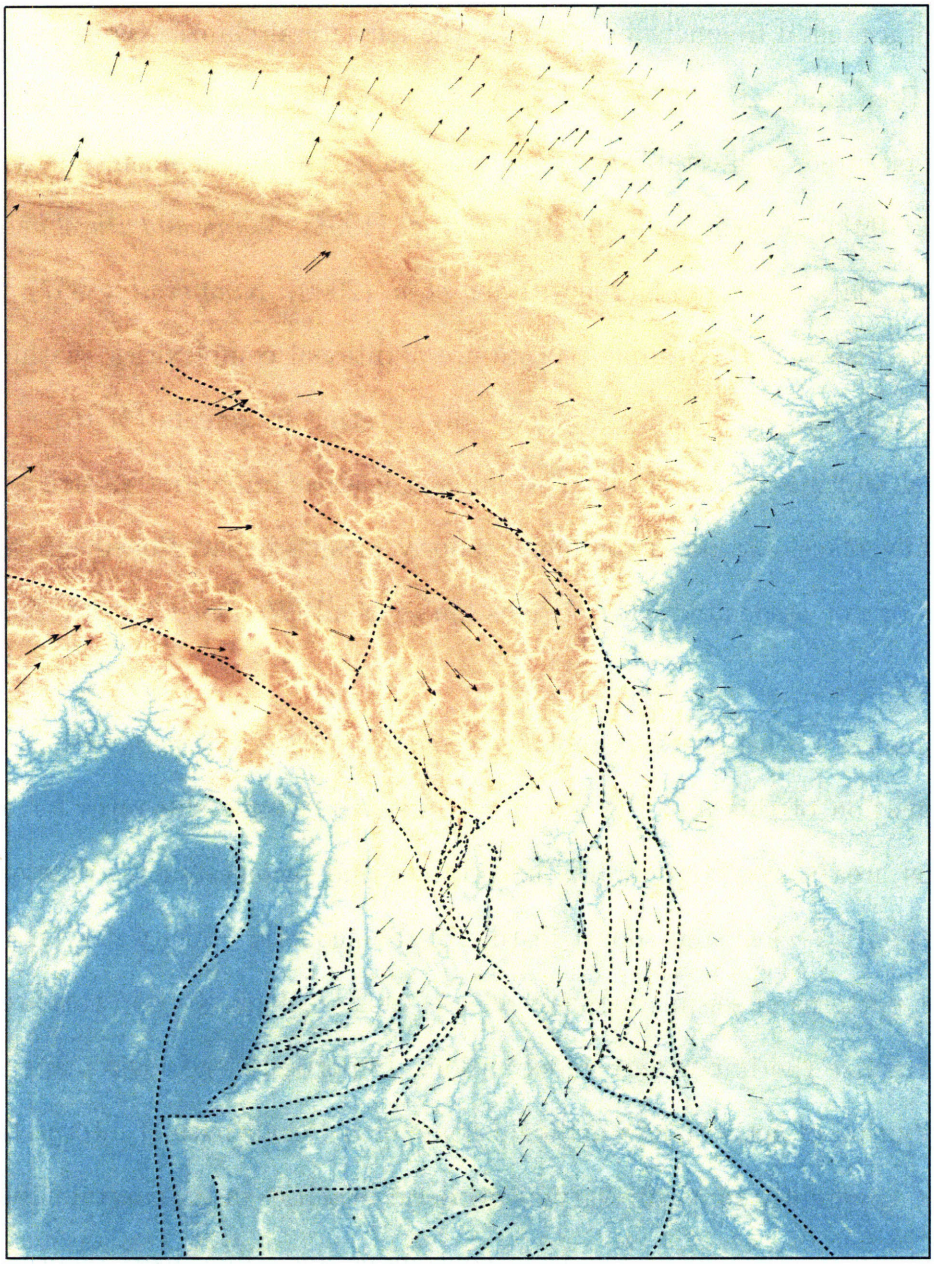

Figure 1-3: GPS velocities relative to South China

velocities can be readily fit by these kinds of models, but important characteristics of the mapped geology remain unexplained.

1.4 Extension, uplift and river incision

The Yulong mountains are a small, but striking range bisected by a deep gorge exceeding 4km in depth and are characterized by high elevations, extreme relief, active normal faults and the exposure of some of the deepest structural levels of the First Bend region. The domal structural geometry and relatively deep exhumation observed in these mountains are a common structural association in extensional terrains; what is unique about the Yulong mountains is that they are an active system and represent an opportunity to understand the processes that result this geometry. Moreover, considerable recent attention has been paid to possible areas where anomalously deep exhumation is in some sense driven by erosional processes (*Zeitler et al.* (2001)), and the Yulong mountains represent an area where similar processes might be taking place.

Chapter 5 describes geomorphologic evidence of high erosion rates being balanced by anomalously high rock uplift rates, accommodated by a closed network of active normal faults (fig. 1-4). The extremely localized region of high uplift rates requires that the brittle, upper crust is underlain by weak material at middle crustal levels. A model is proposed whereby the network of normal faults, the presence of weak crustal material that can respond to local pressure gradients and the ability of erosional processes to balance uplift rates all provide necessary conditions for continued, fast exhumation rates. In essence, the Yulong mountains, as a single feature of the enormous Tibetan orogenic system, represent the product of disparate elements of our understanding of the eastern Tibetan crust: where the coupled processes of strong erosion, weak middle crust and upper crustal extension interact to expose rocks bear-

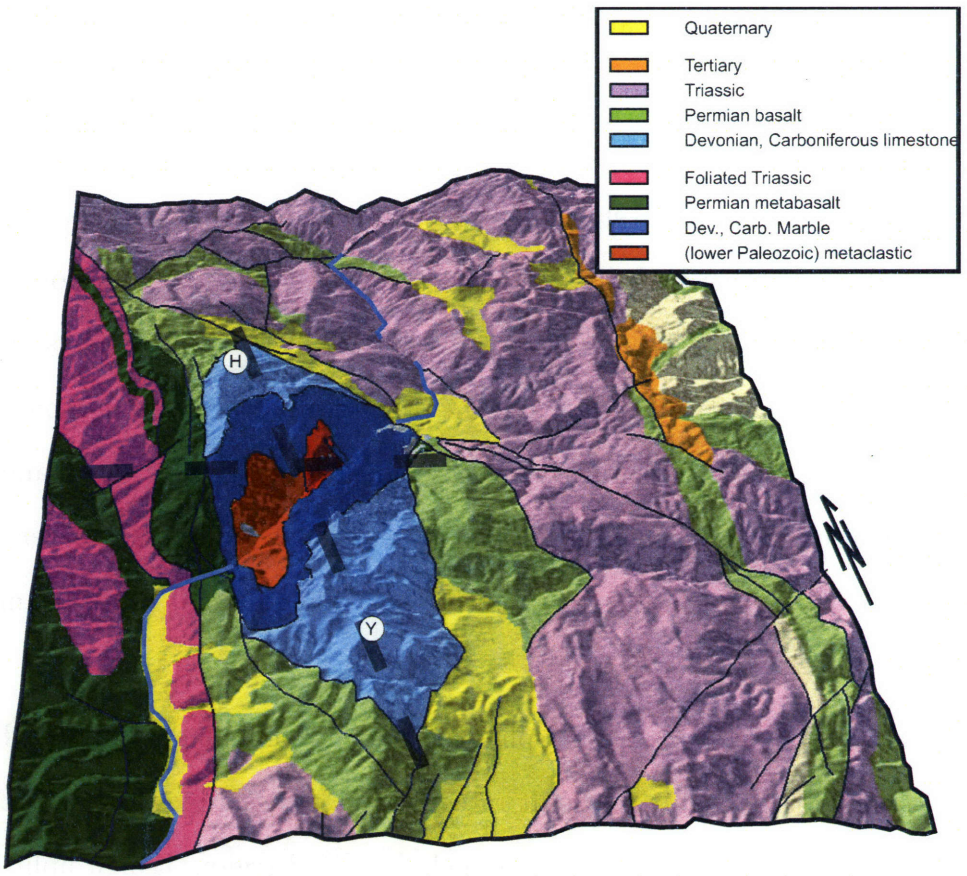

Figure 1-4: The normal fault-bounded Yulong mountains structural culmination.

ing multiple fabrics and the evidence of multiple generations of deformation.

References

Argand, E. (1924), *La tectonique de l'Asie*, Hafner, New York, translated by A.V. Carozzi.

Burchfiel, B. C. (2004), 2003 Presidential address: New technology, new geological challenges, *GSA Today*, *14*, 4–9.

Burchfiel, B. C., C. Studnicki-Gizbert, J. Geissman, Z. Chen, L. Chen, and S. Akciz (submitted), How much strain can continental crust accommodate without developing obvious through-going faults?, submitted to *GSA Special Paper*.

Chen, Z., B. C. Burchfiel, Y. Liu, R. W. King, L. H. Royden, W. Tang, E. Wang, J. Zhao, and X. Zhang (2000), Global positioning system measurements from eastern Tibet and their implications for India/Eurasia intercontinental deformation, *Journal of Geophysical Research*, *105*(B7), 16,215–16,228.

Clark, M. K., and L. H. Royden (2000), Topographic ooze: building the eastern margin of Tibet by lower crustal flow, *Geology*, *28*, 703–706.

England, P. C., and G. A. Houseman (1988), The mechanics of the Tibetan plateau, *Philosophical Transactions of the Royal Society of London A*, *326*, 301–320.

Holt, W. E., J. F. Ni, T. C. Wallace, and A. J. Haines (1991), The active tectonics of the eastern Himalayan syntaxis and surrounding regions, *Journal of Geophysical Research*, *96*(B9), 14,595–14,632.

Holt, W. E., N. Chamot-Rooke, X. L. Pichon, A. J. Haines, B. Shen-Tu, and J. Ren (2000), Velocity field in Asia inferred from Quaternary fault slip rates and global positioning system observations, *Journal of Geophysical Research*, *105*(B8), 19,185–19,210.

Kapp, P., A. Yin, M. T. Harrison, and L. Ding (2005), Cretaceous–Tertiary shortening, basin development, and volcanism in central Tibet, *Geological Society of America Bulletin*, *117*(7-8), 865–878, doi:10.1130/B25595.1.

Kerr, R. A. (2004), GEOPHYSICS: Hammered by India, puttylike Tibet shows limits of plate tectonics, *Science*, *305*(5681), 161a+, doi:10.1126/science.305.5681.161a.

King, R., F. Shen, B. Burchfiel, L. Royden, E. Wang, Z. Chen, Y. Liu, X. Zhang, J. Zhao, and Y. Li (1997), Geodetic measurement of crustal motion in southwest China, *Geology*, *32*, 809–812.

Meade, B. (submitted), Present-day kinematics of the India-Asia collision zone, submitted to *Geology*, 2006.

Metcalfe, I. (1998), Palaeozoic and Mesozoic geological evolution of the SE Asian region: multidisciplinary constraints and implications for biogeography, in *Biogeography and Geological Evolution of SE Asia*, edited by R. Hall and J. Holloway, pp. 25–41, Backhuys Publishers, Leiden , the Netherlands.

Molnar, P., and P. Tapponnier (1978), Active tectonics of Tibet, *Journal of Geophysical Research*, *83*(B11).

Rowley, D. B. (1996), Age of initiation of collision between India and Asia: A review of stratigraphic data, *Earth and Planetary Science Letters*, *145*(1-4), 1–13, doi: 10.1016/S0012-821X(96)00201-4.

Royden, L. H., B. C. Burchfiel, R. W. King, E. Wang, Z. Chen, F. Shen, and Y. Liu (1997), Surface deformation and lower crustal flow in eastern Tibet, *Science*, *276*(5313), 788–790, doi:10.1126/science.276.5313.788.

Sengor, A. M. C., and B. A. Natalin (1996), Paleotectonics of Asia: fragments of a synthesis, in *The Tectonic Evolution of Asia*, edited by A. Yin and M. Harrison, pp. 486–641, Cambridge University Press.

Sengor, A. M. C., D. Altiner, A. Cin, T. Ustaomer, and K. J. Hsu (1984), Origin and assembly of the Tethyside orogenic collage at the expense of Gondwanaland, in *Gondwana and Tethys*, edited by M. G. Audley-Charles and A. Hallam, pp. 119–182, Oxford University Press, Oxford, UK.

Shen, Z.-K., J. LÃ, M. Wang, and R. BÃrgmann (2005), Contemporary crustal deformation around the southeast borderland of the Tibetan Plateau, *Journal of Geophysical Research*, *110*, B11,409+, doi:10.1029/2004JB003421.

Spurlin, M., A. Yin, B. Horton, J. Zhou, and J. Wang (2005), Structural evolution of the Yushu–Nanqian region and its relationship to syncollisional igneous activity, east-central Tibet, *Geological Society of America Bulletin*, *117*(9-10), 1293–1317.

Tapponnier, P., G. Peltzer, R. Armijo, and P. Cobbold (1982), Propagating extrusion tectonics in asia; new insights from simple experiments with plasticine, *Geology*, *10*(12), 611–616.

Tapponnier, P., X. Zhiqin, F. Roger, B. Meyer, N. Arnaud, G. Wittlinger, and Y. Jingsui (2001), Oblique stepwise rise and growth of the Tibet plateau, *Science*, *294*(5547), 1671–1677, doi:10.1126/science.105978.

Wang, E., and C. C. Burchfiel (2000), Late Cenozoic to Holocene deformation in southwestern Sichuan and adjacent Yunnan, China, and its role in formation of the southeastern part of the Tibetan Plateau, *Geological Society of America Bulletin*, *112*, 413–423.

Wang, E., B. Burchfiel, L. Royden, L. Chen, J. Chen, W. Li, and Z. Chen (1998), *Late Cenozoic Xianshuihe-Xiaojiang, Red River, and Dali Fault Systems of Southwestern Sichuan and Central Yunnan, China, GSA Special Paper*, vol. 327, Geological Society of America.

Zeitler, P. K., A. S. Meltzer, P. O. Koons, D. Craw, B. Hallet, C. P. Chamberlain, W. S. F. Kidd, S. K. Park, L. Seeber, M. Bishop, and J. Shroder (2001), Erosion, Himalayan geodynamics, and the geomorphology of metamorphism, *GSA Today, 11*, 4–9, doi:10.1130/1052-5173(2001)011¡0004:EHGATG¿2.0.CO;2.

Zhang, P.-Z., Z. Shen, M. Wang, W. Gan, R. Bürgmann, P. Molnar, Q. Wang, Z. Niu, J. Sun, J. Wu, S. Hanrong, and Y. Xinzhao (2004), Continuous deformation of the Tibetan plateau from global positioning system data, *Geology, 32*, 809–812.

Chapter 2

The early Tertiary Gonjo basin, eastern Tibet: Sedimentary and structural record of the early history of India-Asia collision.

Christopher Studnicki-Gizbert
Li, Z.
Burchfiel, B. C.
Chen, Z.

Abstract

The Gonjo basin consists of a long and narrow belt of lower Tertiary sedimentary rocks that record tectonic and environmental conditions during the early stages of India-Asia collision. The basin fill is dominated by continental sediments reflecting predominantly alluvial fan, fan-delta, floodplain and lacustrine deposition. The presence of aeolian deposits suggests arid conditions at the onset of sedimentation, and may reflect the presence of an orographic rain-shadow. Growth stratal relations indicate that accommodation was created along with the onset of compressional deformation and the generation of structural relief associated with fault-propagation folds. Sediments were derived from proximal locations and deposited into a synclinal trough between bounding antiformal culminations. Deformation outlasted sedimentation, and the Gonjo basin sediments are now part of footwall synclines to bounding reverse faults that broke through the original bounding folds. The preservation of basin-margin facies suggests that the present exposure of Tertiary sediments broadly corresponds with the original extent of the basin. Modern analogues to this basin are found northeast of Tibet, in the form of intermontane basins present between high reverse-fault bounded ranges. Shortening of the basin is generally limited, but the throw on the bounding faults increases from south to north, with perhaps up to 4km of throw on bounding reverse faults in the northern part of the basin. Estimates of regional shortening are hampered by the impossibility of distinguishing late Mesozoic from early Cenozoic deformation. Fold axes and fault traces are parallel, and the two likely phases of deformation must have been coaxial. Strike-slip deformation consisted of distributed left-lateral faults where the uppermost rocks of the basin are shallowly detached, as well as a few prominent left-lateral faults, including one which is on-strike with the active left-lateral Litang fault. Strike-slip faulting definitely post-dates sedimentation, and is not associated with the creation of accommodation space of this basin.

2.1 Introduction

Although it is the type example of a continental collision, the Tibet-Himalaya system remains incompletely understood. This is especially true of the Tibetan plateau, despite recent progress in understanding the late Cenozoic to active tectonics through field studies aided with geodetic, seismological and remote sensing techniques and the earlier late Mesozoic to early Cenozoic history through structural and sedimentological investigations. Many kinematic and dynamic models of the deformation and evolution of the Tibetan plateau have been proposed, and are still a subject of con-

siderable debate. Outstanding issues include: the role and timing of upper crustal shortening and its relationship to crustal thickening (eg. *Kapp et al.* (2005); *Spurlin et al.* (2005)); the role of strike-slip faulting in accommodating both northward indentation of the Indian continent (eg. *Replumaz and Tapponnier* (2003); *Leloup et al.* (1995)) and the localization and propagation of crustal thickening (*Tapponnier et al.* (2001); *Meyer et al.* (1998)); whether the evolution of eastern margin of the Tibetan plateau reflects expulsion of large, rigid terranes (*Replumaz and Tapponnier* (2003); *Leloup et al.* (1995); *Tapponnier et al.* (1982)) or the development of a broad zone of distributed shear and deformation (eg. *Hallet and Molnar* (2001); *Wang and Burchfiel* (1997); *Dewey et al.* (1989)); the contribution of flowing weak middle or lower crust to changes in crustal thickness and elevation (*Royden et al.* (1997); *Clark and Royden* (2000); *Bird*); and whether the active tectonics observed on the northeastern or eastern margins of the Tibetan plateau provide useful analogues for understanding the early Cenozoic history of more central regions of the plateau (*Tapponnier et al.* (2001); *Metivier et al.* (1998); *Meyer et al.* (1998)).

Early Cenozoic continental sediments deposited contemporaneously or soon after the onset of India-Asian collision at $\sim$ 45 - 50 Ma (*Rowley* (1996)) provide an obvious target for gaining insight into the early stages of the growth of the Tibetan plateau. They provide a direct record of erosion and deposition and processes creating accommodation space during the early history of the plateau. Moreover, they suggest a means to distinguish Cenozoic structures from the products of a long and protracted pre-collisional deformation history. These continental sequences are generally found in an arcuate belt that extends from the central plateau into western Yunnan province, mostly within the Qiangtang block (Fig. 2-1). Most of these basins have only been mapped in the course of regional survey mapping (*Qinghai*), but recent detailed structural and sedimentological studies of the Hoh Xil basin (*Wang et al.* (2002); *Liu and Wang* (2001); *Liu et al.* (2003)) and Nanqian–Yushu basins

(*Horton et al.* (2002); *Spurlin et al.* (2005); figure 2-1) have added considerable and much needed detail. These studies have shown that these lower Tertiary sediments were deposited in restricted, narrow basins in the footwalls of thrust faults, and were likely similar to intermontane basins found within the actively shortening Qilian Shan and Tien Shan mountain belts found to the northwest and northeast of the present Tibetan plateau (*Tapponnier et al.* (2001); *Metivier et al.* (1998)).

This paper focusses on early Tertiary rocks exposed in the Gonjo basin, a long ($\sim$ 200km), narrow basin south and east of the Nanqian–Yushu basins and directly north of the eastern Himalayan syntaxis in eastern Tibet. Beyond providing an additional record of deformation and sedimentation during the early stages of continental collision to supplement studies of possibly analogous or related basins farther to the north and west, the Gonjo basin's location makes it uniquely suited for addressing questions as to whether the evolution of the eastern margin of the Tibetan plateau is significantly different from that of central Tibet. In particular, the timing and role of strike-slip deformation and the relationship between shortening and crustal thickening are first-order issues in eastern Tibet. Shortening structures of unequivocally Cenozoic age are difficult to identify, and it has been suggested that much of the crustal thickening here and in western Yunnan province has been accomplished by channel flow of weak middle or lower crustal material from the central plateau (*Clark and Royden* (2000); *Royden et al.* (1997)). Upper crustal deformation may have instead been dominated by strike-slip faulting and block rotation. The Gonjo basin is located where existing large scale maps show an apparent deflection of the predominantly east–west oriented geological trends characteristic of the central plateau into north–south orientations. This apparently describes a broad zone of right-lateral shear wherein crustal blocks are subjected to considerable internal deformation, attenuation and clockwise rotation and possible strike-slip accommodated lateral motion (*Hallet and Molnar* (2001); *Wang and Burchfiel* (1997); *Dewey et al.* (1989)).

In this paper, we describe field relations of the lower Tertiary sediments of the Gonjo basin, and their relationship to thrust and strike-slip faults. We focus on three separate areas of the basin, where we mapped in detail. We describe the sedimentary facies found in the basin, present new age control for these sedimentary rocks, propose depositional environments and compare their setting to likely contemporary analogues found at the modern margins of the Tibetan orogen. The identification of growth stratal patterns provides evidence to suggest that basin subsidence and sedimentation occurred contemporaneously with folding and thrusting along the basin margins. Finally, we evaluate whether Cenozoic shortening in this area is quantifiable or can be distinguished from late Mesozoic tectonism.

2.2 Regional geologic setting

2.2.1 Major geological boundaries and tectonic elements of eastern Tibet and southwestern China.

Eastern Tibet and western Sichuan and Yunnan provinces are underlain by a collage of distinct tectonic elements or "blocks" that accreted to Eurasia from Triassic to Early Jurassic time (*Sengor and Natalin* (1996); *Metcalfe* (1998); fig. 2-1). The Gonjo basin is found within the Qiantang element, which extends from the Pamir mountains and western Tibet and underlies much of central Tibet before being deflected into a north-south orientation in the region north and east of the eastern Himalayan syntaxis (a region also known as the "Three Rivers" or Sanjiang, after the Nu (Salween), Lancang (Mekong) and Jinsha (Yangzi) rivers). South of the Three Rivers region, the Qiangtang block may be correlative to the Lanping-Simao belt, a correlation based on tracing the bounding sutures of the Qiangtang element and several distinct packages of rocks of late Triassic age and younger (B. C. Burchfiel and Z. Chen, map and ms. in preparation, hereafter referenced as *Burchfiel et al.* (In prep.)). The older,

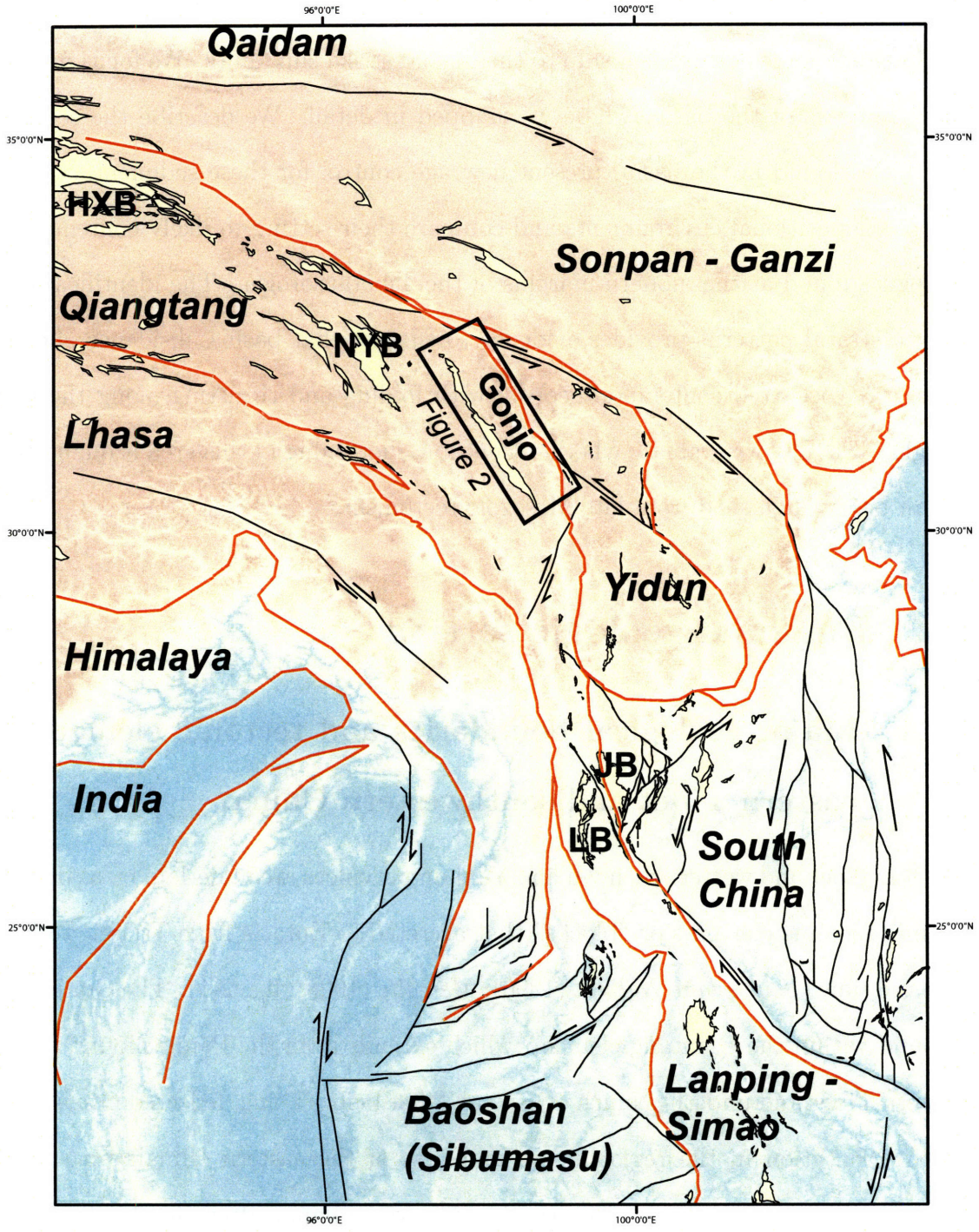

Figure 2-1: Major geological boundaries (in red) and provinces of eastern Tibet and western Yunnan, showing the distribution of early Tertiary basins and their bounding faults. Active strike-slip and extensional faults shown as thin black lines. Basins: HXB: the Hoh Xil basin; NYB: the Nanqian-Yushu basins; JB: the Jianchuan basin; LB: the Lanping basin.

pre-late Triassic, stratigraphy of Qiangtang province differs from that of the Lanping-Simao belt, and a poorly defined suture of middle Triassic age ("Lancangjiang" suture, *Metcalfe* (1998)) may be present in the Three Rivers region.

In the vicinity of the Gonjo basin, the Qiantang element is bounded on its northeastern side by the Triassic Yidun arc terrane and the Jinshajiang suture (*Reid et al.* (2005b); *Sengor and Natalin* (1996)). The Jinshajiang suture can be traced southward through the Three Rivers region into Yunnan, where it appears to be continuous with the Ailao Shan suture (*Metcalfe* (1998); *Burchfiel et al.* (In prep.)). To the southwest, the Bangong-Nujiang suture separates the Qiangtang element from the Lhasa element. This suture appears to extend southward to the Cenozoic Gaoligong and Chongshan shear zones (*Akciz* (2004)), which, like the Cenozoic Ailao Shan shear zone (*Leloup et al.* (1995, 2001)), reactivates older Mesozoic sutures. The Chong Shan shear zone separates Lanping-Simao from the Baoshan element and the Gaoligong Shan separates the probable southern continuation of the Lhasa element from Baoshan (fig. 2-1).

2.2.2 Early Cenozoic syncontractional basins and Cenozoic magmatism.

The Gonjo basin is one of several fault-bounded basins of early Cenozoic age exposed in the Qiangtang and Lanping-Simao elements. To the northwest and west, these include the Hoh Xil (also referred to as the Fenghoushan or Erdaogou) basins (*Wang et al.* (2002); *Liu et al.* (2003); *Liu and Wang* (2001); *Coward et al.* (1988); *Yin et al.* (1988)) and Nanqian-Yushu basins (*Spurlin et al.* (2005); *Horton et al.* (2002)). South of the Three Rivers region, similar rocks are exposed in Lanping-Simao province (*Wang and Burchfiel* (1997)). Other small occurrences of early Tertiary sedimentary rocks occur within the Three Rivers region and in western Yunnan province (*Burchfiel et al.* (In prep.)). Early investigations of these continental Tertiary deposits inter-

preted these as molasse deposits deposited in advance of, and eventually incorporated into, the advancing orogenic front (*Yin et al.* (1988)). However, recent detailed studies of the Hoh Xil and Nangqian-Yushu basins have shown that these basins are filled with terrestrial sequences that were deposited into small restricted and isolated basins (*Horton et al.* (2002); *Spurlin et al.* (2005); *Wang et al.* (2002)). Sedimentation occurred broadly contemporaneously with motion on bounding compressional structures into accommodation space created in the footwalls of the bounding structures. Map relations and stratigraphy described on existing Chinese geological survey maps show suggest similar origins for other Tertiary sections exposed south of the Gonjo basin in the Three Rivers region and into the Lanping-Simao element. The widespread occurrence of Tertiary deposits in the footwalls of reverse faults appears to be characteristic of Qiantang crust (*Kapp et al.* (2005); *Spurlin et al.* (2005); *Horton et al.* (2002)). However, the Gonjo and smaller basins in the Three Rivers corridor have also been interpreted as pull-apart basins (*Hou et al.* (2003); *Li* (1996)).

Other Tertiary rocks are isolated small plutons emplaced at shallow level and related volcanic rocks that are locally interbedded with the early Cenozoic terrestrial sediments. The intrusions form an arcuate belt that parallels the boundaries of Qiangtang and Lanping-Simao and the general distribution of Cenozoic syncontractional sedimentary basins. These intrusions are locally associated with major Cu-Au porphyry type mineral deposits (*Hou et al.* (2003)), and their chemistry suggests a significant component of mantle component, which has been interpreted as suggesting subduction of subcontinental mantle, probably along the Jinsha suture, during early to mid Cenozoic time (*Spurlin et al.* (2005); *Wang et al.* (2001)).

2.2.3 Active tectonics of the eastern margin of the Tibetan plateau.

Geodetic and geological studies have shown that present active structures in eastern Tibet and western Yunnan province consist only of strike-slip and normal faults and accommodate no shortening of the upper crust (*Wang et al.* (1998); *Shen et al.* (2005); *Chen et al.* (2000)). To a first order, the active kinematics are characterized by clockwise rotation of material about the eastern Himalayan syntaxis in a region bounded by the arcuate left-lateral Xianshuihe-Xiaojiang fault system (*Wang et al.* (1998); *Holt et al.* (2000)), although within this region other strike-slip and normal faults define second-order differentially rotating fragments. At present, the eastern margin of the Tibetan plateau comprises high-elevation, low-relief uplands that are currently being dissected and incised by the Jinsha, Nu, and Lancang rivers and their tributaries (*Clark et al.* (2004, in review)). High elevations here reflect thick continental crust (*Li and Mooney* (1998); *Xu et al.* (Submitted)). The absence of active compressional structures requires that all crustal thickening occurred prior to the establishment of the current tectonic regime (in the late mid to late Miocene, *Wang et al.* (1998)), or, if crustal thickening is on-going, it is caused by flow of the lower or middle crust, decoupled from the upper crust (*Clark and Royden* (2000); *Royden et al.* (1997)).

2.2.4 Structural and geological setting of the Gonjo basin

Compilation of existing geological maps (*Qinghai*), together with our own field mapping shows that deformation of Mesozoic and Paleozoic rocks in the vicinity of the Gonjo basin is characterized by upright folds and steep reverse faults (fig. 2-2). Folds are detached at multiple stratigraphic levels, range from fairly open to almost isoclinal in the thinner bedded, more shaley lithologies, and are rarely associated with a

weak, subvertical spaced cleavage. Reverse faults strike parallel to fold axes, appear to be steep where exposed, and typically have very little stratigraphic separation. The deepest stratigraphic levels are Paleozoic rocks exposed immediately west of the Gonjo basin, and a complex of variably metamorphosed Paleozoic sediments and granites adjacent to the Jinsha suture (fig. 2-2), unconformably overlain by Lower Triassic rocks. The strike of the Gonjo basin and its bounding structures is generally parallel to the dominant structural grain, as reflected by the orientation of the fold axes and reverse faults deforming mostly Mesozoic rocks west of the Jinsha suture. There is no evidence of multiple deformation generations (eg. refolded folds, multiple fabric generations) affecting Mesozoic rocks, and the parallelism of these structural trends with structures that deform the Tertiary rocks of the Gonjo basin requires that either all the deformation is Cenozoic in age, or that Cenozoic deformation was coaxial with the earlier (possibly late Triassic, *Reid et al.* (2005a)) deformation. Notable exceptions to the general NNW structural trends are reverse faults that involve Paleozoic basement to the immediate west of the Gonjo basin and that are slightly oblique and unconformably overlain by Gonjo basin sediments, and west and northwest striking high-angle strike-slip faults that cut the Gonjo basin and its bounding structures.

2.3 The Gonjo basin: Stratigraphy

In this section, we describe the pre-Tertiary stratigraphy as a few major packages of rocks bounded by unconformities (fig. 2-2). We then describe the Tertiary stratigraphy of the Gonjo basin, which we have divided into a handful of units based mainly on the identification of easily recognizable, mappable units. In most cases, these also correspond to major facies types.

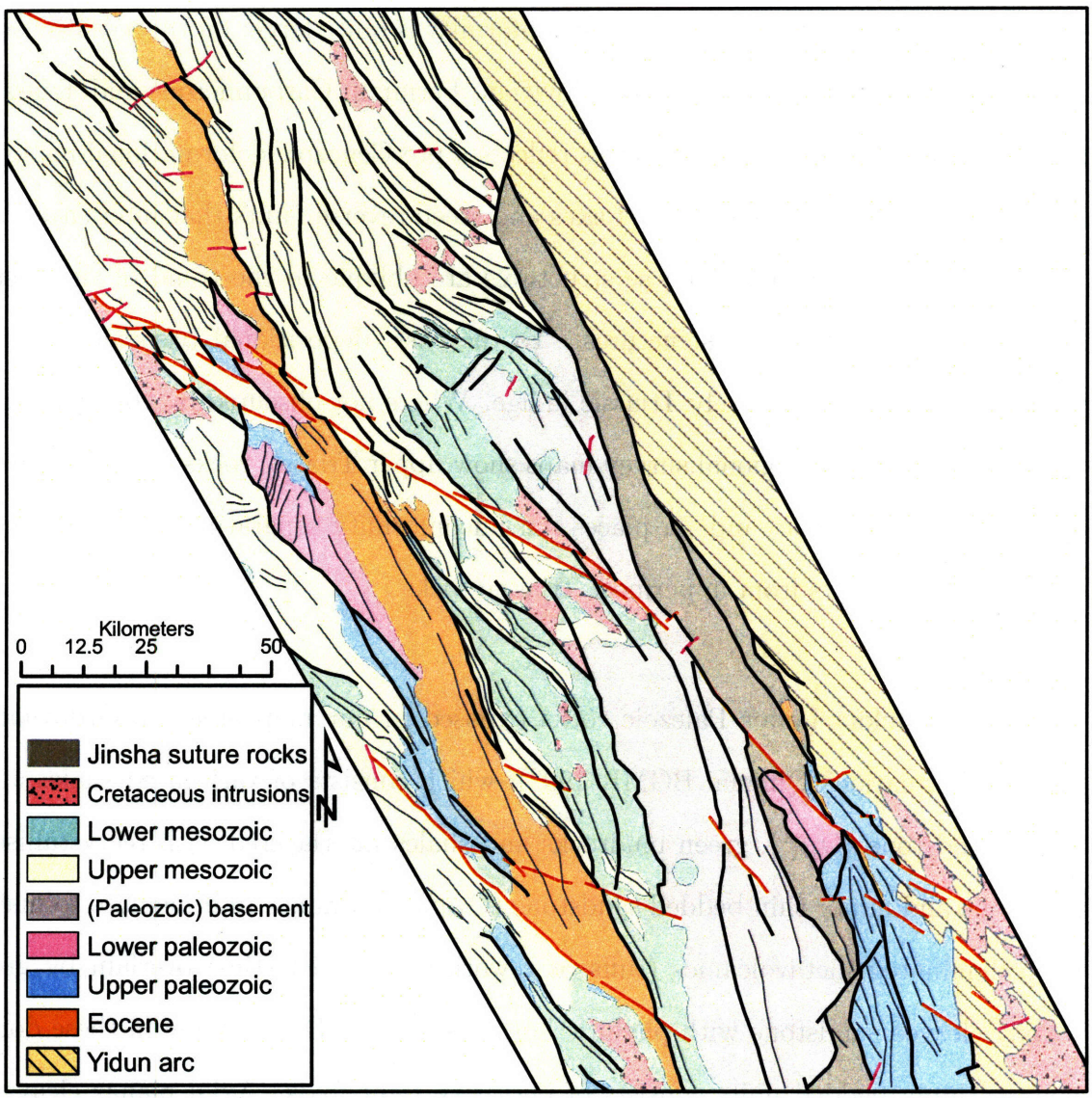

Figure 2-2: Map of the Gonjo basin and its surroundings. Stratigraphy and structure compiled from existing regional geological maps, supplemented by our own mapping along the Chengdu - Lhasa highway, and in the vicinity of the Gonjo basin.

2.3.1 Pre-Cenozoic rocks

Depositional basement to the Gonjo basin consists of marine carbonate and clastic Paleozoic units and a wide range of Triassic units. The range of stratigraphic levels exposed underneath the sub-Tertiary unconformity is quite large: on the western side of the basin, Tertiary rocks overlie Ordovician, Permian, Carboniferous and Triassic units. The range of stratigraphic levels reflects a pre-Cenozoic deformational history, involving the formation of tight fold axes and steep reverse faults that interleave Paleozoic and Mesozoic rocks. These structures are oblique to the trend of the basin and unequivocally younger structures. To the east, depositional basement to the Gonjo sediments is exclusively Triassic in age. Where not obscured by younger compressional structures, regional survey maps show upper Triassic rocks unconformably overlying the Paleozoic, and, in places, an unconformity separating the Lower and Middle Triassic units from uppermost Triassic rocks.

Paleozoic rocks Lower Palezoic rocks exposed in our map area are Ordovician Qinyido Formation (Qinghai BGMR 199?), which consists of variegated shales and minor sandstone (O_1q^1), green mudrocks and shales interlayered with recrystallised limestone and minor thin bedded sandstone (O_1q^2), and minor intermediate to mafic finely laminated metavolcanics (tuffs or reworked volcaniclastics) overlain by grey weakly cleaved sandstone with phyllitic horizons (O_1q^3). Deformation in these dominantly thinly bedded units consists of pervasive tight folds. Axial planar cleavage is dominantly steep, and is crenulated about sub-horizontal axes. Both bedding and cleavage intersect a depositional contact with the Tertiary Gonjo basin rocks at a high angle.

Upper Paleozic rocks are Permian and Carboniferous limestones. The Permian Manchou formation (P_1m) is a deep grey to dark blue-grey, medium to thick bedded (0.5 to 3m) limestone distinguished by minor fossil horizons (crinoid stems, some

minor brachiopods and ammonites) and layers of massive chert and ellipsoidal chert nodules. Carboniferous limestone of units C_2a and C_sl are typically massive, micritic blue-grey limestones with few primary features preserved. Bedding is indistinct, fossils are uncommon, as are interlayered sandstone beds; chert nodules are present but not ubiquitous.

Mesozoic rocks: the Triassic section The Triassic sequence consists of a thick section (>7 km) of mostly marine detrital rocks and carbonates, that are interbedded with mafic to intermediate volcanic rocks. South of the Chengdu-Lhasa highway, a unconformity is mapped between Upper Triassic strata and older rocks, and we therefore break the Triassic into two principal map units in our regional map. The overall depositional setting of these rocks remains unclear. To the west, Upper Triassic rocks lie unconformably over the Carboniferous, with the intervening (< 1.5 km) Permian section almost always absent. Farther to the east, near the Jinsha suture, Paleozoic rocks consist of Ordovician through Carboniferous rocks, are variably metamorphosed, and are intruded by Paleozoic and Mesozoic plutons. The contact between these rocks and the Mesozoic rocks is generally mapped as an unconformity, though this is obscured by later deformation. The northern margin of this sequence of rocks, is an east-west striking, northward dipping fault placing Lower Triassic conglomerate and sandstone on Devonian (?) granite. Faultwards dipping beds of Triassic conglomerate, whose clasts are dominated by granite suggest that this fault may have been an early normal fault, and that Lower Triassic strata may have been deposited in extensional basins.

Above the basal conglomerates, early shoreface sandstones and fluvial conglomerates (T_1) pass into a thick shelf carbonate section (T_2s), which is overlain by distal, fine-grained turbidites (T_2w). Above these rocks, the upper Middle Triassic section ($T_{2-3}j$, Jiangda formation) is quite distinctive and characterised by thick

packages of intermediate to mafic volcanic rocks interbedded with clastic (mostly shales, with some mature sandstones and conglomerates) and rarer carbonate units. Upper Triassic units (T_3ch, T_3q, T_3a, T_3b) consist of a characteristic succession of thin carbonates, terrestrial sediments including coals and fine grained mudstone and sandstone that is regionally extensive.

Contacts within the Triassic section are typically strongly deformed along surfaces sub-parallel to bedding, which is likely the result of flexural slip during the development of the upright folds that characterize this area, as well as detachment horizons accommodating tight folds in the thinner bedded, less competent units. East of the Tertiary Gonjo basin rocks, structural trends within these rocks are parallel to structures deforming the Tertiary section. Where depositional contacts between the Gonjo basin rocks and the Triassic are exposed, however, we always observed an angular unconformity. Therefore, although the Mesozoic rocks alone show no evidence for multiple generations of deformation, some of the deformation of the Mesozoic rocks must have occurred prior to the deposition of the Gonjo basin rocks.

2.3.2 Tertiary rocks

Overview

The Gonjo basin fill is dominated by continental redbed sequences deposited in a narrow, structurally controlled basin. Much of the exposed basin fill is dominated by thinly bedded, fine sand, silt or mud sized sediment (fig. 2-3). In the best exposed section through the basin, near Gonjo village, mudstone, siltstone and fine sandstone represent approximately 70% of the exposed basin fill. Sections on the eastern side of the basin – adjacent to the basin-bounding reverse faults are characterized by coarser facies. Lacustrine facies composed of siltstone, claystone and rarer carbonate beds are common near the top of most sections we observed (fig. 2-3). The general sequence of sedimentary facies exposed in the Gonjo basin is similar to those reported

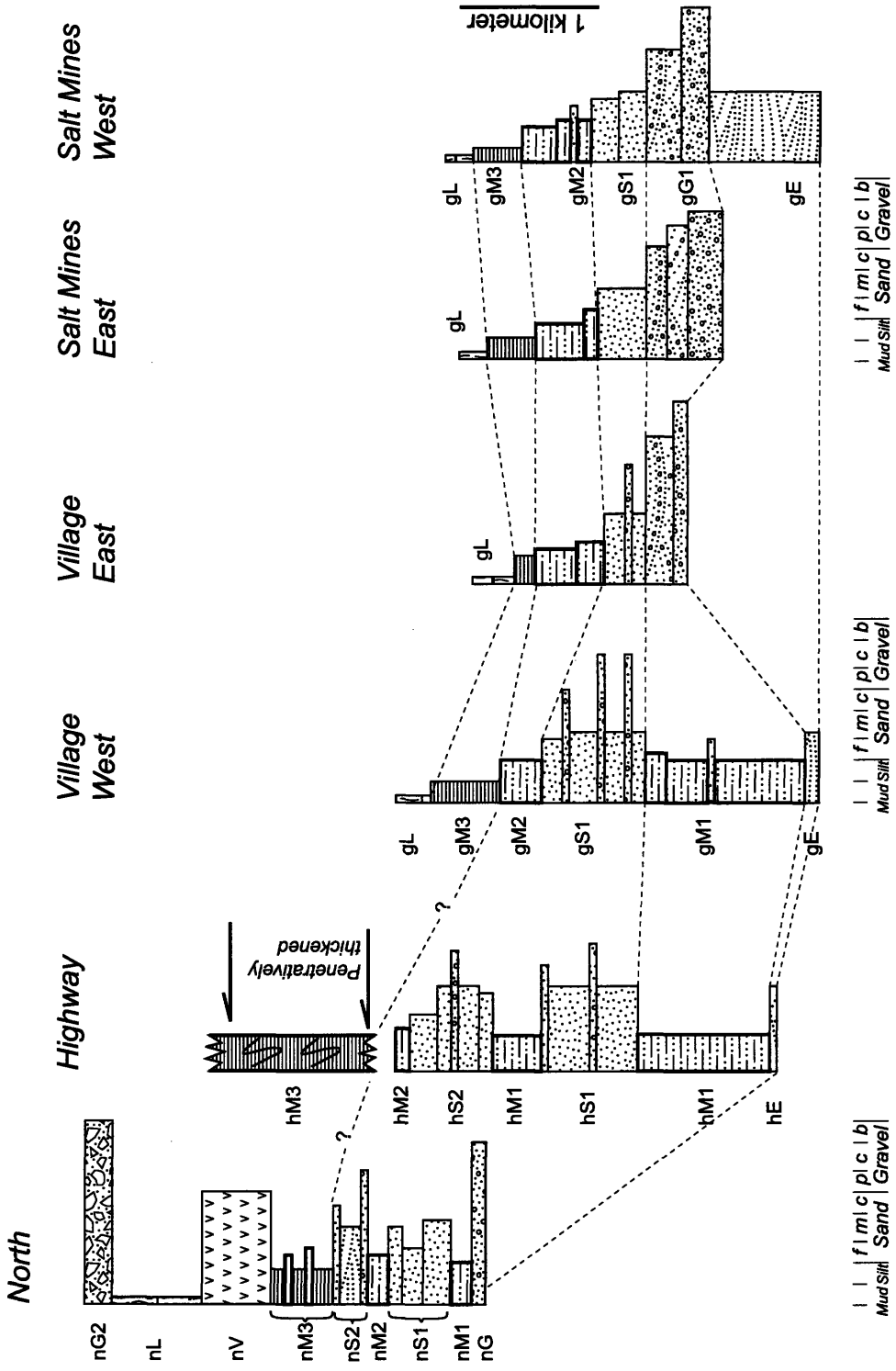

Figure 2-3: Generalized stratigraphic sections for lower Tertiary rocks of the Gonjo basin

by *Horton et al.* (2002) for the basins of the Nanqian–Yushu area. They interpreted these basins as internally drained, structurally controlled basins, and interpreted mud and carbonate deposition as reflecting nearshore lacustrine settings and gravel and sand deposition as fan-delta to alluvial-fan environments.

Tertiary rocks of the Gonjo basin are exposed as a narrow ($\sim$ 20km) but very elongate ($\sim$ 200km) belt of terrestrial sediments. Limited accessibility restricted our fieldwork to detailed selected segments of the basin, and we therefore describe the stratigraphy in terms of the mappable lithostratigraphic units exposed in each of the mapped areas. The best exposure and easiest access is found around the Gonjo village proper and salt mines south of Gonjo village. We refer to these parts of the basin as the "Village" and "Salt Mines" sections (fig. 2-5). The central part of the basin is accessed from the principal highway between Lhasa and Kangding, and we refer to it as the "Highway" section (fig. 2-6). The northernmost section ("North") is the least accessible, but contains volcanic rocks (fig. 2-7) that provide the best age control for these rocks. The generalized stratigraphic columns for all these areas are shown in fig. 2-3. The map units are described for each of the three major sections, in turn. Similar stratigraphic associations were observed in the different sections, and are given similar designations. However, although units can broadly be matched between the different described areas of the basin, no claim to exact time-equivalence is made. In these continental sediments, considerable facies variation can be observed both down-dip and along-strike, and correlated facies may have been developed diachronously.

Gonjo basin south: Village and Salt-Mines areas

Eolian sands and talus deposits (*Unit gE*) In the area near Gonjo, the lower depositional contact of the Gonjo basin rocks with Triassic or Carboniferous rocks is marked by a medium to coarse, extremely well-sorted sandstone of variable thickness. Large foresets, interpreted as dune cross-bedding suggest an eolian origin for this unit

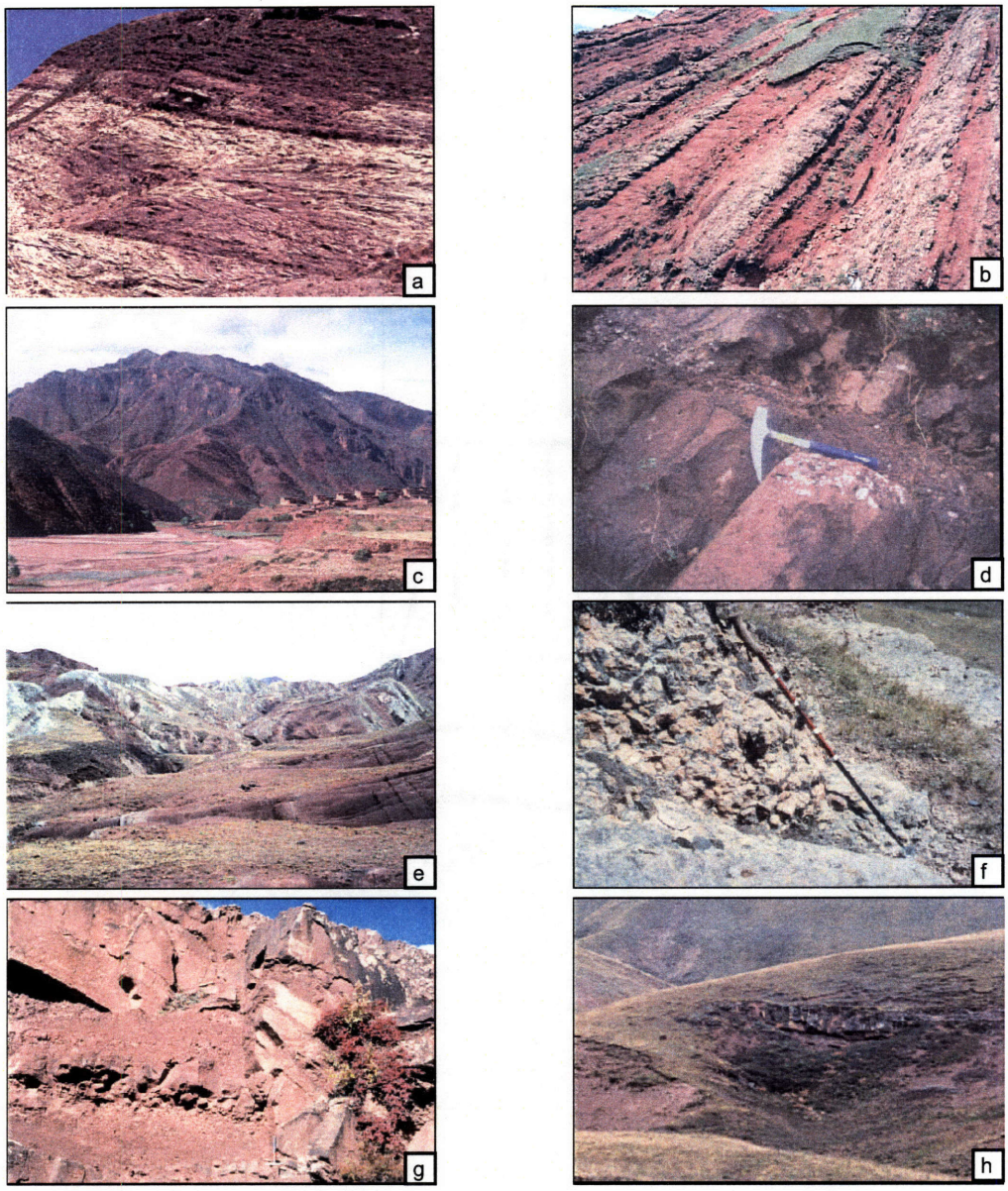

Figure 2-4: Photos of Tertiary sediments of the Gonjo basin. (a) Aeolian beds near Gonjo village; (b) Interbedded gravels and sand beds of unit gG1, interpreted as alluvial fan deposits; (c) View north from Gonjo village. Transition to resistant, cliff-forming beds is the transition between units gM1 and gS1; (d) pebbly lag at the top of laminated to massive sandstone bed in unit gS1; (e) deformed green and yellow carbonaceous shales and carbonates of unit gL; (e) coarse gravel filling incised paleo-caliche surface; (f) floodplain deposits of unit gM2 incised by fluvial channel filled with cross-laminated sandstone; (g) fluvial channel in floodplain deposits in unit nM3.

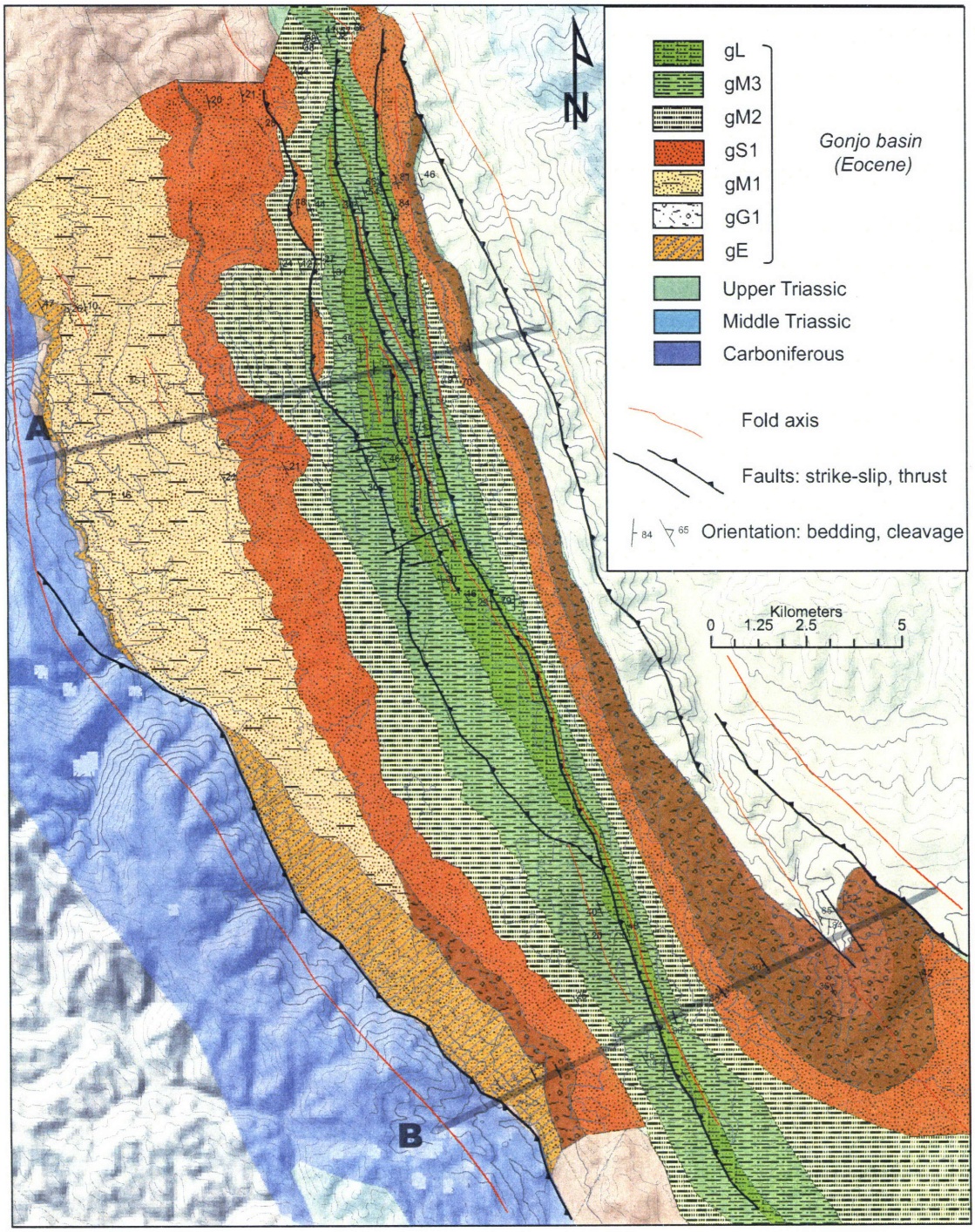

Figure 2-5: Map of the southern part of the Gonjo basin

(fig. 2-4a). To the west of Gonjo village, this unit attains a thickness of up to 70 meters, but its thickness is extremely variable over even short distances. Here, these deposits fill in considerable existing topography underlain by Carboniferous rocks, the local relief on which was on the order of a few hundreds of meters. Blocky, angular, matrix supported, poorly sorted conglomerate whose clasts are entirely local are intercalated with the lowermost eolian sands and are interpreted as talus deposits shed from then-existing cliffs, escarpments and generally steep slopes. On the east side of the basin, along the same section as Gonjo village, the angular matrix supported conglomerate is absent, and dune cross-bedded sandstones lie conformably with the steeply dipping unconformity surface. The dune sands here are much thinner, less than 15 meters. Dune sands are interbedded with thin horizons of well sorted medium sandstones supporting thin, sub-angular pebble size clasts derived from the Triassic slates and phyllites (T3j) immediately underneath the unconformity.

To the south, along the Salt Mines section, well-sorted, dune cross-bedded sandstones are found in the footwall of a reverse fault that places Carboniferous limestones above the Tertiary sandstones. The unconformity and associated proximal conglomerates are not exposed. The dune sand package is much thicker here: up to 200 meters.

Basal conglomerates (*Unit gG1*) Well-rounded pebble to cobble, clast supported conglomerates are present low in the section, above the aeolian sandstones on the east side of the basin along the Gonjo village section, and on both sides of the basin at the level of the Salt Mines. Along the Gonjo village section, these gravels are up to 200 meters thick. Two distinct facies types were identified. The first are thick, moderately sorted, indistinctly bedded cobble conglomerates with clast and matrix supported units, and indistinct internal stratification. Clast compositions include quartz, carbonate and variegated shales that appear to be sourced from the nearby

Triassic units. We interpret these rocks as proximal alluvial fan deposits, with fluvial and debris flow deposition. The second distinct facies consists of 2-3 meter thick beds of well-rounded pebble to cobble, clast supported conglomerates, interbedded with thinner coarse sand to pebbly sandstone beds (fig. 2-4b). Gravel beds have erosive bottoms, show clast imbrication and internal stratification suggesting bar accretion, are well-sorted and dominated by quartz and sandstone clasts. Gravel beds commonly fine upward to a mix of pebbly sandstone and cross-bedded coarse sandstones. We interpret these units as fluvial deposits representing braided river environments or fluvial deposits on the more distal parts of alluvial fans.

Along the Salt Mines section, gravel dominated units are found on both sides of the basin. On the west side of the basin, poorly sorted, poorly stratified, cobble and boulder conglomerates represent debris flow dominated proximal alluvial fans. Clasts are nearly entirely composed of carbonate that appears to be sourced from the nearby Carboniferous limestones thrust over the aeolian sandstones immediately below the gravels. These units grade up into more fluvial, braided river deposits with distinct gravel beds interbedded with coarse sand and pebbly sandstone lenses and thin beds. The east side gravels are apparently much thicker here than in the Gonjo village section, and show the same progression from proximal, debris flow dominated units to more distal, fluvial facies.

Basal mudrocks (*Unit gM1*) Gravel deposits are rare to absent low in the western Gonjo village section. Above the lower section of aeolian deposits, the basal basin fill is a fine-grained facies consisting of thinly bedded medium to fine sands that passes quickly into thin bedded fine and very fine sands and silts. This unit is about 1100 meters thick in the Gonjo village section. Between the Gonjo village section and the Salt Mines section, this unit interfingers with and grades into coarse sands and gravels of the lower Salt Mines section. A general fining upwards sequence de-

fines the bottom of the section, immediately above the aeolian sands, but most of the section is monotonous, punctuated by occasional fine sandstone beds that then grade upwards into very fine sands and silts. The deep red-brown color and weathering of these beds obscures primary structures. Fine lamination and rarer cross-lamination are visible only on rare fortuitously weathered surfaces, usually on recently broken off rock. These rocks may have been deposited entirely in a sub-aqueous environment, perhaps in the most distal parts of fan deltas transporting sediment into a lake. Alternatively, it is possible that these represent floodplain deposits, or sheet flood deposits on distal fans. We found no evidence for fluvial channels in these rocks, but they are poorly exposed.

Sandstone dominated deposits (*Unit gS*) In both the Gonjo village west and Salt Mines west sections, a prominent thick package of cliff-forming sands provides a good mappable unit (fig. 2-4c). This unit is traceable for tens of kilometers along strike, with little change in thickness from the Gonjo village to Salt Mines sections. On the west side of the basin, this sequence is about 750m thick, and we correlate it to a thinner sandstone unit on the east side of the basin, where it ranges from 250 to 300m in thickness. Medium (1-2m) to thick (5-10m) beds of well-sorted, poorly laminated medium to coarse mature sands characterize this unit. Thin beds of fine sand are rare, as are thick (3-4m) horizons of rounded clast supported pebble to cobble conglomerate, and mature matrix supported granule to pebble conglomerates found at the top of reverse-sorted beds (fig. 2-4d). These beds are punctuated by occasional very thick (up to ten meters) beds of completely unlaminated, well-sorted, homogenous sand. Coarsening-up sequences are common. In general, sedimentary structures were rarely observed, although this may be an artefact of the weathering, as lamination and cross-lamination was commonly seen on broken off blocks. Beds are very planar, laterally persistent with only subtle thickness changes observed over

tens of meters and characterized by non-erosive bottoms. These may represent sheet floods on a distal fan or subaqueous deposition via sediment gravity flows in medial or distal fan deltas, as inferred by *Horton et al.* (2002) for apparently similar facies in the Nanqian - Yushu basins to the northwest.

Interbedded fine sand and mudrocks (*Unit gM2*) The cliff-forming sand unit (gS1) grades into a thick sequence of interbedded sandstones and mudrocks, showing a general thinning and fining upwards trend. We place the unit boundary at the last prominent, thick (> 2m) cliff-forming sand bed. The fine grained facies are mostly thinly bedded (< 50 cm) fine to very fine sand, with subordinate ($\sim$ 30%) thinly bedded (< 10 cm) silt and rare clay. Thicker beds of medium grained sandstone and very rare pebble conglomerate beds are also present, and are characterised by erosive bottom contacts and upward fining. These beds are rarer and represent less than 5 % of the total unit thickness. Because the contacts between the mapped units are gradational at both top and bottom, these criteria could not always be precisely applied. Following *Horton et al.* (2002), these rocks may represent subaqueous distal fan delta deposits, with the rare influx of coarser grained material representing the most vigorous gravity flows. Alternatively, these could be floodplain or distal fan deposits. In the Salt Mines section, we found a good exposure of a channel cut into thinly bedded fine sand and silt (fig. 2-4g) and containing trough cross-laminated medium-grained sandstone.

Interbedded mudstones, siltstones and carbonates (*Units gM3, gL*) The most distinctive mappable unit in the area is a 200 meter thick pile of mostly very fine grained rocks (fig. 2-4e). Thinly (< 2 cm) bedded, laminated siltstone and subordinate very fine sandstone grade into siltstone and mudstones interbedded with a series of about a half-dozen striking green and yellow carbonaceous shales and thin carbonate horizons with rare brown, presumably organic rich horizons. Gypsum is present

as veins and fracture fillings. In the Salt Mines area, salt is present in the subsurface and extracted by pumping water through this unit and drying it in evaporating pans. The interbedded claystone, carbonate, and carbonaceous shale units are interpreted as lacustrine deposits, and the presence of evaporites suggests variable lake extent and episodic evaporation of parts of this unit. The green carbonaceous shales provide the only existing age control on the basins in the form of palynological assemblages identified by Chinese stratigraphers as being Eocene in age. The thickness of the carbonate bearing horizons is highly variable and ranges from tens of centimeters where they first appear in the western section to up to ten meters thick within a thrust and fold thickened zone in the center of the basin and at the top of the eastern Gonjo village section. This thickening relation is in contrast to the rest of the rocks in the basin, the overall thickness of which drops off rather dramatically from west to east. The change in thickness is much less clear in the eastern Salt Mines section, where this unit is a locus of penetrative deformation and is exposed as a zone of chaotic gouge bounded by steep reverse faults.

Gonjo basin central: Lhasa Highway area

The western side of the Highway section is broadly analogous to the Gonjo Village and Salt Mines west side sections, with similar map units, and a similar, broadly fining-upwards sedimentary sequence. We emphasize the similarities in our choice of unit names, but, again, the lateral migration of facies types suggests that analogous and correlated units may be diachronously developed. Like the east side of the Gonjo village, the east side of the Lhasa Highway map area consists of a condensed section of mostly coarser grained rocks exposed as the steep limb of a large syncline overturned to the west. We only show a generalized stratigraphic column for the west side of the basin, as tight folds and numerous small scale reverse faults complicate measurement of true original unit thicknesses on the east side. The west side section is homoclinal

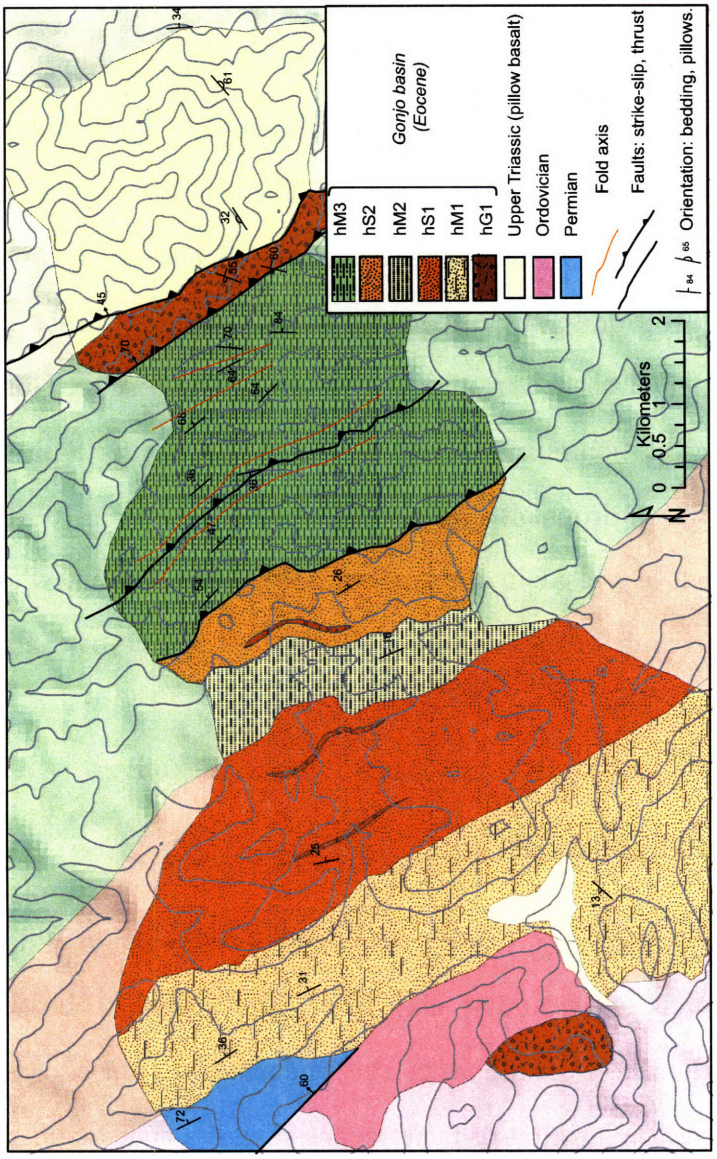

Figure 2-6: Map of the central part of the Gonjo basin, along the Chengdu–Lhasa highway.

up until the uppermost fine grained facies, which steepens abruptly. Numerous tight folds and small reverse faults have effectively penetratively thickened the uppermost unit, and we show this unit only schematically in fig. 2-3. In general, exposure is not as good as farther south, and access is limited to areas easily accessible from the highway.

Basal talus and eolian deposits (*Unit hE*) The western boundary of the basin rocks consists of a few meters of poorly sorted angular matrix supported cobble conglomerates that rest unconformably over steeply dipping Permian carbonates and weakly cleaved Ordovician detrital rocks. These basal conglomerates represent talus and regolith and are overlain by a few tens of meters of well sorted dune crossbedded sandstones that represent aeolian deposits correlatable with similar units described above for the Gonjo Village and Salt Mines sections. Dune crossbed sandstones are not exposed in the steeply dipping eastern section.

Basal proximal gravels (*Unit hG1*) On the east side, basin rocks lie unconformably over Middle to Upper Triassic pillow basalts. Here, the bottom part of the section consists of $\sim$ 150 meters of poorly stratified, subangular to rounded clast supported cobble conglomerates that fine upward into well stratified interbedded clast supported, moderately well sorted 1 - 5 m thick beds of cobble conglomerate interbedded with thinner interbeds of coarse sand. Gravel beds typically fine upwards, have erosive bottoms and show crude cross stratification. Sand beds are cross stratified and often have pebble lag deposits at their bases. The unit as a whole fines upwards, with gravel beds becoming finer grained and thinner, and the proportion of sand beds increasing. As a whole this unit is interpreted as representing progressively more distal alluvial fan deposits, with deposition of the coarser units dominated by debris flows and the interbedded sand and gravel units representing braided river deposits. Clast composition ranges from almost entirely proximally derived basalt at the very

base to a mix of volcanic, quartz and subordinate amounts of carbonate clasts higher up. Sandstone and pebble conglomerate clast compositions are dominated by quartz.

Lower fine-grained sandstones and siltstones (*Unit hM1*) Above the aeolian deposits on the west side of the Lhasa highway area, a thick ($\sim$ 1km), poorly exposed section of shallowly dipping siltstone with subordinate sandstone comprises a large part of the basin fill for this section of the basin. Finer facies are dominated by thinly bedded ($<$ 10 cm), planar laminated very fine sandstones, siltstones and rare claystone. Occasional moderate thickness ($<$ 30 cm) planar beds of fine to medium grained, planar laminated sandstones crop out as resistive ledges but comprise $<$ 5% of this unit. This unit is analogous to the western Gonjo village section unit gM1.

Lower sandstone dominated deposits (*Unit hS1*) Similar to the western Gonjo village section, unit hM1 is overlain by a more resistive, cliff and ledge forming sandstone unit. These rocks are dominantly medium grained, well sorted, laminated sandstones forming generally planar beds generally less than a meter thick, but occasionally up to 5 meters in thickness. Thicker beds tend to be coarser, and often have erosive bottoms, pebbly lag deposits at their bases that grade into coarse sand supported pebbly wackes and fine upwards. Exposure is not very good, and the weathering of these sandstones may be responsible for the lack of observations of sedimentary structure or channel geometries. These units may, like gS1, represent fan delta deposits or subaerially deposited sheet floods on distal alluvial fan surfaces.

Fine grained rocks: fine sandstone and siltstone(*Unit hM2*) Again following the same facies transition as observed farther to the south, hS1 sandstones fine upward into a 300 m thick mixed mudrock and fine sand unit. This unit is dominated by thinly ($<$ 10 cm) bedded siltstones and planar laminated very fine sandstones. Rare, relatively thick ($<$ 1m) beds of ledge forming planar laminated medium grained

sandstone punctuate the sequence, and make up perhaps 10% of the unit. Coarse sandstone and thin horizons of coarse sand supported pebble wacke fining upward to medium sand are rare. This unit is poorly exposed, except along roadcuts.

Upper sand dominated facies (*Unit hS2*) Unlike the Gonjo village and Salt Mines sections, the generally fining upward trend above the hS1 unit is interrupted by the reappearance of another sandstone dominated unit. This unit consists of roughly 600m of relatively thickly bedded sandstones and rarer conglomerate horizons and consists of the same facies as the underlying sandstone unit (hS1). The top 200m of the unit generally fines upwards into a mix of medium to fine sand beds.

Upper siltstones and claystones(*Unit hM3*) The highest unit of the section consists of moderately to steeply dipping thin beds of fine sand to siltstone, with rare thin claystone drapes. This unit is similar to the highest fine grained unit seen in the Gonjo Village section, except for the absence of the green to purple carbonaceous shale and carbonate beds. Numerous small folds and bedding parallel slip surfaces attest to the penetrative thickening of this unit. Tight folds and duplex trains are present in thin (< 10m) zones parallel to the dominant bedding orientation as well as a few larger scale thrust cored anticlines and fault propagation syncline-anticline pairs with wavelengths of tens of meters. The evidence of ubiquitous and near penetrative thickening makes estimating the original thickness of this unit impossible.

Gonjo basin north

The northern part of the Gonjo basin is characterized by very poor access and poor exposure but contains the only volcanic rocks exposed in the basin. We mapped and measured a section in the area of best outcrop exposure and collected a suite of samples in an attempt to establish a paleomagnetic reversal stratigraphy and thus infer subsidence rates. However, many of the sampled sites showed very high within-

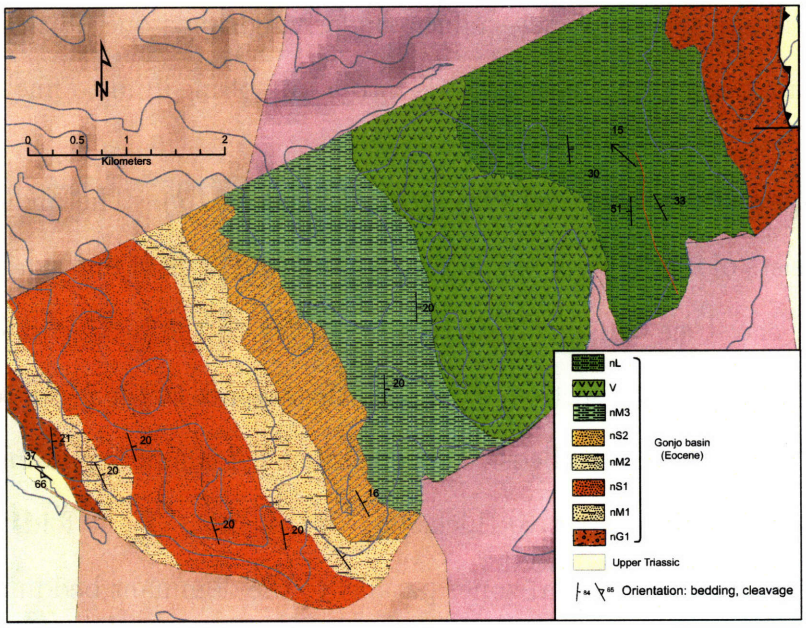

Figure 2-7: Map of the northern part of the Gonjo basin

site dispersion, and there little between-site coherence. Sedimentary facies and the stratigraphic sequence of the northern section differ from the sequences observed farther to the south. A greater proportion of subaerially deposited, fluvial - alluvial facies were found, as well as disconformities marked by paleosol development and erosion. Remote sensing images and existing maps suggest that the upper parts of the southern mapped sections are probably time correlative with the middle part of the northern section. That is, the sedimentary record of the northern section includes younger rocks than in sections to the south, which explains the lack of volcanic rocks in the Lhasa Highway, Gonjo village or Salt Mines sections.

Basal conglomerates (*Unit nG1*) The bottom 50m of the Northern section consists of well-rounded, moderately sorted clast supported conglomerates. These rocks rest upon an angular unconformity with shallowly dipping upper Triassic shales and sandstones that show a weak, subvertical cleavage. The unconformity surface is irregular, and conglomerate fills in narrow, deep paleo-ravines. There appears to be on the order of a few tens of meters of relief over the few hundred meters this contact is exposed. Clast compositions include carbonate and sandstone, with sandstone clasts apparently derived from the underlying Triassic rocks dominating the conglomerate in its lower part. Clasts become progressively less angular and better sorted farther up section, and weak stratification, including rare lenses of cross laminated sands become more common. This unit represents proximal alluvial fans, dominated by debris flows and steep gravel channels.

Lower fluvial – alluvial deposits (*Units nM1, nS1, nM2*) Above the basal conglomerates is a composite section consisting of 150m of fine sands and mudrocks, 450m of medium grained sands punctuated by gravel channels and paleosol horizons, capped by 200m of interbedded siltstone and sandstone. The finer grained unit (NM1) consists of centimeter-scale bedded very fine to medium sandstone interbedded with

tens of centimeter thick medium to coarse cross-laminated sand lenses capped by thin drapes of siltstone. The middle coarser unit (nS1) consists of dominantly medium grained sandstone with minor pebbly lags or pebble wacke and rarer thick (1 - 3m) pebble to small cobble conglomerate interbeds. Gravel deposits are commonly cross-stratified, have erosive bottoms and show a lens like geometry. In places, coarse sand and pebbles are supported by subequal amounts of carbonate cement and fine to medium grained matrix, effectively creating grainstones and wackestones. These carbonate rich horizons show common nodular weathering, as well as pressure solution structures. These horizons appear to have formed pavements, and in places, these paleosurfaces are incised and filled with fluvial gravels. The upper, fine grained unit (nM2) consists mostly of thinly bedded (1 - 2cm) siltstone and very fine sandstone, with planar interbeds of medium to coarse sand and rare pebbly wacke. We interpret these deposits to represent fluvial environments. The finer grained rocks probably represent floodplain deposits, with coarser interbeds representing crevasse splays or migrating sandy channels. The middle, coarser unit may represent frequently avulsing sand to gravel channels in a distal alluvial fan. Development of carbonate rich paleosurfaces may be the result of prolonged subaerial exposure in an arid environment.

Alluvial – fluvial and aeolian(?) sandstones (*Unit nS2*) Unit nS2 consists of 250 meters of medium to coarse sandstone with subordinate amounts of pebble to small cobble conglomerate. Conglomerate beds are generally 1 - 2 m thick, have erosive bottoms, lens-shaped channel geometries, and common lateral accretion cross-stratification structures. Pebble conglomerates and coarse sandstones interbedded with gravels are cross-laminated, have erosive bottoms, and common pebble or cobble lag deposits. We take these coarse facies as representing fluvial deposition on alluvial fan surfaces. Between these coarse facies at the top and bottom of this unit

is a 100 meter thick interval dominated by sandstones, including very well sorted dune cross-bedded medium sandstones that are likely aeolian deposits and fine to medium grained planar sandstones with thin coarse sand to pebble conglomerate lenses. Within both the coarse fluvial–alluvial sediments and dune cross-bedded and more massive sandstones are common thin horizons of matrix (sand) supported pebble or granule conglomerate (wacke) that may be the result of aeolian winnowing of fines. Finally, carbonate rich, nodular weathering, paleo-caliche or pavement surfaces are characteristic of the entire unit, which, together with the possible aeolian deposits suggests aridity and prolonged periods of non-deposition and subaerial exposure.

Fluvial channel and floodplain deposits (*Unit nM3*) Unit nM3 is dominated by fine grained facies, and consists of 450 meters of typically thinly bedded, planar laminated and ripple cross-laminated siltstone and subordinate thin claystone drapes. Interbedded with these fine grained sediments are relatively thin laminated fine to medium sandstone beds and rare discrete medium grained sand channels, with internal ripple, trough cross-stratification and rip-up clasts. We observed a few well exposed channel cross-sections cut into the fine grained deposits that make up the bulk of the unit (fig. 2-4h). We interpret this fine grained unit as representing floodplain, crevasse splay and fluvial channel environments. The unit is capped by a rapidly coarsening up sequence, consisting of thinly bedded cross-laminated medium sands grading quickly to thick ($\sim$ 50 - 70cm) coarse sands and pebble and cobble conglomerates.

Volcanic agglomerate (*Unit nV*) Volcanic and volcaniclastic units in the upper parts of the North Gonjo section consist of lithic agglomerate. Clasts are a mixture of ash and porphyritic flows supported by feldspar, quartz and biotite phyric matrix. Clasts are poorly sorted and range in size from a few milimeters to tens of centimeters, with a complete range of rounding from rounded to angular. Stratification is poor and

indistinct, and lamination is absent. These volcanic units represent porphyroclastic flows and volcanic units reworked in debris flows and mass-wasting events. A thin horizon of volcaniclastic coarse, poorly sorted, angular biotite, quartz and feldspar sandstone immediately underlies the oldest pyroclastic flow unit; other reworked volcaniclastic horizons are rare. Ash-fall tuffs were not found within the poorly exposed 500m thick volcanic unit.

(***Unit nL***) The volcanic sequence is overlain by a very poorly exposed, thick section of red fine sandstone and siltstone, green claystone and carbonaceous shale, thin carbonate beds, thin white chalky ash horizons and rare dark brown organic rich deposits. Sandstone and siltstone units represent only about 15% of the exposed section. We interpret this sequence to represent lacustrine deposits. Significant zones of tight, overturned folds and fractured gouge are present throughout the section which represents the only internal structure in this part of the Gonjo basin and suggests some amount of internal thickening of this unit.

(***Unit nG2***) The highest unit in the Northern section is extremely poorly sorted cobble and boulder conglomerate. Stratification is indiscernable, but appears to be steeper than the homoclinal 20°dip of the rest of the basin. The exact contact between the fine grained lacustrine facies and this unit is covered. Clasts are entirely derived from Triassic limestones, topographically and structurally above these deposits.

2.3.3 Interpretation: the Gonjo basin as restricted intermontane basin

We interpret the sedimentary fill of the Gonjo basin as having been deposited in a narrow, elongate basin whose lateral extent was comparable to that of the presently exposed rocks. We interpret the Gonjo basin stratigraphy as a product of continen-

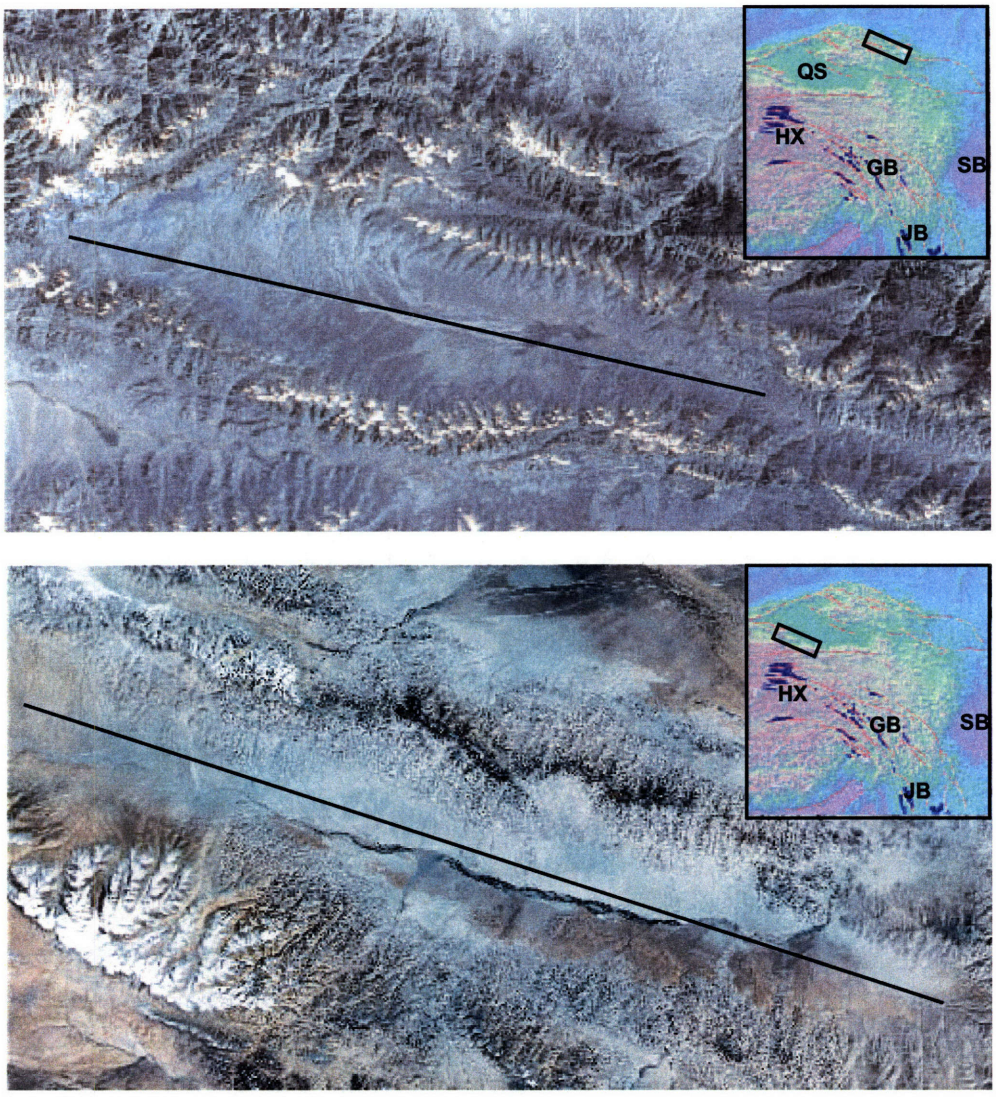

Figure 2-8: Two narrow, elongate basins from northeastern Tibet that may represent modern analogues to the Gonjo basin. Top: intermontane basin perched at high elevations in the Nan Shan ranges. Thin line is 105 km long. Bottom: Intermontane basin south of the Qaidam basin, north of the Kunlun mountains. Line is 175 km long. Sedimentary environments in these basins include bajadas and alluvial fans, meandering river and floodplain environments along the axis of the basin, fan delta and lacustrine deposition, and isolated barchan dune fields. Inset maps show locations relative to eastern Tibet, Tertiary basins in blue. QD: Qaidam basin; HX: Hoh Xil basin; GB: Gonjo basin; SB: Sichuan basin; JB: Jianchuan basin.

tal, mostly fluvial sedimentary environments. Coarse grained facies typically were deposited as alluvial fans, by fluvial or debris flow transport. Finer grained facies represent either distal fan, overbank or crevasse splay floodplain deposition. The finest grained material, and the carbonaceous shales and carbonate rocks represent lacustrine environments. Arid conditions are suggested by aeolian sandstones and possible aolian winnowing of subaerially exposed sediment, creating pebble lags and possible pavement surfaces, especially in the North section. Arid conditions may perhaps reflect basin deposition in a rain shadow created by high topography.

Coarse grained facies are mostly found either immediately above the basal unconformity or at basin margins where we mapped bounding structures that would have been associated with the uplift and erosion of adjacent rocks. Thus, coarse grained rocks form thicker sections on the east side of the basin in the sections mapped in the south and central parts of the basin. In the Salt Mines area, relatively thick sections of coarse conglomerate lie near the bottom of both the western and eastern sections, which is consistent with the basin being bounded by thrusts and thrust-cored anticlines on both sides. The preponderance of finer grained sediment in the Gonjo village and Highway sections suggests that subsidence was rapid enough relative to sediment delivery to confine coarse grained material to the margins, with more distal facies dominating most of the exposed sedimentary section. The general fining-up pattern and transistion to lacustrine facies observed in the central (Highway) and southern (Gonjo Village and Salt Mines) sections, may be interpreted as a tectonic signal: either representing either increased subsidence and consequent transition to underfilled conditions or closure of the basin and the establishment of internal drainage.

The geometry, dominance of terrestrial sedimentary environments, the suggestion of arid conditions, and association of sedimentary facies distributions with bounding structure leads us to suggest that the Gonjo basin was formed as a narrow, intermontane basin. Modern analogous basins might include the arid intermontane basins

caught between thrust bounded ranges in the Argentine Puna and the Qilian Shan and Nan Shan ranges northeast of Tibet. Numerous possible contemporary analogues can be found in thrust fault bounded basins to the northeast of the Tibetan plateau (fig. 2-8).

2.3.4 Age control for Tertiary rocks of the Gonjo basin

The terrestrial redbeds of the Gonjo basin do not lend themselves well to the preservation of fossils that might provide good age control. Previously reported fossils come from the mixed siltstone, claystone and carbonate lacustrine facies that are typically found at the top of the Gonjo basin fill sequence (eg. units gL or nL, or unit Er on the Chinese maps, *Qinghai*). Chinese regional geological studies have reported the following assemblages from these rocks: flora: *Palibinia* sp., *Alstonia* sp., *Carpinus* sp.; palynomorphs: *Ephedripites*; charophytes: *Charites* sp. On the basis of these fossils, these rocks are assigned an early Tertiary, Paleocene to Eocene age.

Rocks of the Gonjo basin are very similar both in facies and structural setting to nearby basins described by *Horton et al.* (2002). Paleogene fossils for these basins include mollusks (*Hippeutis* sp., *Negulus* sp., *Cinima* sp., *Bithynia* sp.), spores (*Pterisiporites* sp.), and plant fossils (*Clelmus* sp.). Interbedded volcanic rocks yielded Ar-Ar ages ranging between 51 to 37 Ma (*Spurlin et al.* (2005)). Considerably farther away (200km to the south, present coordinates), Tertiary sequences near the town of Litang include *Eucalyptus reluensis* sp. nov., *Hemiptelea paradavidii* sp. nov., *Pistacia* sp., *Banksia puryearensis* Berry, *Palibinia pinnatifida* (Reid et Chandler) Tao, *Myrica* sp., *Comptonia* sp., *Albizzia* sp., *Alstonia*? sp., *Viburnum* sp., and *Phyllites* spp.

New age control – Palynology We collected samples for palynological analysis wherever we found fine grained material that appeared to have suffered the

least amount of oxidation and had the potential for preserving organic material. Most of these samples were barren. Two samples had recoverable palynomorphs, and identifiable palynomorphs included *Momipites* sp., *Retitricolporites* sp., *Taxodiaceae/Cupressaceae* sp., *Inaperturites* sp., *Striatricolpites* sp., *Carya* sp., *Psilamonocolpites* sp., *Psilatricolpites* sp., *Tricolpites* sp., *Shizosporis* sp.. *Momipites* is common throughout the Late Eocene and Oligocene of North America; age citations for Tibet and Yunnan are vague and range from Miocene to early Tertiary. These assemblages are very permissive in terms of the possible age ranges of these rocks. The assemblages suggest fairly wet conditions: *Momipites* is a pollen form of the modern genus Engelhardtia, which is a montane genus, with some species found in mountain swamps (see appendix for further details).

New age control – isotope ages of volcanic rocks .

We sampled parts of the thick ($\sim$ 500m) section of volcanic rocks that are exposed in the more northerly parts of the basin for $^{40}Ar/^{39}Ar$ isotope analyses. Conventional mineral separation techniques were used to pick sanidine and biotite phenocrysts which were dated by laser heating of single crystals. Biotite phenocrysts yielded an average weighted age of 43.83 $\pm$ 0.27 Ma (9 crystals, MSWD = 0.84) and a total gas age age of 43.11 $\pm$ 0.35 Ma. Feldspar phenocrysts yielded an average weighted age of 43.02 $\pm$ 0.23 Ma (5 crystals, MSWD = 0.27) and a total gas age of 43.11 $\pm$ 0.35. We interpret these ages as being the age that these rocks were erupted.

2.4 Structural geology

2.4.1 Compressional structures

Overview To first order, for most of its length the Gonjo basin rocks describe a syncline, overturned to the west and bounded to its east by a series of east-dipping

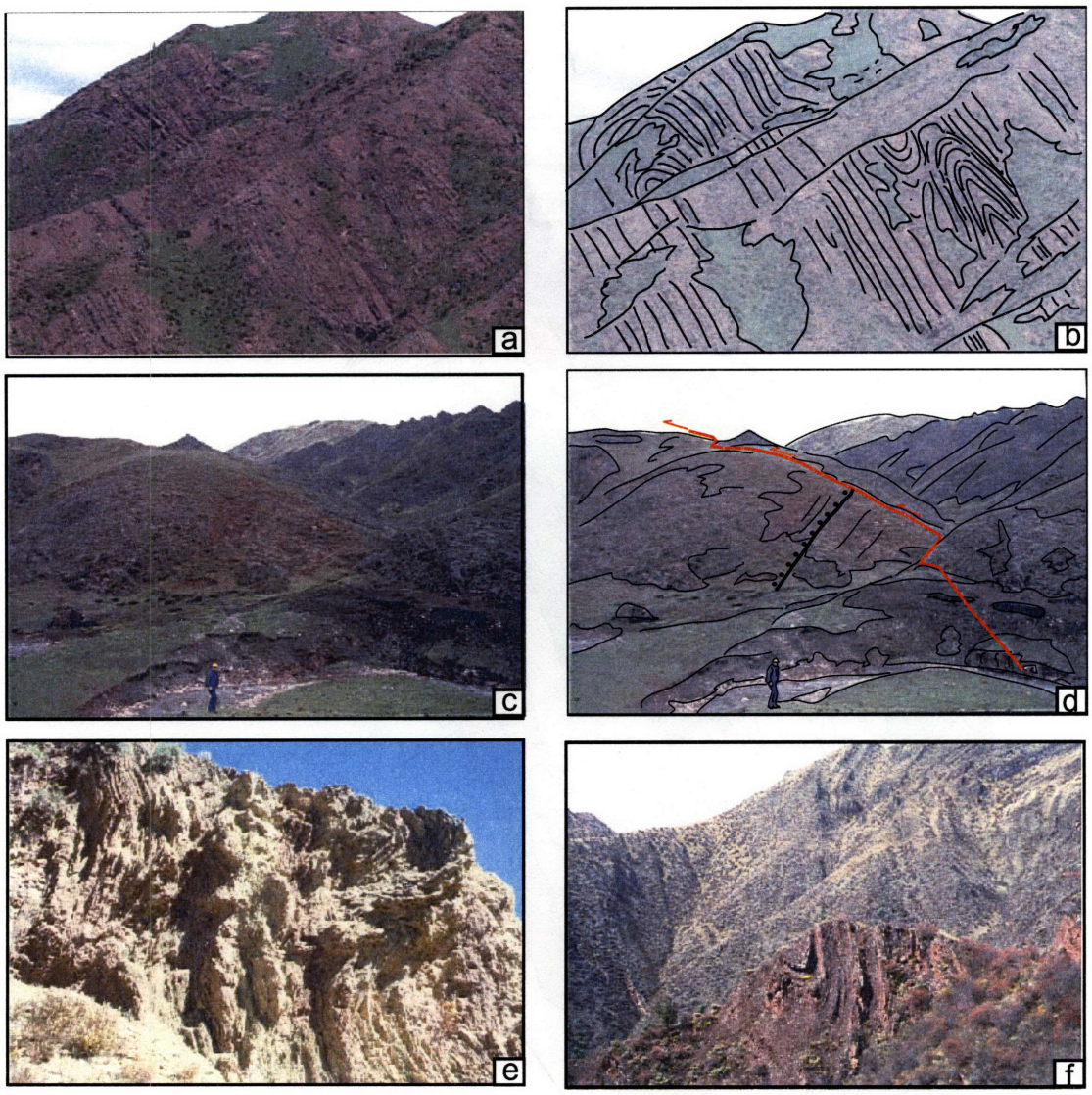

Figure 2-9: (a) and (b) Photo and line drawing of isoclinal, interfolial folds which penetratively thicken thinner, more fine grained lithologies high in the section in the axis of the basin; (c) and (d) photo and line drawing of Tertiary conglomerates in the footwall of thrusted Triassic basalts unconformably overlie the same units; (e) tight, chaotic folds of gypsiferous and carbonate bearing beds in the synclinal axis, Salt Mines area; (f) large scale overturned anticline and syncline, east boundary of Gonjo village section.

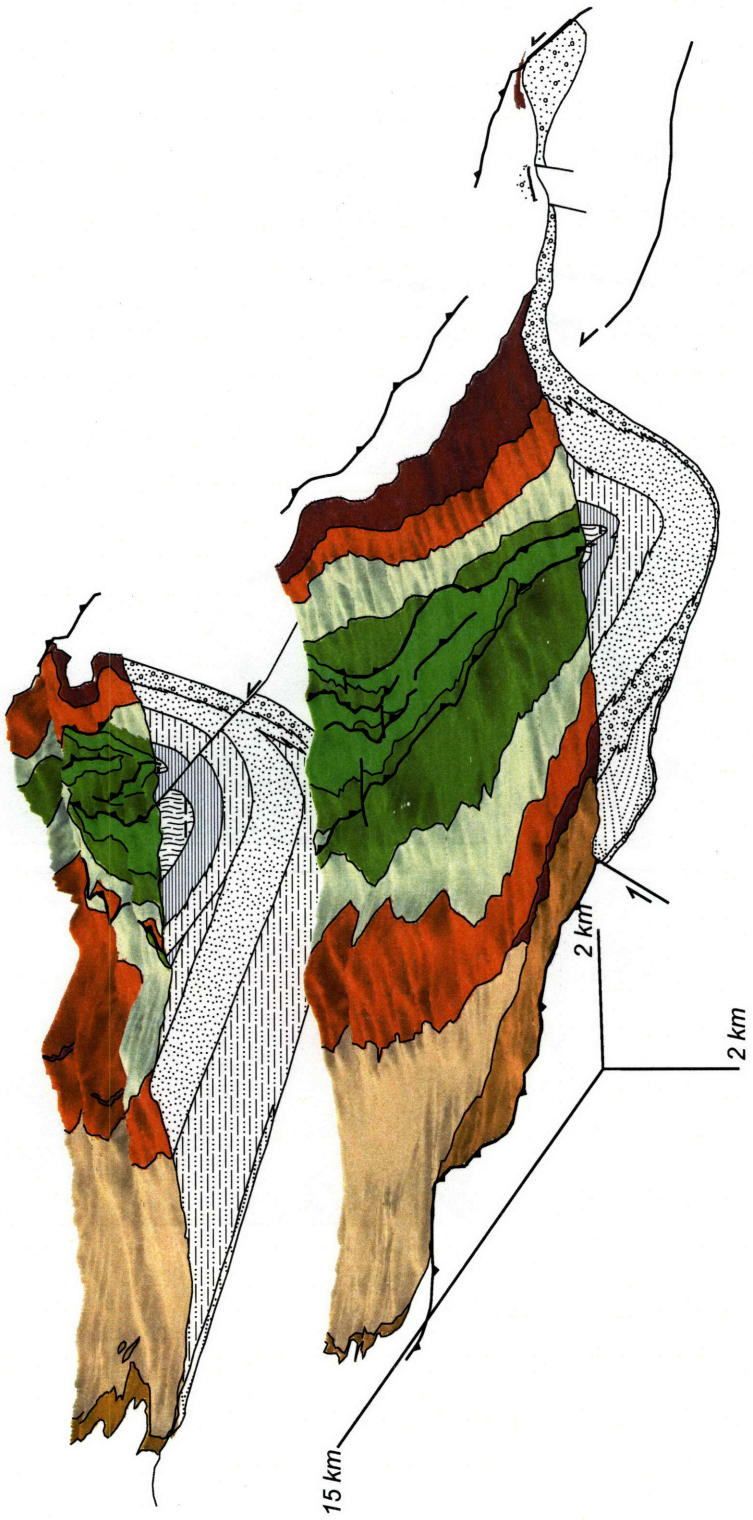

Figure 2-10: Block diagrams of the southern part of the Gonjo basin.

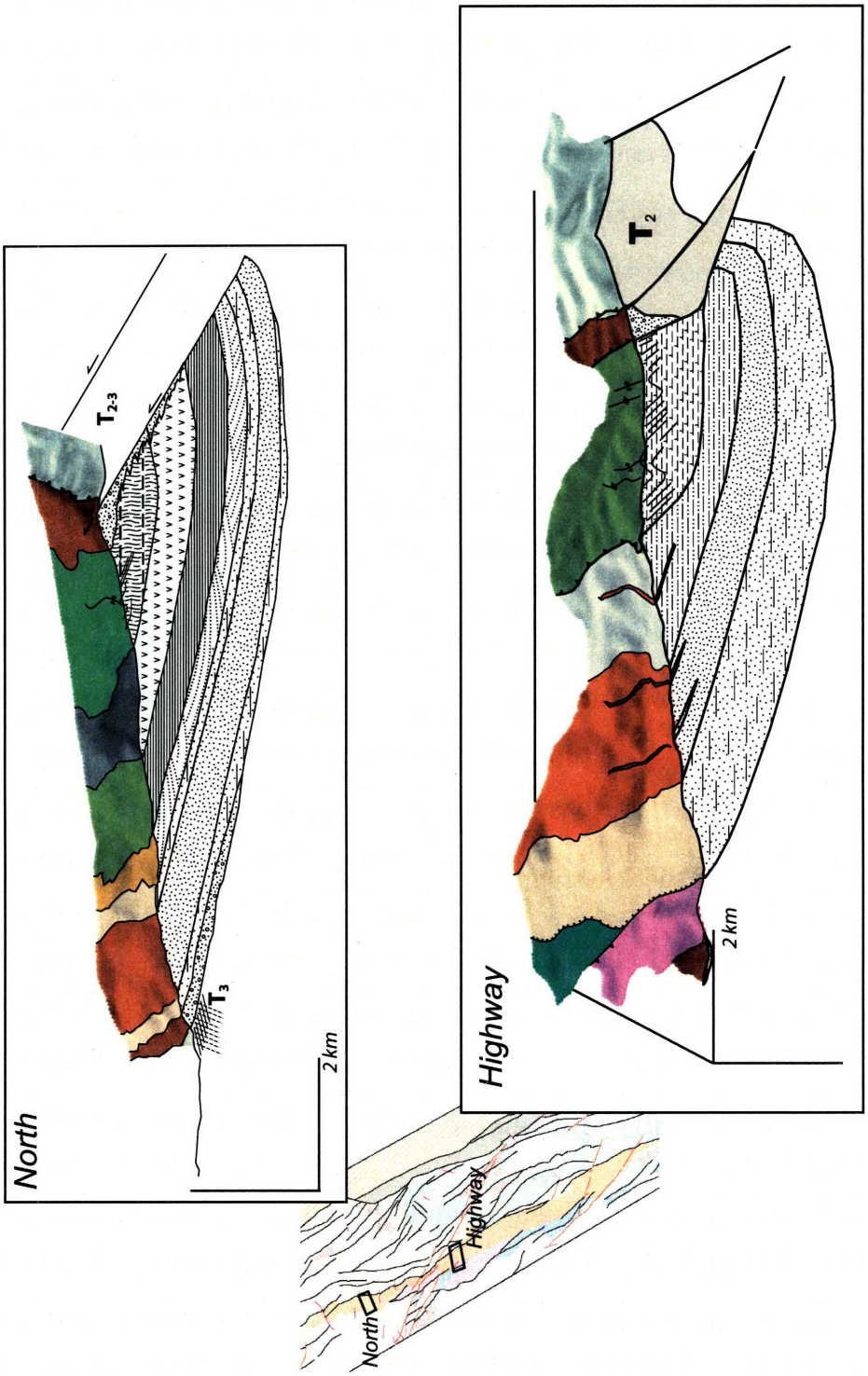

Figure 2-11: (Top) Block diagram of the highway transect, i.e. roughly the middle of the basin. Tight folds detached at a shallow levels in the core of the syncline are shown only schematically. (Bottom) Block diagram of the north section.

reverse faults carrying an antiform of basement rocks. In the Salt Mines section, the basin is bounded by a basement antiform, and reverse faults exposed farther to the north are presumably blind. From the Salt Mines section north, the syncline becomes progressively more asymmetric, and reverse faults break the bounding antiform. Displacement along the eastern bounding reverse faults appears to increase to the north and the north Gonjo section consists entirely of the lower, upright limb of the former syncline. East-verging reverse faults and associated antiforms are also seen on the west side of the basin, where they involve Paleozoic units, but west-verging structures dominate and give the basin its characteristic assymmetric, synclinal geometry.

We broadly divide the shortening structures into three systems of faults and folds. (1) the Eastern system of generally north to north-northwest striking, west verging reverse faults and associated fault-propagation folds; (2) the Western system of discontinuous north to north-northwest striking, east verging reverse faults, many of which are blind and core antiformal culminations; (3) tightly spaced thrust faults and folds that detach high up in the basin fill sequence, along the base of the lacustrine facies. All three of these systems of structures are well-expressed around and south of Gonjo village. To the north, the first set of structures dominates, and the western boundary of the basin rocks is everywhere a gently dipping unconformity.

Eastern reverse faults and related folds

For the entire length of the basin from north to south, the eastern boundary of the basin is bounded by a more or less continuous series of reverse faults and fault cored, generally asymmetric anticlines. In the Salt Mines area, a broad anticline forms the eastern margin of the basin. North of this area, this anticline is broken by a reverse fault which repeats upper Triassic rocks. The west dipping limb of the anticline thus becomes the upright limb of an asymmetric footwall syncline that defines the first order basin geometry. South of the Salt Mines east side fold, the basin boundary is

defined by a reverse fault placing Triassic rocks on the Tertiary section. Although we were not able to access these areas, existing maps show the sub-Tertiary unconformity exposed in the immediate footwall of this structure, suggesting limited stratigraphic separation and throw. At the level of Gonjo village, subvertical Tertiary rocks lie unconformably over Triassic rocks. These are overturned at the northeastern corner of the detailed map area (fig. 2-5); north of here, this fold is broken by a reverse fault presumably coring the overturned anticline. At the level of the Lhasa Highway map, the basin bounding fault places Triassic pillow basalts on Tertiary basin marginal conglomerates, but the throw on this structure is limited to a few hundred meters, because the same basalts are also exposed beneath the sub-Tertiary unconformity in the immediate footwall of the structure.

The maximum possible throw on the eastern bounding structure is along the northern part of the basin, where the pre-Tertiary unconformity is not exposed, and the bounding fault overrides east-dipping Tertiary rocks which presumably at one time formed the shallowly dipping western limb of a footwall syncline to this structures. Throw on the fault cannot be estimated based simple on stratigraphic separation between Triassic rocks on the western side of the basin (clastic rocks of unit T_3ch), and those in the hanging wall of the thrust (carbonates of unit T_3b) since pre-Tertiary shortening is unknown, and no reliable measurements of the original thicknesses of these units are available in any case (stratigraphic separation could vary from 100 meters to perhaps a kilometer and a half, based on the thickness ranges published on regional survey maps). By projecting the sub-Tertiary unconformity, the minimum amount of throw on this structure is 4 kilometers (fig. 2-11).

Shallowly detached tight folds and reverse faults

The nature of the sedimentary fill of the Gonjo basin, specifically, the apparent weakness of the finer grained rocks appears to lend itself to multiple detachment levels.

This is manifest as a small fault cored fold just northwest of Gonjo village proper, penetrative thickening of the uppermost siltstone of the Lhasa Highway section, multiple detached folds and gouge and fracture zones in the uppermost lacustrine facies of the Northern section, but most spectacularly as the train of tight, overturned folds and multiple west verging reverse fault that characterize the upper lacustrine units of the Gonjo village and Salt Mines areas. Most of these features are exposed on the western limb of the first-order basin-scale structure and consistently verge and are overturned to the west. Some of this deformation is simply the result of out-of-syncline thrust sense detachment, flexural slip and quasi-ductile accommodation in the core of the first-order syncline. At the level of the Salt Mines section, all the internal deformation of the uppermost lacustrine units (i.e. unit gL, fig. 2-10) is probably entirely detached at their base. To the north, in the Gonjo Village section, a few hundred meters of inferred separation along the easternmost internal reverse fault may be related to a splay of the main basin bounding structure (cf. fig. 2-10). Along the Lhasa Highway section, the uppermost mudstones are penetratively thickened by pervasive slip surfaces sub-parallel to bedding, meter-scale tight to isoclinal interfolial folds and tens of meter scale fault propagation folds. This shortening must be largely accommodated by a west verging thrust that involves pre-Tertiary rocks. The nearly one kilometer of shortening implied by the block diagram of the North section (fig. 2-11) is considerably greater than the limited throw of the basin-bounding reverse fault.

Western reverse fault and fault-propagation fold

Although the most striking and spectacular deformation is concentrated on the eastern side of the basin, the west side is also characterized by reverse faults and fault-propagation anticlines. West of the town of Gonjo, the western bounding structure is a broad anticline cored by Carboniferous carbonate rocks. Small, east verging reverse

faults presumably splay from the principal reverse fault that cores the broad anticline and expose Carboniferous rocks in the cores of small anticlines. Farther to the south, the previously blind reverse fault is observed to break the fold and places Carboniferous rocks over Tertiary deposits. The displacement on this structure continues to increase to the south, and at the Salt Mines section, Tertiary strata in the footwall of the reverse fault form the steeply dipping west limb of the basin scale syncline (fig. 2-10). Probably related to this is the north-south variation of the lower units of the Tertiary section. Where the west side reverse fault is blind, the lowermost unit consists of fine grained facies of unit gM1. Along the Salt Mines section, this thrust carries Carboniferous carbonates over the lower aeolian unit (gE) and is the source for the coarse alluvial gravels at the bottom of the Salt Mines west section. Notably, increased throw on the west side structure from north to south from Gonjo village to the Salt Mines section is roughly balanced by decreased throw on the east side structure (fig. 2-10).

2.4.2 Cenozoic shortening

East of the basin, Mesozoic rocks are deformed into broad, upright folds, with thinner bedded clastic rocks detached at formation contacts and folded at much tighter wavelengths. Reverse faults are generally steep, and are not associated with significant stratigraphic separation. The deepest stratigraphic levels exposed east of the Gonjo basin are granites and variably metamorphosed Paleozoic sedimentary rocks adjacent to the Jinsha suture, but even this exposure is not indicative of a significant thrust, as lower Triassic rocks rest unconformably on these rocks (fig. 2-2). The fundamental question is how much of the deformation of the rocks exposed between the Gonjo basin and the Jinsa suture is Cenozoic in age. *Reid et al.* (2005a) interpreted the relatively simple deformation of these rocks as being the product of one episode of deformation, and suggested that the age of the deformation was late Triassic to

Jurassic in age. Our mapping has found angular unconformities between Triassic rocks and the Gonjo basin fill, which requires pre-Cenozoic deformation in this area. Compressional structures deforming the Gonjo basin are clearly Cenozoic in age, but these are the only compressional structures within the area west of the Jinsha suture (fig. 2-2) that are unequivocally Cenozoic. Given the lack of multiple generations of deformation in the Triassic rocks away from Gonjo basin, Cenozoic shortening was either limited to the structures directly deforming Tertiary rocks, or was limited to tightening previously existing structures. Therefore, although we can estimate the amount that the Gonjo basin itself has been shortened (the Salt Mines area has been shortened 16 - 22%; the 8km wide Northern section is overthrust by a fault with at least 4km of horizontal displacement), lacking the ability to distinguish between Mesozoic and Cenozoic structures away from the basin, these estimates cannot be extrapolated beyond the narrow corridor within which the basin rocks are exposed.

2.4.3 Relationship between sedimentation and crustal shortening

The unconformity below the Tertiary rocks of the Gonjo basin is exposed almost everywhere along the entire length of the basin, on both west and east sides, with the exception of the northern part of the basin where west-verging reverse faults on the east completely over-ride the marginal facies of the basin. The pre-Tertiary unconformity is developed on a wide range of stratigraphic levels, from Ordovician to Upper Triassic rocks, but even where Tertiary rocks lie above Upper Triassic strata, they do so above an angular unconformity. Moreover, the pre-Tertiary unconformity also overlies a subvertical spaced cleavage developed in the clastic basement lithologies. That is, the nature of this unconformity provides clear evidence of post-late Triassic, pre-Cenozoic compressional deformation in the region. The Gonjo basin rocks are themselves deformed: most of the sedimentary sequence is a shallow to moderately

east-dipping homocline, but, as described above, the strata along the eastern side of the basin are generally steep, and thinner bedded, finer grained lithologies are often deformed by tight folds and reverse faults detaching at high stratigraphic levels. The absence of horizontal Tertiary strata requires that compressional deformation outlasted deposition of strata currently exposed at the surface.

Outcrop scale growth strata

Beyond the obvious pre- and post- early Tertiary shortening, we describe growth stratal relations that suggest that the initiation of Cenozoic shortening began concurrently with the deposition of the Gonjo basin sediment, even if it outlasted sedimentation. This consists of outcrop or hillside scale growth strata low in the sedimentary sequence related to folds and faults on the western side of the southern part of the basin, as well as basin scale patterns of unit thickness changes towards the east side structures, most clearly expressed along the Gonjo village section.

Outcrop or hillside scale growth stratal relations are exposed on the western side of the southern part of the basin. Small anticlines west of Gonjo village cored by Carboniferous limestone involve a few tens of meters of the lowermost fine grained mudrocks and sandstones of unit gM1, above which the Tertiary rocks are not deformed by this structure. East of, and upsection of the fold closure, beds show onlap relations to the nose of the fold (fig. 2-12a). This implies that this fold developed synchronously with some of the earliest deposition of the Gonjo basin rocks.

Along the Salt Mines section, aeolian sands (gE, the youngest Tertiary map unit) on the west side of the basin form the lower limb of a footwall syncline, and are overthrust by Carboniferous limestone. Immediately adjacent to the fault, these beds dip steeply to the east. Upsection, the beds become progressively less steep and units approximately 100 meters up in the section the beds are shallowly dipping and conformable with the rest of the section. The topmost bed shown in fig. 2-12, is the

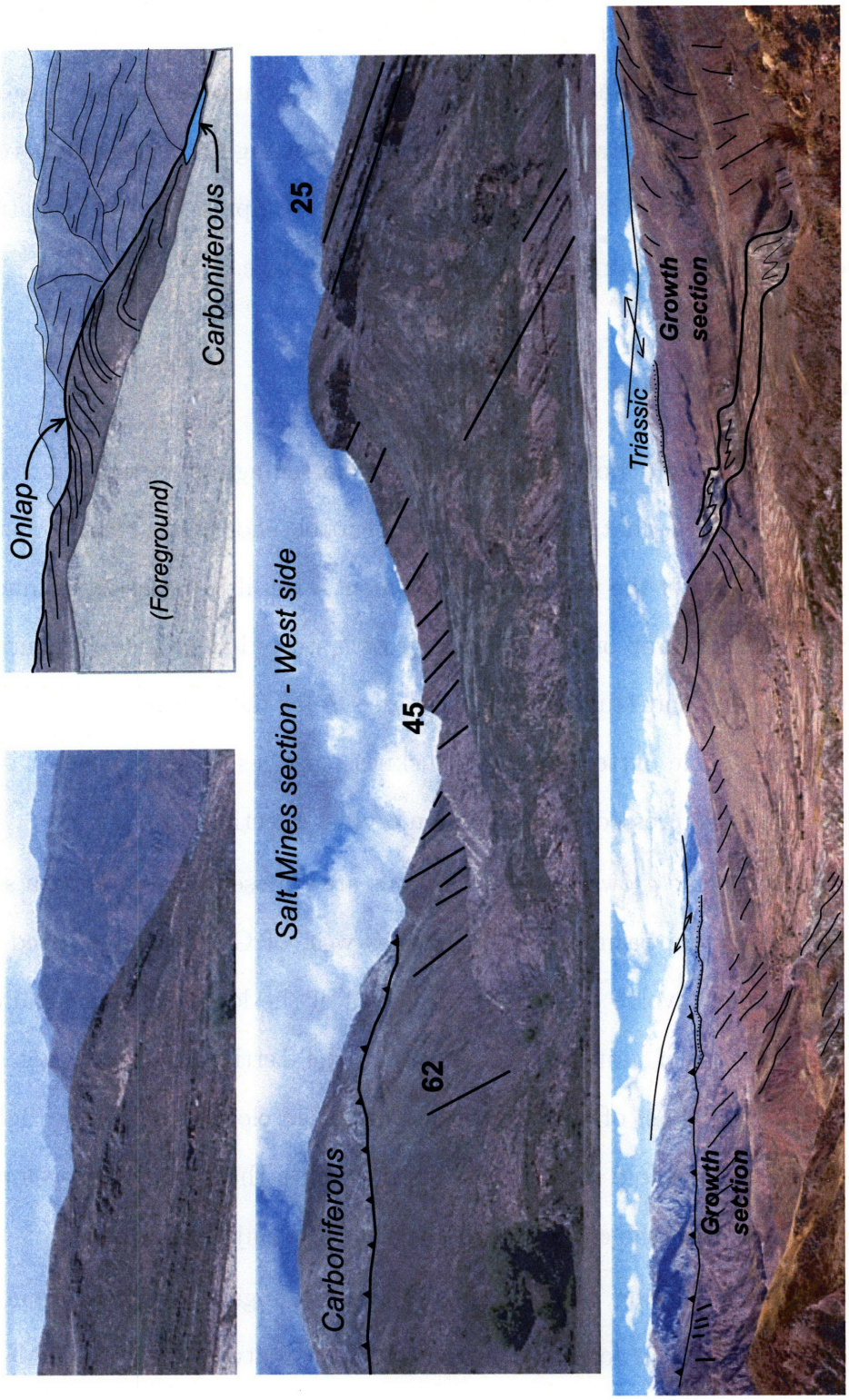

Figure 2-12: Top: onlap relations over the crest of small basement cored anticline, west of Gonjo village. Middle: Growth strata adjacent to western bounging thrust carrying Carboniferous rocks above the basal aeolian section. Prominent thick bed at the right of the photo is the first conglomerate bed, whose clasts are almost entirely derived from the Carboniferous beds. Bottom: view of the Gonjo basin, looking north from the Salt Mines area.

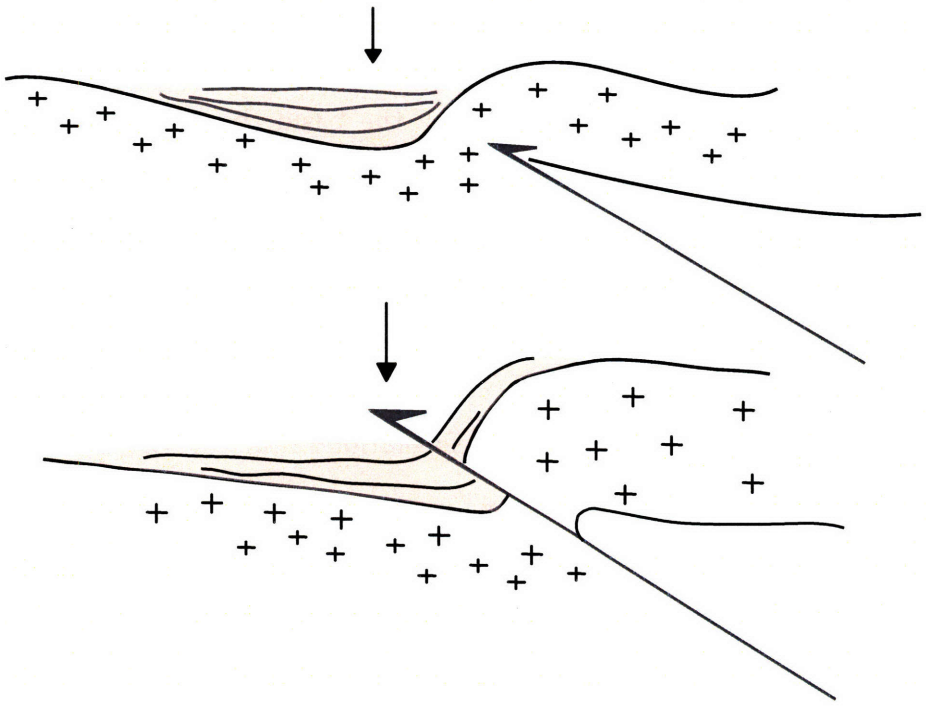

Figure 2-13: Schematic illustration of the relationship between subsidence and shortening structures in the Gonjo basin

first thick cobble conglomerate of the Salt Mines section (unit sG1). The clasts in this bed are almost exclusively derived from the Carboniferous immediately to the west.

Basin-scale growth strata and facies changes

Beyond outcrop (or hillside) scale growth stratal relations that demonstrate that the west side structures bounding the Gonjo basin in the south were active in the early stages of basin sedimentation, changes in total section thickness from west to east reflect variation in accommodation space in the asymmetric west facing syncline that defines the overall geometry of the entire basin. Basin scale accommodation space was determined by the development of the basement cored anticline to the east. The asymmetry of this large scale fold resulted in accommodation space decreasing from

the core of the syncline towards the steep limb of the basin bounding anticlinal uplift to the east (fig. 2-13). The effect of this is the significantly thicker western stratigraphic sections in the southern part of the basin (fig. 2-3). The lowermost strata of both the Gonjo village and Salt Mines sections show the greatest changes in unit thickness from west to east, and although facies variations make exact correlation imprecise, it appears that accommodation space was controlled by the east side structures early in the basin history. Propagation of the blind thrust coring the fold, steepening of the fold and detached deformation in the core of the fold outlasted sedimentation and splays of the fold-coring reverse fault carry the thinner, steepened section the much thicker gently dipping underthrust section, at least at the level of the Gonjo village section.

This geometry superficially appears to differ from the expected geometry of convergent basins. Foreland basins are commonly depicted as wedge of sediment thickening towards a basin bounding thrust (eg. *Jordan* (1995); *Beaumont et al.* (1982)). This geometry results from the simple model conditions of a flexural basin, where the orogenic load of the thrust belt is modeled as a simple linear end-load (eg. *Turcotte and Schubert* (2002)) and is a reasonable approximation for true flexural basins, whose wavelengths typically reach hundreds of kilometres. In detail, where (relative?) subsidence and accommodation space is controlled by blind faults and basement-cored folds rather than the elastic (or viscoelastic) flexure of the entire lithosphere, entirely different stratal geometries are predicted near the bounding structures (fig. 2-13). Before the blind fault breaks the surface, strata are thickest at some distance from the edge of the basin and rapidly thin towards the growth fold. After the reverse fault breaks its growth fold, however, the axis of maximal subsidence is likely to coincide with the tip line of the basin-bounding thrust as the footwall is underthrust. This second stage of growth strata may be represented by the apparent thickening of the green carbonaceous shale marker beds in the lacustrine facies at the top of the Gonjo

village section towards the axis of the basin. This two-stage model of growth stratal geometries – a growth fold stage followed by a fault controlled stage – is similar to the two-stage syn-extensional sedimentary response to the propagation of blind normal faults described in the Suez rift (*Sharp et al.* (2000); *Gawthorpe et al.* (1997)). In a perhaps analogous compressional setting, basins related to the Laramide uplifts of the western North American Cordillera commonly show many of the same stratal geometries (*Jordan* (1995); *Macqueen and Beaumont* (1989); *Jordan* (1995); *Berg* (1962)) near the bounding thrusts and reverse faults.

If the lacustrine deposits are indeed coeval with the growth faults breaking the surface, then splays of the bounding eastern faults deformed deposits in the Gonjo basin very soon after deposition. The competency contrast between carbonates and poorly lithified siltstones and claystones may explain the wild, tight folding of this sequence. The foregoing discussion suggests that (1) the narrow wavelength of the basin is not simply an artefact of preservation, since bounding structures were active from the outset of sedimentation; (2) the development of accommodation space for the Gonjo basin sediments can be explained entirely in terms of the structural relief generated during compressional deformation.

2.4.4 Strike-slip faulting

The narrow and elongate geometry of the Gonjo basin has led some (*Hou et al.* (2003); *Li* (1996) to interpret its origin as a pull-apart basin. Such a model requires strike-slip faults with traces striking parallel to the basin, a series of secondary normal faults at high angle to the strike of the basin causing subsidence, and predicts specific growth stratal patterns. Specifically, for a north-south trending pull-apart basin, units should show thickness changes in a north-south direction, and syn-tectonic sediments should strike oblique to the basin boundaries. We found no north-south variations in unit thickness that would suggest the presence of secondary structures oblique to the

main basin bounding faults and all units strike parallel to the compressional basin-bounding structures. In our mapping, we found no evidence for significant strike-slip deformation parallel to the basin on the basin-bounding faults. Furthermore, on regional geological maps (*Qinghai*), the fault defining the western boundary of the basin can be traced southward for a considerable distance, and the map relations do not provide any evidence for strike-slip motion along this structure. This fault as mapped, dips steeply ($\sim$ 60 °) to the east, and appears to be a thrust for its entire length.

Although basin-parallel strike-slip faults were not found, strike-slip faults that strike at a high angle to the basin bounding structures are common. We group these into three sets. The first consists of three major north-west striking left-lateral faults that offset basin units and the main basin bounding faults. The second is a system consisting of a large number of east striking left-lateral faults with very small amounts of slip on any one structure that is associated with the highly deformed lacustrine rocks near Gonjo village. The last set is a number of small east to north-east striking right lateral faults that affect the northern-most part of the basin. In all cases, strike-slip deformation along these structures post-dates sedimentation and shortening and some of these faults may be quite young.

Northwest striking late left-lateral faults

Three important northwest striking left-lateral faults are indicated on the large scale map of the basin (fig. 2-2). Two of these truncate the southern end of the basin and displace the main mapped eastern-bounding reverse fault. A third, the apparently largest of the three, offsets the entire basin about two-thirds the way up its length and complicates the correlation of the North Gonjo basin stratigraphic section with those mapped to the south. The southern faults are shown as dipping towards the basin rocks and having both reverse and normal separation on the regional maps.

Although poorly exposed, we were able to trace out the northernmost of the two southern faults. Where we traced the fault, it was subvertical, and we suspect that part of the apparent ambiguities on the older maps are the result of the trace of this fault being closely coincident with a pre-Cenozoic, northeast dipping fault. Based on map relations suggesting that all three of these faults offset the main basin bounding structures, as well as truncate facies trends, these faults must be younger than the shortening structures in this area. In particular, although we were not able to access the northernmost of the three northwest striking faults, we note that it is coincident with a geomorphically well-expressed lineament traceable on both DEMs and remote sensing imagery and exactly along strike with the active Litang fault to the southeast, at least raising the possibility that these structures are quite young and may have been active since Pliocene time.

Distributed left-lateral faults

High-angle faults with small offsets are ubiquitous throughout the region, but there is a particular concentration of these associated with the steeper, pervasively folded and faulted lacustrine strata in the core of the basin in the southern map area (Gonjo Village and Salt Mines areas). Commonly, sets of small (<1m) offset faults are spaced at the scale of one or two metres. These faults are predominantly subvertical (60-90°dips, mean 85°) and trend anywhere from 260-280°(mean 265°). Slickenstraie and fault cylindricity are uncommon but where present, these pitch at low angles on the fault surface (0-30°). Although dextral and sinistral senses of separation (taken to be offset, given the low angle of slickenlines and the consistency of sense of offset for the complete range of bed orientations) are observed, over 80% of faults (out of a random sample of about 65) show left-lateral offset.

These faults are most easily recognized where beds are steeper and more distinct, especially in unit L, characterized by alternating green shale, carbonate and drab red

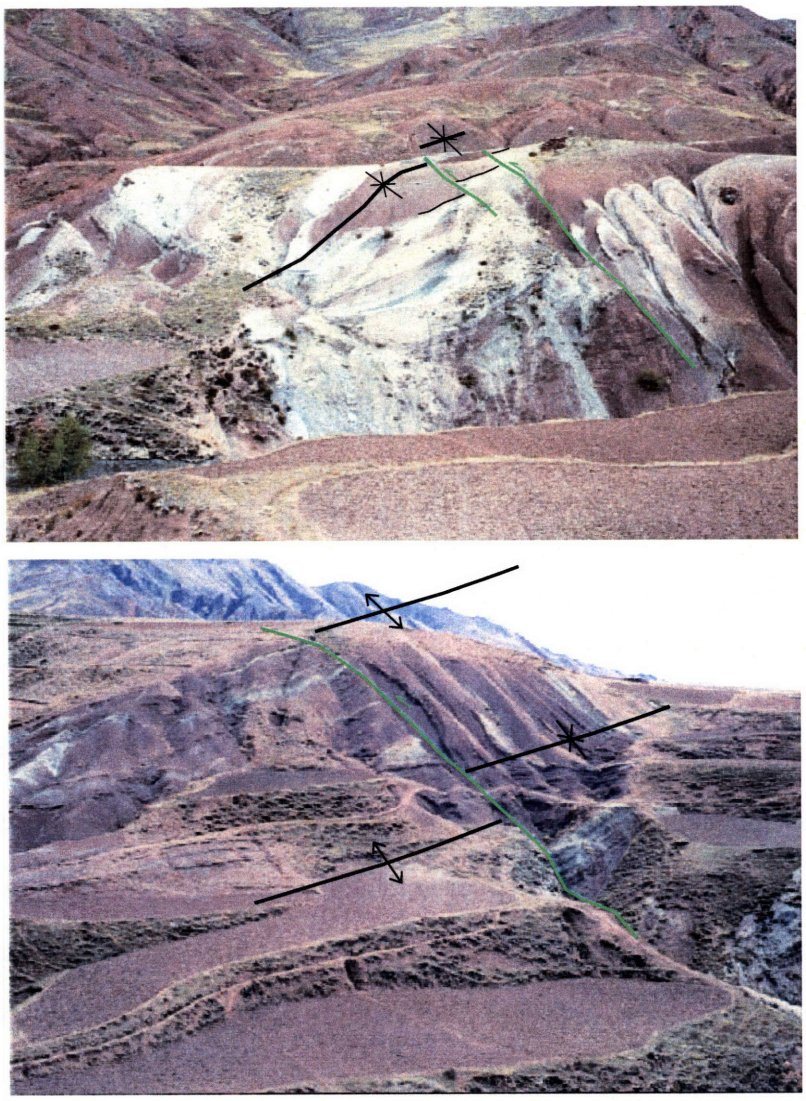

Figure 2-14: Outcrop relations show that distributed, small offset strike-slip faults offset shortening structures without modifying their geometry and therefore postdate them. Top: Syncline cut by two small left-lateral faults; Bottom: Syncline-anticline pair cut by left-lateral fault with $\sim$ 10 meters of separation.

siltstone and claystone. It is possible that the greater density of these faults in the core of the basin may reflect an observational bias. Nevertheless, the association of these faults with shallowly detached and highly deformed beds appears to be real. This may reflect a kinematic association between these strike slip faults and the numerous thrusts and folds of variable throw and wavelength. Alternatively, there may be a relationship between strain partitioning and weak and shallowly detached rocks. In detailed mapping and of individual folds and minor reverse faults that were offset by some of these faults we found neither tightening of the folds or evidence of greater throw on reverse faults across these structures.

2.5 Discussion

Structural and depositional setting The Gonjo basin reflects deposition of proximally derived continental sediments into an intermontane basin formed between thrust bounded ranges in a manner analogous to modern intermontane basins found to the northeast of the Tibetan plateau. In this respect, the Gonjo basin rocks share a similar depositional and structural setting to the other early Tertiary basins found farther to the west in the central parts of the Tibetan plateau (*Horton et al.* (2002); *Spurlin et al.* (2005); *Wang et al.* (2002); *Liu and Wang* (2001)). Like those basins, the identification of growth strata implies that sedimentation occurred in the early stages of upper crustal shortening. Despite the narrow and elongate geometry of the Gonjo basin rocks that may be taken as suggestive of strike-slip faulting during basin development, we found that strike-slip faulting definitely post-dates sedimentation and compressional deformation. The geometry of sedimentary stratal packages is furthermore inconsistent with strike-slip faulting either creating accommodation space in a releasing-bend setting, or active strike-slip faulting during sedimentation, as described in the Ridge basin of California (*Crowell* (2003)).

Cenozoic shortening *Spurlin et al.* (2005) prepared balanced cross-sections across the lower Tertiary Nanqian-Yushu and related basins and proposed that nearly 40% shortening occurred in early Cenozoic time in a region only a few tens of kilometers northwest of the northern Gonjo basin. In the region around the Gonjo basin, we find abundant evidence for pre-Tertiary shortening. Structures that may have been formed during the Mesozoic deformation identified by *Reid et al.* (2005a) are parallel to the unequivocally Cenozoic structures that directly involve the Gonjo basin rocks. Away from the Gonjo basin, Cenozoic deformation may have reactivated older structures and simply tightened pre-existing folds or reactivated pre-existing faults. As a result, we cannot constrain the amount of Cenozoic shortening of rocks between the Jinsha suture and the Gonjo basin. We do note, however, that the structural style of this region consists of broad, upright folds and reverse faults associated with limited amounts of stratigraphic separation. The shortening of the Gonjo basin itself consists of a single broad fold, and the throw on reverse faults bounding the basin on its east side is generally quite limited. In short, in order to have the upper crust shorten by as much as proposed by *Spurlin et al.* (2005) for the Nanqian-Yushu region, either most, if not all, of the deformation away from the Gonjo basin is Cenozoic, or shortening was accommodated on structures that are not exposed in this region.

Cenozoic crustal thickening At present, the region around the Gonjo basin is underlain by thick continental crust, which accounts for the high average elevations in this area. Considerable pre-Cenozoic crustal thickening cannot be discounted, given the evidence of pre-Cenozoic deformation in the form of angular unconformities between upper Triassic and the Tertiary rocks of the Gonjo basin. *Reid et al.* (2005a) considered the deformation of the Triassic rocks east of the Gonjo basin to be Cretaceous in age. Evidence of arid conditions during deposition of the Gonjo basin sediments – particularly the aeolian facies that occur at the base of the section

in south and central parts of the basin – at least raises the possibility of the basin having been located in the rain shadow of high topography.

Nevertheless, the present high elevation of the Gonjo basin cannot be completely accounted for by late Mesozoic and early Cenozoic crustal thickening accompanying upper crustal shortening. The basin is perched more than two kilometers above the elevation of the Jinsha river, but incision of the landscape is incomplete, and most of the Gonjo basin rocks are exposed upstream of knickpoints that represent the extent of river incision propagation. The timing of river incision in this area is unknown, but low-temperature thermochronology of rocks exposed at the bottoms of canyons cut by the major rivers draining the eastern margin of the plateau suggests that major incision of the plateau margin occurred in the late Miocene (*Clark et al.* (2005)). That is, there is a significant lag between the latest upper crustal shortening and river incision, which could reflect late uplift of the plateau margin without accompanying upper crustal deformation.

Tertiary rocks and structures of the Three Rivers area the distribution of early Tertiary basins of the eastern plateau margin defines an arcuate belt that is east-west trending on the central plateau and north-south trending in Yunnan province (fig. 2-1). Like the Gonjo basin and other Tertiary rocks exposed in the central plateau, they are generally found in synclinal troughs in the footwalls of reverse faults of limited throw. Both in Tibet and into Yunnan province, these basins follow the dominant structural grain. Southeast of the Gonjo basin, basin orientations reflect east-west shortening whereas crustal thicknesses and elevations decrease steadily from northwest to southeast. That is, the apparently minor upper crustal shortening is highly oblique to, and does not explain, the gradient in crustal thickness.

Strike-slip deformation We found no evidence for strike-slip motion parallel to the basin-bounding faults. In particular, we can rule out strike-slip deformation as

being a mechanism for the creation of accommodation space for the Gonjo basin sediments in a pull-apart or releasing step-over setting and stratal patterns do not support a transpressive setting during basin development. Strike-slip deformation is present in this area, and consists of east-west or northwest-southeast trending structures that definitively post-date folding and reverse faulting. We note that the orientation and shear sense of northwest-southeast faults is the same as the active Litang fault mapped to the southeast. In particular, the most prominent such fault, which crosses the basin 1/3 of the length from north to south, is almost perfectly in line with the Litang fault, and is clearly traceable on both remote sensing images and DEMs. This raises the possibility that not only do these faults post-date shortening in this area, but they may be quite young. Also interesting is the very distributed and poorly localized nature of the ubiquitous small-offset faults that deform the tightly folded and shallowly detached lacustrine sediments in the southern part of the basin. The presence of gypsum, salt and weak shale lithologies clearly accommodates the tight geometry of the folds and the detached style of deformation of these units. The apparent association of poorly localized, distributed strike-slip faulting with these rocks also suggests to us that the shallow detachment surfaces may also play a role in strain localization of strike-slip faulting.

The lack of early strike-slip affecting the rocks of the Gonjo basin has implications for the nature of strike-slip deformation regionally. Any potential major translation or rotation of the Gonjo basin rocks has to have been accommodated by faults away from the basin, and the nearest candidate is along the trace of the Jinshajiang suture, tens of kilometers to the east of the basin. That is, early translation or rotation did not occur concurrent with penetrative shear deformation. The apparent deflection of geological trends from the central Tibetan plateau and south into the Three Rivers area that suggests a wide zone of right-lateral shear is likely a young feature.

Acknowledgements

We thank John Geissman, Joel Johnson and Brandon MacElroy for careful reading editing of early versions of this paper and providing very helpful comments that significantly improved the manuscript. The first author was supported by the Fonds Pour la Recherche en Sciences et Technologies (Québec) graduate student grant. Research for this study was funded by NSF awards EAR 0003571 and EAR 8904096.

References

Akciz, S. O. (2004), Structural and geochronological constraints on the ductile deformation observed along the Gaoligong Shan and Chong Shan shear zones, Yunnan (China), Ph.D. thesis, MIT.

Beaumont, C., C. E. Keen, and R. Boutilier (1982), A comparison of foreland and rift margin sedimentary basins, *Philosophical Transactions of the Royal Society of London. Series A, Mathematical and Physical Sciences*, *305*, 295–317.

Berg, R. R. (1962), Mountain flank thrusting in Rocky Mountain foreland, *AAPG Bulletin*, *46*(11), 2019–2032.

Bird, P. (), Lateral extrusion of lower crust from under high topography, in the isostatic limit, *Journal of Geophysical Research*, *96*(B6), 10,275–10,286.

Burchfiel, B. C., Z. Chen, et al. (In prep.), Tectonostratigraphic map of eastern Tibet and Yunnan province, map and accompanying notes in preparation.

Chen, Z., B. C. Burchfiel, Y. Liu, R. W. King, L. H. Royden, W. Tang, E. Wang, J. Zhao, and X. Zhang (2000), Global positioning system measurements from eastern Tibet and their implications for India/Eurasia intercontinental deformation, *Journal of Geophysical Research*, *105*(B7), 16,215–16,228.

Clark, M. K., and L. H. Royden (2000), Topographic ooze: building the eastern margin of Tibet by lower crustal flow, *Geology*, *28*, 703–706.

Clark, M. K., L. M. Schoenbohm, L. H. Royden, K. X. Whipple, B. C. Burchfiel, X. Zhang, W. Tang, E. Wang, and L. Chen (2004), Surface uplift, tectonics, and erosion of eastern Tibet from large-scale drainage patterns, *Tectonics*, *23*, TC1006+, doi:10.1029/2002TC001402.

Clark, M. K., M. A. House, L. H. Royden, K. X. Whipple, B. C. Burchfiel, X. Zhang, and W. Tang (2005), Late Cenozoic uplift of southeastern Tibet, *Geology*, *33*(6), 525–528.

Clark, M. K., L. H. Royden, K. X. Whipple, B. C. Burchfiel, X. Zhang, and W. Tang (in review), Deformation of a regional low-relief relict lanscape (erosion surface) in eastern Tibet, *Journal of Geophysical Research - Earth Surface*.

Coward, M. P., W. S. F. Kidd, P. Yun, R. M. Shackleton, and Z. Hu (1988), The structure of the 1985 Tibet geotraverse, Lhasa to Golmud, *Philosophical Transactions of the Royal Society of London, Series A*, *327*, 307–336.

Crowell, J. C. (2003), Tectonics of the Ridge Basin region, southern California, in *Evolution of the Ridge Basin, southern California: An interplay of sedimentation and tectonics*, edited by J. C. Crowell, Geological Society of America Special Paper 367, pp. 157–203, Geological Society of America.

Dalrymple, G. B., and W. A. Duffield (), High precision ^{40}ar/^{39}ar dating of Oligocene rhyolites from the Mogollon-Datil volcanic field using a continuous laser system, *Geophysical Research Letters*, pp. 463–466.

Dewey, J., S. Cande, and W. Pitman (1989), The tectonic evolution of the India/Eurasia collision zone., *Ecolgae Geologicae Helvetiae*, *82*, 717–734.

Gawthorpe, R. L., I. R. Sharp, J. R. Underhill, and S. Gupta (1997), Linked sequence stratigraphic and structural evolution of propagating normal faults, *Geology*, *25*(9), 795–798.

Hallet, B., and P. Molnar (2001), Distorted drainage basins as markers of crustal strain east of the Himalaya, *Journal of Geophysical Research*, *106*(B7), 13,697–13,710.

Holt, W. E., N. Chamot-Rooke, X. L. Pichon, A. J. Haines, B. Shen-Tu, and J. Ren (2000), Velocity field in Asia inferred from Quaternary fault slip rates and global positioning system observations, *Journal of Geophysical Research*, *105*(B8), 19,185–19,210.

Horton, B. K., A. Yin, M. Spurlin, J. Zhou, and J. Wang (2002), Paleocene–Eocene syncontractional sedimentation in narrow, lacustrine-dominated basins of east-central Tibet, *Geological Society of America Bulletin*, *114*, 771–786.

Hou, Z., H. Ma, Z. Khin, Y. Zhang, M. Wang, Z. Wang, G. Pan, and R. Tang (2003), The Himalayan Yulong porphyry copper belt: Product of large-scale strike-slip faulting in eastern Tibet, *Economic Geology*, *98*(1), 125–145.

Jordan, T. E. (1995), Retroarc foreland and related basins, in *The Tectonics of Sedimentary Basins*, edited by C. Busby and R. Ingersoll, Blackwell Science, Cambridge, Ma.

Kapp, P., A. Yin, M. T. Harrison, and L. Ding (2005), Cretaceous–Tertiary shortening, basin development, and volcanism in central Tibet, *Geological Society of America Bulletin*, *117*(7-8), 865–878, doi:10.1130/B25595.1.

Leloup, P. H., R. Lacassin, P. Tapponnier, U. Scharer, D. Zhong, X. Liu, L. Zhang, S. Ji, and P. T. Trinh (1995), The Ailao Shan-Red River shear zone (Yunnan, China), Tertiary transform boundary of Indochina, *Tectonophysics*, *251*(1-4), 3–84, doi:10.1016/0040-1951(95)00070-4.

Leloup, P. H., N. Arnaud, R. Lacassin, J. R. Kienast, T. M. Harrison, T. T. P. Trong, A. Replumaz, and P. Tapponnier (2001), New constraints on the structure, thermochronology, and timing of the Ailao Shan-Red River shear zone, SE Asia, *Journal of Geophysical Research*, *106*(B4), 6683–6732.

Li, S., and W. D. Mooney (1998), Crustal structure of China from deep seismic sounding profiles, *Tectonophysics*, *288*(1-4), 105–113, doi:10.1016/S0040-1951(97)00287-4.

Li, T. (1996), The process and mechanism of the rise of the Qinghai-Tibet plateau, *Tectonophysics*, *260*, 45–53, doi:10.1016/0040-1951(96)00075-3.

Liu, Z., and C. Wang (2001), Facies analysis and depositional systems of Cenozoic sediments in the Hoh Xil basin, northern Tibet, *Sedimentary Geology*, *140*(3-4), 251–270, doi:10.1016/S0037-0738(00)00188-3.

Liu, Z., X. Zhao, C. Wang, S. Liu, and H. Yi (2003), Magnetostratigraphy of Tertiary sediments from the Hoh Xil basin: implications for the Cenozoic tectonic history of the Tibetan plateau, *Geophysical Journal International*, *154*(2), 233–252, doi: 10.1046/j.1365-246X.2003.01986.x.

Macqueen, H., and C. Beaumont (1989), Mechanical models of tilted block basins, *American Geophysical Union Monograph*, *48*, 65–71.

Metcalfe, I. (1998), Palaeozoic and Mesozoic geological evolution of the SE Asian region: multidisciplinary constraints and implications for biogeography, in *Biogeography and Geological Evolution of SE Asia*, edited by R. Hall and J. Holloway, pp. 25–41, Backhuys Publishers, Leiden , the Netherlands.

Metivier, F., Y. Gaudemer, P. Tapponnier, and B. Meyer (1998), Northeastward growth of the Tibet plateau deduced from balanced reconstruction of two depositional areas: The Qaidam and Hexi Corridor basins, China, *Tectonics*, *17*(6), 823–842.

Meyer, B., P. Tapponnier, L. Bourjot, F. Metivier, Y. Gaudemer, G. Peltzer, G. Shunmin, and C. Zhitai (1998), Crustal thickening in Gansu-Qinghai, lithospheric mantle subduction, and oblique, strike-slip controlled growth of the Tibet plateau, *Geophysical Journal International*, *135*(1), 1–47, doi:10.1046/j.1365-246X.1998.00567.x.

Qinghai, B. (), *Qinghai Bureau of Geology and Mineral Resources*, 1:200000 Regional Map Series, various sheets, various years.

Reid, A., C. Wilson, and S. Liu (2005a), Structural evidence for the Permian-Triassic tectonic evolution of the Yidun Arc, eastern Tibet, *Journal of Structural Geology*, *27*, 119–137, doi:10.1016/j.jsg.2004.06.011.

Reid, A. J., C. J. Wilson, D. Phillips, and S. Liu (2005b), Mesozoic cooling across the Yidun Arc, central-eastern Tibetan Plateau: A reconnaissance 40Ar/39Ar study, *Tectonophysics*, *398*(1-2), 45–66, doi:10.1016/j.tecto.2005.01.002.

Renne, P. R., C. C. Swisher, A. L. Deino, D. B. Karn, T. Owens, and D. J. DePaolo (1998), Intercalibration of standards, absolute ages and uncertainties in $^{40}Ar/^{39}Ar$ dating, *Chemical Geology*, *145*, 117–152.

Replumaz, A., and P. Tapponnier (2003), Reconstruction of the deformed collision zone between India and Asia by backward motion of lithospheric blocks, *Journal of Geophysical Research*, *108*(B6), 2285+, doi:10.1029/2001JB000661.

Rowley, D. B. (1996), Age of initiation of collision between India and Asia: A review of stratigraphic data, *Earth and Planetary Science Letters*, *145*(1-4), 1–13, doi: 10.1016/S0012-821X(96)00201-4.

Royden, L. H., B. C. Burchfiel, R. W. King, E. Wang, Z. Chen, F. Shen, and Y. Liu (1997), Surface deformation and lower crustal flow in eastern Tibet, *Science*, *276*(5313), 788–790, doi:10.1126/science.276.5313.788.

Sengor, A. M. C., and B. A. Natalin (1996), Paleotectonics of Asia: fragments of a synthesis, in *The Tectonic Evolution of Asia*, edited by A. Yin and M. Harrison, pp. 486–641, Cambridge University Press.

Sharp, I. R., R. L. Gawthorpe, J. R. Underhill, and S. Gupta (2000), Fault-propagation folding in extensional settings: Examples of structural style and synrift sedimentary response from the Suez rift, Sinai, Egypt, *Geological Society of America Bulletin*, *112*(12), 1877–1899, doi:10.1130/0016-7606(2000)112¡1877:FPFIES¿2.0.CO;2.

Shen, Z.-K., J. LÃ, M. Wang, and R. BÃrgmann (2005), Contemporary crustal deformation around the southeast borderland of the Tibetan Plateau, *Journal of Geophysical Research*, *110*, B11,409+, doi:10.1029/2004JB003421.

Spurlin, M., A. Yin, B. Horton, J. Zhou, and J. Wang (2005), Structural evolution of the Yushu–Nanqian region and its relationship to syncollisional igneous activity, east-central Tibet, *Geological Society of America Bulletin*, *117*(9-10), 1293–1317.

Tapponnier, P., G. Peltzer, R. Armijo, and P. Cobbold (1982), Propagating extrusion tectonics in asia; new insights from simple experiments with plasticine, *Geology*, *10*(12), 611–616.

Tapponnier, P., X. Zhiqin, F. Roger, B. Meyer, N. Arnaud, G. Wittlinger, and Y. Jingsui (2001), Oblique stepwise rise and growth of the Tibet plateau, *Science*, *294*(5547), 1671–1677, doi:10.1126/science.105978.

Turcotte, D., and G. Schubert (2002), *Geodynamics*, John Wiley and Sons, New York.

Wang, C., Z. Liu, H. Yi, S. Liu, and X. Zhao (2002), Tertiary crustal shortening and peneplanation in the Hoh Xil region: implications for the tectonic history of the northern Tibetan plateau, *Journal of Asian Earth Sciences*, *20*(3), 211–223, doi:10.1016/S1367-9120(01)00051-7.

Wang, E., and B. Burchfiel (1997), Interpretation of Cenozoic tectonics in the right-lateral accomodation zone between the Ailao Shan shear zone and the eastern Himalayan syntaxis, *International Geology Review*, *39*, 191–219.

Wang, E., B. Burchfiel, L. Royden, L. Chen, J. Chen, W. Li, and Z. Chen (1998), *Late Cenozoic Xianshuihe-Xiaojiang, Red River, and Dali Fault Systems of Southwestern Sichuan and Central Yunnan, China*, *GSA Special Paper*, vol. 327, Geological Society of America.

Wang, J.-H., A. Yin, T. M. Harrison, M. Grove, Y.-Q. Zhang, and G.-H. Xie (2001), A tectonic model for Cenozoic igneous activities in the eastern Indo-Asian collision zone, *Earth and Planetary Science Letters*, *188*(1-2), 123–133, doi:10.1016/S0012-821X(01)00315-6.

Xu, L., S. Rondenay, and R. D. Van der Hilst (Submitted), Velocity structure beneath southeastern Tibet from teleseismic receiver functions, submitted to Physics of Earth and Planetary Interiors.

Yin, J., J. Xu, C. Liu, and H. Li (1988), The Tibetan plateau: regional stratigraphic context and previous work, *Philosophical Transactions of the Royal Society of London, Series A*, *327*(11), 5–52.

Appendix A : Palynology

Samples that appeared to have suffered least oxidization and greatest potential preservation of organic material were selected for palynological analysis. Samples were prepared using standard sample preparation techniques including washing in distilled water and HNO_3, dissolution of carbonate and silicate minerals in HCl and HF acids, sieving and mounting on microscope slides. Sample processing was performed by PaleoLab in the Woodlands, TX. Slides and residues were shipped to Biostratigraphy.com, LLC in Garland, TX for sample analysis. Dr. O. Colmenares performed the palynological enumeration. Dr. Pierre Zippi performed the kerogen and thermal alteration analysis, and re-examined all the samples. Dr. Zippi is responsible for the age, paleoenvironment, and thermal maturation interpretations of the samples. For each sample, palynological species are listed along with the number of specimens observed. The kerogen particle types are listed in order of semi-quantitative relative abundance. The thermal alteration index (TAI) is estimated from spore color. Equivalent vitrinite reflectance values (%Ro) and maximum temperature (T°C and T°F) are estimated from TAI. Age significant taxa are used to propose possible age ranges for samples and probable paleoenvironments are interpreted from floral composition.

1E68 Zamu area

Poor preservation of the organic matter.
Barren of palynomorphs.
Kerogen: Abundant black opaque charcoal, rare dark tracheids and insoluble minerals.
TAI: Unknown; no in-situ pollen/spores observed.
Age: Unknown.
Paleoenvironment: Unknown

1E61B Zamu area

Poor preservation of the organic matter.

Count	Palynomorph
45	Momipites sp. (circular amb, triporate with simple pori, psilate)
4	Fungal spores, broken
3	Taxodiaceae/Cupressaceae spp
2	Inaperturites sp.
2	Retitricolporites sp.
1	(Salix? prolate, finely reticulate, less than 20 μm)
2	Striatricolpites sp.
1	Carya sp. (amb like Bombacaceae, finely reticulate)
1	Fragment of reticulate pollen/spore
1	Fragment of verrucate pollen/spore
1	Psilamonocolpites sp. 1
1	Psilatricolpites sp. 1 (small size, prolate)
1	Psilatricolpites sp. 2

Kerogen: Abundant black opaque charcoal, rare dark tracheids and insoluble minerals.
TAI: 3 (pollen thermally altered, substantial burial). Estimated %Ro=0.85, T°C=122
Age: Momipites is common throughout the Late Eocene and Oligocene of North America. Age citations for Tibet and Yunnan are vague and range from Miocene to Early Tertiary.
Paleoenvironment: Momipites is a pollen form-genus of the modern genus Engelhardtia (Juglandaceae). Modern species require summer rainfall, high humidity, warm winters and an almost non-seasonal climate, such as wet tropical, moist tropical, premontane wet, and premontane rain forest. Engelhardtia is a montane genus, with some species found in mountain swamps.

1E57A South Gonjo, west side

Poor preservation of the organic matter.

Count	Palynomorph
45	Indet spore? subtriangular central body? surrounded by thinner membrane
43	Indet alga? sp
3	Tricolpites (Tricolporites)? sp.
1	Bisaccate? (Pinaceae)
1	Broken Retitricolpites
1	Degraded Cicatricosisporites
1	Schizosporis sp (Zygnemataceae)

Kerogen: Abundant black opaque charcoal, rare dark tracheids and insoluble minerals.
TAI: 3 (pollen thermally altered, substantial burial). Estimated %Ro=0.85, T°C=122
Age: Unknown; similar thermal maturity to 1E61B. The two dominant taxa are not known and probably represent new species.
Paleoenvironment: Lacustrine.

1E24A South Gonjo basin, east of salt mines

Poor preservation of the organic matter.

Count	Palynomorph
85	Calamospora sp (thin wall, folded faint trilete)
75	Calamospora sp. cf. C. tangpuensis Qian, Zhao et Wu 1983
42	cf. Piceaepollenites sp.
18	Deltoidospora sp. (triangular amb, psilate)
8	Dictyophyllidites sp. cf. D. harrisi Couper 1958
8	Protoconiferous sp. cf. P. phylloides (Qiam et Wuan) Hua 1986
6	Broken trilete spores
6	Todisporites sp. cf. T. major Couper 1950
4	Deltoidospora sp. (triangular amb, slightly granulate)
4	Inaperturopollenites sp.
4	Tetrads
3	Cycadopites spp
2	Alisporites? sp.
2	Cyathidites sp.
2	Lophotriletes sp. 2
2	Retitriletes sp.
2	Taxodiaceaepollenites hiatus
1	Cyathidites sp. cf. C. australis Couper 1953
1	Exesipollenites? Sp.
1	Fungal filament?
1	Fungal spores (broken)
1	Lophotriletes sp. cf. L. delicatus Ouyang et Li 1980
1	Glomus (mycorrhizal fungi) recent contamination?

Kerogen: Abundant black opaque charcoal, rare dark tracheids and insoluble minerals.
TAI: 2+ to 3- (pollen thermally altered, substantial burial). Estimated %Ro=0.70, T°C=107
Age: The presence of Glomus spp canbe interpreted two ways: 1) the specimen is contamination from plant roots penetrating the outcrop sample; 2) the specimen is in-situ and the age is sub-Recent, probably Quaternary, with the older, darker fossils reworked from Early Mesozoic coals. Calamospora tangpuensis is known only from the Late Triassic of coal-bearing strata of Hunan (Xiang) and Jiangxi (Gan) District (Qian, Zhao and Wu 1983). Lophotriletes delicatus was reported

from the Late Permian (Ouyang and Li 1980), however, the age of the host-coal was latter re-interpreted as Early Triassic (Mao et al 1984). Although these ages are in close agreement, both taxa were not assigned directly to the original species (i.e. "cf" the Latin abbreviation for compare with). The ages of the remainder of the assemblage are all long-ranging, but consistent with a Triassic or Early Mesozoic. The absence of angiosperm pollen also helps to restrict this age of this sample to Jurassic or older.
Paleoenvironment: Fluvial/paludal, wet forest? Palynology of field samples from the Gonjo basin, Eastern Tibet and Lijiang area, Yunnan, China.

1E22A Gonjo village section

Barren of palynomorphs.
Kerogen: Abundant dark tracheids and black charcoal/coal.
TAI: Unknown; no in-situ pollen/spores observed.
Age: Unknown.
Paleoenvironment: Unknown

1E21A Gonjo, East margin

Poor preservation of the organic matter.

Count	Palynomorph
1	Glomus spp (contamination?)
1	Betula (contamination?)

Kerogen: Abundant black charcoal/coal and rare dark tracheids.
TAI: Unknown; no in-situ pollen/spores observed
Age: Unknown
Paleoenvironment: Unknown

1E19C Gonjo, Zamu area

Barren of palynomorphs.
Kerogen: Abundant black charcoal/coal and insoluble minerals.
TAI: Unknown; no in-situ pollen/spores observed
Age: Unknown.
Paleoenvironment: Unknown

Appendix B: $^{40}Ar/^{39}Ar$ geochronology

Ages for volcanic rocks exposed in the northern part of the Gonjo basin were determined by dating feldspar and biotite phenocrysts extracted from the groundmass. Samples prepared using standard mineral separation techniques. Samples were coarsely crushed, and sieved. Biotite, muscovite and K-feldspar minerals were separated using electomagnetic techniques, heavy liquids and hand-picking. Feldspar concentrates were ultrasonically etched c. 10% HF acid for 5-7 mins. All concentrates were further cleaned in ultrasonically with distilled water and ethanol, re-sieved, and re-picked to approximately 99% purity.

The final separates were in copper foil and irradiated in the McMaster University reactor, Canada without Cd-shielding. Argon was extracted from the irradiated samples by single crystal laser-fusion with an Ar-ion laser, and measured using a MAP 215-50 rare gas mass spectrometer equipped with a Johnson MM-1 electron multiplier operated at a gain of c. 10,000. Values for the irradiation parameter J were determined relative to 28.34 Ma for co-irradiated Taylor Creek sanidine (*Dalrymple and Duffield*; *Renne et al.* (1998)), and is known to better than 0.25% (1σ) for all samples. Corrections for interfering reactions were 0.000672 for 39Ar/37Ar(Ca), 0.000280 for 36Ar/37Ar(Ca), and 0.025 for 40Ar/39Ar(K).

$^{40}Ar/^{39}Ar$ model ages for each gas extraction step were calculated assuming an initial $^{40}Ar/^{39}Ar$ value of 295.5 and are assigned a 2σ uncertainty that reflects propagated analytical errors and the reactor flux monitor J. Total-fusion results are reported as a weighted mean age of all crystals fused, calculated using the inverse of the variance as the weighting factor.

Incremental Heating		36Ar(a)	37Ar(ca)	38Ar(cl)	39Ar(k)	40Ar(r)	Age ± 1σ (Ma)	40Ar(r) (%)	39Ar(k) (%)	K/Ca ± 1σ
4A028@4 42.00 W		0.00007	0.01146	0.00000	0.00475	0.12110	44.13 ± 2.09	85.25	7.16	0.203 ± 0.006
4A028@4 43.00 W		0.00027	0.01166	0.00000	0.00465	0.11879	44.28 ± 2.43	59.96	7.00	0.195 ± 0.006
4A028@4 44.00 W		0.00007	0.01375	0.00000	0.00522	0.13051	43.28 ± 1.70	87.12	7.87	0.186 ± 0.005
4A028@4 45.00 W		0.00003	0.00010	0.00006	0.04628	1.14894	43.02 ± 0.21	99.26	69.69	232.926 ± 462.133
4A028@4 46.00 W		0.00055	0.01200	0.00004	0.00551	0.13293	41.82 ± 1.70	44.92	8.30	0.225 ± 0.006

Information on Analysis		Results	40(r)/39(k) ± 1σ	Age ± 1σ (Ma)	MSWD	39Ar(k) (%,n)	K/Ca ± 1σ
Sample	ZEC-84						
Material	Feldspar (single xl)	**Weighted Plateau**	24.8287 ± 0.1181 ± 0.48%	43.02 ± 0.23 ± 0.53%	0.27	100.00	0.201 ± 0.007
				External Error ± 0.23	1.06	5 Statistical T ratio	
				Analytical Error ± 0.20	1.0000	Error Magnification	
Irradiation	cl149-	**Total Fusion Age**	24.8780 ± 0.1936 ± 0.78%	43.11 ± 0.35 ± 0.81%		5	0.665 ± 0.008
J-value	0.000972			External Error ± 0.35			
Standard	28.34			Analytical Error ± 0.33			

Figure 2-15: Data table for $^{40}Ar/^{39}Ar$ geochronology of feldspar phenocrysts in volcanic rocks of the northern Gonjo basin

Incremental Heating		36Ar(a)	37Ar(ca)	38Ar(cl)	39Ar(k)	40Ar(r)	Age ± 2σ (Ma)	40Ar(r) (%)	39Ar(k) (%)	K/Ca ± 2σ
4A028@5(	58.00 W	0.00049	0.00027	0.00011	0.03442	0.86025	43.30 ± 0.61	85.70	10.07	63.285 ± 116.828
4A028@6(	60.00 W	0.00022	0.00018	0.00010	0.02237	0.56053	43.40 ± 0.93	89.76	6.54	60.095 ± 168.481
4A028@5(	54.00 W	0.00025	0.00216	0.00015	0.05136	1.29571	43.71 ± 0.42	94.53	15.02	11.660 ± 2.321
4A028@5(	57.00 W	0.00012	0.00061	0.00011	0.03311	0.83650	43.76 ± 0.57	95.85	9.69	26.525 ± 22.084
4A028@5(	51.00 W	0.00022	0.00042	0.00015	0.04700	1.18901	43.82 ± 0.39	94.80	13.75	55.490 ± 61.318
4A028@5(	53.00 W	0.00024	0.00154	0.00016	0.05361	1.35868	43.90 ± 0.35	95.02	15.68	17.052 ± 4.561
4A028@5(	52.00 W	0.00086	0.00012	0.00013	0.03668	0.93064	43.95 ± 0.58	78.53	10.73	150.275 ± 587.295
4A028@5(	56.00 W	0.00009	0.00000	0.00011	0.03841	0.97811	44.12 ± 0.51	97.35	11.23	0.000 ± 0.000
4A028@5(	59.00 W	0.00010	0.00434	0.00014	0.02490	0.63682	44.30 ± 0.95	95.50	7.28	2.808 ± 0.335

Information on Analysis	
Sample	ZEC-82
Material	Biotite (single xl)
Irradiation	cl149-
J-value	0.000972
Standard	28.02

Results		40(r)/39(k) ± 2σ	Age ± 2σ (Ma)	MSWD	39Ar(k) (%,n)	K/Ca ± 2σ
Weighted Plateau		25.2962 ± 0.0989 ± 0.39%	43.82 ± 0.27 ± 0.63%	0.84	100.00 9	2.574 ± 0.350
			External Error ± 0.27	2.31	Statistical T ratio	
			Analytical Error ± 0.17	1.0000	Error Magnification	
Total Fusion Age		25.2914 ± 0.1055 ± 0.42%	43.81 ± 0.28 ± 0.64%		9	17.380 ± 2.576
			External Error ± 0.28			
			Analytical Error ± 0.18			

Figure 2-16: Data table for $^{40}Ar/^{39}Ar$ geochronology of biotite phenocrysts in volcanic rocks of the northern Gonjo basin

Chapter 3

Structural and tectonic evolution of the First Bend of the Yangzi River region, Western Yunnan, China

Christopher Studnicki-Gizbert
Yizhao Wang
B. Clark Burchfiel
Liangzhong Chen

Abstract

We outline structural relationships and the tectonic evolution of rocks in the region around the First Bend of the Jinsha (Yangzi) river in western Yunnan (near 27N, 100E). Here, Cenozoic deformation related to the on-going collision between India and Asia is superimposed upon an earlier complex deformational history. We describe fabric relationships in schists and phyllites of the Shigu formation and rocks exposed in the core of the Yulong mountains and their relationships to early Tertiary sediments and active deformation. The Shigu Formation rocks show evidence for four generations of deformation and are unconformably overlain by broadly warped and tilted Tertiary redbeds of the upper Jianchuan basin. In the Yulong mountains, active normal faults bound a sequence of metamorphic rocks which have suffered an analogous history of superposed deformation. Middle Triassic metamorphism and folding related to deformation along the Jinshajiang suture zone was followed by late Mesozoic west-directed fold and thrust nappes that are responsible for the dominant fabrics in this region. Early Tertiary deformation involved apparently discrete reverse faults with limited throw, ruling out any major contribution in the Cenozoic to crustal thickening in this region. The currently active tectonic regime probably began no earlier than the middle or late Pliocene and consists of a transtensional network of normal and left-normal faults. The most dramatic manifestation of this deformation is the anomalously high Yulong mountains. Here, a closed network of normal faults bounds an antiformal structural culmination that exposes some of the deeper structural levels of the region.

3.1 Introduction

Northwest of Lijiang, Yunnan, the Jinsha (Yangzi) river makes the first of its unusual, hairpin bends as it flows from the high Tibetan plateau through to Sichuan and central China. The region around this bend (which we simply refer to as "the First Bend") is notable as it is near the intersection of several first-order geological and tectonic boundaries of the eastern margin of the plateau, and exposes a variety of different structural and stratigraphic levels in a small geographic area. In this area, the quality of bedrock exposure and access is considerably better than in most of Yunnan province, and geological mapping reveals a long, complex tectonic history in the rocks of the eastern margin of the Tibetan plateau that has heretofore been largely undescribed in the English language literature. These rocks are sometimes

described as being part of the "South China foldbelt"– which is an imprecise term that is applied to deformed rocks of South China paleogeographic affinity, regardless of the age or setting of their deformation (cf. *Wang et al.* (1998) for a discussion).

The eastern margin of the Tibetan plateau is characterized by a complex collage of geological units, whose paleogeographic affinities and tectonic histories are poorly known. Unraveling some of these complexities is of first-order importance for Tibetan tectonics for at least two reasons. First, distinguishing Cenozoic from older structures is a necessary first step towards being able to characterize the contribution made by collision of India with Asia to crustal deformation and thickening here. Second, being able to precisely locate first-order geological boundaries is crucial to reconstructing the early Cenozoic history of this area, which may have been dominated by significant terrane motions (eg. *Replumaz and Tapponnier* (2003). Previous work has mostly focussed either on the active deformation (*Wang et al.* (1998); *Chen et al.* (2000); *He and Tsukuda* (2003); *Socquet and Pubellier* (2004)) or on the relatively high grade Cenozoic shear zones, such as the Ailao Shan (*Leloup et al.* (1995, 2001)), Chongshan and Gaoligong Shan (*Akciz* (2004)). In this paper, we outline the structural relationships and tectonic evolution of rocks with South China affinity in this region from early Mesozoic metamorphism through early Tertiary compressional deformation to active transtensional tectonics. We seek to place time brackets on fabrics and structures and attempt to disentangle Cenozoic deformation from the older history.

Some of the deepest structural levels of the South China fold belt – or, rather, deformed rocks of South China affinity exposed along the eastern margin of the Tibetan plateau – are exposed in the region around the First Bend. Near the first bend, garnet-muscovite-biotite schists of the Shigu Formation grade into chlorite grade rocks and these are themselves juxtaposed against unmetamorphosed South China (Yangzi platform) units. Farther to the east, the transition between rocks penetratively strained and multiply deformed at low metamorphic grades and the upper crustal fold-thrust

belt deformational style characteristic of the deformation exposed in most of the rest of South China (*Wang et al.* (1998); *Hsu et al.* (1988)). A unique perspective on the relationship between the two deformational styles is provided by the geology of the Yulong Xueshan ("Jade Dragon Snow Mountains"), the subject of a reconnaisance tectonic study by *Lacassin et al.* (1996). This small, isolated mountain range is characterized by anomalously high elevations (up to 5500m), is bounded by active normal faults and is bisected by the Jinsha river, which has carved a nearly 4 km deep canyon through the heart of the range. Within this range, the polydeformed Paleozoic section is juxtaposed against unmetamorphosed low-grade upper Paleozoic and lower Mesozoic rocks.

In this paper, we exploit the variety of structural levels exposed in the First Bend region in order to disentangle the long and complex tectonic history of these rocks and thereby begin to address first-order questions about the tectonic development of the eastern margin of the Tibetan plateau, including: How old are the dominant fabrics and structures in these rocks? What was the extent and style of early Cenozoic deformation and shortening? What effects might the pre-Cenozoic tectonics of this region have had on the extent and style of Tertiary or active tectonics? We begin by first outlining the general geological context of the region. We describe the major geological provinces, their boundaries and the major deformational events at a regional scale from Mesozoic assembly through to young and active tectonics. We then describe the structural and geological relationships we observed in the First Bend region, beginning with early Cenozoic structures and then describing and interpreting fabric relations in metamorphic rocks exposed in this region. We then outline a tectonic interpretation that emphasizes the importance of a previously unrecognized late Mesozoic episode of compressional deformation.

3.2 Regional geologic context

Major geological boundaries in the First Bend region are somewhat imprecisely located, and the nomenclature of the various recognized tectonic elements or provinces is far from established. Figure 5.2 shows the distribution of major geological untis and our interpretation of their boundaries based on the compilation of 1:200K geological survey maps (*BGMR Yunnan* (1990); *Burchfiel et al.* (In prep.)). The First Bend region comprises part of what is sometimes referred to as the Yunling Collage ((*Wang et al.*, 1998; *Hughes et al.*, 2002)). To the north are the Three Rivers fold belt and Yidun arc, which extend southward from the eastern Tibetan Plateau. The Lanping-Simao consists of geological units to the southwest. Much of the initial juxtaposition of these units is thought to have occurred in early Mesozoic time (*Metcalfe* (1998); *Sengor and Natalin* (1996)), but Cenozoic deformation – notably possibly large translations along strike slip faults localized on older terrane boundaries (eg., *Leloup et al.* (1995, 2001); *Akciz* (2004)) has modified and obscured the original relationships. Correlation of sutures recognized on the Tibetan plateau (eg. the Jinsha suture) with boundaries in Yunnan is the subject of some debate (eg. *Metcalfe* (1998) and *Roger et al.* (2003)). In this region, the Jinsha-Benzilan suture is the contact between the deepest levels of the South China block with rocks of Lanping-Simao-Qiangtang affinity (*Metcalfe* (1998)), and is here overlapped and stitched by upper Triassic sediments and granites respectively (*BGMR Yunnan* (1990)). These rocks are themselves unconformably overlain by the weakly deformed Tertiary rocks of the Jianchuan basin.

3.2.1 Three Rivers Fold belt

The Three Rivers fold belt is named after the Jinsha (Yangzi), Lancang (Mekong) and Nu (Salween) rivers, which flow almost parallel for nearly 1000km from the north of

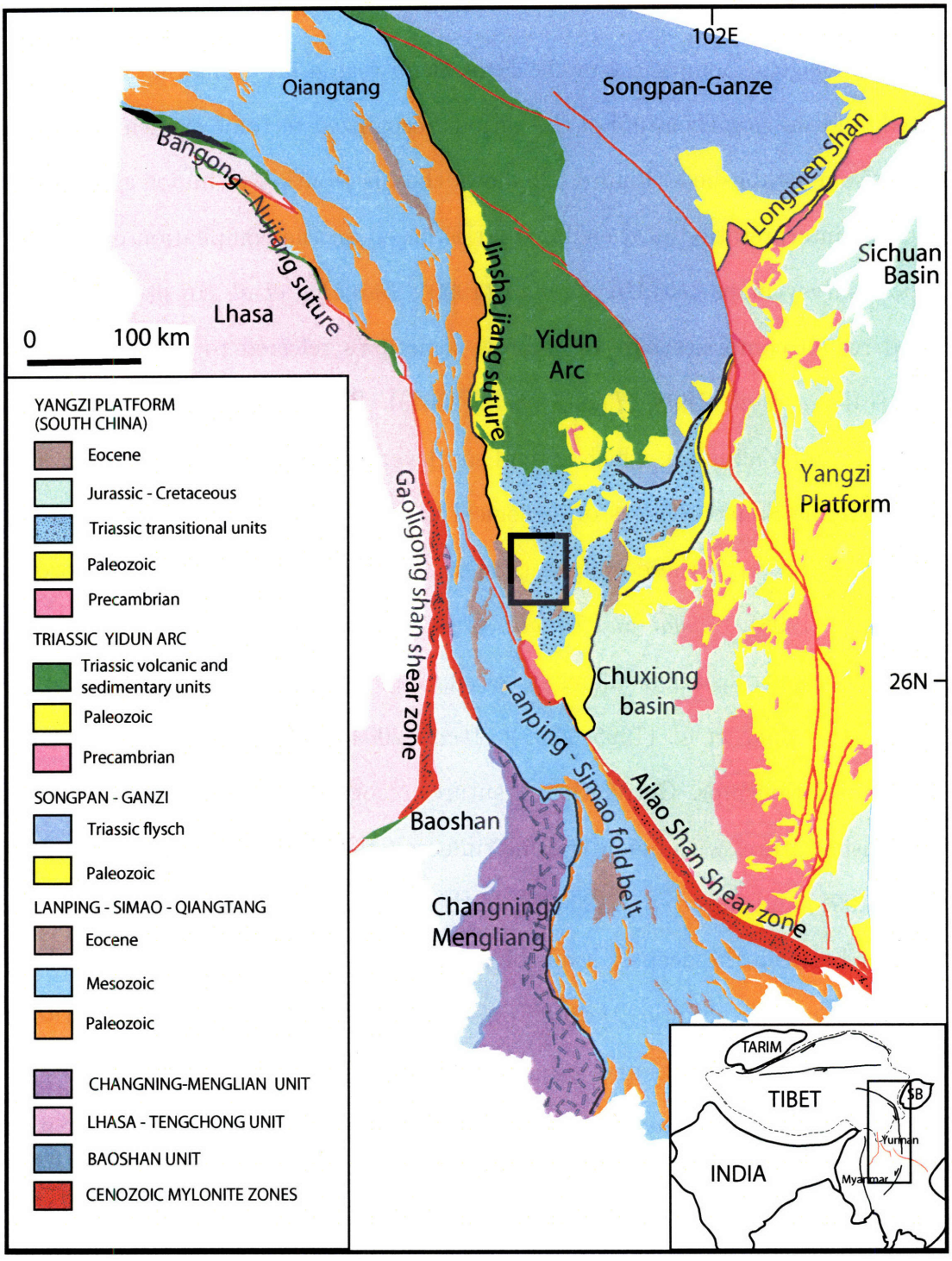

Figure 3-1: Main geologic provinces of Eastern Tibet and Southwest China. Box shows location of study area, and location of figure 3.5. Thin red lines represent active faults; for a complete map of active structures, see figure 5.2.2.

the Eastern Himalayan Syntaxis to near the Yulong mountains. The close parallelism of these major continental rivers and the lack of well-developed tributaries along their extremely straight and parallel courses has led *Hallet and Molnar* (2001) to speculate that these rivers represent strain markers in a broad zone of right-lateral shear that accommodates the northward motion of the Eastern Himalayan syntaxis into Asia. The interpretation of this area as a wide shear zone is a fairly old one, and is suggested by the apparent rotation of dominantly E-W geological trends of the Tibetan plateau into north-south orientations in the Three Rivers region (*Dewey et al.* (1989); *England and Molnar* (1990)). In particular, the Qiangtang block of the Tibetan plateau appears to have suffered the brunt of this deformation: beyond the rotation of faults and contacts into N-S orientations, the Qiangtang narrows considerably from hundreds of kilometers in Central Tibet to tens of kilometers in the Three Rivers region. South of the active Zhongdian fault, Qiangtang rocks merge into Lanping-Simao rocks, with which they are likely correlated (figs. 5.2,5.2.2). The interpretation of this region as a broad shear zone depends on the contiguity of geological markers and the correlation between Qiangtang and Lanping-Simao. In particular, the various sutures joining units in Tibet (eg. the Bangong-Nujiang and Jinshajiang sutures) can be correlated with major sutures or shear zones in Yunnan. Compilations of Chinese geological survey maps, together with field checking (B. C. Burchfiel and Z. Chen, map and ms. in prep), furthermore suggest that there are a number of distinct packages of rocks that might be followed from the plateau, through the zone of strong deformation of the Three Rivers fold belt and into Yunnan. It is, however, unclear what mechanisms (e.g. uniform simple shear or semi-distributed faulting and block rotation) or structures might be responsible for the apparent right-lateral deflection and attenuation of geological trends. Finally, the timing of this deformation is unclear, although the contiguity of geological markers suggests that it must post-date any lateral extrusion of large terranes (eg. *Leloup et al.* (1995, 2001);

Replumaz and Tapponnier (2003)).

East of the Jinshajiang suture, Triassic and older rocks in the Three Rivers fold belt are commonly metamorphosed to low (chlorite–sericite) grade, show multiple fabric generations, and are generally strongly deformed with a characteristically strong stretching lineation and/or prominent crenulation lineation. Locally, metamorphic grade is higher, and is characterized by biotite-muscovite-garnet assemblages and deformed syn-metamorphic leucogranites (*Reid et al.* (2005a)). Multiple deformations and high strain complicate the interpretation of the affinities of even low-grade rocks within this belt. Paleozoic units can be correlated with the South China (Yangzi platform) stratigraphy, with the Permian Emei Shan basalts, in particular, as a prominent and distinctive marker unit. The Mesozoic stratigraphy is less clear, as units related to the Yidun arc and arc-related basins grade into and interfinger with the Triassic stratigraphy of South China.

3.2.2 Yidun Arc

The Yidun Arc primarily consists of large Triassic granitoid plutons in Eastern Tibet, associated volcanic and volcaniclastic rocks and former forearc or backarc sequences (*Reid et al.* (2005a,b); *Wang and Burchfiel* (2000); *BGMR Yunnan* (1990)). The latter rocks are typically strongly and multiply deformed chlorite phyllites, intercalated with marbles and metavolcanics, isolated mafic or ultramafic blocks and local exposures of Paleozoic rocks. This series of rocks is well-exposed along the western boundary of the Yidun arc, and is interpreted as a melange unit that represents the location of the Jinshajiang suture in this region. The suture zone rocks extend from the active Ganzi fault on the Tibetan plateau to where they are overlain by Eocene rocks of the upper Jianchuan basin just west of the present study area. North of the First Bend region, near the town of Litang, metamorphic grade drops moving east away from the suture, and Triassic volcanogenic and arc-marginal basin rocks lack

cleavage and show good preservation of both fossils and primary sedimentary and volcanic structures.

South of where the arc plutons are exposed – i.e. the Yidun arc proper – in the vicinity of the First Bend region, upper Triassic rocks are part of a transitional unit: these rocks contain interfingering deep-water and near-shore or terrestrial sequences with local volcanogenic deposits. This represents a widely exposed "transitional" sequence between the flysch-like facies of the Yidun arc and its related basins and the Songpan-Ganzi basin and littoral Yangzi platform sequences (fig. 5.2).

3.2.3 Lanping-Simao Fold Belt

The Lanping-Simao fold belt is dominated by terrestrial red beds of mainly Jurassic to early Tertiary age. Age control in these poorly exposed red beds is poor; it generally consists of palynological or floral assemblages, with rare vertebrate fossils providing the most solid age control (*BGMR Yunnan* (1990)). Furthermore, this area is heavily cultivated or forested, is deeply weathered and generally characterized by extremely poor exposure (generally, just roadcuts). Apart from the redbeds, exposures of Paleozoic to early Mesozoic rocks are present along the western and eastern edges of the terrane and in small isolated areas within the belt. Isolated patches of coal-bearing Pliocene sediments are locally preserved. These rocks have suffered significant non-rigid deformation in Cenozoic time, including considerable clockwise rotation of small scale fault bounded blocks (*Wang and Burchfiel* (1997); *Sato et al.* (2001); *Geissman et al.* (2001); *Geissman et al.* (submitted)). With the exception of the Pliocene sediments (and the uppermost Tertiary rocks, which are only broadly folded), Lanping-Simao rocks are generally deformed by reverse faults, small strike-slip faults and upright folds. Most structural features trend NW-SE, sub-parallel to the boundaries of this terrane. The western boundary is defined by the Cenozoic left-lateral transpressional Chong Shan shear zone and its continuation as a reverse

fault further to the south along the Lancang (Mekong) river (*Akciz* (2004)). Near the First Bend region, the eastern boundary of Lanping-Simao is marked by the active (?) Tongdian fault which more or less follows the Jinshajiang suture (the suture proper is buried under upper Triassic rocks and Tertiary sediments of the Jianchuan basin for much of this length). South of the First Bend region (southwest of the towns of Dali and Midu), the Lanping-Simao belt is bounded by the schists and phyllites of the Song Ma - Ailao Shan suture (*Metcalfe* (1998)) and mylonites of the Cenozoic Ailao Shan shear zone (*Leloup et al.* (1995, 2001)). Except where the Tongdian fault and Jianchuan basin obscure the original relations, both the eastern and western fault boundaries of Lanping-Simao have reverse components to them (*Schoenbohm et al.* (2005); *Wang and Burchfiel* (1997); *Akciz* (2004)), and Lanping-Simao units are everywhere in the footwalls of these faults.

Paleozoic rocks of Lanping-Simao fold belt are generally of Cathaysian affinities, whereas the Qiangtang block exhibits Gondwanaland faunas and floras up to the Early Permian(*Sengor and Natalin* (1996)). Qiangtang rocks are separated from Lanping-Simao rocks by the Early Triassic Lancangjiang suture (*Metcalfe* (1998)). Hence, beyond the superficial similarity between the Mesozoic red beds of Lanping-Simao to red beds of the Qamdo basin in southern Qiangtang, the correlation of Lanping-Simao with Qiangtang rests on the similarities of the middle and upper Triassic rocks of both terranes. As noted earlier, the specific contiguity of these terranes through the Three Rivers zone depends on the contiguity of various distinctive rock units and, especially, the Jinshajiang suture. An additional complication is the possibility that large parts of Qiangtang-Lanping-Simao were translated large distances parallel to belt (*Leloup et al.* (2001); *Replumaz and Tapponnier* (2003)).

3.2.4 Yangzi platform and South China

Around the First Bend proper, rocks have South China – Yangzi platform affinities. These rocks are exposed in most of Sichuan and Yunnan provinces, and extend from the edge of the Tibetan plateau to the Ailao Shan metamorphic rocks. In Yunnan, these rocks are invariably folded and often referred to as the South China fold belt (eg. *Wang et al.* (1998)). This terminology is imprecise, however, since there were likely a number of temporally and geographically separate deformational episodes, the timing or setting of each being somewhat poorly constrained (cf. *Wang et al.* (1998)). The Yangzi platform (and thus South China fold belt) rocks consist of a late Precambrian basement of typically metamorphic rocks overlain by an early Paleozoic dominantly clastic sequence, itself overlain by a late Paleozoic shallow marine carbonate sequence. Permian carbonates are overlain by the distinctive and wide-spread late Permian Emeishan flood basalts (*Thompson et al.* (2001)). The Paleozoic sequence is locally incomplete, and considerable variability makes stratigraphical correlation a challenge. Possibly related to this is a north-south trending zone of basement rock exposures broadly defining the "Kungdian high", a region that likely experienced periodic exposure and erosion in Paleozoic and early Mesozoic time(cf. the discussion of the Kungdian high in Sichuan province in *Burchfiel et al.* (1995)). Triassic rocks consist of a lower predominantly carbonate or mixed clastic - carbonate section and, in the middle Triassic, either deep-water turbidite deposits (flysch) characteristic of the Songpan-Ganzi terrane of the northern Tibetan plateau or near-shore clastic deposits characteristic of most of central Yunnan. Upper Triassic rocks are clastic rocks intercalated with occasional terrestrial sequences (particularly where the middle Triassic shows a more near-shore character) and mafic to intermediate volcanic rocks.

Jurassic and Cretaceous rocks are mostly limited to thick accumulations of terrestrial red bed sequences in the Chuxiong basin. The Chuxiong basin is dominated by Mesozoic rocks, but local exposures of poorly dated early Tertiary red beds occur.

The Chuxiong basin is likely the foreland basin to the Mesozoic mountain belt that was the continuation of the Longmenshan orogen in Sichuan province (*Burchfiel et al.* (1995)). Minor folding and small-displacement thrusts locally affect Chuxiong basin rocks up to early Tertiary in age. Tertiary rocks are also exposed in the footwalls of minor reverse faults around Lijiang and in the Jianchuan basin. These rocks are described in greater detail below.

3.3 Regional tectonics of the Three Rivers region and western Yunnan

By the end of the Triassic, with the exception of the Lhasa terrane, all of the tectonic elements or terranes of the Three Rivers area were juxtaposed along the various sutures now cropping out throughout Yunnan and Tibet (*Metcalfe* (1998); *Sengor and Natalin* (1996)). These regions were then subject to a complicated and protracted history of deformation from mid Mesozoic to present time. The earliest Mesozoic deformational history, which presumably may have accompanied the suturing of the youngest terrane boundaries (eg. the Early Triassic Lancangjiang suture, *Metcalfe* (1998)), is the most poorly documented and least constrained. We believe that is is reflected in the development of early fabrics and pro-grade metamorphism exposed in the deeper structural levels in this region. Subsequently, the main regional deformational events are related to the Jurassic–Cretaceous Longmenshan orogeny (*Burchfiel et al.* (1995); *Wallis et al.* (2003); *Huang et al.* (2003) and early Tertiary to present India–Asia collision.

3.3.1 Early Mesozoic metamorphism and deformation

Apart from high grade metamorphism related to major Cenozoic Gaoligong, Chong Shan and Ailao Shan shear zones, exposures of metamorphic rocks are relatively

uncommon in the region shown in figures 5.2 and 5.2.2. Upper greenschist to amphibolite rocks are found in the core of the Longmen mountains, south of the Longmen mountains in normal fault and detachment bounded domal culminations, and in a discontinuous belt adjacent to the Jinsha suture from the area of the First Bend north to the town of Dege in Tibet. In the Longmen mountains, *Huang et al.* (2003) used U-Pb and Rb-Sr data to argue for two episodes of metamorphism at c. 204 – 190 Ma and then c. 168 – 158 Ma, with subsequent slow cooling after c. 138 Ma. *Wallis et al.* (2003), using U-Pb and Ar-Ar systems, also found evidence for Mesozoic, as well as early Cenozoic (c. 65 Ma) Barrovian metamorphism and deformation for this area. South of the Longmen mountains, high grade rocks are exposed in the core of three normal fault bounded culminations: the Qiasi, Changqiang and Jianglang domes. The last was the subject of a detailed structural study by *Yan et al.* (2003), who interpreted the Jianglang dome as a Cordilleran core complex and cited c. 177 Ma K-Ar ages for exhumation along low-angle detachment faults. Finally, a discontinuous belt of variable grade metamorphic rocks extends from the present study area north to where the Yidun arc is juxtaposed against the Qiangtang block along the Jinsha suture. Ar-Ar ages from some of these exposures as well as various generations of granites, together with fabric studies led *Reid et al.* (2005a,b) to argue that the main episode of metamorphism here was related to the accretion of the Yidun arc and Qiangtang block with the Songpan–Ganzi terrane in the early to middle Triassic, with rapid cooling of metasedimentary rocks from c. 244 to c. 210 Ma. Apart from the early Cenozoic ages reported by *Wallis et al.* (2003) and Jurassic ages reported by *Yan et al.* (2003), most of the metamorphism and high grade deformation of rocks exposed in eastern Tibet and western Yunnan is early to middle Triassic in age, and thought to be related to the assembly of the various terranes or tectonic blocks of this region during the Indosinian orogeny *Sengor and Natalin* (1996).

3.3.2 Late Mesozoic fold and thrust belts: the Longmenshan Orogen and its continuation in Yunnan

In Yunnan, thin-skinned deformation of the Yangzi platform rocks began in early Jurassic time and persisted into the Cretaceous (*Wang et al.* (1998)). This deformation represents the southward continuation of deformation in the Longmen mountains, which form the western margin of the Sichuan basin to the north (*Burchfiel et al.* (1995); *Wallis et al.* (2003); *Huang et al.* (2003)). Generally east-vergent deformation was accompanied with the accumulation of thick mostly terrestrial sediments in the Sichuan and Chuxiong foreland basins *Meng et al.* (2005); *Wang et al.* (1998). Apart from common folds, two major thrust faults can be followed into Yunnan. As in the Longmen Shan, the eastern limit of the thrusts corresponds, more or less, to the extent of flysch-like deposition in the upper Triassic rocks (*Wang et al.* (1998); *Burchfiel et al.* (1995)). The easternmost thrust places Paleozoic rocks over both Triassic rocks as well as Jurassic foreland rocks, and apparently terminates in a large refolded recumbent anticline near Dali. Here, the mainly northeast trending, east-southeast verging Longmen Shan age structures abruptly bend to north-south, west-verging orientations. Generally, Longmen Shan age structures verge east-southeast west and north of the active Chenghai fault whereas possibly contemporaneous structures verge west in a corridor from Dali to at least Zhongdian. It is unclear what process is responsible for the abrupt hairpin syntaxis around which the Mesozoic structures are folded. Apart from the major thrusts outlined above and perhaps a few other faults, the structural style is dominated by tight, commonly overturned, thin skinned folds, without associated fabric development.

3.3.3 Cenozoic tectonic evolution

Early Cenozoic tectonics include folding, shortening and rotation of the Lanping-Simao belt, limited shortening in Yangzi rocks, significant strike-slip and transpression on at least three major faults (and perhaps other, less-prominent faults), and rotation and shear of rocks within the Three Rivers zone. Limited crustal shortening accompanied significant clockwise rotation, translation and shear of deforming crustal blocks bounded by the major Gaoligong Shan, Chong Shan and Ailao Shan structures (*Geissman et al.* (2001); *Sato et al.* (2001); *Geissman et al.* (submitted); *Akciz* (2004); *Wang and Burchfiel* (1997); *Leloup et al.* (1995, 2001)). Most of the translation, rotation and shear deformation appears to be limited to the Lanping-Simao rocks, west of the Jianchuan basin and Jinshajiang suture. In the present study area, evidence for upper crustal shortening is limited to the tilting of rocks below the mid-Jianchuan basin unconformity and to minor faults with 100s of meters of throw in the Lijiang area – these are described in detail below. In Lanping-Simao, Cenozoic upper crustal shortening is similarly limited to broad, upright folds and minor reverse faults (*Wang and Burchfiel* (1997); *Geissman et al.* (submitted)).

The apparently minor upper crustal shortening during Cenozoic time has naturally raised the question of how great crustal thicknesses and correspondingly high elevations were developed in eastern Tibet and western Yunnan. Low-relief surfaces are widely developed over both metamorphic rocks associated with the major early faults and the deforming blocks that they bounded (*Schoenbohm et al.* (in press); *Clark et al.* (2005, in review); *Clark* (2003); *Wang et al.* (1998)) and dramatic incision of an older, lower relief landscape is characteristic of much of Yunnan and eastern Tibet. Elevation and subsequent incision of the landscape has been suggested as being the result of channel flows of lower or middle crustal material that thickened the crust with little or no contribution from upper-crustal shortening (*Clark et al.* (in review); *Clark and Royden* (2000)). Low temperature thermochronometry and

the ages of sediments found on the high elevation relict surface suggest that crustal thickening began in mid to late Miocene time in eastern Tibet (*Clark et al.* (2005)) and in early Pliocene time in central Yunnan (*Schoenbohm et al.* (in press); *Wang et al.* (1998)). An important outstanding question is what the mean elevations and crustal thicknesses were prior to late Cenozoic incision.

3.3.4 Young and active tectonics

The active tectonics of eastern Tibet are characterized to a first order by the clockwise rotation of crustal material about the eastern Himalayan syntaxis (*Wang et al.* (1998)). The arcuate left-lateral Xianshuihe and Xiaojiang faults bound this rotating region (the Chuan Dian fragment, e.g. *Wang et al.* (1998); *Yoshioka et al.* (2003); *Tamai et al.* (2004)) to the northeast and east from the eastern Tibetan plateau to the Red River fault (fig. 5.2.2). These first-order kinematics are well-established from mapping of active faults (*Wang et al.* (1998)), modelling of combined seismic strain release, fault slip-rates and geodetic velocities (*Holt et al.* (2000)), and geodetic data (*Shen et al.* (2005); *Chen et al.* (2000); *King et al.* (1997); *Zhang et al.* (2004)). Both geological and geodetic data show additional second-order complexities to this simple picture. Within the clockwise rotating region, smaller blocks are bounded by Jianchuan-Lijiang-Zhongdian fault system, and the Chenghai, Tongdian, Batang and Litang faults. The combined geodetic velocity field of *Chen et al.* (2000); *Zhang et al.* (2004) shows that an east-west component of extension is superimposed on the first-order clockwise rotation. This extension is associated with the Chenghai fault and the transtensional Jianchuan-Lijiang-Zhongdian (JLZ) fault system and causes differential rotation of a block bounded by the JLZ and Chenghai faults. The southeastern margin of this block consists of a wedge shaped region characterized by north-south trending, east-west extending Quaternary extensional basins linked by left-lateral northeast trending strike-slip or oblique strike-slip faults (figure 3-3).

Figure 3-2: Young and active faults of Yunnan. The left-lateral Xianshuihe fault bounds a broad region rotating clockwise about the eastern Himalayan syntaxis and extending east-west south of it. Focal mechanism solutions are drawn from the Harvard CMT catalogue. Boxes show the locations of the study area and figures 3-3 and 3.5

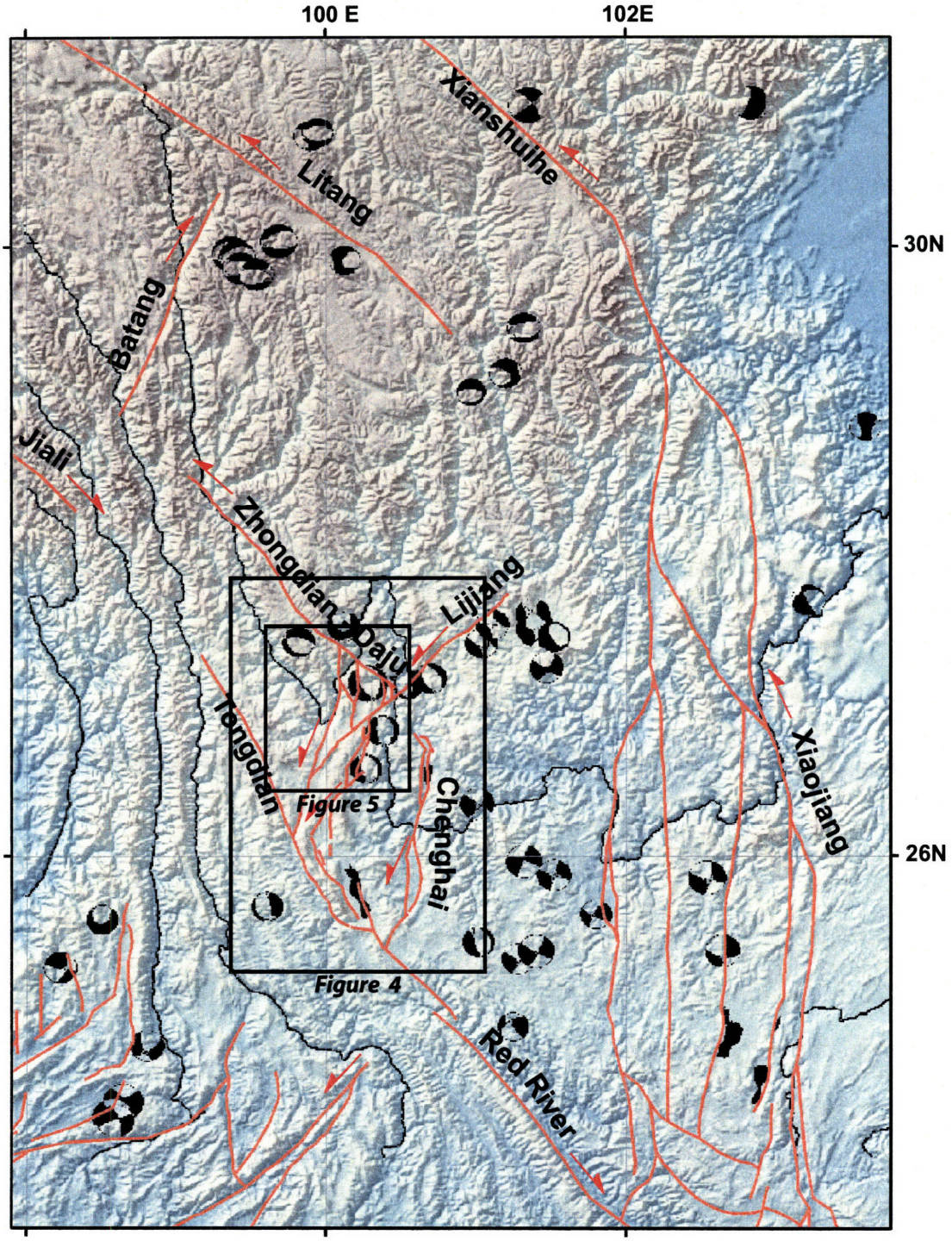

The normal fault bounded Yulong mountains are located at the apex of this wedge. North of the Yulong mountains, the block is bounded by the Daju and Zhongdian faults. None of the mapped active faults accommodate any shortening of the upper crust. Focal mechanism solutions are dominated by normal fault mechanisms and geodetically determined velocities are consistent with the lack of active shortening (fig. 5.2.2).

The region is seismically active, with a particular concentration of both major and minor quakes spatially associated with the Yulong mountains and the apex of the wedge of transtensional active faulting. Harvard CMT solutions show that all major ($M > 5$) events are extensional, with a very small strike-slip component. Most striking were the 1997 M 7 and M 6 (aftershock) earthquakes that ruptured the oblique-normal Daju and Xueshan faults that define the eastern boundary of the Yulong mountains (*Chen and Xu* (2000); *He et al.* (2001); *Akamatsu et al.* (1998)). *Lacassin et al.* (1996) noted the presence of active normal faults on the eastern boundary of this range, but did not consider these to be relevant to the structural and tectonic evolution of the range.

3.4 Early Cenozoic rocks and structures of the First Bend area

Early Cenozoic deposits in the First Bend area consist of accumulations of terrestrial clastic sediments. Although it is difficult to precisely establish the age of these redbeds, these rocks are crucial for distinguishing Cenozoic from earlier structures. We note two general associations for early Tertiary deposits in this area. First, deposits comprising the Jianchuan basin originally formed in what was probably a laterally more extensive basin, and the mechanisms responsible for basin subsidence are unclear. Second, Tertiary sediments were also deposited in very narrow, structurally

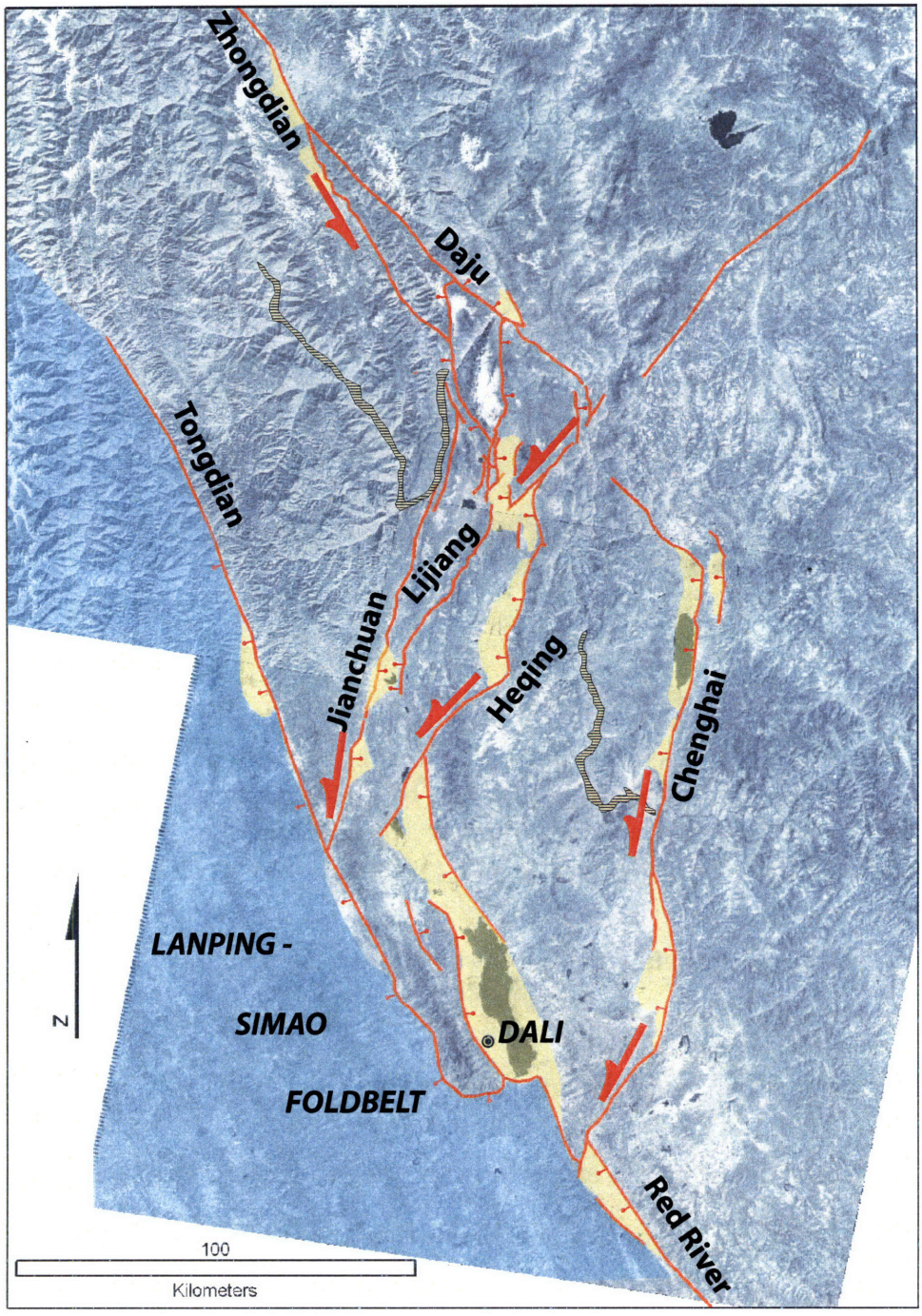

Figure 3-3: Quaternary basins associated with the transtensional Dali - Lijiang fault system. Hatched areas along the Jinsha river represent reaches where the river is alluviated upstream of the Yulong mountains and in response to subsidence in the hangingwall of the Chenghai faults

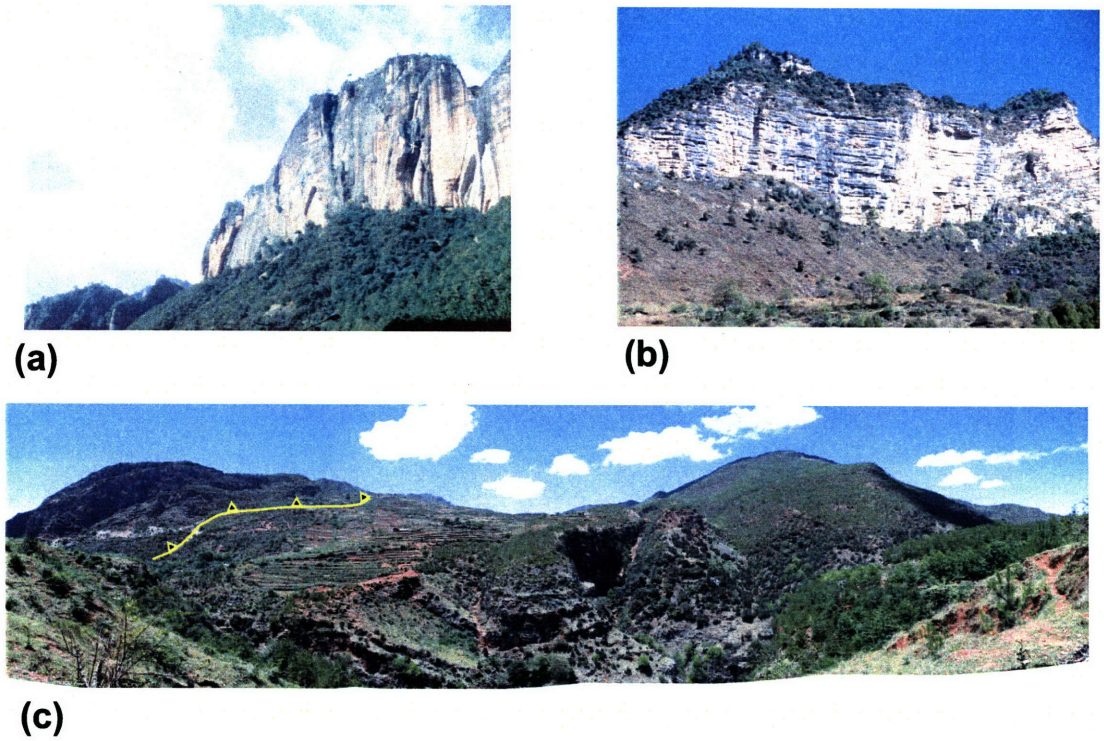

Figure 3-4: Tertiary rocks of the First Bend region. (a) Tall cliffs of aeolian sediments of the upper Jianchuan basin near Liming; (b) Flat lying fluvial gravels and sands of the uppermost Jianchuan basin; (c) Tertiary rocks in the footwall of a small reverse fault near Lijiang

controlled basins in the immediate footwalls of reverse faults.

3.4.1 Tertiary Jianchuan basin

The Jianchuan basin consists of a relatively thick (>1000 m) sequence of red terrestrial sediments of early Tertiary age. The basin can be broadly separated into two parts, separated by an angular unconformity. The lower section is poorly exposed and seen only near the southern margin of the basin. The upper section involves almost a kilometer of terrestrial red beds that overlie both the lower, deformed section and the high grade Shigu metamorphic rocks. The upper section is cut by alkaline sills and shallow plutons. The Jianchuan rocks are found in a rhomb-shaped area

bounded to the west by (old, inactive) normal and thrust faults and to the southeast by the Jianchuan fault, an active normal-left-slip fault (*Wang et al.* (1998)). To the northeast, the Jinsha river has cut through both the Tertiary section and at least 1000 meters of the underlying Shigu metamorphic rocks. On the northeast and north margins, the basal unconformity is exposed where the Jianchuan sediments have been stripped off their Shigu basement. To the west, the active (?) left-lateral transtensional Tongdian fault juxtaposes Triassic rocks against the red beds of the Lanping-Simao fold belt. This last fault may mark the continuation of either or both the Ailao Shan shear zone and the Red River fault, although we note that the geomorphic expression of the Tongdian fault does not continue south of its intersection with the Jianchuan fault and it is difficult to reconcile left-lateral and normal slip on the Tongdian (*Wang et al.* (1998)) with the young (and possibly active) right-lateral slip on the Red River (*Schoenbohm et al.* (2006); *Cong and Feigl* (1999); *Weldon et al.*; *Allen et al.* (1984); *Replumaz et al.* (2001)).

Lower section

The lower parts of the Jianchuan basin series consist of thinly bedded red mudstones with minor fine sandstone interlayers. The total thickness of this lower part is unclear, since it is very poorly exposed. Most outcrops of this lower section are steeply tilted, in contrast with the overlying upper section which is characterized by generally shallow dips and very broad, gentle folds. Ages reported on existing Chinese maps (*BGMR Yunnan* (1990)) are early Tertiary, and are based on rare algal and ostracod fossils. Existing maps correlate these rocks with similar lithologies to the west near the town of Lanping, where Cretaceous redbeds of the Lanping–Simao province grade into lower Tertiary (i.e. Paleogene) sediments. This correlation is, however, inconsistent with tectonic interpretations that invoke hundreds if not thousands of kilometers of offset along structures that purportedly separate these rocks (eg. *Leloup et al.* (1995,

2001); *Chung et al.* (1997)).

Upper section

To the south, the upper Jianchuan sediments overlie the lower section above an angular unconformity. In the North, the upper section rests unconformably on the high grade Shigu metamorphic schists. Rocks immediately above the unconformity consist of a very poorly sorted matrix and clast supported pebble conglomerate whose clasts are angular and consist entirely of biotite-muscovite schist and obviously proximally derived. This basal conglomerate is very distinct from other conglomerates in the Jianchuan sediments, whose clasts are of mixed provenance and never include schist (or marble or phyllite). The schists must therefore have been exposed at the time the basal conglomerate was laid down, but once covered they were no longer available to be eroded, transported and deposited. The lack of metamorphic rock clasts higher in the section despite these rock types dominating lithologies to the north and east implies that the original lateral extent to the north and east of the Tertiary rocks was considerably greater than the present exposure.

The upper Jianchuan rocks are subdivided into three main mappable units. Ages come from the middle unit of the upper section (E2b, *BGMR Yunnan* (1990)) and are based on an ambiguous floral assemblage. Above the basal unconformity, the lowest unit (E2m, *BGMR Yunnan* (1990) maps) is composed of a distinct thick eolian section and fluvial conglomerates and sandstones. Clasts in most of the coarse upper Jianchuan rocks are mostly dominated by quartz vein material, carbonates, and rare volcanics. No metamorphic clasts are observed. Clast composition suggests that the source rocks were either Triassic rocks of Lanping-Simao currently found in fault contact to the west or unmetamorphosed Triassic rocks of South China affinity transported from much farther to the east or northeast.

Like the lower, steeply tilted section of the Jianchuan basin, the upper, less-

deformed section is correlated on existing maps with units a few tens of kilometers to the west near the town of Lanping. Near Lanping, the upper section lies above an angular unconformity, and consists of a much less deformed, gently folded upper section dominated by well-sorted medium grained predominantly fluvial sandstones, with many of the same facies types as the Jianchuan upper section. Poor exposure and general lack of distinct marker beds presents a difficulty in establishing a definite correlation between the units. Nevertheless, it should be noted that the correlation of both the upper and lower parts of the Jianchuan basin with similar rocks near Lanping is at odds with tectonic models of this region invoking strike-slip faults with hundreds of kilometers of separation separating these basins (eg. *Leloup et al.* (2001, 1995); *Replumaz and Tapponnier* (2003)).

Alkaline sills and hypabyssal intrusions

The Jianchuan basin and underlying Shigu metamorphic rocks are intruded by an extensive series of alkaline hypabbysal sills, dykes and small plutons. These rocks are part of a regionally extensive belt of isolated alkaline intrusions found throughout Yunnan and in a long discontinuous belt that follows the structural trends of the Three Rivers belt and continues to outcrop in the eastern plateau of Tibet (*Wang et al.* (2001); *Zhang and Scharer* (1999); *Chung et al.* (1997)). Existing age control for these rocks consists of Rb-Sr and K-Ar ages cited by the regional survey mapping of these areas (*BGMR Yunnan* (1990)) and newer, more precise Ar-Ar (eg. *Wang et al.* (2001)) and U-Pb (*Zhang and Scharer* (1999)) determinations. Other possibly related young igneous rocks include a poorly documented ultra-potassic dyke swarm (lamprophyres and minettes) that is present throughout the eastern plateau, the Three Rivers zone and the present study area. One of these dykes (a lamprophyre) is exposed along the Tiger Leap gorge section.

In Yunnan, rocks of this series have received some focussed attention, including

extensive trace element geochemistry and precise Ar-Ar age determinations. *Wang et al.* (2001) have interpreted these rocks as mantle-derived melts produced during intracontinental subduction of Lanping-Simao rocks underneath Yangzi rocks along the Ailao Shan zone. Alternatively, these rocks may be analogous to modern potassic volcanic rocks erupting in northern Tibet, just south of the Kunlun mountains. It is not clear that the Jianchuan alkaline intrusives are straight-forwardly related to subduction along the Ailao Shan, since similar rocks are also present to the west of the boundary and the Ailao Shan shear zone does not crop out continously to the west of the study area.

The Jianchuan alkaline rocks consist of sills, dykes and small plutons that are seen to intrude both the terrestrial sediments of the Upper Jianchuan basin and the Shigu metamorphic rocks that underlie these. They consist of massive or jointed distinctive white weathering medium grained clinopyroxene and amphibole bearing syenite, and are commonly quarried in this area for monument and facing stone. Mafic (biotite - amphibole after clinopyroxene) xenoliths are common, and typically form subangular centimeter or smaller scale inclusions in the rock. It is likely that at least some of the pyroxenes in the groundmass are xenocrysts derived from disaggregated versions of these xenoliths.

Age control of Tertiary alkaline intrusions Previous geochronological work on these rocks includes a U-Pb age reported in *Zhang and Scharer* (1999) of 35.1 Ma. We separated sanidine from a sill near Liming for Ar-Ar dating and obtained a good plateau age of 40.00 +/- 0.42 Ma (MSWD = 0.99, and Appendix A), which we consider a crystallization age. The discrepancy between these two ages more than likely reflects different pulses of magmatism over a protracted period of time, which is consistent with the broad range of ages reported for similar rocks regionally. The age of the sill reported here provides a minimum age for the upper Jianchuan basin

fill.

3.4.2 Fault-related Tertiary basins near Lijiang

Notable Tertiary rocks in the First Bend area also include terrestrial sediments related to minor reverse faults such as near the city of Lijiang and town of Mingyin. These basins consist of elongate but narrow sediment accumulations in the footwall of minor reverse faults. Both the Lijiang and Mingyin basins are on the order of tens of kilometers long, but less than a kilometer wide and are bounded on their west sides by east-verging thrust faults. Accommodation space for sediment accumulation is created by subsidence in the footwall synclines to the faults, and sediment accumulations are thickest near the bounding fault. Near Lijiang, the entire section of sediment from the basal unconformity to the overthrust hanging wall rocks is well exposed, and consists of a few hundred meters of fill. Sediments above the basal unconformity are pebbly conglomerates and coarse sandstones derived from adjacent Triassic limestones and represent alluvial fan deposits. Reverse faults related to these sediments trend N-S, verge eastward and are characterized by very limited throw (<1 km). These structures are the only unequivocally Cenozoic structures and it appears that early Tertiary upper crustal shortening was rather limited. We note that these minor faults and basins are more or less parallel to other mapped compressional structures farther to the east. These, such as faults that bound the Chuxiong basin, are mostly east verging Mesozoic structures that suffered minor reactivation in early Tertiary time.

3.5 Metamorphic rocks of the South China fold belt: low-grade polydeformed foliated Yangzi platform rocks and Shigu group schists

In most of Yunnan, exposures of Yangzi / South China rocks are characterized by deformation without significant fabric development. In the First Bend area, however, deeper structural levels are exposed. In particular, we mapped a chlorite isograd which represents the boundary between South China / Yangzi rocks whose deformation occurred in an upper crustal, shallowly detached structural setting with those that are characterized by penetrative fabric development and show a record of multiple generations of deformation (fig. 3.5). The isograd more or less follows the trace of what was likely the earlier trace of the Quaternary Jianchuan fault. At present, slip on the Jianchuan fault is transferred to normal faults bounding the Lijiang basin, well to the east of the isograd. This isograd is then deflected by the antiformal uplift of the Yulong mountains and, in the area around the Yulong mountains, is mostly coincident with the major normal fault system (the Xueshan and Daju faults) bounding the range to the East. West of the isograd towards the Jinsha-Benzilan suture, progressively higher metamorphic grades are exposed.

The highest grade rocks exposed in the First Bend region are the Shigu formation pelitic schists, which are tentatively assigned lower Paleozoic or upper Proterozoic ages on existing maps. Lower grade – though still penetratively deformed – rocks generally structurally above (though perhaps locally interleaved with) these can be reliably correlated with the well-known Yangzi / South China stratigraphy. Between the Shigu formation exposures and rocks exposed in the Yulong mountains culmination, existing maps show an apparently complete Paleozoic to lower Mesozoic section, albeit commonly disrupted by numerous faults and map-scale folds. Many of these faults are associated with significant omission of section – particularly, the common

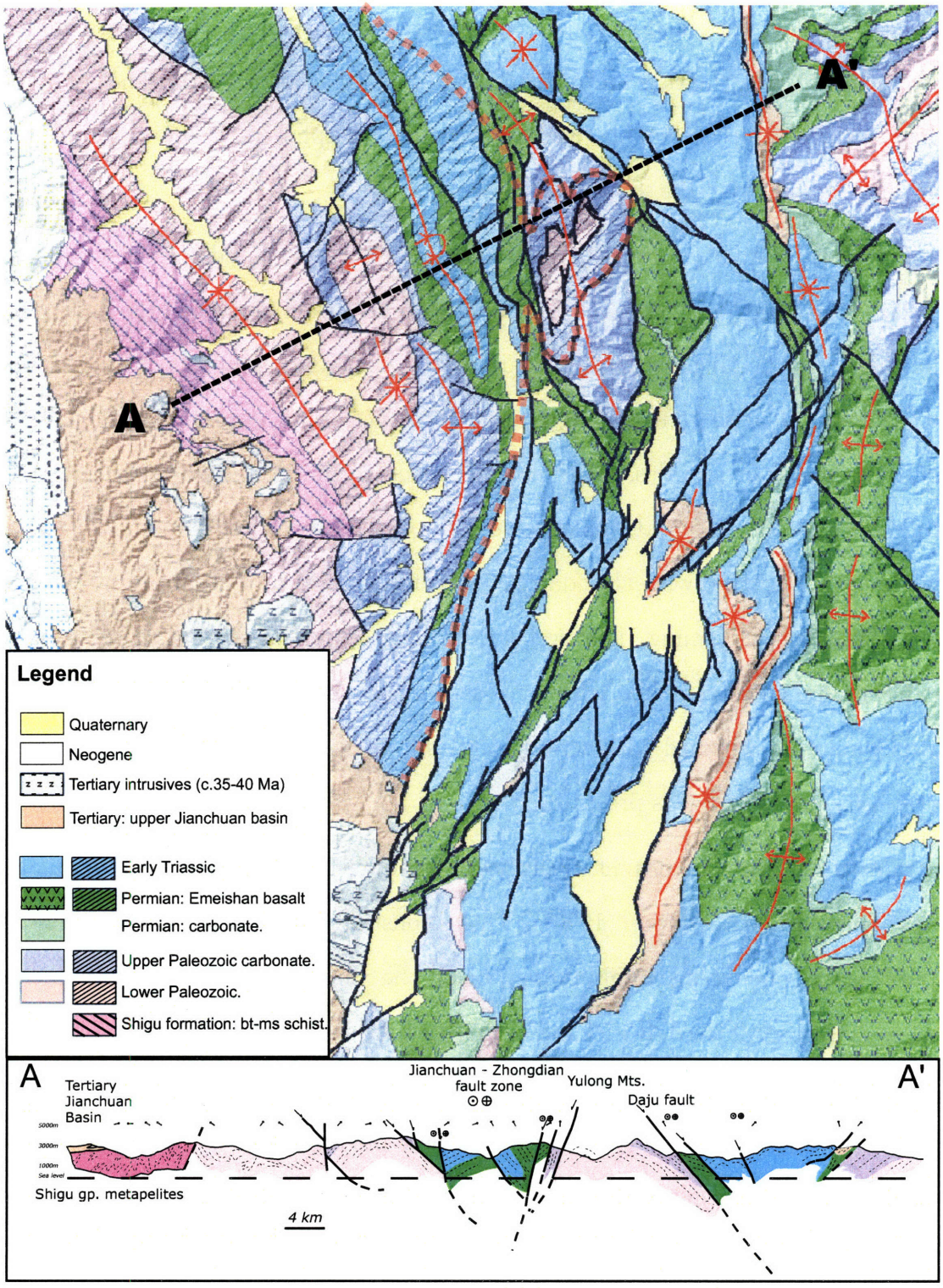

Figure 3-5: Geological map of the First bend region. Dashed line and hatching indicates foliated rocks west of the Yulong mountains culmination. Heavy black lines are Quaternary faults related to the Dali - Lijiang transtensional fault system.

juxtaposition of high and low grade metamorphosed lower Paleozoic clastic rocks against ductilely deformed Devonian carbonates (now marbles). In all units, multiple generations of deformation are recognizable from superposed fabrics and folds. The Shigu rocks are unconformably overlain by unmetamorphosed, weakly deformed early Tertiary sediments of the Jianchuan basin.

The Shigu Formation consists of variably metamorphosed and polydeformed metapelitic rocks that mostly crop out to the west of the Jinsha river from the first bend of the Jinsha (at the town of Shigu) to south of the Zhongdian fault some fifty kilometers to the north. The Shigu rocks are mostly pelitic, with rarer psammitic lithologies and no calc-silicates or marbles. Metamorphic grade within the Shigu formation ranges from lower greenschist grade (chlorite-sericite phyllites) to lower amphibolite (biotite-muscovite +/- garnet with abundant leucogranite dykes) rocks that are well exposed near the village of Liming. During fieldwork related to this present study, we found no aluminum silicates in the schists. Where weakly metamorphosed, thin psammite horizons are interlayered with sericite schists, but no primary structure (apart from compositional layering) is preserved.

Existing Chinese maps tentatively ascribe a lower Paleozoic or Precambrian age to these rocks (*BGMR Yunnan* (1990)). This is consistent with the regional stratigraphy (pure clastic sequences are only present below the Silurian; significant clastic rocks do not re-appear until the Triassic, and even then they are interbedded with volcanic and carbonate rocks). Also, the Shigu rocks are broadly structurally below the distinct, weakly metamorphosed calc-silicates, marbles, phyllites and metavolcanic rocks to the east that are reliably correlated with well-known middle and upper Paleozoic sequences.

Like many of the rocks in the Three Rivers region east of the Jinshajiang suture, the Shigu rocks bear multiple fabric generations. Compositional layering is transposed into the dominant fabric, which itself is multiply crenulated. The main tranposition

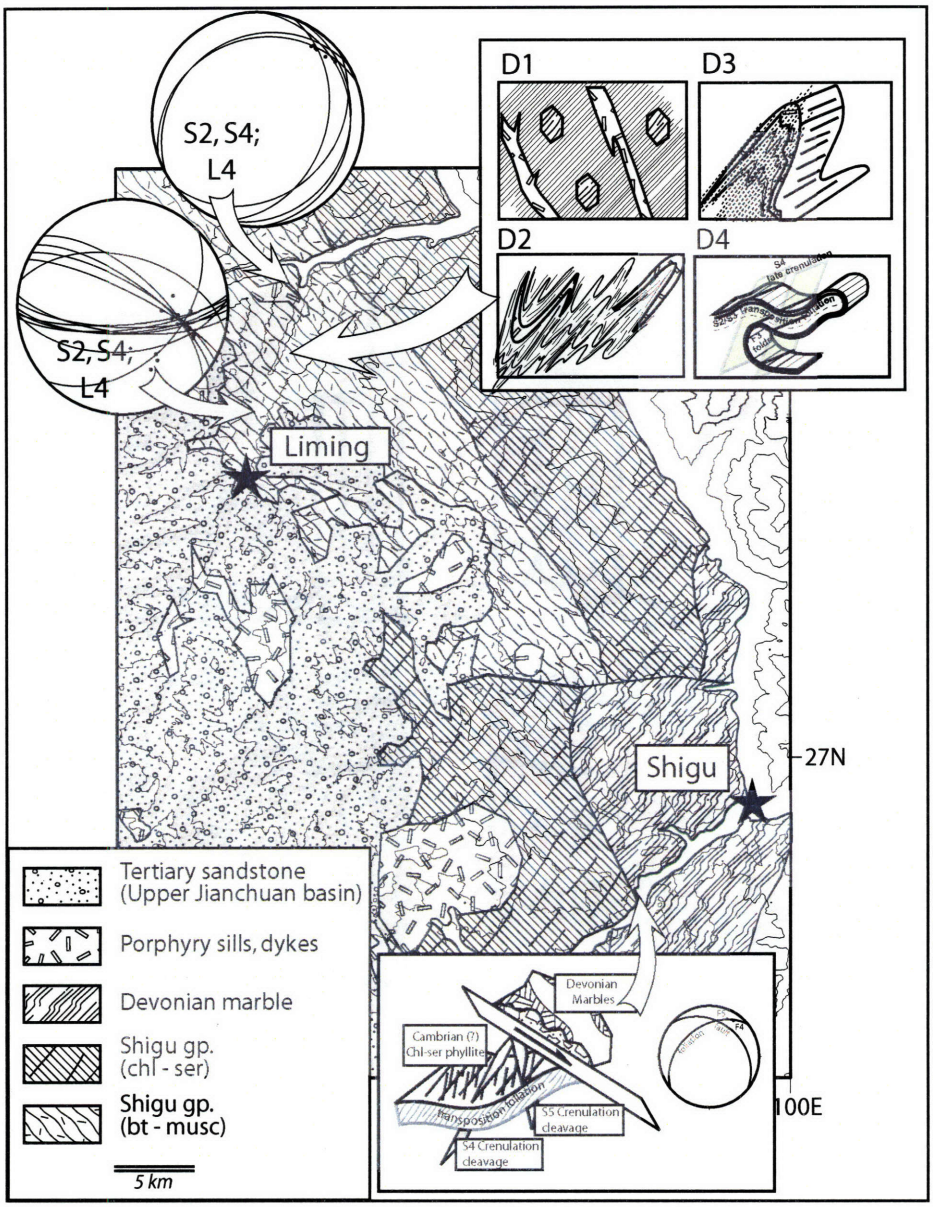

Figure 3-6: Structural relations of the Shigu formation schists and phyllites. Stereonets to the top and left show orientations of S_{main} and L_{main} measured from Liming to the contact with chlorite sericite grade rocks. Lower inset cartoon shows relations between chl-ser grade Shigu formation rocks and overlying Devonian marbles. Upper inset cartoon shows the general structural style of the main fabric forming deformation generations. Tertiary rocks lie unconformably over the polydeformed schists and phyllites, and have suffered only gentle warping and tilting.

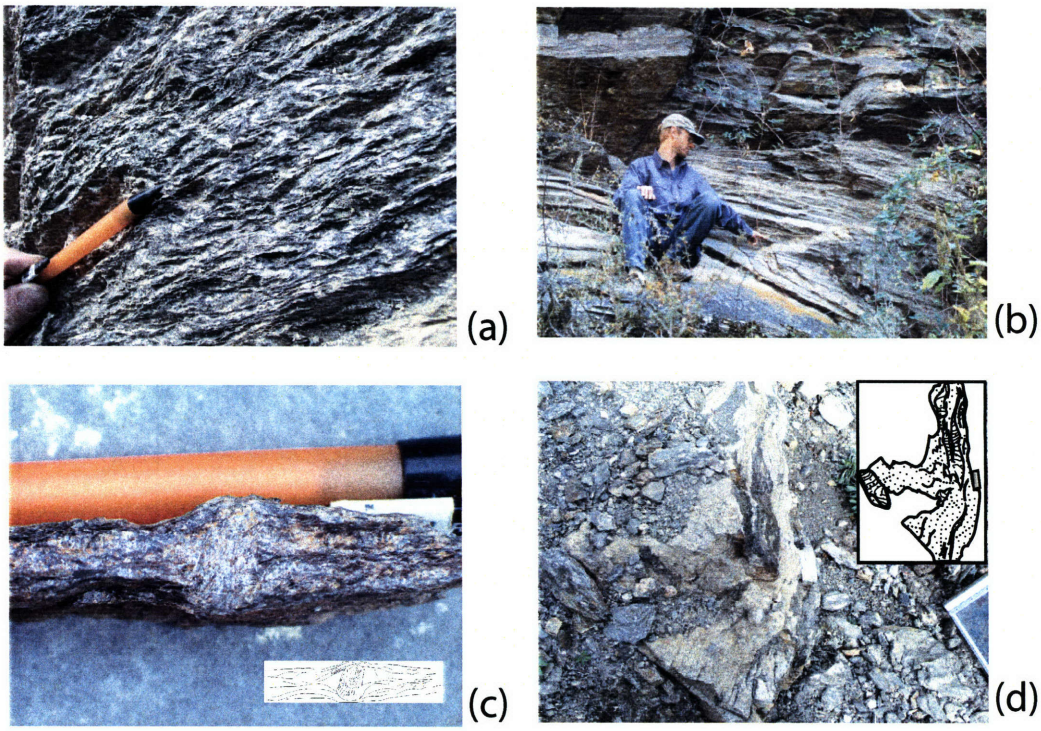

Figure 3-7: Shigu formation rocks. (a) Characteristic view of multiply crenulated Shigu biotite-muscovite schists; (b) Geologist pointing parallel to the strong stretching lineation typically parallel to recumbent mesoscale folds. Note folded leucogranite in the hinge of the fold; (c) Thoroughly retrogressed garnet porphyroblast still shows vestiges of pre-metamorphic inclusion trails; (d) Foliated and sheared leucogranite with deformed schist xenoliths.

foliation is itself related to the folding of an earlier, tectonic fabric that can be recognized in the hinges of rootless, isoclinal, interfolial folds. Moreover, inclusion trails in garnet are discontinuous and oblique to the main fabric, although these could be a primary fabric or related to an early formed slaty cleavage. Therefore, S_{main} is at least an S2 fabric, which we refer to as S_{Sg2}. S_{Sg2} fabrics are folded about tight mesoscale folds folds (F_{Sg3}) whose hinges are parallel to a very strong stretching lineation (L_{Sg3}) and well-developed mineral lineations are the most striking fabric elements in all outcrops. L_{Sg3} and F_{Sg3} orientations are extremely consistent at outcrop scale, but are variable over larger distances, which we believe is the result of larger than outcrop scale folds. This last generation of folds is likely related to a pervasive late crenulation and crenulation cleavage (F_{Sg4} and S_{Sg4}, respectively).

Relationships between deformation and metamorphism are reasonably clear. Garnet growth was pre-kinematic with respect to S_{Sg2}. Garnets are almost always completely retrogressed to clots of biotite, plagioclase, chlorite and rusty oxides. S_{Sg2} is typically wrapped around these retrogressed pseudomorphs, which are not obviously stretched, fractured or otherwise deformed. Sheets and veins of a weakly foliated, medium to fine grained, equigranular magnetite biotite monzogranite are common in the higher grade rocks and folded about F_{Sg3}. The timing of granite intrusion with respect to metamorphism or earlier deformations is equivocal, but we presume they are broadly contemporaneous with metamorphism. Higher grade garnet-biotite bearing facies and lower grade chlorite-sericite rocks appear to be interleaved (although the outcrop is too poor to be certain of this relationship), suggesting that the tight folding of D_{Sg3} affected variably metamorphosed lithologies juxtaposed by faults predating D_{Sg3} folding.

Upper Paleozoic and lower Triassic rocks west of the Yulong mountains that structurally overlie the Shigu rocks appear to be characterized by fabric relationships analogous to those seen in the Shigu rocks. In particular, Devonian and Carboniferous

Generation	Planar fabric elements	Linear fabric elements	Metamorphism	Possible age
pre-D1(?)	Inclusion trails in garnets; ambiguous whether tectonic or primary.	Not observed	Inclusion trails could be primary, or reflect an early compaction-related slaty cleavage.	If primary, then Cambro-Ordovician. Otherwise unknown.
$D_{Sg}1$	Early tectonic fabric, folded and transposed into main transposition foliation (S2)	Rootless, interfolial fold hinges.	Bt + Mus +/- Gt. Concordant leucogranite veins and sheets.	Post-dates deposition of the South China stratigraphic section (at least up to the early to middle Triassic).
$D_{Sg}2$	Main transposition foliation. Transposition of early fabrics, compositional layering, transposition of leucogranite veins and sheets.	Not observed.	Unknown.	Unknown.
$D_{Sg}3$	Subtle crenulation cleavage, axial planar to mesoscopic folds.	Tight mesoscopic folds, very strong stretching lineation, mineral lineation.	Chlorite grade.	Possibly related to the continuation of the Longmenshan orogen (Jurassic to Cretaceous). Definetly pre-dates lower Jianchuan basin deposition (poorly dated, probably early Eocene).
$D_{Sg}4$	Latest crenulation; forms pervasive upright crenulation cleavage.	Crenulation axes.	No metamorphism: crenulation cleavage developed by rotation of pre-existing phyllosilicates and pressure solution.	Possibly related to deformation of the lower Jianchuan basin rocks, definetly pre-dates upper Jianchuan basin deposition (Eocene) and potassic sills (40 Ma).

Table 3.1: Interpretation of multiple generations of deformation in the Shigu formation. Ages are somewhat speculative, see text for details.

ductilely deformed, recrystallized marbles of uncertain metamorphic grade are folded at a variety of scales, these folds deform an existing transposition fabric, and are associated with striking stretching lineations. This deformation therefore appears to have affected a pile of rocks including higher and lower grade Shigu rocks, the metamorphosed Devonian to lower Permian carbonate section, metavolcanic Permian rocks and the lower Triassic mixed clastic and carbonate section. Unit contacts are typically faulted, and are commonly characterized by significant omission of stratigraphic section, particularly at the base of the Devonian. Near the town of Shigu, several good exposures show Devonian marbles faulted against (Cambrian?) Shigu phyllite (figure 3-6). Apparently similar relationships are shown in several places on the existing maps, although we were not able to access outcrops on the east side of the river, upstream from Shigu and the First Bend. Near Shigu, the fault contact is not associated with ductile fabric in the lower Shigu rocks and is instead characterized by a few meters of gouge and fault breccia. We suggest that stratigraphic omission below the Devonian units is the result of extensional tectonics related to the early history of the transtensional Jianchuan-Zhongdian fault zone. Presently, there is no evidence for active faults west of the Yulong mountains, but the very straight course of the Jinsha river immediately downstream of the bend proper is consistent with early left-lateral motion along structures west of the Yulong mountains.

3.5.1 Age constraints

Protolith ages for the Shigu formation are variously reported on existing Chinese maps as either lower Paleozoic and/or Precambrian. As discussed above, this age is uncertain, and based solely on the Shigu rocks being found structurally below units whose correlation with the well-established South China stratigraphy is more certain. The ages of deformation are even more uncertain, apart from the fact that the Shigu rocks are unconformably overlain by unmetamorphosed and only weakly deformed

early Tertiary terrestrial sediments of the Jianchuan basin. In table 1, we present our interpretations and hypotheses regarding the age of the various deformational generations and the fabrics they produce. These are based on: 1) the development of the main transposition foliation affects all rocks west of the Yulong mountains, and so must post-date the youngest rocks in the deformed section (i.e. lower Triassic); 2) folding of the main foliation and development of the strong stretching and crenulation lineation postdates retrogression of peak metamorphic phases; 3) at least two major regional tectonic events are likely to have affected these rocks: first, juxtaposition of South China rocks with Lanping-Simao rocks against the Jinshajiang suture and second, the southward continuation of the Jurassic - Cretaceous Longmenshan orogen which affects rocks in Yunnan to the Jinshajiang - Ailaoshan sutures; 4) the Shigu formation is overlain by unmetamorphosed, uncleaved rocks of the early Tertiary Jianchuan basin. These rocks are described in greater detail below, but an angular unconformity within these rocks suggests the existence of early Eocene deformation; 5) finally, we have acquired a few Ar/Ar ages from Shigu group schists and potassic sills that intrude sediments of the Jianchuan basin.

We report here the first radioisotope ages from the Shigu formation rocks in the form of Ar/Ar cooling ages for biotite and muscovite collected from 2-mica leucogranites that intruded the schists but are deformed about F_{Sg3} fold hinges. We obtained plateau and inverse isochron ages for muscovite of 227.5 +/- 2.4 Ma (MSWD = 0.05) and 224.6 +/- 22.1 (MSWD = 0.02), respectively. We were unable to determine statistically significant plateau or inverse isochron ages from biotite; the total gas fusion age for these samples is 213.2 +/- 1.1 Ma. We emphasize that these ages are preliminary, reconnaissance thermochronological ages. These cooling ages could conceivably represent cooling after peak metamorphism and melt intrusion, cooling due to extensional exhumation or cooling post-D3 deformation. Normal fault contacts and missing section are common in the area, but we found no ductile fabrics

associated with these faults, even in Devonian marbles, suggesting that these faults were responsible for only limited unroofing. We prefer the interpretation that D3 deformation is Longmenshan orogen age (early Jurassic to Cretaceous), since that is the most consistent with what is known of the regional tectonics of the region.

3.6 Metamorphic rocks of the Yulong mountains culmination: the Tiger-Leap Gorge transect

The Yulong mountains are an anomalously high elevation range of glaciated mountains bisected by the Jinsha river, which carves a 3.5 km deep gorge ("Tiger - Leap Gorge") through its center. To a first order, the range is a doubly plunging antiformal structure bounded by active normal faults. Tiger - Leap gorge is cut through mylonitic marbles, polydeformed low-grade pelitic rocks, thinly bedded and cleaved meta-turbidites and quartzites that represent the deepest structural levels exposed in the core of the Yulong mountains culmination. As a result of the combination of spectacular exposure and easy access afforded by a road built along the gorge, previous geological investigations of the Yulong mountains have focussed their attentions along this transect – which is cut entirely through penetratively deformed, cleaved and metamorphosed rocks. The most recent study was a reconnaissance structural and thermochronological study by *Lacassin et al.* (1996), who recognized the general antiformal structure that is cut by the gorge. However, previous work has neglected to describe the multiple generations of fabrics and structures that preceded antiformal folding, and either ignored or down-played the role normal faults played in the structural and tectonic evolution of this mountain range. Furthermore, although Tiger - Leap gorge is cut entirely in metamorphosed rocks, the northern and southern margins of the range, however, are underlain by Devonian to Permian uncleaved and unmetamorphosed rocks. In this section, we describe the structures and fabric

relations of rocks of Tiger-Leap gorge, and their relationships to unmetamorphosed and uncleaved rocks structurally above them or in the hanging walls of the active normal faults that bound the Yulong mountains.

With the exception of the extremely pure mylonitic marbles, which are most likely deformed Devonian (and perhaps Carboniferous) limestones, other metamorphic rocks within the core of the range resist easy correlation to the known Yangzi stratigraphy. Meta-clastic lithologies structurally below the marbles have been assigned a variety of different protolith ages, from Precambrian to lower Devonian. Since the lower Paleozoic Yangzi stratigraphy is dominated by clastic lithologies, we tentatively assume that the meta-clastic rocks are derived from these strata. However, it is unclear whether the protoliths of the Yulong clastic rocks are the same as the protoliths of the Shigu formation rocks. Both are lower Paleozoic (or older), but we failed to find a number of distinct marker units exposed in Tiger Leap gorge (in particular, a very distinct dune-crossbedded quartzite unit) in exposures of the Shigu formation that we were able to examine. A lower Devonian age (cited in *Lacassin et al.* (1996) and early regional scale compilation maps) seems unconvincing in light of the fact that lower Devonian and Silurian rocks in the South China stratigraphy are generally pure limestones or carbonate dominated mixed limestones and marly clastic lithologies. If either the lower Paleozoic or Precambrian (less likely) ages are correct, there appears to be section missing at the contact between marbles and structurally underlying rocks. This contact between marbles and clastic rocks is everywhere a brittle fault contact. This relationship is reminiscent of that between Devonian marbles and low grade Shigu metaclastic rocks exposed near Shigu described above.

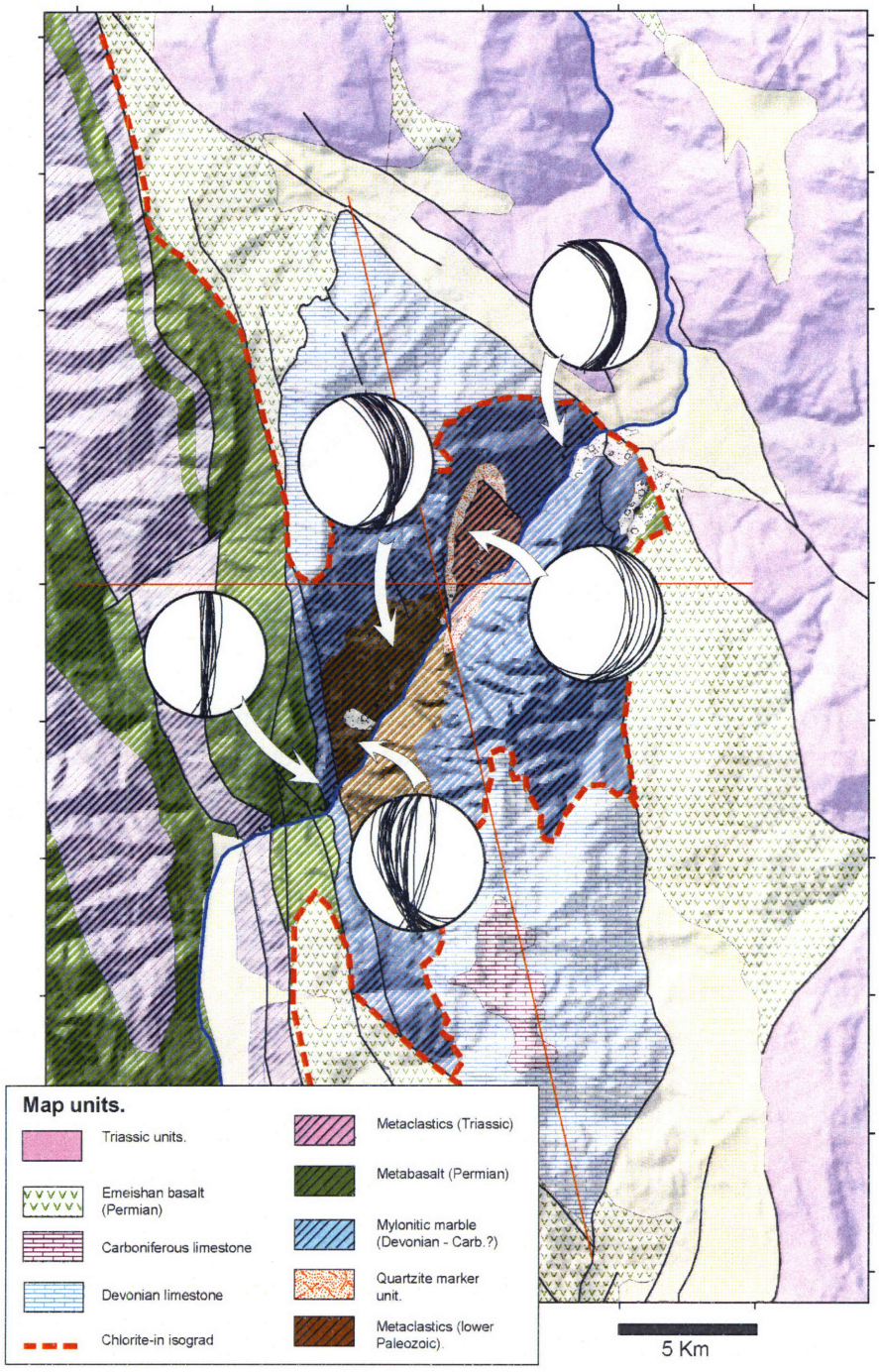

Figure 3-8: Geological map of the Yulong mountains. Stereonets plot the main transposition fabric. Thin orange lines show the trace of the cross-sections through the range (figures 3-9).

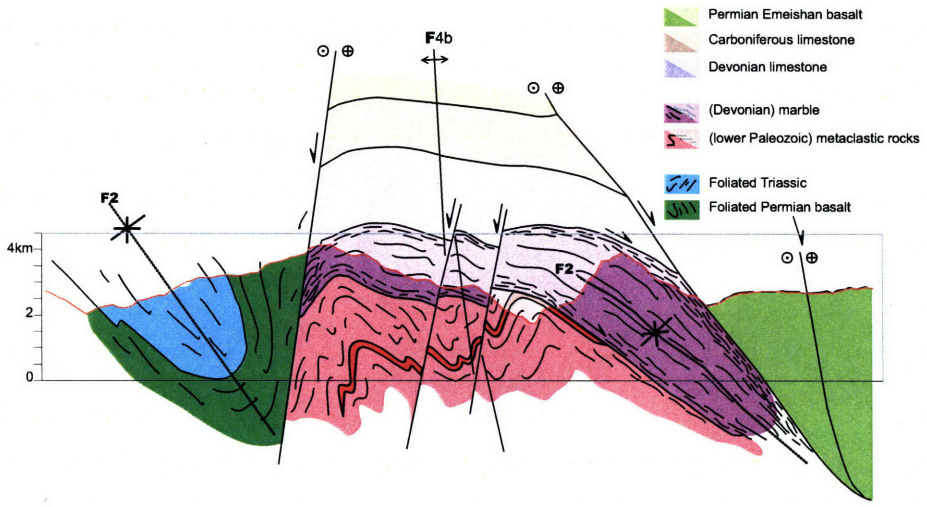

Figure 3-9: East-west oriented cross-section through the Yulong mountains. Dashed vertical line shows the trace of the N-S cross-section. No vertical exaggeration.

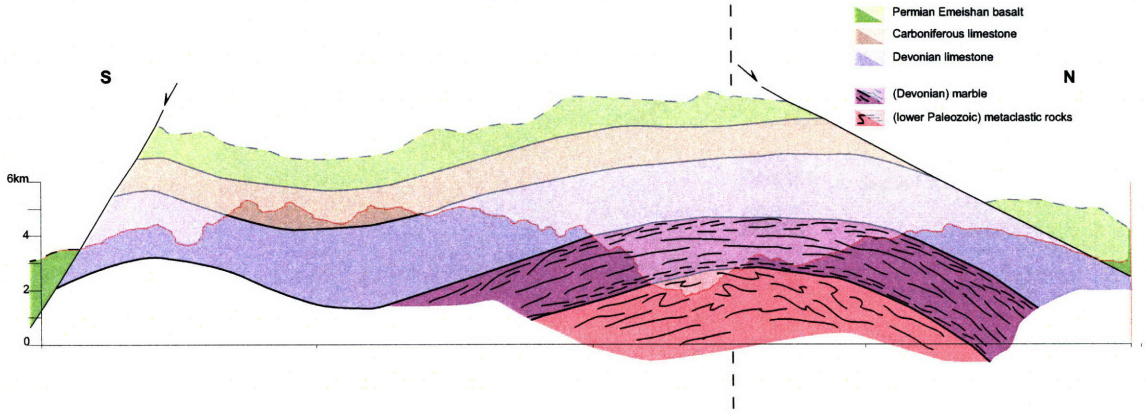

Figure 3-10: North-south oriented cross-section through the Yulong mountains. Dashed vertical line shows the trace of the E-W cross-section. No vertical exaggeration.

Figure 3-11: Stereonets of fabric elements of metaclastic rocks within the Tiger Leap gorge. Plots are of the main transposition foliation (S0 = S1) in chlorite phyllites and bedding in metaturbidites and quartzites.

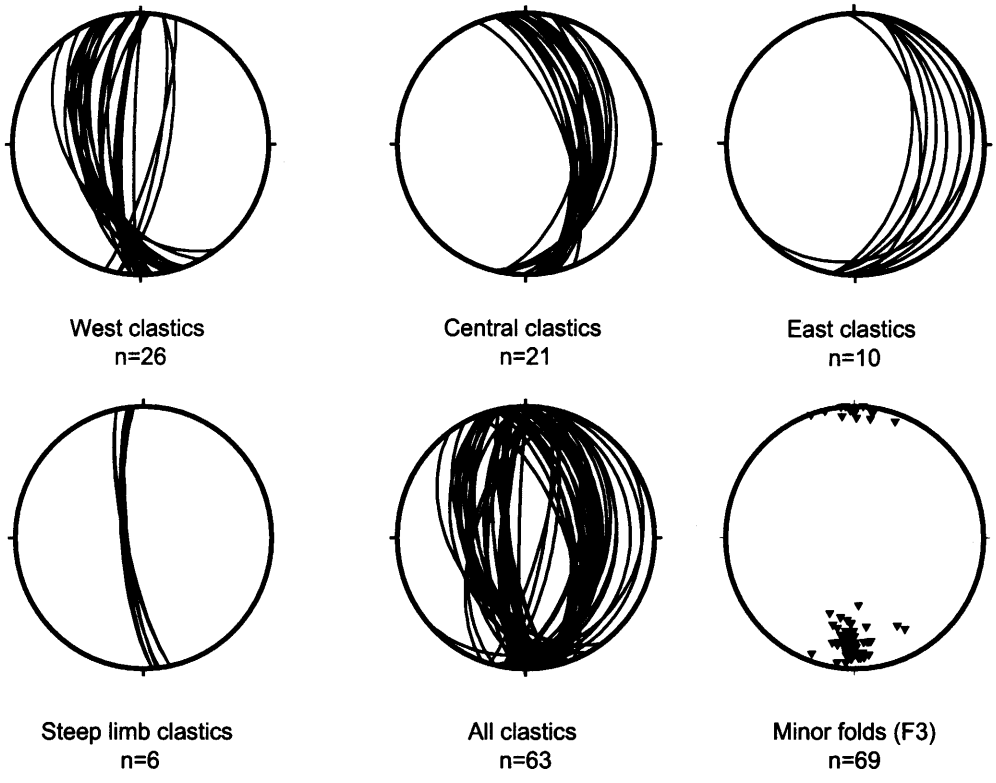

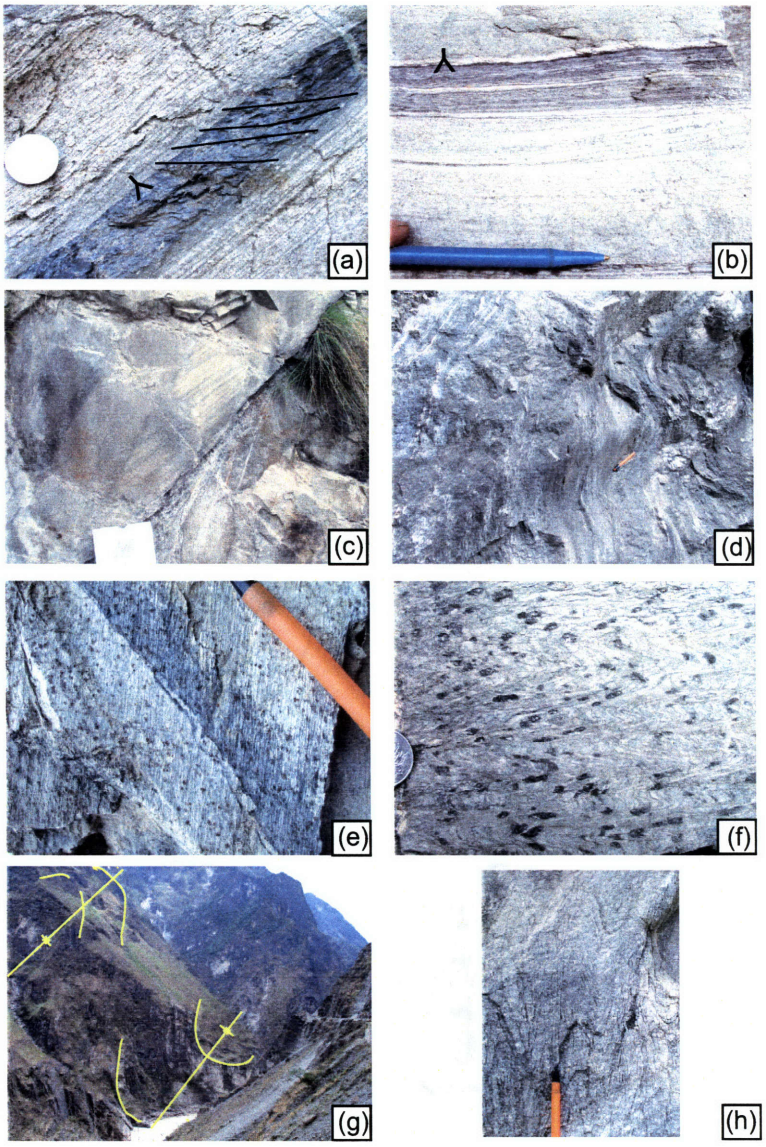

Figure 3-12: Mesoscale fabrics of metamorphic rocks within the Tiger Leap gorge. (a) Cleavage within shaley interval in sandstones is oblique to bedding; younging direction requires these beds be on the lower, upright limb of a recumbent syncline; (b) Cross-lamination in sandstones provide younging direction; (c) large scale cross-lamination in quartzite beds; (d) shallowly plunging minor folds parallel to inferred map scale fold deform S1 cleavage; (e) crenulation lineation (F2) overprints earlier intersection lineation (L1); (f) clots of chlorite-sericite after chloritoid (?) are folded about F2 fold axes; (g) large scale folds of competent quartzite marker unit; (h) subvertical pressure solution cleavage is the only fabric plausibly related to late doming of the Yulong rocks.

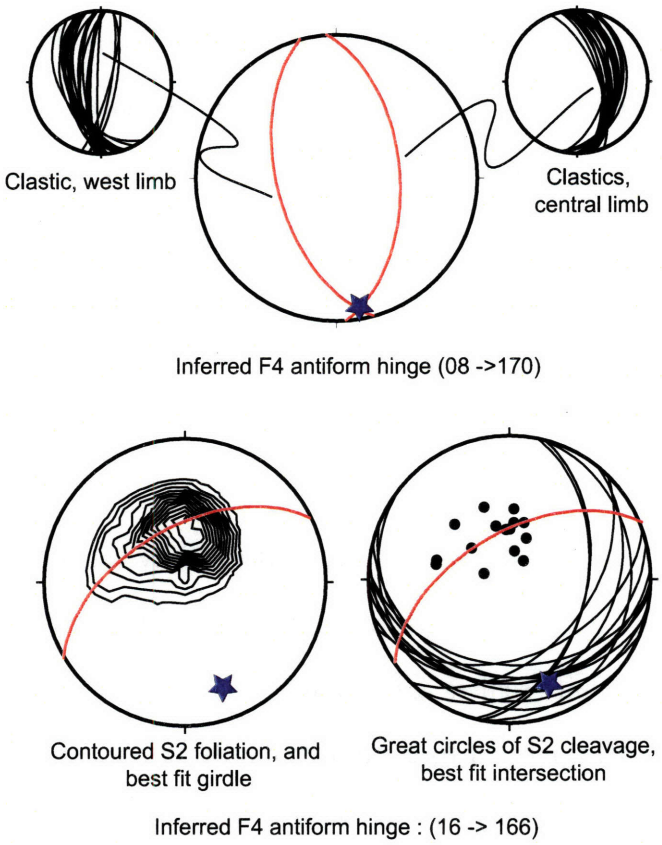

Figure 3-13: Two approaches to inferring orientation of the late, F4 antiform. Cleavage and facing relations require that clastic rocks be on the same limb of the major F2 structure. Any variation must therefore be later. [Top] Intersection of two limbs of the antiform yields the hinge. [Bottom] Contoured poles to S2 foliations (π plot) and intersection of great circles of S2 axial planar foliations (β plot) yield essentially same result.

3.6.1 Metamorphism, early fabric formation, and recumbent folding

All rocks exposed in the gorge show abundant evidence for multiple deformations. The most obvious deformation, and the one most responsible for the large-scale structural geometry of the range is an antiformal upright folding of the units within the bounding normal faults. This deformation is superimposed upon an early deformational history characterized by multiple fabric generations. This early history is associated with a very strong stretching lineation, itself always parallel to the axes of minor folds of earlier metamorphic fabric. We submit that the early fabrics (pre-antiformal doming) are analogous to fabrics in variably metamorphosed rocks to the west of the range (especially, within the Shigu metamorphic rocks).

Early fabrics

The earliest structures (D_{Y1}) include the main foliation (S_{Y1}), defined by various low-grade micas: chlorite and sericite are dominant, with phlogopite in marble units. Biotite is rare, and limited to a few psammite schists and partings within some quartzite layers. The early (S_{Y1}) fabric is mostly parallel to compositional layering, especially the more pelitic rocks. In thinly interbedded meta mudstones and sandstones (turbidites?), primary sedimentary structure is preserved in the sand layers and bedding parallel metamorphic fabric is poorly developed and often absent (fig. 3.6.1a, b, c). In the phyllitic units, on the other hand, small, rootless isoclinal folds (F_{Y1}) transposed into S_{Y1} were commonly observed. Very distinct porphyroblasts grew in all units save the marbles. These porphyroblasts have been thoroughly retrogressed, and are commonly observed as rusty chlorite-rich patches that are folded about crenulations of S_{Y1} (fig. 3.6.1f). Where apparently least retrogressed and deformed, they appear to be chloritoid. However, in thin section, these porphyroblasts have high birefringence, due to complete replacement by sericite +/- chlorite. Porphyroblast growth

is presumed syn-S_{Y1}, but only because the porphyroblasts are so badly retrogressed that any earlier fabric that might have been represented by inclusion trails and the like is completely obscured.

D_{Y2} recumbent, west-verging folding

The composite S_{y0}–S_{y1} layering is itself refolded by a map-scale recumbent fold. Bedding, cleavage and numerous sedimentary facing indicators (fig. 3.6.1a, b, c) require that the metaclastic rocks of Tiger Leaping gorge form the upright limb of a map-scale recumbent syncline that closes to the east and is overturned to the west. Mesoscopic minor folds within these rocks which fold S_{Y1} fabric have fold hinges and axial planes generally parallel to the interpreted larger scale fold, and are interpreted as parasitic, second or third order folds (fig. 3.6.1d). The F_{Y2} recumbent folds are associated with an axial planar cleavage (S_{Y2}) and numerous minor folds, crenulations and, locally, sheath folds in quartzite (F_{Y2}). In places, chlorite-sericite clots after the M_{Y1} porphyroblasts are folded about the F_{Y2} minor folds (fig. 3.6.1f). F_{Y2} minor folds are commonly parallel to a ubiquitous strong stretching and mineral lineation (L_{Y2}). In the phyllitic lithologies where S_{Y1} is most strongly expressed, the late (S_{Y2}) axial planar cleavage is a crenulation cleavage, and overprints a first generation intersection lineation (S_{Y0} X S_{Y1}, fig. 3.6.1e). In the sandier lithologies, S_{Y1} fabric is poorly developed or absent, and the only well-developed fabric is the S_{Y2} axial planar cleavage, oblique to the orientation of bedding within these rocks (fig. 3.6.1a). Apart from outcrop-scale minor folds, a larger scale (amplitude and wavelength in the 10s of meters scale) hinge is clearly exposed where a distinctive 100 meter thick horizon of relatively pure quartzites provides a marker for tracing the fold geometry (fig. 3.6.1g). These quartzites cross the road at the vertical to overturned limb of a second-order F_{Y2} syncline. On the north side of the gorge, beds defining the steep, near vertical limb can be traced to their (faulted) contact with the marbles, where they turn, dip

east, and define the upright (higher) limb of an F_{Y2} anticline. The general sense of overturn of this second order fold, as well as the inferred map-scale fold and mesoscopic sheath folds in quartzites all suggest overturn, and presumably transport, in a top to the west sense. This is consistent with shear sense indicators reported by *Lacassin et al.* (1996).

Marble fabrics

Fabrics in the marbles are more difficult to assign to specific phases of deformation, since early fabrics are generally completely overprinted by later deformational episodes. This likely reflects the ease at which calcite flows ductilely at even low metamorphic grades characteristic of the later deformation generations. Near the margins of the range, in particular, marble fabrics are parallel to the bounding young and active normal faults. On the other hand, in the core of the range, the marble fabrics appear to be folded about the inferred map-scale recumbent fold. Phlogopite-rich partings within the marbles provide the only record of multiple deformations in the form of oblique sets of crenulation hinges, which indicate refolding of early fabrics. The most prominent such crenulation is parallel to the extremely prominent stretching lineation found throughout the range and parallel to the hinge of the inferred map-scale recumbent fold.

3.6.2 Late fabrics and structures

Spectacular sections of marble mylonite are exposed on both the western and eastern margins of the Tiger Leap gorge transect. These rocks are extremely pure calcite marble, except for very local phlogopite and sericite along isolated partings in the rock. Planar fabric is intense, and lineations are ubiquitous and strongly developed. Linear fabric elements consist of crenulations of phologopite along cleavage partings, the stretching and/or alignment of oxides and phlogopite decorating these partings. Two

Generation	Planar fabric elements	Linear fabric elements	Metamorphism	Interpretation and possible age
$\mathbf{D}_{Y1}$	S1 fabric in pelitic lithologies (phyllites).	Interfolial minor folds	Chloritoid, chlorite.	Early regional metamorphism (pre-early to middle Triassic, based on correlation with Shigu metamorphism).
$\mathbf{D}_{Y2}$	Transposition foliation in phyllites. Axial planar cleavage oblique to bedding in meta-turbidites.	Strongly developed stretching lineation in all lithologies, crenulation axes, intersection lineations in units where tectonic fabrics can be distinguished from bedding or compositional layering.	Early porphyroblasts thoroughly retrogressed (chlorite - sericite).	West directed recumbent fold nappes. Longmenshan age (Jurassic - Cretaceous)?
$\mathbf{D}_{Y3}$	Ambiguous: recrystallisation of phlogopite in marbles. No penetrative fabric or crenulation in structurally lower clastic rocks.	None.	Unknown. Recrystallisation of phlogopite in marbles could occur at low greenschist grade.	Regionally, early Tertiary reverse faults. 31.4 +/- 6.6 Ma (Ar-Ar) and 43 Ma (Rb-Sr) ages from phlogopite in marbles.
$\mathbf{D}_{Y4a}$	Mylonites and chlorite - sericite brittle - ductile shear zones in eastern marbles.	Spectacular stretching lineation in eastern marbles. Minor assymetric folds of quartz - carbonate veins and bouding necks in brittle - ductile shear zones.	Low greenschist grade.	Late Miocene or early Pliocene extension representing early stages of presently active tectonics.
$\mathbf{D}_{Y4b}$	No penetrative planar fabrics, some minor sub-vertical spaced pressure solution cleavage.	Doubly-plunging antiformal range-scale doming.	Low greenschist grade to none.	Late Miocene or early Pliocene to present.
$\mathbf{D}_{Y5}$	No penetrative planar fabrics. Brittle normal and transtensional faults bounding the Yulong mountains.	None.	None: brittle faults cutting surficial deposits.	Active normal and transtensional faults accommodating differential uplift of the Yulong mountains.

Table 3.2: Interpretation of multiple generations of deformation in the Yulong mountains. We use subscripts to distinguish between deformation phases identified in the Yulong mountains from those documented in the Shigu formation (table 1), although we believe that the early fabrics at least are broadly correlatable. See text for details on age interpretation.

crenulation generations are observed in the western marbles. The eastern marbles are somewhat different: strong fabrics and stretching and mineral lineations are best developed near the contact with the structurally lower clastic rocks and towards the western margins of the range, where particularly intense fabrics are developed. Between these two zones of more strongly developed fabric is a central domain of foliated, but poorly or even not lineated marbles. Some hint of primary compositional layering is locally observable looking perpendicular to the foliation and down-dip, parallel to the orientation of the stretching lineation.

Interpretation of Early Tertiary isotope ages from recrystallized phlogopite

Lacassin et al. (1996) reported a Rb-Sr isochron age of 43 Ma based on the analysis of different sized fractions of phlogopite collected from marbles on the east side of the range, immediately adjacent to the contact between the eastern marbles and clastic rocks structurally beneath them. They interpreted these marbles as being the decollement to southward directed thrusts and argued that this age represented the recrystallization of phlogopite during this event. From the same site we collected phlogopite for Ar-Ar analysis, and obtained an isochron age of 36 +/- 2 Ma (MSWD 1.24) that is reasonably close to the ages of *Lacassin et al.* (1996) (see Appendix for details). Of the eastern marbles, these are the ones least affected by the extensional overprint. We also collected phlogopite from marbles near the eastern margin of the range and the active range bounding normal faults. This sample site consisted of a coarse phlogopite present in a very discrete horizon in marble mylonites overprinted by extensive brittle fractures. We were unable to determine statistically significant plateau or isochron ages for this sample; the total gas fusion age is 31.3 +/- 0.2 Ma. We cannot, however, discount the possibility that these ages are simply the result of hydrothermal alteration: phlogopite is rare in these extremely pure marbles, and is present only along very distinct and discrete partings. If so, then no real significance

can be attached to these ages. On the other hand, regionally, small east verging reverse faults deform early Tertiary (Eocene - Oligocene) terrestrial sediments, so we cannot entirely discount the possibility that an Eocene age deformation has affected rocks in this area. If so, this would be a rather cryptic deformation, with no fabrics, folds or faults in the Yulong mountains that can be unequivocally interpreted as being related to these ages.

Eastern-most marbles and brittle - ductile extensional shear zones (D_{y5a})

The eastern-most marbles are characterized by particularly intense mylonites and ubiquitous, spectacular mineral (trails of oxides) and stretching lineations that are overprinted by brittle-ductile extensional shear zones that are broadly parallel to the main mylonite foliation. Outside of these brittle-ductile extensional shear zones, we found no unequivocal shear sense indicators. The orientation of the strong lineations in the easternmost marbles is oblique to early (D_{Y2}) linear fabric elements. Whereas D_{Y3} linear fabrics (lineations, minor folds and crenulations) are shallowly plunging and north-south trending, the lineations in the eastern marbles trend east of north, with more easterly trends apparent closer to the eastern margin of the marbles. The progressively more easterly trends suggests that earlier (likely D_{Y2} generation) fabrics were rotated into a new orientation with progressive strain. We therefore regard the fabrics in the eastern marbles to belong to an entirely different deformation generation, and, in fact, related to early stages of the presently active extensional deformation. Since we cannot discount the possibility of early Tertiary deformation in this area, we refer to this generation as D_{Y4}.

In the pure marbles, all fabrics are perfectly parallel and penetrative and kinematic indicators are absent. However, on the eastern margin of the Tiger-Leap transect, the mylonitic fabric is locally overprinted by chlorite-sericite (+/- phlogopite) brittle-ductile shear zones. These zones either anastomose around coherent, meter-scale

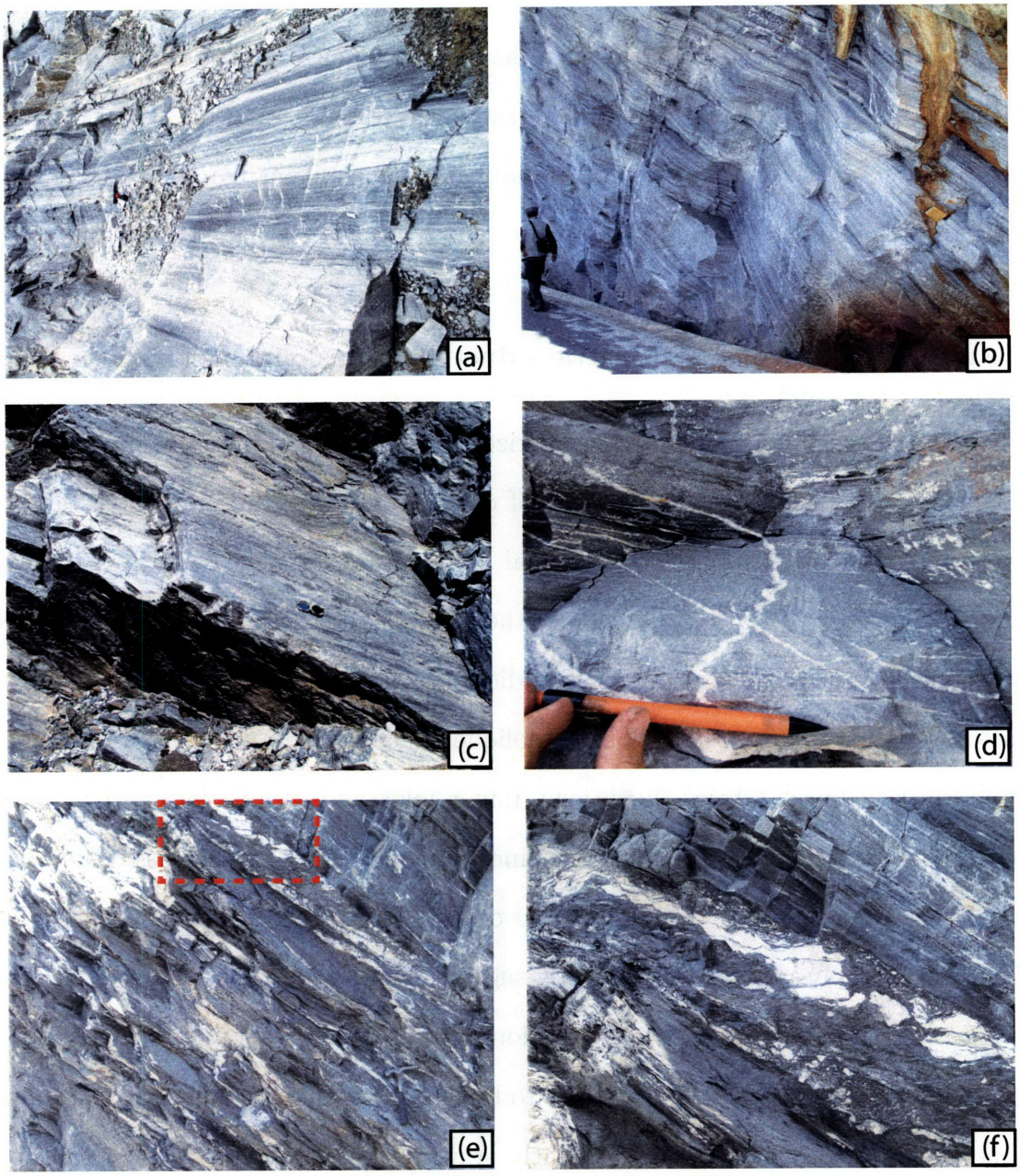

Figure 3-14: Mesoscale fabrics in mylonitic marbles. (a) Mylonitic marble on the west side of the Yulong mountains; (b) east dipping mylonitic marbles of the east side; (c) down dip lineation in eastern marbles; (d) progressively deformed vein sets in eastern marble, photo taken perpendicular to the foliation and parallel to the stretching lineation; (e) brittle-ductile shear zones overprinting marble mylonite; (f) close up of (e), showing top side down shear sense.

lenses of mylonite or form fabric-parallel zones. A wide variety of kinematic indicators are apparent in these zones (fig. 5-6). Where the brittle-ductile zones define meter-scale lenses of coherent marble, these are typically asymmetrical, whose asymmetry defines normal-sense, top to the east slip. Within east-dipping, fabric parallel zones, C/S fabrics, shear bands, σ and δ winged inclusions (of white calcite within a dark chloritic groundmass), domino structures and asymmetrical folds all indicate top to the east (normal sense) slip (*Hanmer and Passchier* (1991); *Simpson and Schmid* (1983) and references therein). Farther to the east, marbles become intensely fractured, and steep and eastward-dipping fracture sets dominate. These then transition into zones of breccia and fault gouge incorporating chloritic mafic material presumably derived from the Permian basalts exposed to the east. The area of breccia and fault gouge is coincident with the trace of the main range-bounding fault, an active normal or oblique normal fault that is defined by the obvious and spectacular facetted range front. The succession of progressively more brittle deformation, together with the normal-sense, top to the east kinematics reflects the exhumation of material in the footwalls of the range-bounding normal faults from depths at which calcite flows ductilely by dislocation glide or creep to the surface, where the deformation is associated with breccia and gouge related to the active range bounding normal faults.

Late antiformal refolding (D4b)

The gross antiformal structure of the range is the result of a late (F_{Y4b}) fold that we interpret as doming in the footwall of the range-bounding normal faults. The orientation of the F_{Y4b} hinge is well defined by the intersection of refolded S_{Y2} transposition fabrics and by best-fit girdles of oblique S2 axial planar cleavages measured in the weakly deformed mixed sand and mud metaclastic lithologies (fig. 3.6.1). The F_{Y4b} fold trends nearly north-south, and, where it is bisected by the Tiger Leap gorge, plunges shallowly ($\sim$10 deg) to the south. The overall structure, however, is doubly-

plunging: the fold plunges to the north at the northern end of the range, where Permian basalts are juxtaposed with weakly foliated carbonates across a north-dipping normal fault. The F_{Y4b} antiform is not associated with penetrative axial planar fabric development or mesoscale minor folds. The only mesoscale structures that can be plausibly related to the development of the late F_{Y4b} antiform (apart from the range-bounding normal faults, see below) is a locally developed steeply dipping pressure solution cleavage in quartzite near the middle of the transect (fig. 3.6.1h). L_{Y4a} linear fabrics in the eastern most mylonitic marbles are oblique to the inferred trend of the F_{Y4b} hinge, but we believe that late ductile shear of the east side marbles is kinematically and dynamically linked to the overall antiformal uplift of the range.

The doubly-plunging geometry of the late antiform produces an overall domal geometry to the range (fig. 3-15). Unlike earlier fabrics and structures, this deformation is entirely local to the Yulong mountains and, in particular, it is expressed only within the young and active faults bounding the range. Unlike *Lacassin et al.* (1996), we do not interpret the domal geometry as a the product of the interference of distinct fold generations. Late upright folds with east - west trending fold hinges and axial surfaces that would be required to produce the domal geometry are not present anywhere in the region. Instead, we believe that the doubly plunging geometry of the antiform is the product of a single tectonic episode, and is related to doming of the footwalls of the range-bounding normal faults. Since these faults are active, antiformal doming of the range is likely on-going. The abrupt steepening and narrowing of the Jinsha river as it crosses the bounding faults and steep hillslopes characterized by frequent large landsliding events represent geomorphic metrics of anomalously high uplift rates within the bounding normal faults that support this contention.

The crest of the antiform is coincident with the greatest amount of exhumation: where the Jinsha river flows out of the range, the bounding normal faults places unmetamorphosed middle Triassic rocks against a condensed, penetratively sheared

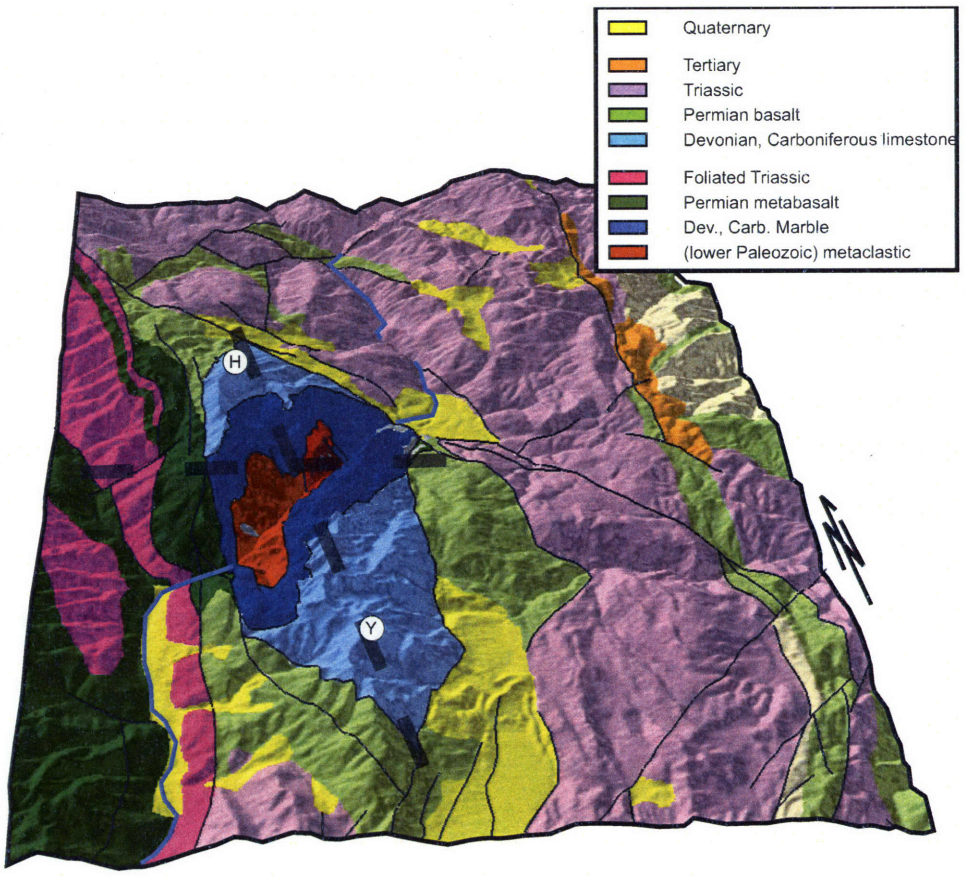

Figure 3-15: Oblique aerial view simulated by draping the geological map over a digital elevation model. View to the north, 1.5X vertical exaggeration. The Jinsha river is traced out in blue; thick dashed lines show the locations of the cross-sections of figures 3-9, 3-10. Circled letters show the locations of the Haba (5360m) and Yulong summits (5596m).

section of Permian phyllonite, which itself lies on the Devonian marble mylonite. This represents a stratigraphic separation of at least 4.5km, but this does not take into account the difference in metamorphic grade across the normal faults. At the northern and southern margins of the range, the bounding faults connect together in complex ways, but in both places the amount of separation across the faults is much lower. The northern margin of the range (the northern slopes of Haba mountain) is characterized by a moderate angle, domed normal fault reminiscent of the extensional "turtlebacks" of Death valley (*Wright et al.* (1974)), which places unmetamorphosed Permian Emeishan basalt above sheared, but not mylonitic, carbonate that is likely Devonian, but perhaps could be Carboniferous. The far less accessible southern margin of the range consists of a complex mosaic of steeper, intersecting faults. Here, unmetamorphosed Carboniferous limestone retaining many primary structures and unstrained fossils is juxtaposed against rocks from somewhere near the middle of Permian Emeishan basalt sequence. The lack of a marked difference in metamorphic grade makes stratigraphic separation a potentially useful measure of total vertical separation, but the lack of reliable marker beds in the Permian basalts complicates this estimate. However, since the total measured thickness of the Emeishan basalts in this area is reported as $\sim$ 3km (*BGMR Yunnan* (1990)), this represents a maximum estimate of vertical throw across these faults. Finally, we note that the maximum exhumation and the crest of the actively doming antiform is exactly coincident with the >3.5 km deep gorge which we feel suggests a causal link between uplift and the dramatic incision of the Jinsha river, similar to the links between river incision and doubly-plunging antiforms which have been noted in fold and thrust belts (eg. *Simpson* (2004) and references therein).

Active, brittle normal faulting

The Yulong mountains are located at the northern margin of a roughly 50km wide zone of active transtensional faulting extending from the town of Dali east to the Chenghai fault and bounded to the north by the extension of the Daju fault (fig. 3-3). Major faults include the Jianchuan, Lijiang and Daju faults and the entire zone is characterized by north-south trending normal and left-normal faults associated with narrow, elongate Quaternary basins linked by NE striking left-normal transtensional faults that act as transfer structures. The age of inception of these faults is not very well known. *Wang et al.* (1998) compiled palynological, paleontological and C14 ages from sediments in Quaternary basins associated with these faults. The oldest ages are Late Pliocene ($\sim$ 2.4 Ma) fossils and palynomorphs found in the Lijiang basin. We collected organic-rich material in small sag basins associated with normal and left-normal faults associated with the Yulong basins for palynological analysis. None of our samples yielded very tight age constraints, and all assemblages were consistent with Pliocene or younger ages (Appendix B). The Yulong mountains themselves are entirely contained within a network of normal and oblique left-normal faults that define a rhomb-shaped region between the Plio-Quaternary Lijiang basin, and the active Daju fault. While the most of the faults in the regional transtensional network from Dali to the Daju fault are associated with Plio-Quaternary basins, the Yulong mountains themselves are characterized by anomalously high elevations and extremely rugged topography in the footwall of the rhomb-shaped region defined by active normal faults.

The range-bounding faults are geomorphically well-expressed by steep, facetted scarps and are easily traced both in the field and on digital elevation models and satellite imagery. The range-bounding faults are not perfectly symmetrical. The western and southern boundary faults are defined by very steep cliff faces, vertical scarps and their traces are not deflected by the topography, notably the more than

3 kilometers of relief associated with the upstream side of Tiger Leap gorge. The eastern boundary is marked by an obvious, east-dipping surface and well-developed facets. South of the outlet of Tiger Leap gorge, the boundary fault (sometimes referred to as the Xueshan fault) strikes north-south and clear evidence of active faulting is evidenced by the (oblique normal) offset of glacial moraines and by scarps cut on landslide debris and colluvial material. At the outlet of Tiger Leap gorge the bounding fault (the Daju fault) assumes a northwest strike, and the obvious surface is sub-parallel to, if slightly steeper than, the east-dipping mylonites and brittle-ductile shear zones in its footwall. To the north, the Daju fault is connected with the western boundary fault on the north side of Haba mountain, and eventually connects with the active (?) trace of the left-lateral Zhongdian fault farther to the northwest. The eastern faults are more obviously active: beyond the considerable geomorphic evidence for activity, numerous large (M >5, including the 1996 M7 event) earthquakes are associated with these faults.

3.6.3 Unfoliated, unmetamorphosed Paleozoic rocks of the Yulong mountains

Despite the unparalled exposure and easy access it affords, rocks exposed in Tiger Leap gorge are not representative of all lithologies found within the Yulong mountains. At high elevations at the northern and southern margins of the range, rocks are unmetamorphosed and unfoliated limestones of Devonian and Carboniferous age. We interpret the marbles exposed in the Gorge are metamorphic equivalents of these distinctive massive and thickly bedded limestones. If this is correct, then the Yulong mountains appears to contain a juxtaposition of polydeformed metamorphic rocks with their unmetamorphosed equivalents. Extremely rugged and inaccessible terrain precluded a detailed investigation of this relationship (our mapping took us to elevations of 5400m, but without technical mountaineering equipment, this is only possible

in very few places). It appears that the lower Devonian limestones grade into weakly foliated carbonates which themselves overlie the mylonitic marbles with Devonian (and perhaps Carboniferous) protoliths. We propose that the entire stratigraphy was repeated by a major west-vergent thrust that overlies the west-closing recumbent syncline that deforms the foliated rocks currently exposed in Tiger Leap Gorge. On this interpretation, rocks of the First Bend region cropping out to the west of the Yulong mountains – which are as young as middle Triassic, were, at one point, in the footwall of a major west verging fault carrying unmetamorphosed South China rocks.

3.7 Summary of timing constraints

Throughout the paper, we have pointed out the available constraints on the age and timing of various rock units and structures. Here, we summarize these, and highlight their limitations.

Stratigraphy and protolith ages We rely on the established South China (Yangzi platform) stratigraphy, although we note that unit thicknesses are often reported as fairly broad ranges on Chinese survey maps and are often variable from sheet to sheet. Given the passive margin or continental platform setting that is inferred for deposition of rocks up until middle or late Triassic time, this is unlikely to be entirely real. Instead, it is likely a result of generally poor exposure in most of Sichuan and Yunnan provinces, coupled with a complex and protracted Mesozoic to Recent deformational history that remains poorly documented and understood. Nevertheless, the general stratigraphy is well-known and well-established, and we exploit it for the identification of the protoliths for most of the metamorphosed and penetratively deformed rocks exposed west of the Yulong mountains. Notably, the Shigu formation is likely the equivalent of the the upper Precambrian to lower Paleozoic clastic section; metaclastic rocks exposed in Tiger Leap gorge are likely lower Paleozoic (Cambrian

to Ordovician); pure marbles are probably derived from thick and massive Devonian and Carboniferous limestones. The thick Permian Emeishan basalts are similarly distinctive.

Regional Mesozoic tectonics We attempt to frame our interpretations of the ages of various fabrics and deformation generations in the context of what is known about regional tectonic events. In particular, middle Triassic suturing of South China with Lanping Simao along the Jinshajiang suture and Jurassic to Cretaceous compressional deformation related to the southward continuation of the Longmenshan orogen in Yunnan province represent two obvious candidates for interpreting the older deformation generations in these rocks. We suggest that early fabrics in the Shigu formation (Table 1: D_{Sg1}/D_{Sg2}) and foliated clastic rocks in Tiger Leap gorge (Table 2: D_{y1}) are related to the early Mesozoic deformation, an interpretation consistent with the work of *Reid et al.* (2005a,b), who concluded that early fabrics and metamorphism was Triassic in age. On the other hand, we submit that the characteristic recumbent folding and associated strong stretching lineations of all foliated First Bend rocks (D_{Sg3} in Shigu rocks, D_{Y2} in the Yulong mountains) probably reflect Longmenshan age (Jurassic–Cretaceous) deformation, for a number of reasons discussed below.

Early Tertiary sediments The presence of an angular unconformity in the early Tertiary Jianchuan basin is evidence for possibly significant deformation at this time. Unfortunately the lower Jianchuan basin strata are very poorly exposed, and it is impossible to say much about the nature or extent of this deformation. Rocks of the upper Jianchuan basin unconformably overlie both the lower Jianchuan sequence and the Shigu schists, but are only broadly warped and tilted. This limits the extent of significant upper crustal deformation later than when these rocks were laid down – before the intrusion of potassic sills and dykes from c.40 – 35 Ma.

Isotope geochronology Most of the foliated rocks in the First Bend area are low greenchist grade chlorite - sericite bearing rocks and there are few young igneous units, presenting few opportunities for isotope geochronology. Nevertheless, we have presented a handful of new Ar-Ar ages, including micas in leucogranites in the Shigu Formation, sanidine in sills and dykes intruding the Jianchuan basin sediments and phlogopite found in marbles exposed at the eastern margin of Tiger Leap gorge. We interpreted these ages as cooling, crystallisation and recrystallisation or alteration ages, respectively. In the Shigu rocks, micas yield c. 227 Ma ages, and are similar to the early Triassic Ar-Ar ages that *Reid et al.* (2005b) determined for metamorphic rocks north of the study area, along the Jinshajiang suture. A sill intruding the Jianchuan basin yielded a c. 40 Ma Ar-Ar age, and related rocks were dated using U-Pb as being c. 35 Ma *Zhang and Scharer* (1999).

Most difficult to interpret are the c. 32 Ma ages from phlogopite in the Yulong mountains. *Lacassin et al.* (1996) interpreted Rb-Sr ages from these rocks as reflecting recrystallization of the phlogopite during a major regional tectonic where the marbles formed the decollement to thrust fault systems propagating to the south. In our own mapping, we found very few unequivocally Tertiary aged reverse faults, characterized by very limited throw, and oriented north-south. Also, as noted above, $>$ 40 Ma rocks in the upper Jianchuan basin escaped major deformation, so we believe that early Tertiary deformation in this region was limited to relatively minor E-W directed compression. That is, while it is possible that these early Tertiary ages reflect recrystallization during deformation, our interpretation of the style and significance of early Tertiary deformation differs from *Lacassin et al.* (1996).

Quaternary basins Although imprecisely dated, the oldest sediments found in Quaternary basins associated with active transtensional faults provides a loose constraint for the inception of active transtensional faulting. Samples we collected for

palynological analysis found in fluvial sediments derived from the Yulong mountains failed to provide better constraints than reported by *Wang et al.* (1998): the oldest ages are late Pliocene ($\sim$ 2 - 2.4 Ma). Palynomorph assemblages in our samples are consistent with Quaternary ($>$ 1.8 Ma) or late Pliocene ages. Normal faults bounding the Yulong mountains are active and kinematically linked to this fault system, so these ages roughly constrain the inception of extension, antiformal doming and footwall uplift of the Yulong mountains.

3.8 Discussion: Tectonic evolution of the First Bend region

In this paper, we have combined compilation and review of existing published maps and reports on the local and regional geology with reconnaissance and detailed field checking and mapping to construct a first order interpretation of the structure and tectonic evolution of rocks in the vicinity of the First Bend of the Jinsha river. In particular, we have focussed on the highest grade rocks in the area (the Shigu formation), the best exposure of large amounts of physical and structural relief (the Yulong mountains and Tiger Leap Gorge) and Cenozoic sediments. By combining these perspectives, we are able to propose a reasonable interpretation of the tectonic history of the First Bend area.

3.8.1 Early Triassic metamorphism along the Jinsha suture

Ar-Ar ages of c. 227 Ma for micas in leucogranites intruding the relatively high grade schists of the Shigu formation are consistent with the range of ages reported by *Reid et al.* (2005b) for metamorphic rocks near the Jinshajiang suture north of our study area. In this area, early metamorphism and associated fabrics affected all rocks up to early Triassic in age, so the age of metamorphism is broadly constrained to be

between early and late Triassic age. This metamorphism is interpreted as being the result of the assembly of the Qiantang, Yidun arc and South China tectonic elements during the Indosinian orogeny (*Sengor and Natalin* (1996)).

3.8.2 Correlation of fabrics between the Yulong mountains and Shigu formation

Although we do not intend our labels for deformation generations (eg. D1, D2, etc.) for the Shigu formation rocks and Tiger Leap gorge rocks to exactly correspond, we do think that some of the deformation generations can be correlated between the two areas. We believe that early fabric development and metamorphism in the Yulong mountains (D_Y1) is part of a regional event and so correlates with the earlier fabrics observed in the Shigu rocks (D_Sg1, D_Sg2). These early fabrics are recumbently folded; these folds are themselves associated with a strong stretching and crenulation lineation which is the most striking fabric element in all foliated rocks from the Shigu schists (D_{Sg3}) to the rocks exposed in the core of the Yulong mountains (D_{Y2}). Clots of chlorite–sericite after thoroughly retrogressed garnet (in the Shigu schists) and chloritoid (?) in the Yulong rocks are folded about minor folds related to this deformation.

Not all deformation generations observed in these two areas have equivalents. The latest crenulation affecting the Shigu formation rocks – which we suspect is early Tertiary in age and somehow related to the angular unconformity in the Jianchuan basin – does not seem to have an obvious equivalent set of fabrics in the Tiger Leap gorge rocks. Similarly, late deformation related to (late Pliocene to present) extensional unroofing and antiformal doming is confined to the Yulong mountains, though brittle normal faults juxtaposing Shigu low grade phyllite and Devonian marbles may represent young reactivation of these contacts during an early stage of regional transtensional deformation.

3.8.3 The importance of late Mesozoic deformation

The most striking fabric elements in the foliated rocks in this area are related to recumbent folds that overprint early metamorphism and fabric development. In the Yulong mountains, foliated rocks with probable Paleozoic protoliths are found as the lower limb of a east-closing recumbent syncline structurally overlain by an unmetamorphosed section that ranges from Devonian to Permian in age. We interpret this relationship as a west-verging thrust, and submit that late fabrics and folds in the foliated rocks are related to compressional deformation. The timing of this deformation can only be loosely bracketed between the development of early fabrics (post-early Triassic and pre-227 Ma cooling) and the age of the weakly deformed Tertiary sediments of the Jianchuan basin that unconformably overlies the Shigu rocks. We propose that Longmenshan (Jurassic - Cretaceous) age deformation has affected these rocks. Elsewhere in Yunnan, the deposition and deformation of foreland basin sequences in the Sichuan and Chenghai basins provides a means of establishing the age. In the First Bend region, middle to late Mesozoic terrestrial sediments dominate the Lanpin-Simao tectonic element immediately to the west, but the possibility that significant terrane displacement related to the Ailao Shan shear zone (*Leloup et al.* (1995); *Replumaz and Tapponnier* (2003) occurred along a boundary between our study area and rocks in the Lanping-Simao complicates the possibility of linking the two. In the absence of a sedimentary record, constraining the age this deformational event recorded in unmetamorphosed or low grade rocks is a challenge. The late compressional deformation may have occurred as late as earliest Tertiary, raising the possibility of crustal thickening and high elevations in this area prior to Cenozoic deformation related to India-Asia collision.

3.8.4 Limited Cenozoic shortening and implications for crustal thickening

Our mapping has failed to find evidence for significant and widespread Cenozoic upper crustal shortening. Unequivocally Cenozoic reverse faults are isolated structures with limited amounts of throw. These structures are oriented north-south and accommodate east-west shortening, suggesting that they cannot be responsible for the regional topographic gradient from the high plateau to the north to near sea-level elevations to the south. Furthermore, the timing of river incsion into a regional low relief paleo-landscape observed at high elevations suggests that crustal thickening and consequent surface uplift in this area occurred in Miocene to Pliocene times (*Clark et al.* (in review); *Schoenbohm et al.* (in press); *Wang et al.* (1998)), much later than the age of Cenozoic shortening structures in this region. Leaving early Cenozoic shortening aside, the question remains: if there was relatively high topography created during Mesozoic compressional deformation, had this completely decayed by the time of late Cenozoic river incision? We look forward to paleoelevation studies of Tertiary sediments in this region to further constrain the evolution of crustal thickness and topography in this region.

Acknowledgements

We thank Sinan Akciz, Kip Hodges and Nick Austin for reading early drafts of this paper. Malcolm Pringle provided much appreciated help with the Ar-Ar geochronology. Funding for this study was provided by NSF Continental Dynamics grants EAR 0003571 and EAR 8904096. The first author was also supported by a graduate student fellowship from the Fonds de Recherche pour la Nature et les Technologies (Quebec).

References

Akamatsu, J., H. Morikawa, N. Nishimura, K. Onoue, M. Nakamura, N. Seto, M. Komazawa, L. Jiang, K. Li, Q. Luo, and Y. Wang (1998), Bedrock structure in Lijiang basin and its seismic effects, in *Effects of Surface Geology on Seismic Motion*, edited by K. Irikura, K. Kudo, H. Okada, and T. Sasatani, pp. 725–732.

Akciz, S. O. (2004), Structural and geochronological constraints on the ductile deformation observed along the Gaoligong Shan and Chong Shan shear zones, Yunnan (China), Ph.D. thesis, MIT.

Allen, C. R., K. Sieh, A. Gillespie, Y. Han, B. Zhang, and C. Zhu (1984), Red River and associated faults, Yunnan province, China: Quaternary geology, slip rates, and seismic hazard, *Geological Society of America Bulletin*, *95*(6), 686–700.

BGMR Yunnan (1990), *Yunnan Bureau of Geology and Mineral Resources*, 1:200000 Regional Map Series, various sheets.

Burchfiel, B., Z. Chen, Y. Liu, and L. Royden (1995), Tectonics of the Longmen Shan and adjacent regions, central China, *International Geology Review*, *37*, 661–735.

Burchfiel, B. C., Z. Chen, et al. (In prep.), Tectonostratigraphic map of eastern Tibet and Yunnan province, map and accompanying notes in preparation.

Chen, Y. T., and L. S. Xu (2000), A time-domain inversion technique for the tempospatial distribution of slip on a finite fault plane with applications to recent large earthquakes in the Tibetan Plateau, *Geophysical Journal International*, *143*, 407–416, doi:10.1046/j.1365-246X.2000.01263.x.

Chen, Z., B. C. Burchfiel, Y. Liu, R. W. King, L. H. Royden, W. Tang, E. Wang, J. Zhao, and X. Zhang (2000), Global positioning system measurements from eastern Tibet and their implications for India/Eurasia intercontinental deformation, *Journal of Geophysical Research*, *105*(B7), 16,215–16,228.

Chung, S.-L., T.-Y. Lee, C.-H. Lo, P.-L. Wang, C.-Y. Chen, N. T. Yem, T. T. Hoa, and W. Genyao (1997), Intraplate extension prior to continental extrusion along the Ailao Shan-Red River shear zone, *Geology*, *25*, 311–314.

Clark, M. K. (2003), Late Cenozoic uplift of southeastern Tibet, Ph.D. thesis, MIT.

Clark, M. K., and L. H. Royden (2000), Topographic ooze: building the eastern margin of Tibet by lower crustal flow, *Geology*, *28*, 703–706.

Clark, M. K., M. A. House, L. H. Royden, K. X. Whipple, B. C. Burchfiel, X. Zhang, and W. Tang (2005), Late Cenozoic uplift of southeastern Tibet, *Geology*, *33*(6), 525–528.

Clark, M. K., L. H. Royden, K. X. Whipple, B. C. Burchfiel, X. Zhang, and W. Tang (in review), Deformation of a regional low-relief relict lanscape (erosion surface) in eastern Tibet, *Journal of Geophysical Research - Earth Surface*.

Cong, D. C., and K. Feigl (1999), Geodetic measurement of horizontal strain across the Red River fault near Thac Ba, Vietnam, 1963-1994, *Journal of Geodesy*, *73*(6), 298–310, doi:10.1007/s001900050247.

Dalrymple, G. B., and W. A. Duffield (), High precision ^{40}ar/^{39}ar dating of Oligocene rhyolites from the Mogollon-Datil volcanic field using a continuous laser system, *Geophysical Research Letters*, pp. 463–466.

Dewey, J., S. Cande, and W. Pitman (1989), The tectonic evolution of the India/Eurasia collision zone., *Ecolgae Geologicae Helvetiae*, *82*, 717–734.

England, P., and P. Molnar (1990), Right-lateral shear and rotation as the explanation for strike-slip faulting in eastern Tibet, *Nature*, *344*, 140–142.

Geissman, J., B. C. Burchfiel, C. Studnicki-Gizbert, S. Akciz, and L. Chen (submitted), Complexities in the early Cenozoic extrusion of crustal fragments around the eastern Himalayan syntaxis, *Geosphere*.

Geissman, J. W., L. Chen, J. Yin, and B. Burchfiel (2001), Paleomagnetic Data Bearing on Tectonic Rotations in Northern Indochina South of the Ailao Shan Shear Zone, *AGU Fall Meeting Abstracts*, pp. A296+.

Hallet, B., and P. Molnar (2001), Distorted drainage basins as markers of crustal strain east of the Himalaya, *Journal of Geophysical Research*, *106*(B7), 13,697–13,710.

Hanmer, S., and C. W. Passchier (1991), *Shear sense indicators: a review*, Paper 90 - 17, Geological Survery of Canada.

He, H., and E. Tsukuda (2003), Recent progresses of active fault research in China, *Journal of Geography (Tokyo Geog. Soc.)*, *112*, 489–520.

He, H., T. Oguchi, R. Zhou, J. Zhang, and S. Qiao (2001), Damage and seismic intensity of the 1996 Lijiang earthquake, China: A GIS analysis, *Tech. rep.*, Center for Spatial Information Science, University of Tokyo, Tokyo, Japan.

Holt, W. E., N. Chamot-Rooke, X. L. Pichon, A. J. Haines, B. Shen-Tu, and J. Ren (2000), Velocity field in Asia inferred from Quaternary fault slip rates and global positioning system observations, *Journal of Geophysical Research*, *105*(B8), 19,185–19,210.

Hsu, K., S. Sun, J. Li, H. Chen, H. Pen, and A. M. C. Sengor (1988), Mesozoic overthrust tectonics in South China, *Geology*, *16*, 418–421.

Huang, M., R. Maas, I. S. Buick, and I. S. Williams (2003), Crustal response to continental collisions between the Tibet, Indian, South China and North China Blocks: geochronological constraints from the Songpan-Garze orogenic belt, western China, *Journal of Metamorphic Geology*, *21*, 223–240, doi:10.1046/j.1525-1314.2003.00438.x.

Hughes, N., S. Peng, and H. Luo (2002), Kunmingaspis (Trilobita) putatively from the Yunling Collage and the Cambrian history of the Eastern Himalayan syntaxial region, *Journal of Paleontology*, *76*(4), 709–717.

King, R., F. Shen, B. Burchfiel, L. Royden, E. Wang, Z. Chen, Y. Liu, X. Zhang, J. Zhao, and Y. Li (1997), Geodetic measurement of crustal motion in southwest China, *Geology*, *32*, 809–812.

Lacassin, R., U. SchÃrer, P. H. Leloup, N. Arnaud, P. Tapponier, X. Liu, and L. Zhang (1996), Tertiary deformation and metamorphism SE of Tibet: The folded Tiger-leap decollement of NW Yunnan, China, *Tectonics*, *15*(3), 605–622.

Leloup, P. H., R. Lacassin, P. Tapponnier, U. Scharer, D. Zhong, X. Liu, L. Zhang, S. Ji, and P. T. Trinh (1995), The Ailao Shan-Red River shear zone (Yunnan, China), Tertiary transform boundary of Indochina, *Tectonophysics*, *251*(1-4), 3–84, doi:10.1016/0040-1951(95)00070-4.

Leloup, P. H., N. Arnaud, R. Lacassin, J. R. Kienast, T. M. Harrison, T. T. P. Trong, A. Replumaz, and P. Tapponnier (2001), New constraints on the structure, thermochronology, and timing of the Ailao Shan-Red River shear zone, SE Asia, *Journal of Geophysical Research*, *106*(B4), 6683–6732.

Meng, Q.-R., E. Wang, and J.-M. Hu (2005), Mesozoic sedimentary evolution of the northwest Sichuan basin: Implication for continued clockwise rotation of the South China block, *Geological Society of America Bulletin*, *117*, 396–410, doi: 10.1130/B25407.1.

Metcalfe, I. (1998), Palaeozoic and Mesozoic geological evolution of the SE Asian region: multidisciplinary constraints and implications for biogeography, in *Biogeography and Geological Evolution of SE Asia*, edited by R. Hall and J. Holloway, pp. 25–41, Backhuys Publishers, Leiden , the Netherlands.

Reid, A., C. Wilson, and S. Liu (2005a), Structural evidence for the Permian-Triassic tectonic evolution of the Yidun Arc, eastern Tibet, *Journal of Structural Geology*, *27*, 119–137, doi:10.1016/j.jsg.2004.06.011.

Reid, A. J., C. J. Wilson, D. Phillips, and S. Liu (2005b), Mesozoic cooling across the Yidun Arc, central-eastern Tibetan Plateau: A reconnaissance 40Ar/39Ar study, *Tectonophysics*, *398*(1-2), 45–66, doi:10.1016/j.tecto.2005.01.002.

Renne, P. R., C. C. Swisher, A. L. Deino, D. B. Karn, T. Owens, and D. J. DePaolo (1998), Intercalibration of standards, absolute ages and uncertainties in $^{40}Ar/^{39}Ar$ dating, *Chemical Geology*, *145*, 117–152.

Replumaz, A., and P. Tapponnier (2003), Reconstruction of the deformed collision zone between India and Asia by backward motion of lithospheric blocks, *Journal of Geophysical Research*, *108*(B6), 2285+, doi:10.1029/2001JB000661.

Replumaz, A., R. Lacassin, P. Tapponnier, and P. H. Leloup (2001), Large river offsets and Plio-Quaternary dextral slip rate on the Red River fault (Yunnan, China), *Journal of Geophysical Research*, *106*(B1), 819–836.

Roger, F., N. Arnaud, S. Gilder, P. Tapponnier, M. Jolivet, M. Brunel, J. Malavieille, Z. Xu, and J. Yang (2003), Geochronological and geochemical constraints on Mesozoic suturing in east central Tibet, *Tectonics*, *22*(4), 1037+, doi: 10.1029/2002TC001466.

Sato, K., Y. Liu, Z. Zhu, Z. Yang, and Y. Otofuji (2001), Tertiary paleomagnetic data from northwestern Yunnan, China: further evidence for large clockwise rotation of the Indochina block and its tectonic implications, *Earth and Planetary Science Letters*, *185*, 185–198.

Schoenbohm, L., B. C. Burchfiel, and L. Chen (in press), Propagation of surface uplift, lower crustal flow, and Cenozoic tectonics of the southeast margin of the Tibetan plateau, *Geology*.

Schoenbohm, L. M., C. B. Burchfiel, C. Liangzhong, and Y. Jiyun (2005), Exhumation of the Ailao Shan shear zone recorded by Cenozoic sedimentary rocks, Yunnan Province, China, *Tectonics*, *24*, TC6015+, doi:10.1029/2005TC001803.

Schoenbohm, L. M., C. B. Burchfiel, L. Chen, and J. Yin (2006), Miocene to present activity along the Red River fault, China, in the context of continental extrusion, upper-crustal rotation, and lower-crustal flow., *Geological Society of America Bulletin*, doi:10.1130/B25816.1.

Sengor, A. M. C., and B. A. Natalin (1996), Paleotectonics of Asia: fragments of a synthesis, in *The Tectonic Evolution of Asia*, edited by A. Yin and M. Harrison, pp. 486–641, Cambridge University Press.

Shen, Z.-K., J. LÃ, M. Wang, and R. BÃrgmann (2005), Contemporary crustal deformation around the southeast borderland of the Tibetan Plateau, *Journal of Geophysical Research*, *110*, B11,409+, doi:10.1029/2004JB003421.

Simpson, C., and S. Schmid (1983), An evaluation of criteria to deduce the sense of movement in sheared rocks, *Geological Society of America Bulletin*, *94*(11), 1281–1288.

Simpson, G. (2004), Role of river incision in enhancing deformation, *Geology*, *32*, 341–344.

Socquet, A., and M. Pubellier (2004), Cenozoic deformation in western Yunnan (China–Myanmar border), *Journal of Asian Earth Sciences*, *24*, 495–515.

Tamai, M., Y. Liu, L. Z. Lu, M. Yokoyama, N. Halim, H. Zaman, and Y.-i. Otofuji (2004), Palaeomagnetic evidence for southward displacement of the Chuan Dian fragment of the Yangtze Block, *Geophysical Journal International*, *158*, 297–309.

Thompson, G. M., J. R. Ali, X. Song, and D. W. Jolley (2001), Emeishan basalts, SW China: reappraisal of the formation's type area stratigraphy and a discussion of its significance as a large igneous province, *Journal of the Geological Society, 158*, 593–599.

Wallis, S., T. Tsujimori, M. Aoya, T. Kawakami, K. Terada, K. Suzuki, and J. Hyodo (2003), Cenozoic and Mesozoic metamorphism in the Longmenshan orogen: Implications for geodynamic models of eastern Tibet, *Geology, 31*(9), 745–748, doi:10.1130/G19562.1.

Wang, E., and B. Burchfiel (1997), Interpretation of Cenozoic tectonics in the right-lateral accomodation zone between the Ailao Shan shear zone and the eastern Himalayan syntaxis, *International Geology Review, 39*, 191–219.

Wang, E., and C. C. Burchfiel (2000), Late Cenozoic to Holocene deformation in southwestern Sichuan and adjacent Yunnan, China, and its role in formation of the southeastern part of the Tibetan Plateau, *Geological Society of America Bulletin, 112*, 413–423.

Wang, E., B. Burchfiel, L. Royden, L. Chen, J. Chen, W. Li, and Z. Chen (1998), *Late Cenozoic Xianshuihe-Xiaojiang, Red River, and Dali Fault Systems of Southwestern Sichuan and Central Yunnan, China, GSA Special Paper*, vol. 327, Geological Society of America.

Wang, J.-H., A. Yin, T. M. Harrison, M. Grove, Y.-Q. Zhang, and G.-H. Xie (2001), A tectonic model for Cenozoic igneous activities in the eastern Indo-Asian collision zone, *Earth and Planetary Science Letters, 188*(1-2), 123–133, doi:10.1016/S0012-821X(01)00315-6.

Weldon, R., K. Sieh, C. Zhu, Y. Han, J. Yang, and S. Robinson (), Slip rate and recurrence interval of earthquakes on the Hong He (Red River) fault, Yunnan, PRC.

Wright, L., J. Otton, and B. Troxel (1974), Turtleback surfaces of Death Valley viewed as phenomena of extensional tectonics, *Geology, 2*(2), 53–54.

Yan, D., M. Zhou, H. Song, and Z. Fu (2003), Structural style and tectonic significance of the Jianglang dome in the eastern margin of the Tibetan plateau, China, *Journal of Structural Geology, 25*, 765–779.

Yoshioka, S., Y. Liu, K. Sato, H. Inokuchi, L. Su, H. Zaman, and Y. Otofuji (2003), Paleomagnetic evidence for post-Cretaceous internal deformation of the Chuan Dian Fragment in the Yangtze block: a consequence of indentation of India into Asia, *Tectonophysics, 376*(1-2), 61–74.

Zhang, L.-S., and U. Scharer (1999), Age and origin of magmatism along the Cenozoic Red River shear belt, China, *Contributions to Mineralogy and Petrology, 134*, 67–85.

Zhang, P.-Z., Z. Shen, M. Wang, W. Gan, R. Bürgmann, P. Molnar, Q. Wang, Z. Niu, J. Sun, J. Wu, S. Hanrong, and Y. Xinzhao (2004), Continuous deformation of the Tibetan plateau from global positioning system data, *Geology*, *32*, 809–812.

Appendix: $^{40}Ar/^{39}Ar$ geochronology

$^{40}Ar/^{39}Ar$ ages were determined by dating feldspar phenocrysts in the Jianchuan basin sills, biotite and muscovite from coarse grained leucogranite dykes intruding the Shigu formation schists and coarse phlogopite present along rare partings in the Yulong mountains marbles. Samples prepared using standard mineral separation techniques. Samples were coarsely crushed, and sieved. Biotite, muscovite, phlogopite and K-feldspar minerals were separated using electromagnetic techniques, heavy liquids and hand-picking. Feldspar concentrates were ultrasonically etched c. 10% HF acid for 5-7 mins. All concentrates were further cleaned in ultrasonically with distilled water and ethanol, re-sieved, and re-picked to approximately 99% purity.

The final separates were packed in copper foil and irradiated in the McMaster University reactor, Canada without Cd-shielding. For all samples, argon was extracted from the irradiated samples by step-heating of bulk samples using a double vacuum resistance furnace, and measured using a MAP 215-50 rare gas mass spectrometer equipped with a Johnson MM-1 electron multiplier operated at a gain of c. 10,000. Values for the irradiation parameter J were determined relative to 28.34 Ma for co-irradiated Taylor Creek sanidine (*Dalrymple and Duffield*; *Renne et al.* (1998)), and is known to better than 0.25% (1σ) for all samples. Corrections for interfering reactions were 0.000672 for 39Ar/37Ar(Ca), 0.000280 for 36Ar/37Ar(Ca), and 0.025 for 40Ar/39Ar(K).

$^{40}Ar/^{39}Ar$ model ages for each gas extraction step were calculated assuming an initial $^{40}Ar/^{39}Ar$ value of 295.5 and are assigned a 2σ uncertainty that reflects propagated analytical errors and the reactor flux monitor J. Release spectra illustrate model

ages for step-heating analyses as a function of the amount of ^{39}Ar released in each step. Plateau ages are defined as comprising at least 3 consecutive steps representing more than 50% of the total ^{39}Ar gas released and whose ages are within 2σ error of the weighted mean value.

Biotite from the Shigu formation leucogranites and phlogopite from the Yulong marbles has release spectra which failed to meet the criteria for a plateau age. We calculated ages from linear fits of the data on $^{36}Ar/^{40}Ar$ versus $^{39}Ar/^{40}Ar$ isotope correlation diagrams. Failing a statistically significant age determination from either age spectra or inverse isochron plots, a total gas age is calculated from the pooled age from all heating steps and is equivalent to a conventional K/Ar age.

3.8.5 Plots and data tables

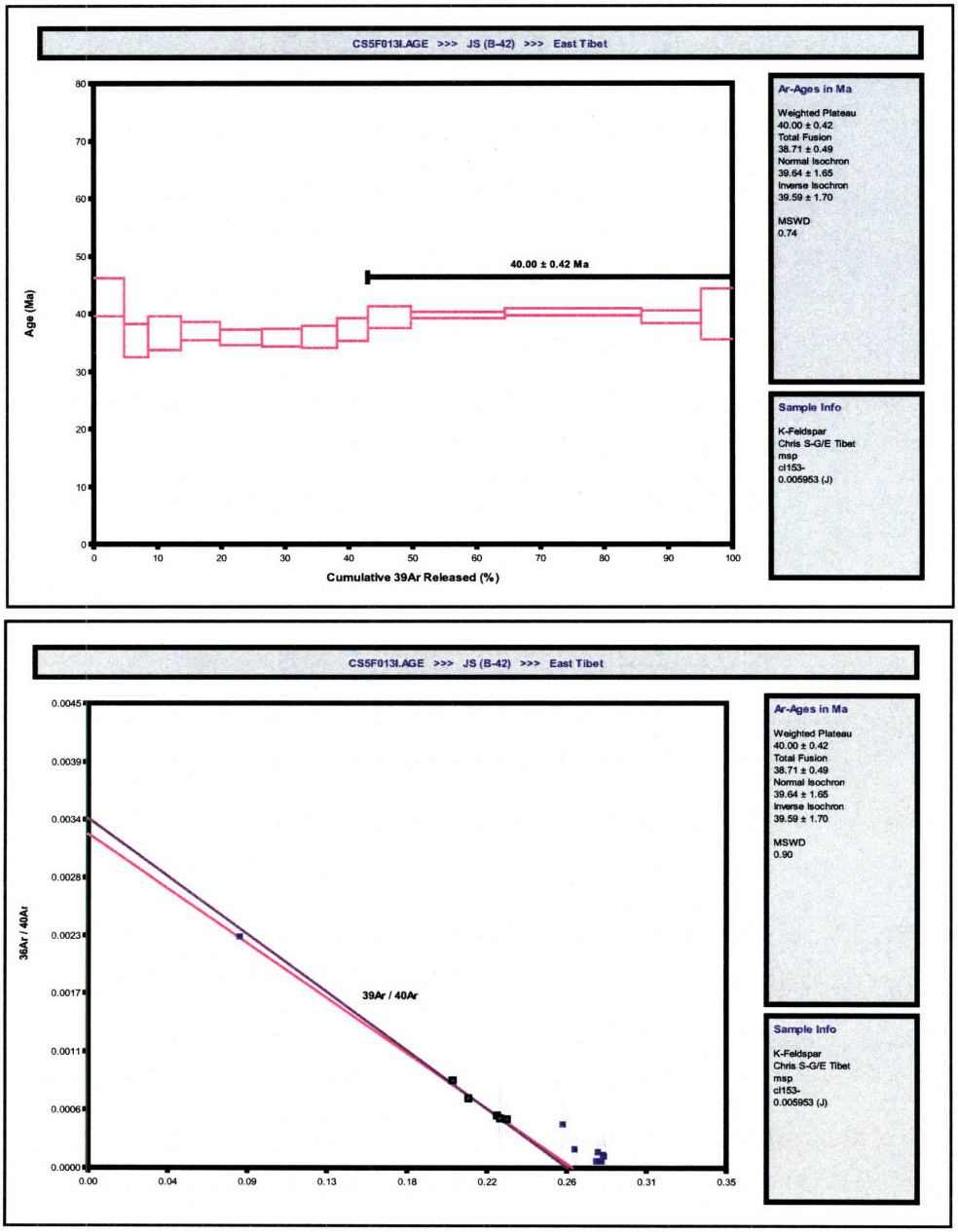

Figure 3-16: Plateau and inverse isochron plots for Jianchuan basin sills

Incremental Heating		36Ar(a)	37Ar(ca)	38Ar(cl)	39Ar(k)	40Ar(r)	Age (Ma)	2σ	40Ar(r) (%)	39Ar(k) (%)	K/Ca	2σ
5F013I.01	973 C	0.00103	0.00888	0.00418	0.03887	0.15726	42.93	3.32	33.92	4.70	2.145	0.247
5F013I.02	1023 C	0.00005	0.00824	0.00036	0.03121	0.10394	35.42	2.89	87.01	3.77	1.856	0.116
5F013I.04	1123 C	0.00001	0.01052	0.00031	0.04296	0.14817	36.66	2.97	97.49	5.19	2.001	0.269
5F013I.05	1173 C	0.00001	0.01122	0.00033	0.05079	0.17696	37.03	1.56	97.41	6.14	2.219	0.095
5F013I.06	1223 C	0.00003	0.01024	0.00034	0.05460	0.18466	35.96	1.31	94.87	6.60	2.613	0.104
5F013I.07	1273 C	0.00002	0.00772	0.00027	0.05125	0.17292	35.87	1.52	95.67	6.19	3.253	0.165
5F013I.08	1323 C	0.00002	0.00586	0.00025	0.04530	0.15354	36.04	1.91	96.12	5.47	3.787	0.362
5F013I.09	1373 C	0.00003	0.00361	0.00050	0.04026	0.14133	37.32	1.97	94.02	4.87	5.461	0.837
5F013I.10	1433 C	0.00011	0.00529	0.00196	0.05563	0.20648	39.42	1.87	85.60	6.72	5.154	0.750
5F013I.11	1493 C	0.00027	0.00809	0.00535	0.12139	0.45528	39.84	0.58	84.61	14.67	7.351	0.711
5F013I.12	1573 C	0.00056	0.01921	0.00713	0.17714	0.67311	40.36	0.58	79.75	21.41	4.518	0.140
5F013I.13	1673 C	0.00032	0.01702	0.00378	0.07739	0.28797	39.53	1.07	74.78	9.35	2.229	0.073
5F013I.14	1873 C	0.00008	0.01888	0.00330	0.04065	0.15300	39.98	4.42	85.45	4.91	1.055	0.029

Table 3.3: Data table for sample JS, Jianchuan basin sill.

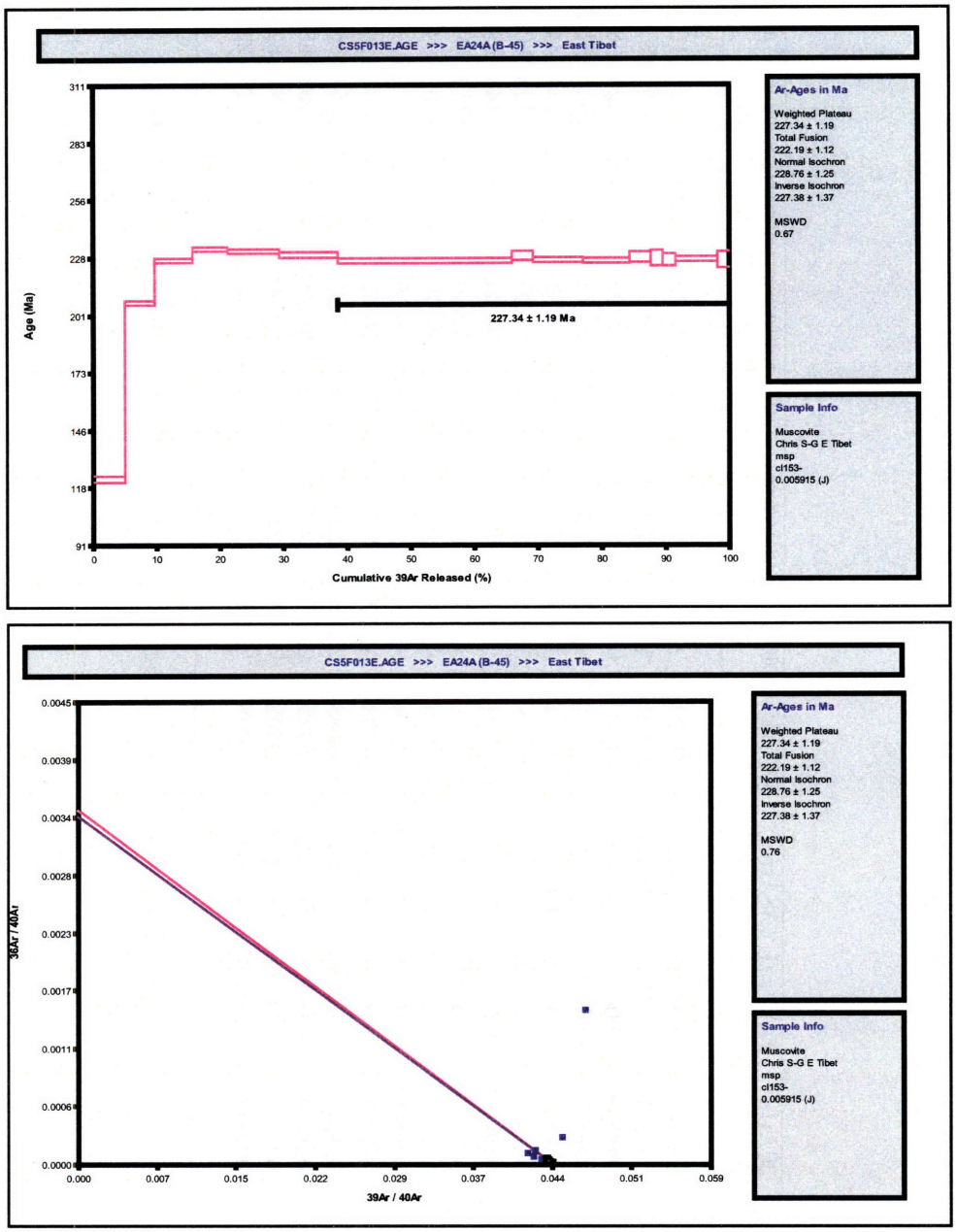

Figure 3-17: Plateau and isochron for muscovite from leucogranites intruding Shigu formation schists

Incremental Heating		36Ar(a)	37Ar(ca)	38Ar(cl)	39Ar(k)	40Ar(r)	Age (Ma)	2σ	40Ar(r) (%)	39Ar(k) (%)	K/Ca	2σ
5F013C.1	660 C	0.00781	0.00325	0.00254	0.24529	2.91099	122.39	1.66	55.72	4.92	37.016	8.972
5F013C.2	710 C	0.00139	0.00116	0.00095	0.23494	4.82677	206.90	1.05	92.06	4.71	99.184	77.082
5F012C.3	750 C	0.00096	0.00122	0.00087	0.30110	6.82873	227.10	1.02	95.90	6.04	120.498	65.777
5F013D.1	780 C	0.00070	0.00023	0.00069	0.27334	6.35796	232.56	1.08	96.74	5.48	578.801	2124.125
5F013D.2	800 C	0.00074	0.00149	0.00088	0.40884	9.46175	231.46	0.95	97.63	8.20	134.344	81.965
5F013D.3	820 C	0.00050	0.00180	0.00103	0.45318	10.41132	229.87	1.31	98.49	9.09	123.560	196.127
5F013D.4	840 C	0.00165	0.00466	0.00283	1.36884	31.02328	226.96	1.05	98.34	27.45	143.808	115.802
5F013E.1	870 C	0.00004	0.00071	0.00019	0.16471	3.77381	229.28	2.24	99.60	3.30	114.059	1236.632
5F013E.2	900 C	0.00012	0.00182	0.00071	0.39259	8.90563	227.15	1.14	99.49	7.87	105.894	121.568
5F013E.3	940 C	0.00010	0.00226	0.00062	0.36520	8.27876	227.01	1.08	99.55	7.32	79.227	104.873
5F013E.4	980 C	0.00002	0.00082	0.00025	0.16293	3.72036	228.55	2.50	99.77	3.27	97.176	217.027
5F013E.5	1020 C	0.00002	0.00082	0.00019	0.09168	2.08866	228.06	3.78	99.61	1.84	54.656	122.065
5F013E.7	1120 C	0.00009	0.00026	0.00025	0.10329	2.34361	227.21	2.82	98.78	2.07	194.883	1427.244
5F013E.8	1200 C	0.00014	0.00198	0.00066	0.33005	7.50354	227.62	1.25	99.36	6.62	81.482	131.979
5F013E.9	1400 C	0.00008	0.00192	0.00024	0.09098	2.06429	227.20	3.87	98.78	1.82	23.223	31.407

Table 3.4: Data table for muscovite from leucogranites intruding Shigu formation schists

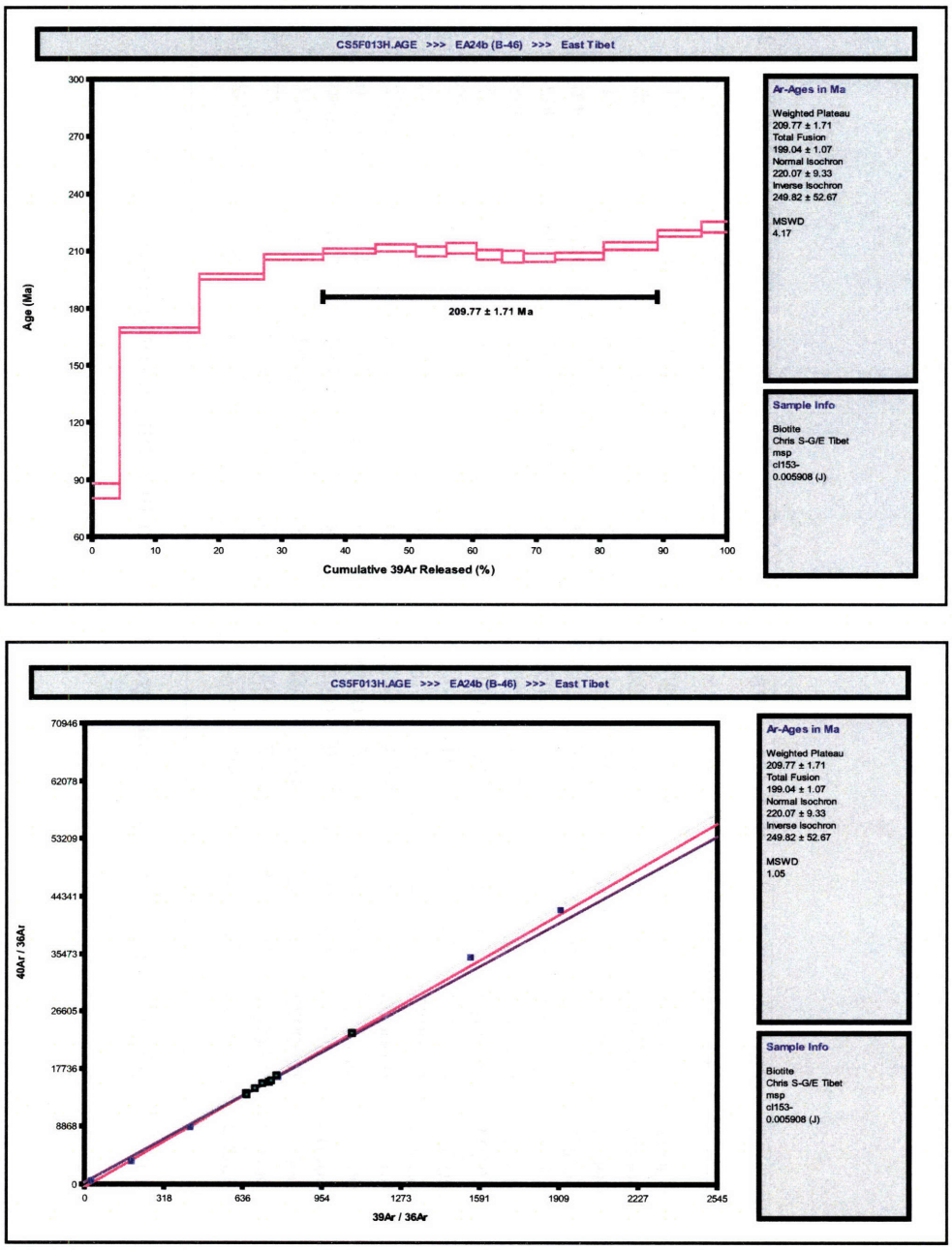

Figure 3-18: Plateau and inverse isochron plots for biotite from leucogranites intruding Shigu formation schists.

Incremental Heating		36Ar(a)	37Ar(ca)	38Ar(cl)	39Ar(k)	40Ar(r)	Age (Ma)	2σ	40Ar(r) (%)	39Ar(k) (%)	K/Ca	2σ
5F013H.01	873 C	0.00097	0.00029	0.00037	0.02576	0.20821	84.17	3.91	41.97	4.32	44.011	76.675
5F013H.02	973 C	0.00039	0.00041	0.00063	0.07493	1.24287	168.66	1.33	91.29	12.57	89.705	150.352
5F013H.03	1003 C	0.00014	0.00045	0.00051	0.06115	1.19250	196.74	1.29	96.46	10.26	66.871	137.524
5F013H.04	1033 C	0.00007	0.00042	0.00046	0.05561	1.14496	207.09	1.46	98.08	9.33	64.566	131.174
5F013H.05	1063 C	0.00007	0.00021	0.00041	0.04923	1.02962	210.20	1.31	97.87	8.26	116.062	249.941
5F013H.06	1093 C	0.00005	0.00026	0.00029	0.03762	0.79345	211.83	1.87	98.11	6.31	69.958	216.725
5F013H.07	1133 C	0.00004	0.00010	0.00019	0.02902	0.60644	210.04	2.69	97.76	4.87	142.167	764.420
5F013H.08	1173 C	0.00004	0.00009	0.00018	0.02804	0.59121	211.80	2.78	97.97	4.70	144.752	5160.460
5F013H.09	1203 C	0.00003	0.00035	0.00020	0.02345	0.48552	208.21	2.67	98.00	3.93	32.953	87.725
5F013H.10	1233 C	0.00003	0.00003	0.00013	0.02054	0.42326	207.30	3.01	97.74	3.44	342.862	13178.600
5F013H.11	1273 C	0.00004	0.00015	0.00026	0.02915	0.59887	206.66	2.13	97.73	4.89	93.496	814.967
5F013H.12	1313 C	0.00006	0.00030	0.00041	0.04589	0.94716	207.58	1.85	98.02	7.70	76.080	75.036
5F013H.13	1353 C	0.00005	0.00033	0.00046	0.05060	1.07103	212.58	2.03	98.61	8.49	74.941	355.308
5F013H.14	1393 C	0.00002	0.00022	0.00038	0.04147	0.90776	219.40	1.53	99.19	6.96	94.177	196.076
5F013H.15	1473 C	0.00002	0.00002	0.00023	0.02368	0.52655	222.65	2.75	99.04	3.97	640.762	49304.485

Table 3.5: Data table for muscovite from leucogranites intruding Shigu formation schists

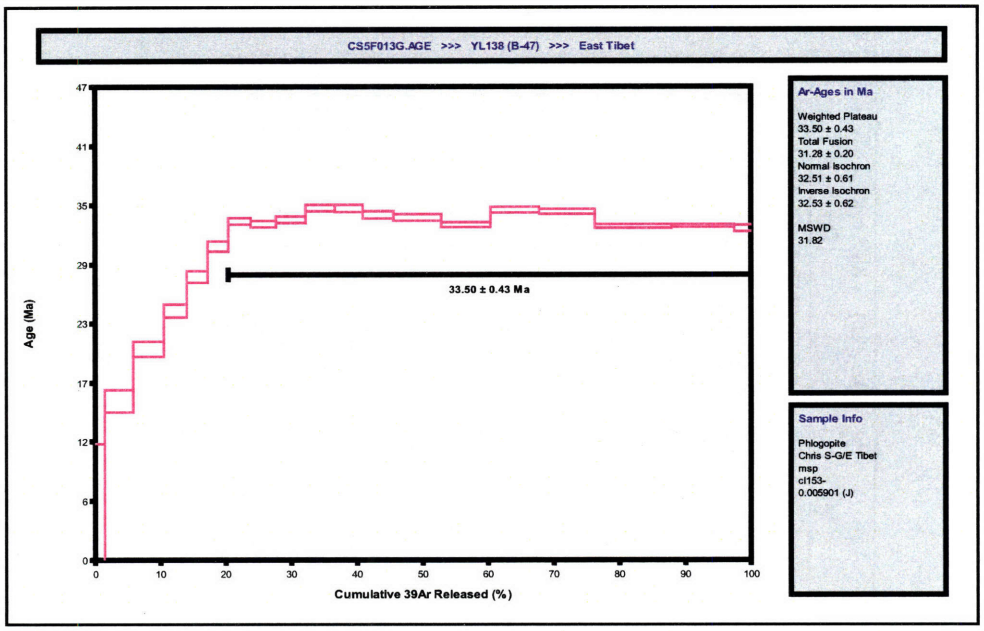

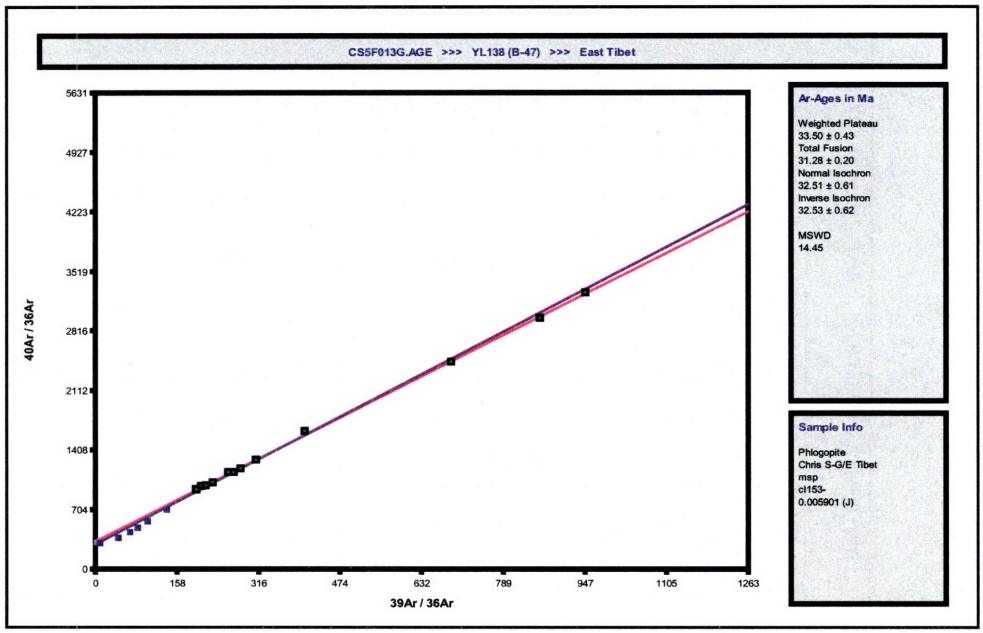

Figure 3-19: Plateau and inverse isochron plots for sample YL-138A, phlogopite from marbles in the Yulong mountains. Neither the age spectra nor inverse isochron ages yield interpretable ages, and we use the total gas fusion age for this sample.

Incremental Heating		36Ar(a)	37Ar(ca)	38Ar(cl)	39Ar(k)	40Ar(r)	Age (Ma)	2s	40Ar(r) (%)	39Ar(k) (%)	K/Ca	2s
5F013G.01	551 C	0.03246	0.00719	0.00271	0.27947	0.14442	5.49	5.93	1.48	1.47	19.045	2.010
5F013G.02	650 C	0.01802	0.02297	0.00285	0.82005	1.21374	15.69	1.14	18.50	4.31	17.495	0.762
5F013G.03	700 C	0.01314	0.02399	0.00251	0.88686	1.74605	20.84	0.78	30.89	4.66	18.113	0.748
5F013G.04	730 C	0.00811	0.01471	0.00180	0.66636	1.54994	24.59	0.65	39.11	3.50	22.199	1.387
5F013G.05	760 C	0.00602	0.01019	0.00144	0.61099	1.61571	27.93	0.57	47.40	3.21	29.386	2.878
5F013G.06	790 C	0.00434	0.00910	0.00145	0.60397	1.77050	30.94	0.48	57.73	3.18	32.528	2.721
5F013G.08	850 C	0.00210	0.00721	0.00152	0.65504	2.07366	33.39	0.31	76.51	3.44	44.504	5.281
5F013G.09	880 C	0.00259	0.00932	0.00189	0.73068	2.29640	33.15	0.33	74.58	3.84	38.399	4.304
5F013G.10	910 C	0.00369	0.01362	0.00196	0.84460	2.68658	33.55	0.34	70.71	4.44	30.376	2.161
5F013G.11	940 C	0.00417	0.01626	0.00214	0.85737	2.82196	34.70	0.32	69.23	4.51	25.830	1.564
5F013G.12	970 C	0.00421	0.01665	0.00190	0.82048	2.69926	34.69	0.35	68.11	4.31	24.147	1.344
5F013G.13	1000 C	0.00446	0.01698	0.00225	0.87822	2.83422	34.03	0.35	67.91	4.62	25.346	1.253
5F013G.14	1040 C	0.00649	0.02301	0.00328	1.39200	4.45828	33.78	0.30	69.54	7.32	29.646	1.648
5F013G.15	1080 C	0.00534	0.01846	0.00326	1.43687	4.50680	33.09	0.25	73.64	7.55	38.149	2.601
5F013G.16	1120 C	0.00544	0.02427	0.00313	1.40417	4.59693	34.52	0.26	73.69	7.38	28.355	1.323
5F013G.17	1160 C	0.00398	0.01744	0.00353	1.61473	5.25531	34.32	0.21	81.19	8.49	45.370	2.134
5F013G.18	1200 C	0.00322	0.01407	0.00484	2.22173	6.92924	32.90	0.16	87.30	11.68	77.359	6.183
5F013G.19	1270 C	0.00191	0.01280	0.00426	1.81353	5.66401	32.95	0.16	90.28	9.53	69.413	4.581
5F013G.20	1400 C	0.00056	0.00289	0.00113	0.48315	1.49767	32.70	0.32	89.39	2.54	81.850	21.741

Table 3.6: Data table for sample YL-138A, phlogopite from marbles in the Yulong mountains.

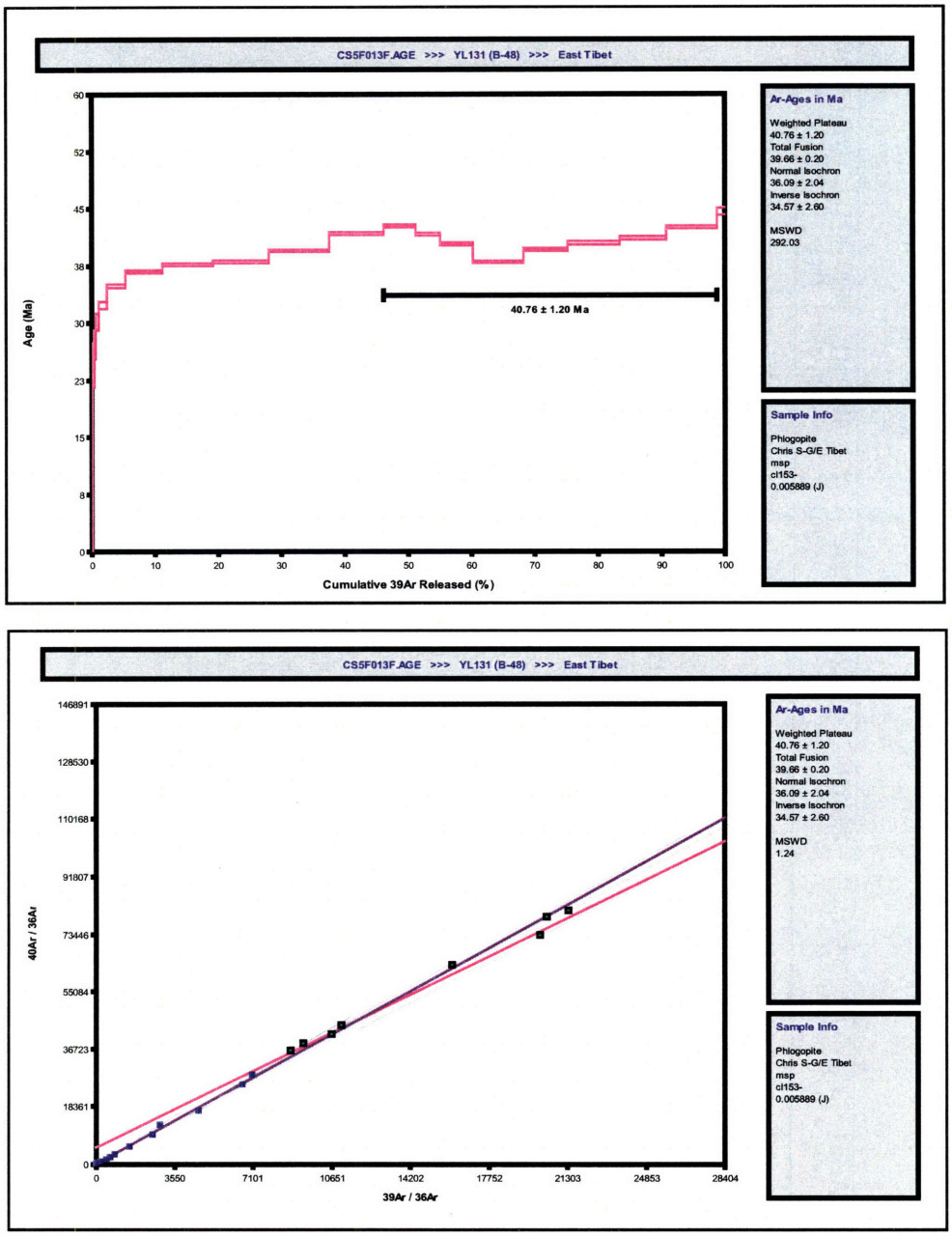

Figure 3-20: Plateau and inverse isochron plots for sample YL-131, phlogopite from marbles in the Yulong mountains. The age spectra do not yield an interpretable age, but we use the inverse isochron age.

Incremental Heating		36Ar(a)	37Ar(ca)	38Ar(cl)	39Ar(k)	40Ar(r)	Age (Ma)	2s	40Ar(r) (%)	39Ar(k) (%)	K/Ca	2s
5F013F.01	550 C	0.00633	0.00359	0.00131	0.03561	0.03251	9.67	9.35	1.71	0.13	4.863	4.888
5F013F.02	650 C	0.00074	0.00662	0.00039	0.05671	0.13225	24.61	2.87	37.65	0.21	4.198	0.620
5F013F.03	700 C	0.00039	0.02053	0.00026	0.07576	0.19649	27.35	1.86	62.55	0.28	1.808	0.078
5F013F.04	730 C	0.00027	0.01142	0.00027	0.12544	0.36119	30.34	1.04	81.17	0.47	5.382	0.347
5F013F.05	760 C	0.00050	0.00028	0.00061	0.32023	0.98759	32.47	0.43	86.37	1.20	569.114	1416.150
5F013F.06	790 C	0.00095	0.00071	0.00152	0.79351	2.63744	34.97	0.24	89.78	2.97	551.417	566.305
5F013F.07	820 C	0.00105	0.00124	0.00289	1.57633	5.52708	36.87	0.18	94.05	5.90	624.176	350.427
5F013F.08	850 C	0.00083	0.00178	0.00387	2.14862	7.71893	37.77	0.17	96.25	8.05	590.746	320.812
5F013F.09	880 C	0.00050	0.00145	0.00437	2.33508	8.47887	38.17	0.17	97.62	8.75	788.929	441.041
5F013F.10	910 C	0.00039	0.00181	0.00480	2.56257	9.64960	39.57	0.17	98.19	9.60	691.969	322.986
5F013F.11	940 C	0.00032	0.00141	0.00431	2.28281	9.09017	41.82	0.18	98.35	8.55	790.693	606.343
5F013F.12	970 C	0.00015	0.00091	0.00249	1.34865	5.49698	42.79	0.20	98.58	5.05	723.976	626.810
5F013F.13	1000 C	0.00009	0.00040	0.00185	1.04354	4.14482	41.71	0.21	98.72	3.91	1291.643	2861.845
5F013F.14	1040 C	0.00013	0.00097	0.00251	1.38994	5.34791	40.42	0.19	98.65	5.21	703.631	612.206
5F013F.15	1353 C	0.00011	0.00148	0.00369	2.12847	7.71515	38.10	0.17	98.92	7.97	703.100	344.667
5F013F.16	1120 C	0.00009	0.00024	0.00340	1.86380	7.03809	39.68	0.21	98.98	6.98	3755.280	21811.931
5F013F.17	1160 C	0.00011	0.00023	0.00397	2.17067	8.37921	40.55	0.20	98.99	8.13	4557.110	30407.055
5F013F.18	1200 C	0.00012	0.00130	0.00339	1.95964	7.68980	41.22	0.21	98.91	7.34	738.278	885.286
5F013F.19	1270 C	0.00023	0.00131	0.00392	2.13493	8.67380	42.66	0.19	98.63	8.00	801.593	426.568
5F013F.20	1400 C	0.00012	0.00003	0.00066	0.34714	1.47623	44.62	0.43	97.10	1.30	6289.471	200110.390

Table 3.7: Data table for sample YL-131, phlogopite from marbles in the Yulong mountains.

Chapter 4

Seismological, geodetic and geologic perspectives on the active tectonics of eastern Tibet and southern China: a review

Christopher Studnicki-Gizbert
B. Clark Burchfiel
Robert W. King
Zhiliang Chen
Liangzhong Chen

Abstract

A compilation of the active faults of the eastern margin of the Tibetan plateau, southwestern China and northern Myanmar is presented based on a review of published literature, maps, seismicity records, remote sensing analyses and fieldwork. Major faults are identified and all available slip-rate estimates for these faults are summarized. This geologic perspective of the active tectonics of the eastern Tibetan borderlands is compared with the perspective from geodetic measurements. Published GPS measurements from two separate networks are combined and these are then used to constrain a deforming block model. We choose the model geometry such that it conforms as closely as possible to the mapped geology in order to highlight differences between the two. Modeled slip rates on the block boundaries are found to be generally consistent with published or cited geologic slip-rate estimates on major faults in this region. Discrepancies between a block model description and the mapped geology occur where geologic strain is diffuse and poorly localized. Notable examples of these areas are the southern strands of the Xiaojiang fault system north of the Red River and within the Lanping-Simao fold belt. Although these broad zones of deformation are poorly described by narrow block boundaries, block modeling proves to be a useful tool for identifying these regions and quantifying the strain they accommodate.

4.1 Introduction

The eastern margin of the Tibetan plateau has been long been a focus of attention of studies examining continental deformation and response to collisional tectonics. Early western work recognized that the topography, seismicity, and distribution of faults in eastern Tibet and southwestern China were related to the on-going collision of the Indian sub-continent with Eurasia (*Tapponnier and Molnar* (1976); *Molnar and Tapponnier* (1978); *Molnar and Deng* (1984)). Alternative explanations and descriptions of continental deformation in this area became subjects of considerable debate. Two end-member descriptions of the deformation were that the deformation of Eurasian continental material occurred in a continuous, distributed fashion that could be reasonably approximated by considering the Eurasian continent to behave as a viscous fluid (*England and Houseman* (1988); *England and Molnar* (1990); *Holt et al.* (1991, 2000) or that continental deformation could be idealized in terms of the plate-like motions of relatively few rigid blocks bounded by fast-slipping vertical

strike-slip faults (*Avouac and Tapponnier* (1993); *Tapponnier et al.* (1982, 1986); *Replumaz and Tapponnier* (2003)). Field studies of Cenozoic deformation in this area has tended to either emphasize discrete, localized high strain zones (eg. *Leloup et al.* (1995)) or complex, distributed deformation (*Wang et al.* (1998); *Wang and Burchfiel* (1997)). Similarly, there is considerable disagreement as to the slip-rates on major faults both in eastern Tibet as well as the Kunlun and Altyn Tagh faults north of Tibet, with the proponents of block-like continental deformation tending to prefer fast slip rates on a few major strike-slip faults.

Despite its promise, the recent availability of GPS based geodetic data has not done much to settle the debate. Geodetic based estimates of slip-rates for some of the major faults – particularly the Altyn Tagh fault (*Wallace et al.* (2004); *Shen et al.* (2001)) – are often considerably lower than some reported geologically determined slip-rates, but the apparent contradiction has been explained by possible secular variation in fault slip-rate, such that the short-term rates measured by geodetic methods need not match the long-term rates estimated by measuring the offset of dated geomorphic piercing-points (*Chevalier et al.* (2005)). The apparently continuous velocity field derived from geodetic measurements on the plateau has been taken to imply continuous, distributed deformation there (*Zhang et al.* (2004)), but the same data are equally or better explained in terms of the motions of a small number of fault-bounded blocks and elastic strain accumulation at block boundaries (*Meade* (submitted)).

In this paper, we combine geologic and geodetic perspectives of the active tectonics of eastern Tibet and southwestern China to address both the larger first-order questions raised above as well as to gain insight into the specific tectonics of this region. In particular we pose the following questions: (1) what are the slip-rates of the major faults in this region? (2) to what extent are slip-rate estimates based on geodetic data consistent with geologic slip-rate estimates? (3) to what extent can the deformation be explained in terms of a small number of deforming blocks? (4)

what is the appropriate characterization of areas where geodetic techniques measure significant strain, but no through-going faults are present?

4.2 Active faults of eastern Tibet and southwest China

We have compiled a map that shows the distribution of active faults in eastern Tibet, southwest China and northern Indochina (fig. 4-1). The location of these faults is known from previous geologic work, tracing the faults on remote sensing images and our own field mapping. The criteria we use to identify active faults is whether they are associated with large (M >5) earthquakes in any of the earthquake catalogues we use (described below), whether they offset Quaternary geomorphic features, whether they are associated with significant historical earthquakes or by examining geodetic velocities in the vicinity. Some of the fault locations are uncertain: We suspect that the Jiali fault is kinematically linked to the Sagaing fault and to normal faults responsible for subsidence and basin formation south of the eastern Himalayan syntaxis and east of the Sagaing fault in a manner similar to that shown by *Lee et al.* (2003) (their figure 1). The actual location of faults in this area is difficult to establish on remote sensing imagery. Our fieldwork in this area was not very helpful as the area in question is some of the most remote and inaccessible terrain in eastern Tibet. We are also unsure of how far the Lijiang fault projects to the northeast, and whether it is connected to the Litang fault. This area is characterized by considerable diffuse microseismicity, and relocation of seismic events by *Yang et al.* (2005) shows a less diffuse pattern of seismicity that suggests a possible link, but DEMs and remote sensing imagery are unequivocal at best. Finally, it is unclear whether all of the geomorphically well expressed northeast trending faults along the China – Myanmar border region are active.

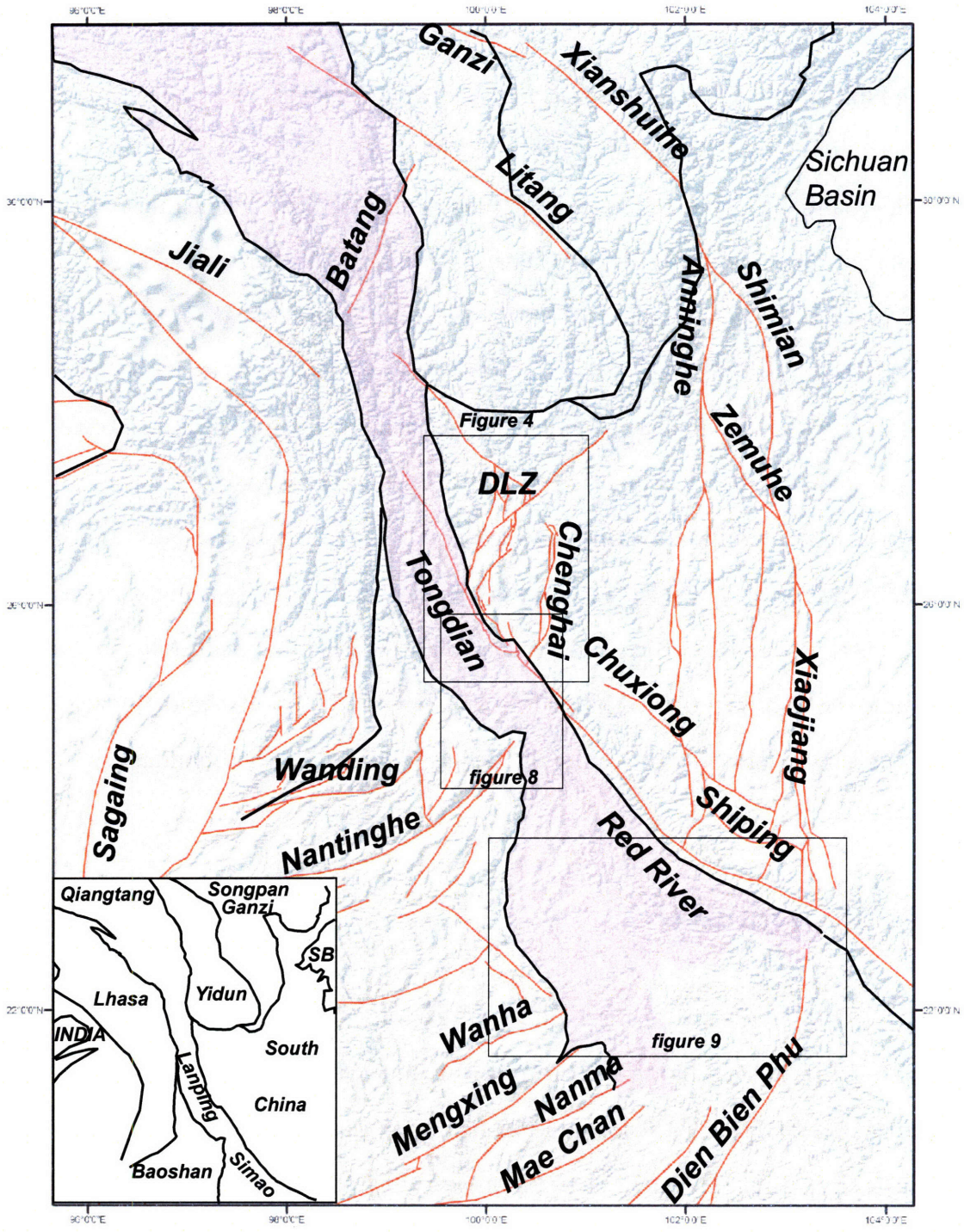

Figure 4-1: Active faults and major geologic boundaries of eastern Tibet and southwestern China. Active faults are in red, major boundaries in black. Inset shows the names of the major blocks or tectonic elements of the region. SB: Sichuan basin; DLZ: Dali-Lijiang-Zhongdian fault system, see fig. 4-4 for detailed fault map. Boxes show locations of figures 4, 8 and 9.

This map differs from other published maps of the distribution of active faults in this area. In particular, most active fault maps show one or two north-south striking active faults along the Nu (Salween) and Lancang (Mekong) river valleys where these run very close together and parallel with the Jinsha (Yangzi) rivers in the "Three Rivers" (Sanjiang) area (eg. *Shen et al.* (2005), their figure 1). The unusually narrow, straight and elongate river courses have been interpreted as the result of the three river drainages being caught in wide zone of right-lateral shear (*Hallet and Molnar* (2001)). Detailed mapping of the Cenozoic Chong Shan and Gaoligong Shan shear zones in this area has found no evidence of active faulting in this area (*Akciz* (2004)), and the area is relatively quiet seismically. Second, although geomorphically well-expressed active faults are easily mapped north of the Red River fault and south of the Lanping-Simao foldbelt, there are no clear, geomorphically well-expressed active faults cutting across the belt itself that would connect mapped faults to the north and and south of the belt. Mapped faults appear to stop at the boundaries of the Lanping-Simao fold belt, but, notably, deform and deflect the boundaries.

4.3 Seismicity

Eastern Tibet and southwestern China are characterized by considerable seismicity, much of it diffuse. In figure 4-2, we plot earthquakes from three separate seismicity catalogs. First, we show the focal mechanism solutions provided by the Harvard CMT catalog (fig. 4-2a). By themselves, these are subject to considerable uncertainty as to location, but these are readily corrected using either the relocated events of *Sun et al.* (2004) or the locations from local networks provided by the CSB. The second catalog consists of events recorded and located by the Chinese Seismological Bureau catalogue from local networks of seismometers (fig. 4-2b). There is some uncertainty in the precise location of these events, mainly due to the simple velocity model used.

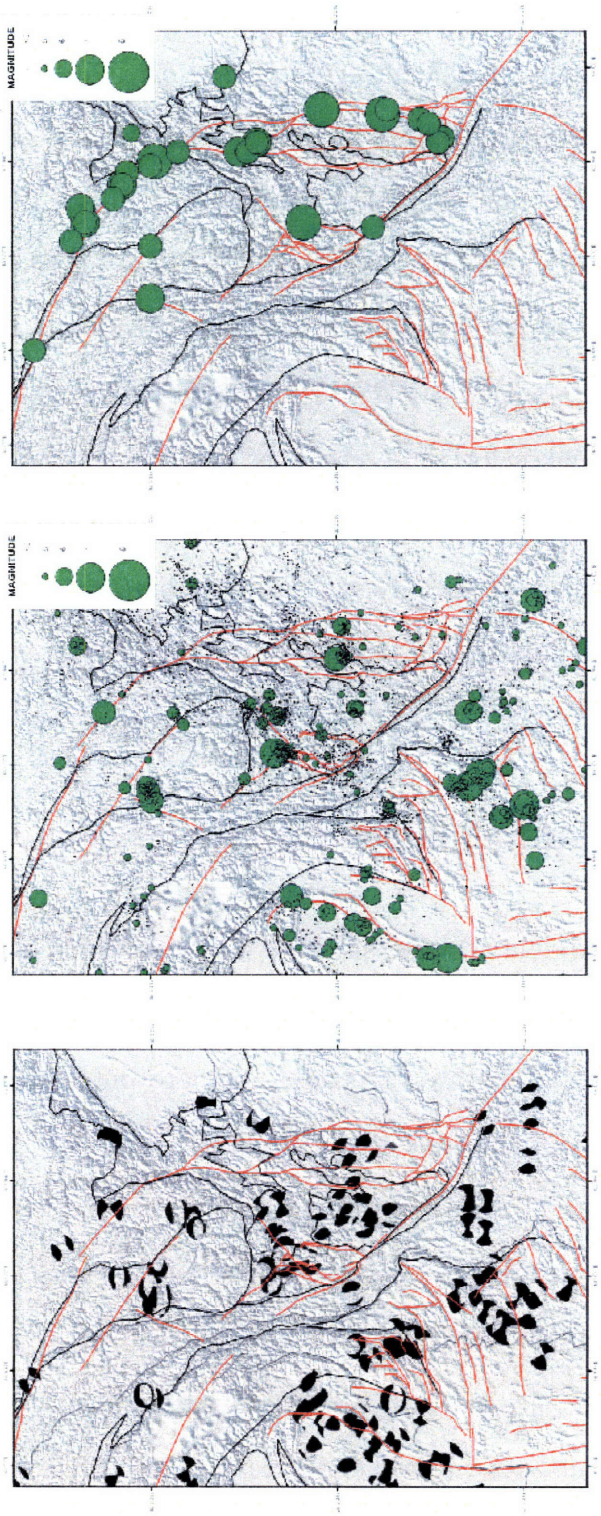

Figure 4-2: (A) Earthquakes and focal mechanisms from the Harvard CMT catalog; (b) earthquake locations from the CSB catalog. Location of events after 1990 are relocated using a regional velocity model *Sun et al.* (2004); (c) Pre-1970 and historic earthquakes compiled from *Molnar and Deng* (1984), *Yang et al.* (2005) and *Papadimitriou et al.* (2004)

Relocation of these events using better velocity models, particularly of the crust, for events later than 1990 have shown significant errors in the original locations of events (*Sun et al.* (2004)). Other relocation efforts include that of *Yang et al.* (2005), who used the double-difference relocation algorithm. In figure 4-2b, we have used *Sun et al.* (2004) for events after 1990, and the uncorrected CSB catalog for events prior to 1990. The third catalog we show consists of historic (pre-1900) and pre-1970 events as compiled by *Molnar and Deng* (1984); *Yang et al.* (2005) and *Papadimitriou et al.* (2004) (fig. 4-2c). Earthquakes for these catalogs always plot precisely on mapped faults, because the compilers try to match an event recorded in the historical literature with a mapped fault trace. Especially in the more distant past and for remote locations, these catalogs are incomplete, and there are clear biases.

4.4 Review of slip-rate estimates

In this section, we compile the available geologic slip-rate determinations for all the faults shown in figure 4-1. Relatively few slip rate estimates have been published in the western literature, but many slip rate determinations are only available as internal institutional reports, or are published in the Chinese geological literature. Apart from published slip rate estimates we were able to find, our compilation also relies on reviews of the Chinese literature as provided by *Papadimitriou et al.* (2004), *He and Tsukuda* (2003) and *Allen et al.* (1991). The compiled slip rate determinations in tables 1–3, and show them graphically in figure 4-3. We split this section into three parts, corresponding to (1) the Xianshuihe, Xiaojiang and related faults; (2) the Red river fault and faults between the Xiaojiang fault system and the Lanping-Simao fold belt; and (3) faults west of the Lanping-Simao fold belt, including the Sagaing fault. In the text, we focus on geologic slip rate determinations; we list the geodetically based slip-rate estimates of *Chen et al.* (2000) and *Shen et al.* (2005) in the tables.

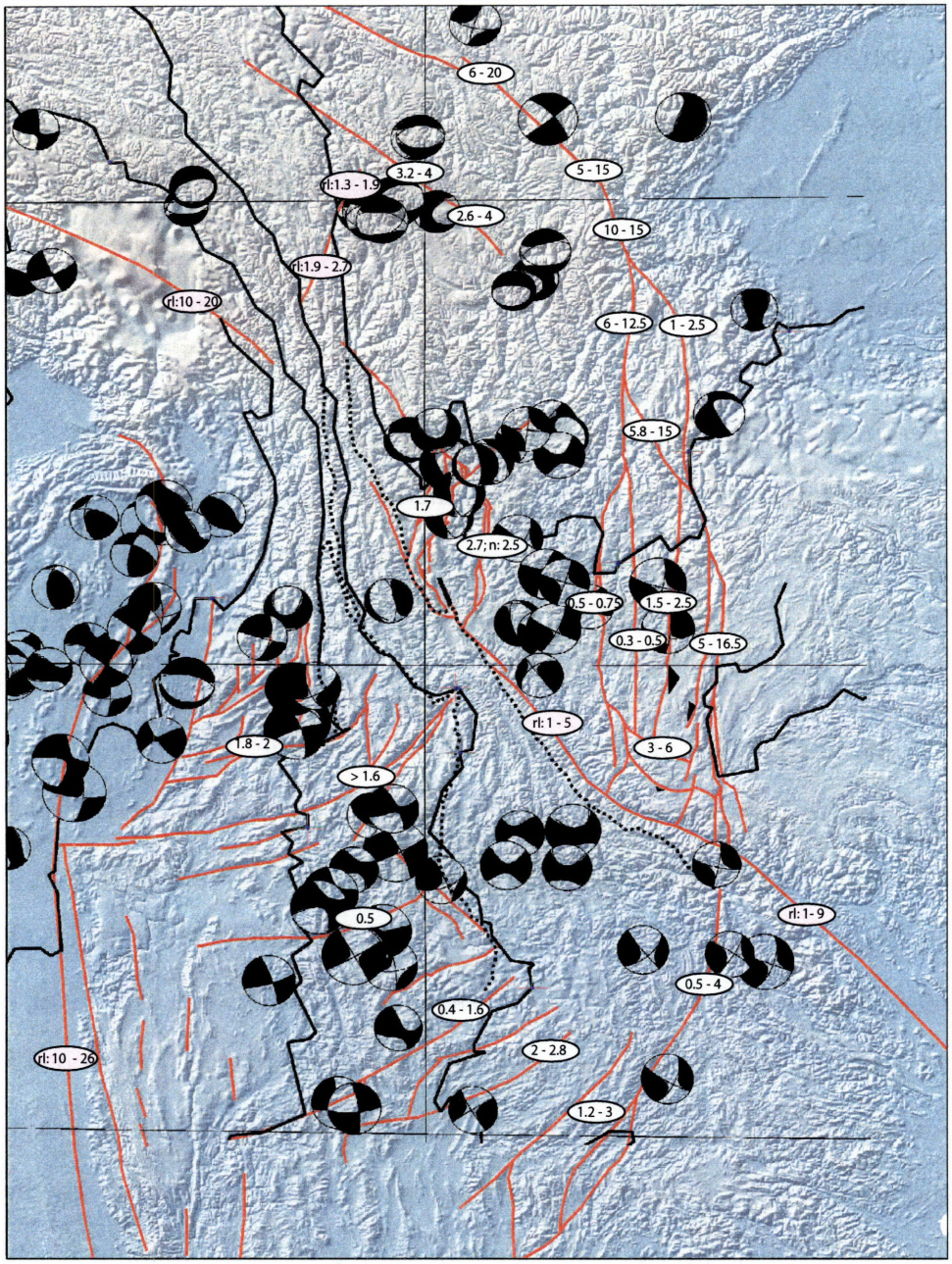

Figure 4-3: Geologically determined slip rates for the region. See tables for details and references and text for discussion. White bubbles indicate left-lateral rates, pink bubbles are right lateral rates. Normal-sense slip indicated by prefix "n".

4.4.1 The Ganzi, Xianshuihe, Xiaojiang and related faults

The Xianshuihe – Xiaojiang fault system is the main northeastern and eastern boundary between upper crustal fragments rotating clockwise about the Eastern Himalayan syntaxis and as such is the most important set of faults for understanding the first order tectonics of this region (*Wang et al.* (1998)). Six historical earthquakes of magnitude 7 or greater have occurred along this fault zone. Its importance in terms of regional tectonics and kinematics was noted early on by *Tapponnier and Molnar* (1976); *Molnar and Tapponnier* (1978), and more recently emphasised by *Holt et al.* (1991); *King et al.* (1997); *Chen et al.* (2000) and especially *Wang et al.* (1998). The fault system – sometimes referred to as the Kangding fault system – comprises a series of fault segments linked across stepovers or bends. These include the Ganzi - Yushu fault of the Eastern Tibetan plateau and the Xianshuihe fault proper between Ganzi and Shimian. At Shimian, the fault begins to split into multiple strands: the Shimian and Anninghe faults south of Shimian and the Zemuhe, Xiaojiang and other minor faults farther to the south. Where the fault system approaches the Red River, individual splays are so numerous that shear deformation occurs across a zone approximately 150 kilometers wide (*Wang et al.* (1998); *Schoenbohm et al.* (2006)). The most comprehensive report on the geology of the entire fault system from Ganzi to the Red River is *Wang et al.* (1998), who provided detailed maps of different parts of the fault system and synthesized regional scale mapping and reports in the Chinese literature, and identify several offset piercing points along different parts of the fault system. Their estimates of slip-rates are made by taking the total amount of offset and dividing by the less well-known duration that the faults were though to have been active. They suggested a rate of 15 – 30 mm/yr (assuming inception at 4 and 2 Ma, respectively) for the segment of the Xianshuihe fault north of where it begins to splay, with slip-rates along any one fault diminishing as the fault system splays into multiple strands.

Fault	Slip Rate (mm/yr) geologic	Geodetic	Source
Ganzi			No slip-rate estimates available
XXH West	13		*Papadimitriou et al.* (2004)
	6 to 10		*He and Tsukuda* (2003)
		10	*Chen et al.* (2000)
		8 to 12	*Shen et al.* (2005)
	15		*Yang et al.* (2005)
	15		*Wang et al.* (1998)
XXH Central	12 to 13		*Papadimitriou et al.* (2004)
	15		*Wang et al.* (1998)
XXH East	15		*Wang et al.* (1998)
	9.5 to 10		*Papadimitriou et al.* (2004)
Anninghe	6 to 10		*He and Tsukuda* (2003)
	12.5		*Wang et al.* (1998)
		2 to 6	*Shen et al.* (2005);Includes Shimian fault
Shimian	2.5		*Wang et al.* (1998)
Zemuhe	5.8 to 8.5		*He and Tsukuda* (2003)
		5 to 9	*Shen et al.* (2005)
Xiaojiang	7		*Wang et al.* (1998)
		5 to 9	*Shen et al.* (2005)
	6.4 to 8.8		*Yang et al.* (2005)
	13 to 16.5		*He and Tsukuda* (2003); all on east strand
Faults west of Xiaojiang	8		*Wang et al.* (1998); Distributed among many strands
		0	*Shen et al.* (2005)
Shiping (right lateral)	-3 to -6		*He and Tsukuda* (2003)

Table 4.1: Slip rates for the faults of the Xianshuihe-Xiaojiang fault system. Positive values are left-lateral slip.

The Ganzi fault

The Ganzi segment is located on the Tibetan plateau, with an eastern termination is near to and to the east of the town of Ganzi. Here the Ganzi appears to overlap the western termination of the Xianshuihe fault proper in a northward stepping, releasing stepover. Extensional strain predicted by such a step-over is not reflected in the topography, but *Allen et al.* (1991) map dozens of NNE trending normal faults and cite possible normal sense earthquake solutions in this area. Near Ganzi the fault lies in a prominent linear valley, bounded by the glaciated peaks of the Chola Shan mountain ranges (max. elevation near 6100m) to the south and abrupt escarpments to the north. Geomorphic evidence of left-lateral active slip on this fault is obvious and ubiquitous and includes dozens of bent and offset drainages and offset alluvial and debris flow fans as well as a 15 km offset of the Yalong river. Previous workers have suggested that the anomalously high Chola ranges to the south are the result of transpression along the fault (*Wang et al.* (1998); *Wang and Burchfiel* (2000); *He and Tsukuda* (2003); *Allen et al.* (1991)). However, there is no geomorphic or seismic evidence of active reverse faults along the foot of the range. Instead, granites of the Chola Shan are separated from the volcanic rocks outcropping to the north by a northward dipping, dip-lineated mylonite in carbonate and calc-silicate rocks in the presumed footwall of generally northward dipping fault scarps related to the active Ganzi fault. Southward dipping escarpments on the north side of the valley suggests a graben morphology. Active subsidence of the valley is reflected in the profile of the Yalong river as it crosses the valley. The Yalong river makes an abrupt change from steep and incisional north of the Ganzi valley to shallow, alluviated and meandering within the valley. South of Ganzi and the (most active) fault, the Yalong river then plunges through one of the deepest and steepest bedrock gorges in eastern Tibet. We suggest, therefore, that the Ganzi fault is actually transtensional, and that the high elevation of the Chola ranges may, instead, reflect rift-flank uplift.

We were unable to find any geologically determined slip-rate estimates for the Ganzi fault.

Xianshuihe fault

The Xianshuihe fault proper extends from north of the eastern termination of the Ganzi fault southeast of the Dadu river, where it splits into the Anninghe and Shimian splays. *Wang et al.* (1998) proposed slip-rates of between 15 to 30 mm/yr, based on $\sim$ 60 kilometers of offset along this fault, and a proposed age of 2 to 4 Ma for the inception of faulting. *Papadimitriou et al.* (2004) provide the most detailed compilation of historical seismicity and fault slip rates for a dozen separate sections of the Xianshuihe, Anninghe and Zemuhe faults. Most of the slip rates they cite are geologic rates from measured offsets of dated features, but some are based on historical seismicity and assumptions about average recurrence interval. For the Xianshuihe, slip rates range from 13 mm/yr to 9.5 mm/yr, with rates decreasing from the Luhuo segment (westernmost segment of the Xianshuihe fault proper) to the Anninghe fault. *He and Tsukuda* (2003) cite a rate of 6 – 10 mm/yr for the Xianshuihe fault northwest of the town of Kangding. *Allen et al.* (1991) reported the results of a neotectonic studies along a segment of the Xianshuihe fault from Ganzi to Kangding. Based on offsets of geomorphic markers, they suggested a Quaternary slip-rate of 15 +/- 5 mm/yr along the northwest segment of their study area and a much lower rate of $\sim$ 5 mm/yr near Kangding. Slip-rates published in the Chinese literature they review suggested 5 – 10 mm/yr and $<$ 5 mm /yr for the northwestern and southeastern portions, respectively. *Allen et al.* (1991) also suggested that some segments of this fault were likely creeping at around 6 mm/yr, from measurements reflecting 13 years of measurements following the 1973 M 7.6 Luhuo earthquake. Using a historical seismicity catalogue and the method of *Kostrov* (1974), *Molnar and Deng* (1984) proposed a slip rate of 10 – 15 mm/yr for the Xianshuihe fault near Kangding, with the lower rate resulting

from inclusion of earthquakes from the historical (pre 1920) record.

Anninghe, Zemuhe and Shimian faults

South of about 29°latitude, the Xianshuihe splits onto two main splays, the Anninghe and Shimian faults. Farther south, the Anninghe fault splays into the Zemuhe fault, which connects back to the Shimian fault. *He and Tsukuda* (2003) cited a rate of 6 – 10 mm/yr for the Anninghe fault and 5.8 – 8.5 mm/yr for the Zemuhe fault. *Wang et al.* (1998) determined total offsets of 50km and 10km for the Anninghe and Shimian faults, respectively, which, assuming a 4 Ma age of inception for these faults, results in rates of 12.5 mm.yr and 2.5 mm/yr. *Shen et al.* (2005)'s estimates based on geodetic data are somewhat lower. They infer a total rate of 4±2 mm/yr for both the Anninghe and Shimian (Daliangshan) faults.

Xiaojiang and related faults

South of the the Anninghe, Zemuhe and Shimian faults, at least four major splays together form the Xiaojiang fault system. *He and Tsukuda* (2003) cite a Quaternary slip rate of 13 – 16.5 mm/yr for the easternmost strand of the Xiaojiang fault, though it is not clear where this determination applies, and whether it applies to a single strand of the Xiaojiang fault or to the cumulative slip-rate across all the multiple strands in the southern region of this fault zone. From west to east, *Wang et al.* (1998) report offsets of 3km, 2km, 10km and 28km across the four principal strands of the Xiaojiang fault system. For inception ages of 2 – 6 Ma, these offsets result in slip rates of 0.5-1.2 mm/yr, 0.33-0.8 mm/yr, 1.67-4 mm/yr and 4.67-11.2 mm/yr. For their preferred 4 Ma age of inception, the rates are 0.75 mm/yr, 0.5 mm/yr, 2.5 mm/yr and 7 mm/yr. Using geodetic data, *Shen et al.* (2005) estimated a rate of 7±2 mm/yr for the easternmost strand of the Xiaojiang fault system, and were unable to detect motion on the other splays (although this might be a result of their

data filtering technique, which removed stations within 15 to 30 km of faults).

The strands of the Xiaojiang fault system are linked together by minor splays and two major east-west striking right-lateral faults: the Qujiang and Shiping (Jianshui) faults. *Burchfiel and Wang* (2003) interpreted these faults as originally left-lateral faults that now bound small fragments that rotate counterclockwise between major strands of the Xiaojiang fault system. *Burchfiel and Wang* (2003) noted that these faults are associated with only small right-lateral separation, and therefore suggested that their slip-rates must be small and not regionally significant. Alternatively, *He and Tsukuda* (2003) suggest that the low slip rates cited by *Allen et al.* (1984) for the parallel Red River fault to the south may be the result of transfer of right slip to these faults. They note that several M > 6 earthquakes are associated with this area and cite Chinese studies suggesting 3 to 6 mm/yr of slip. Earthquake focal mechanisms in the area of these faults cannot distinguish between left-slip on a strand of the north-south trending Xiaojiang fault system or right-slip on a east-west trending right lateral fault.

4.4.2 The Red River fault, and faults northeast and east of the Lanping-Simao fold belt

The Red River and Tongdian faults

The right-lateral Red River fault is parallel to the exhumed left-lateral mylonites of the Ailao Shan shear zone (*Leloup et al.* (1995, 2001)), and its importance in the large scale tectonics of the region has been the subject of considerable debate. Early interpretations of the Red River fault suggested that it was a major structure that accommodated the extrusion of a large, rigid block north of the fault in much the same way as the older left-lateral mylonites of the adjacent Ailao Shan shear zone had been interpreted as having accommodated hundreds of kilometers of motion. Estimates of

Fault	Segment	Slip Rate geologic	Geodetic	Source
Tongdian			0 to -4	*Shen et al.* (2005)
			0 to 4 ext.	*Shen et al.* (2005)
Lijiang			3	*Shen et al.* (2005)
		1.7		*Wang et al.* (2000)
Zhongdian		less than 6		*Burchfiel and Wang* (2003)
Litang			4	*Shen et al.* (2005)
		4		*Papadimitriou et al.* (2004)
		2.6 to 4.4		*Zhou et al.* (2005)
Batang		1.3 to 2.7		*Zhou et al.* (2005)
Chenghai			<7 ext	*Shen et al.* (2005)
		2.7 and 2.5 ext		*Wang et al.* (2000)
Longlin			-6	*Shen et al.* (2005)
Red River	Northwest	-4 to -6		*Yang et al.* (2005)
		-3 to -7		*Allen et al.* (1984)
		-1 to -4		*Weldon et al.*
		-2.6 to -4		*He and Tsukuda* (2003)
	Southeast	-7 to -9		*Yang et al.* (2005)
	Vietnam		-1 to -5	*Cong and Feigl* (1999)

Table 4.2: Slip rates for faults northeast of the Lanping-Simao foldbelt

the slip-rate on this fault are variable, but generally are only modest. *Allen et al.* (1984) inferred 2-5 mm/yr, based on restoring offset streams and assuming "maximum credible rate of incision" of these streams. *Replumaz et al.* (2001) estimated a slip rate of 5 mm/yr, based on their match of offset streams which yielded 25km of total offset and assuming dextral reactivation of the Ailaoshan shear zone at 5 Ma. Detailed mapping by *Schoenbohm et al.* (2006) showed a longer history of right lateral faulting that preceded river incision and suggested that right lateral rates may have been greater prior to epirogenic uplift of the landscape and subsequent incision. Their mapping and interpretations further suggested that active right-lateral slip rates on this fault ought to be variable and should decrease from where the fault intersects with splays of the Xiaojiang fault system to the southeast. *Weldon et al.* trenched the main strand of fault in the Gasa valley, and estimated a slip-rate of 2 mm/yr and a recurrence interval for major earthquakes on this faults of between 5000 to 7000

years. They did not trench the fault at the foot of the Ailao shan mountains, or other strands of this pull-apart and suggested that the slip rate for the entire fault 1 to 4 mm/yr. Faster rates were suggested by *Yang et al.* (2005) who cited studies in the Chinese literature that estimated rates of between 4 to 6 mm/yr northwest of the westernmost strand of the Xiaojiang fault and between 7 to 9 mm/yr where the fault interacted with the Xiaojiang fault. Strangely enough, *He and Tsukuda* (2003) cite a review by same author as cited by *Yang et al.* (2005), but report a much lower rate of 2.6 to 4 mm. It is not clear how these slip rates were determined.

Existing geodetic slip rate estimates suggest very slow values and possible inactivity on this fault. *Shen et al.* (2005) infer a rate of 1±2 mm/yr northwest of the Xiaojiang fault. A slip-rate estimate based on a combination of triangulation surveys and GPS in Vietnam suggested slip rates of less than 5 mm/yr or lower (*Cong and Feigl* (1999)), but they admit large uncertainties in their estimates and could not rule out inactivity of this fault in Vietnam.

It is difficult to trace the Red River fault northwest of where it intersects with the Chenghai fault in the Midu basin. *Schoenbohm et al.* (2006)'s mapping suggested that it may connect with a fault east of Dali, bounding the Erhai Quaternary extensional basin there. West of Dali, high grade rocks are exposed in the normal-fault bounded Diancang Shan (*Leloup et al.* (2001); *Wang et al.* (1998)). Normal (right-normal?) faults on the west side of this high grade massif strike north to an intersection with the Jianchuan fault, and continue as the Tongdian fault, which appears in the field to be mainly a normal fault. *Shen et al.* (2005) call this the Red River Fault Northwest, and report a geodetically derived estimate of 2±2 mm/yr of right lateral slip and at least 2 mm/yr of extension on this structure.

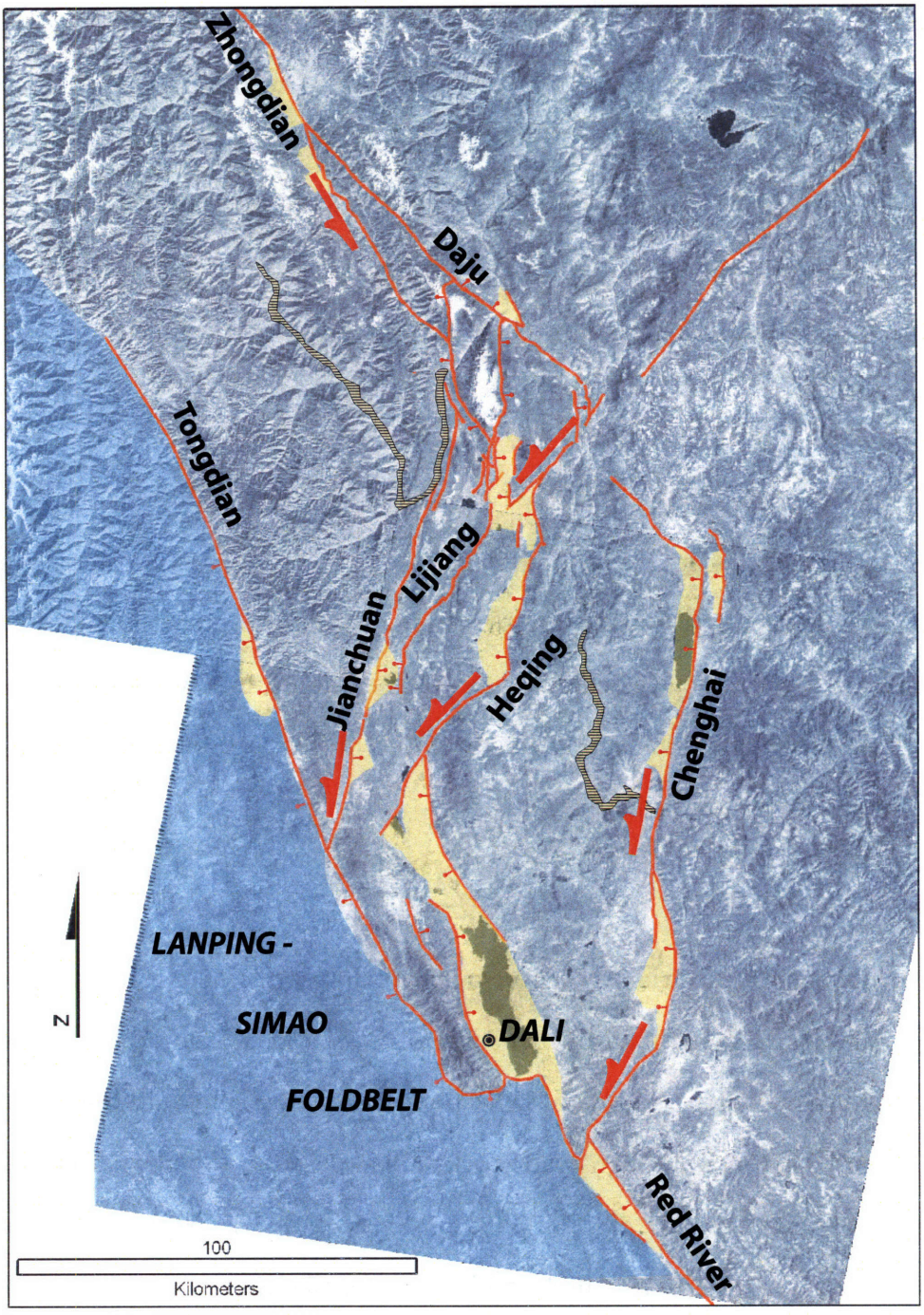

Figure 4-4: Faults of the Yunling collage. Plio-Quaternary basins are shaded yellow, and alluviated stretches of the Jinsha river are shown as a hatched pattern.

The Yunling collage: Dali, Jianchuan, Lijiang, Zhongdian and Chenghai transtensional faults

The Yunling collage comprises a network of interrelated transtensional faults and related Quaternary basins between the towns of Zhongdian and Dali (*Wang et al.* (1998), fig. 4-4). The left-lateral northwest-southeast striking Zhongdian fault bounds this region to the northeast and connects with a series of northeast striking left-normal faults that transfer extension between north-south striking normal and left normal faults and associated north-south trending Pliocene-Quaternary extensional basins. *Armijo et al.* (1989) interpreted these basins as extensional pull-aparts linking the Red River fault with the Zhongdian (on this interpretation, a right lateral fault) and Jiali faults. The Zhongdian fault, however, offsets fold axes, unit contacts and the Jinsha (Yangzi) river in a left-lateral sense (*Burchfiel and Wang* (2003); *Wang et al.* (1998)) and cannot be traced in the field, on remote sensing imagery or on geologic maps past the southwestern extension of the right lateral Batang fault. *Wang et al.* (1998) interpreted these faults as defining a small block, whose independent motion of the larger clockwise rotations regionally explained left-lateral faulting. Extensional basins here were explained as pull-apart structures. However, normal fault mechanisms dominate the available seismicity record, all of the faults we mapped in this region are either normal or left-normal, and we suspect that east-west extension drives differential rotation of small fault bounded crustal fragments here. Very few slip-rate determinations are available for faults in this area. An engineering study for hydroelectric development in this region cited left-lateral slip-rates of 1.7 mm/yr and 2.7 mm/yr for the Lijiang and Chenghai faults, respectively, and a normal-sense slip-rate of 2.5 mm/yr for the Chenghai fault (*Wang et al.* (2000)). No information on how these slip-rates were determined is available.

Fault	Slip Rate geologic	Geodetic	Notes	Source
Jiali	-10 to -20			*Armijo et al.* (1989)
	-2 to -12		Central plateau Jiali and related faults	*He and Tsukuda* (2003)
Sagaing	-10 to -26			*Bertrand and Rangin* (2003)
Wanding	1.8 to 2			*Lacassin et al.* (1998)
Natinghe	>1.6			*Lacassin et al.* (1998)
Wan Ha	0.5			*Lacassin et al.* (1998)
Mengxing	0.4 to 1.6			*Lacassin et al.* (1998)
Nanma	2 to 2.8			*Lacassin et al.* (1998)
Mae Chan	0.3		Assuming 5 Ma age; other faults to the south accommodate 1.2 to 3 mm/yr	*Lacassin et al.* (1998)
Dien Bien Phu	0.5 - 4			*Zuchiewicza et al.* (2004)

Table 4.3: Slip rates for faults west and southwest of the Lanping-Simao foldbelt

The Litang and Batang faults

The Batang and Litang structures are a right-lateral and left-lateral pair of faults northeast of the eastern Himalayan syntaxis. A 1989 earthquake swarm of earthquakes occurred where these two apparent conjugate faults intersect. Focal mechanisms indicate north-south extension, consistent with the kinematics of the conjugate faults. Slip rate estimates for the Litang fault are 4 mm/yr (*Xu et al.* (2003), as cited by *Papadimitriou et al.* (2004)), and 3.8±0.6 mm/yr for the southeastern end of the fault and 2.8±0.2 mm/yr near where the fault intersects the Batang fault (*Zhou et al.* (2005)). The Batang fault slip rate has been estimated as 2.35±0.35 mm/yr at the southwestern end of the fault and 1.6±0.3 mm/yr near Batang village, where the fault offsets the Jinsha (Yangzi) river.

4.4.3 Faults southwest and west of the Lanping-Simao fold belt

The Jiali and Sagaing faults

The right lateral Jiali fault is a prominent fault that extends from the central Tibetan plateau to north of the eastern Himalayan syntaxis. *Armijo et al.* (1989) proposed slip rates on the order of 10 - 20 mm/yr, and suggested that it connected with the Red River fault via the Zhongdian fault. The Zhongdian fault is a left-lateral structure that cannot be traced much farther northwest than where it crosses and offsets the Jinsha (Yangzi) River. The Jiali fault itself is difficult to trace east of the syntaxis, although some evidence can be found on remote sensing imagery for *Lee et al.* (2003)'s suggestion that this fault terminates into two southeastward striking splays – the Puqu and Parlung faults. The Puqu fault is then shown to ultimately connect with the Sagaing fault. This fault has a prominent role in *Replumaz and Tapponnier* (2003)'s reconstruction of Cenozoic block motions, and they assign it a slip rate of 10±5 mm/yr, and total displacement 180 to 250km. *He and Tsukuda* (2003) cite an estimate of 2 - 12 mm/yr to this fault, though this slip rate applies farther to the west in the central Tibetan plateau.

The Saigang fault is one of the longest and most rapidly slipping faults in Asia, and accommodates much of the relative motion between India and Indochina. *Bertrand and Rangin* (2003) dated young basalt flows offset by the fault, but poor exposure resulted in considerable uncertainty as to the total amount of offset. They determined a right-lateral slip-rate of 18±8 mm/yr. Considerable additional relative motion between India and Asia is accommodated by tranpressional faults in the Indo-Burman ranges (*Satyabala* (2003)), though their contribution has not been quantified.

The Nantinghe, Dien Bien Phu and faults southwest of the Lanping-Simao belt

West and southwest of the southwestern boundary of the Lanping-Simao foldbelt, active faults consist of north south trending normal faults linked by arcuate, generally northeast trending left-lateral faults that act as transfer faults. Normal faults are particularly common north of the Wanding fault, in the Tengchong region. Here, east west extension is associated with Quaternary volcanism (*Wang and Burchfiel* (1997)). Both the normal and left-lateral strike slip faults have clear geomorphic expression. The left-lateral faults offset the major, deeply incised rivers in the region (*Lacassin et al.* (1998)). With the exception of the Dien Bien Phu fault, none of these faults cross the southwest boundary of the Lanping-Simao belt, though slip may continue past their northeastern terminations and deform the boundary itself (*Burchfiel et al.* (submitted)). *Lacassin et al.* (1998) propose slip-rates based on river offsets and assuming an age for the onset of left-lateral faulting. They propose that left-lateral slip may have begun between 20 and 5 Ma, but there are no constraints on this estimate. For the latest proposed age of initiation, the total left lateral slip between the Wanging and Dien Bien Phu faults ranges from 12 to 17.7 mm/yr. The Dien Bien Phu fault is the farthest southeast of these faults, and appears to act as a transfer fault for north-south trending grabens to the north. *Zuchiewicza et al.* (2004) dated Quaternary sediments in pull-aparts near the China-Vietnam border associated with the Dien Bien Phu fault and inferred a rate between 0.5 and 4 mm/yr.

Most of the faults southwest of the Lanping-Simao fold belt consist of northeast striking left-lateral faults and associated north-south striking normal faults. Apart from these are a few northwest striking faults with apparent right-lateral shear sense. The most prominent of these is Longlin fault, which is likely associated with several major earthquakes (*Guo et al.* (2000)). We are not aware of any geologic slip-rate determinations. Using a profile of GPS velocities across the fault, *Shen et al.* (2005)

inferred a rate of 6 mm/yr.

4.5 Geodetic perspectives on active deformation

Geologic approaches to describing the active tectonics of this region together describe a consistent picture of at least the first order active kinematics of this region. However, the review of published or cited slip rate estimates and mapping of active faults reveals not only considerable inconsistency in the estimates of fault slip rates, but also generally poor characterization of many of the second-order characteristics of the active tectonics. *Wang et al.* (1998) recognized the presence of independently deforming smaller crustal fragments associated with the Jianchuan, Lijiang, Chenghai and Zhongdian faults, but provided no slip-rate estimates. There is little recognition of the importance of normal faulting and extension, despite common normal fault mechanisms shown, for example, in the CMT catalogue (fig. 4-2a). *Wang et al.* (1998) and *Schoenbohm et al.* (2006) demonstrated that left-lateral strain becomes progressively more distributed and poorly localized on the Xianshuihe–Xiaojiang fault system moving from the Anninghe and Zemuhe faults south towards the Red River, but *Wang et al.* (1998)'s reported offset on the strands of the southern Xiaojiang fault system are at odds with the appearance of almost completely even strain distribution between all the strands of the fault network suggested by the broad deflection of the Red River fault and rocks of the now inactive Ailao Shan shear zone. Other estimates of fault slip rates for the Xiaojiang fault system appear to only consider slip on the easternmost strand. Finally, southwest of the Lanping-Simao fold belt, *Lacassin et al.* (1998) identify about a half-dozen arcuate left-lateral faults, each slipping very slowly, and thus suggesting the overall clockwise rotation of the upper crust about the eastern Himalayan syntaxis occurs in a much more distributed manner than in regions to the north. Between these faults, and faults north of the Red River and Tongdian

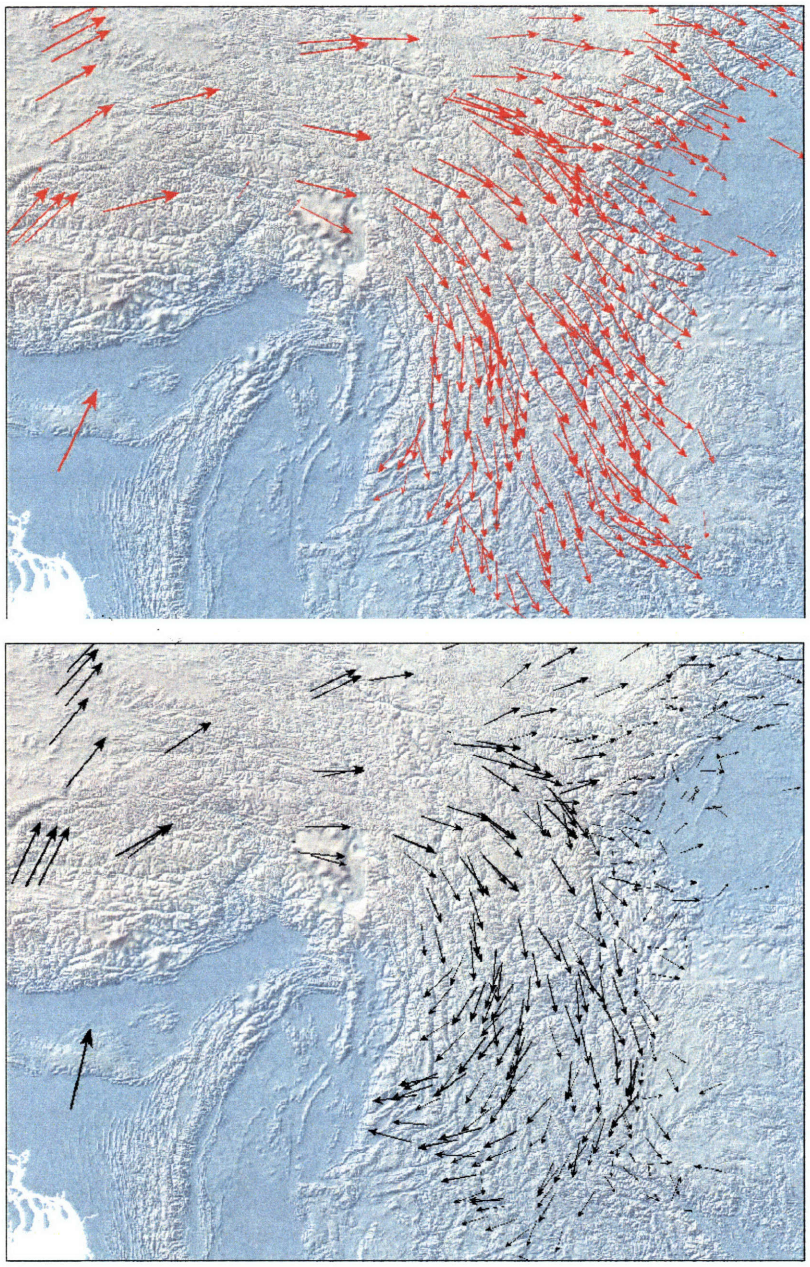

Figure 4-5: Top: GPS velocities shown relative to Eurasia. Bottom: GPS velocities shown relative to South China, defined by minimizing velocities of stations east of the Xiaojiang fault and within the Sichuan Basin.

faults, the Lanping-Simao fold belt exposes no obvious through-going faults, although it is seismically active, and it appears as though left-lateral slip must somehow be transferred across these rocks (*Burchfiel* (2004); *Burchfiel et al.* (submitted)).

Recently available geodetic measurements of crustal strain provide an important data set for helping resolve some of these ambiguities. The earliest results (*King et al.* (1997); *Chen et al.* (2000)) from a relatively sparse network of GPS stations supported the first-order picture of clockwise rotation deduced by mapping (*Wang et al.* (1998)) or modeling of seismic strain release (*Holt et al.* (1991)) and provided a means of estimating the short-term slip rates on the Xianshuihe–Xiaojiang fault. Recently, the considerably denser network of *Chen et al.* (2004) and *Zhang et al.* (2004) in this area was exploited by *Shen et al.* (2005) to provide slip-rate estimates for many of the second-order faults as well. *Shen et al.* (2005) estimated slip-rates by considering selected profiles across faults and comparing velocities sufficiently far from the faults such that the effects of elastic strain due to interseismic locking of the faults would hopefully not affect the estimates (tables 4.4.1 and 4.4.2). For the most part, their slip rate estimates are consistent with at least some of the geologically based slip rate estimates. They also showed that, after removing stations near active faults, the remaining GPS velocities could be well explained by rigid rotations of only a few major independent fault bounded blocks.

In this section, we combine geodetic measurements of *Chen et al.* (2004); *Zhang et al.* (2004) with data from the MIT-Chengdu GPS network (*Chen et al.* (2000)) to attempt to quantify the short-term slip rates of major faults in the region and to assess to what extent the deformation in this region can be characterized by the rotation of a small set of independent blocks. The resulting velocity field clearly shows the first-order kinematics of clockwise rotation of material west of the Xianshuihe–Xiaojiang fault system about the eastern Himalayan Syntaxis (figure 4-5). We use the block modeling code developed and described by *Meade and Hager* (2005), that fits the

observed geodetic data to the velocities predicted by both the angular velocity vector describing the rotation of each independent block and the expected elastic strain due to the locking of the fault boundary according to a simple model of a dislocation in an elastic half-space (eg. *Savage and Burford* (1973); *Okada* (1985)). Slip-rates for faults forming the block boundaries are then solely determined by the orientation of the boundary and the angular velocity of the block. The advantage of this approach over estimating slip-rates from profiles across faults is that it explicitly considers the interseismic elastic strain contribution to the observed geodetic velocities, and measurements made near faults are included in the inversion.

This approach requires defining a number of block boundaries that form closed and continuous boundaries. For the most part, the block boundaries are coincident with the locations of mapped faults but the model geometry departs from the mapped geology in two respects. First, block boundaries may be present where no faults are mapped, either because deformation occurs in a broad zone of distributed shear or because we do not know the precise location of these faults. Block modeling is actually useful in these situations, because it may provide insight into the deformation of a certain region where the geologic information is equivocal or absent. Second, the model geometry might represent a zone where deformation is distributed along many parallel fault splays as a single boundary. This may occur where the slip-rates on each individual strand is too small, or the GPS data are too sparse to distinguish the effect of one single fault or a number of closely parallel faults. The faults described by *Lacassin et al.* (1998) southwest of the Lanping-Simao fold belt provide an example. There are about a half-dozen prominent faults and a number of smaller splays with very slow slip-rates and we have no geodetic data for large parts of the region between the boundaries of Lanping-Simao and India.

We tested over two dozen alternate model geometries for this region, in an effort to (1) better determine short-term slip-rates on the major faults in the region; (2) assess

the deformation of areas where no obvious faults are present; (3) assess the importance of the independent deformation of crustal fragments west of the Xianshuihe–Xiaojiang fault system; and (4) compare a deforming block model description of the active tectonics to geologic data regarding the location and distribution of faults. We describe two of these models. The first is a "simple model" that intentionally neglects the presence of faults west of a boundary defined by the Xianshuihe–Xiaojiang fault system and the Dien Bien Phu fault. The second is our "preferred model" that reflects our best effort at finding a model geometry that adequately fits the observed geodetic data and conforms most closely to the geometry of mapped faults.

4.5.1 Simple model

The "Simple Model" attempts to fit geodetic data with the simplest representation of the deformation east of the eastern Himalayan syntaxis where rotation is accommodated entirely by slip along the Xianshuihe–Xiaojiang fault system and the Dien Bien Phu faults (fig. 4-6). Although this description captures the first-order characteristics of the deformation, the residual velocities demonstrate the importance and nature of deformation internal to the principal rotating block. Residuals show a significant west-directed (in a South China fixed frame) component to the velocities that emphasizes the importance of east-west extension accommodated by the faults of the Dali-Lijiang-Zhongdian system, the Chenghai fault, north-south trending normal faults in the Tengchong region and left-lateral slip on faults southwest of the Lanping-Simao fold belt described by *Lacassin et al.* (1998). The importance of deformation west of the Xianshuihe–Xiaojiang and Dien Bien Phu fault is also shown by the disparity between the fault slip rates estimated by the model and geologic slip rate determinations. The Dien Bien Phu fault, in particular, must slip much faster in the model than the slip rate estimate of *Zuchiewicza et al.* (2004), suggesting that much if not most of the relative motion of the crust between South China and regions

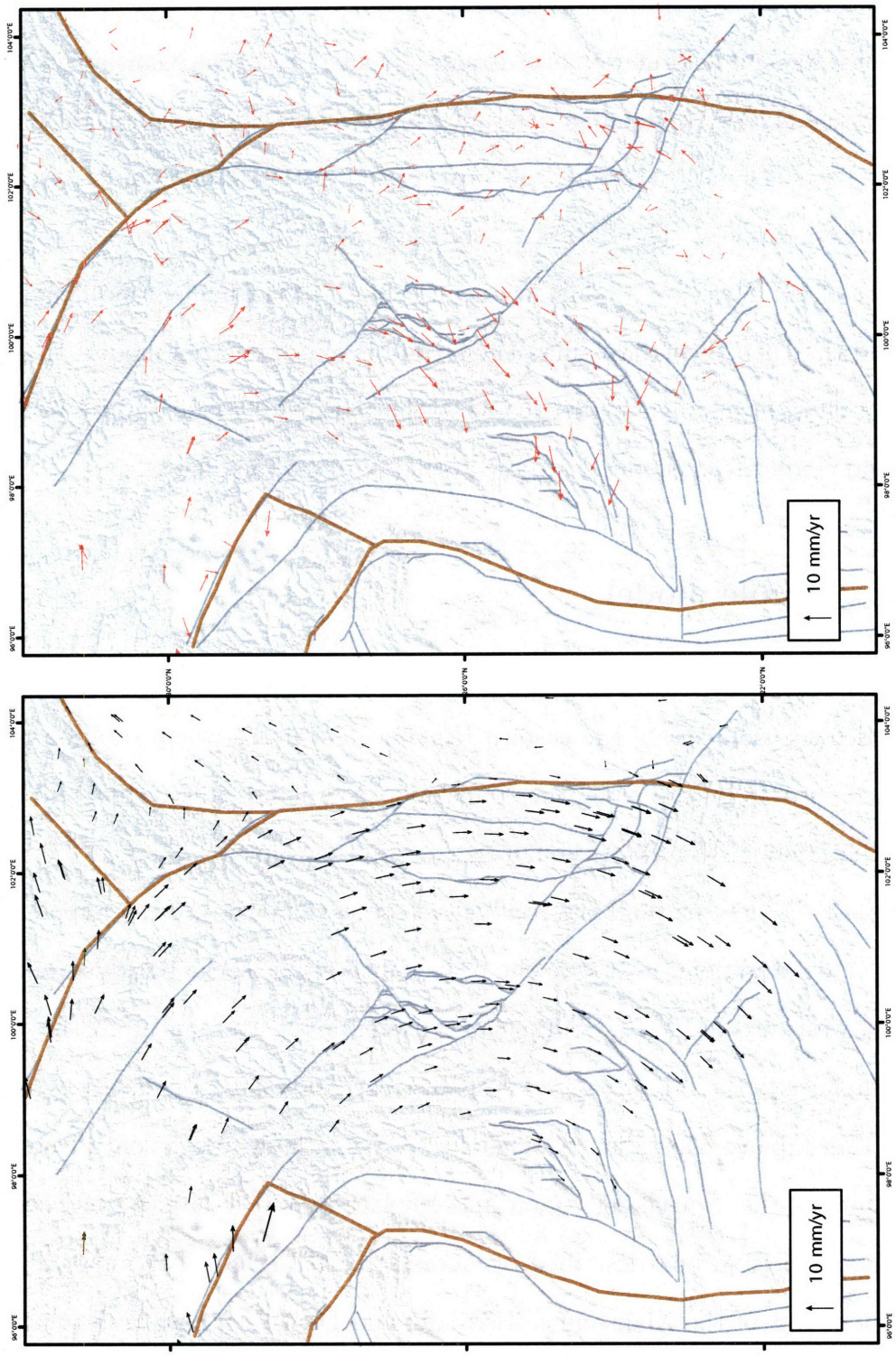

Figure 4-6: Left: Modelled geodetic velocities assuming no internal deformation of the region west of the Xianshuihe-Xiaojiang-Dien Bien Phu fault. Right: Residual velocities, note west directed velocities in western part of the block. Block boundaries in brown, 15km locking depth.

east of the Sagaing fault is accommodated by faults or shear zones west of the Dien Bien Phu fault.

4.5.2 Preferred model

Figure 4-7 shows the block geometry, and modeled and residual velocities for our preferred block model description. As noted above, we tested over two dozen alternate block geometries. The "best" model not only produces an acceptable fit to the geodetic data, but is broadly consistent with the distribution of mapped faults. In principle, a block model that defines an independent block for each GPS station would produce a perfect fit, but would have to essentially ignore the mapped geology. Such a description would be logically equivalent to perfectly continuous deformation, such as proposed for the Tibetan plateau by *Zhang et al.* (2004). Reasonable fits can be accommodated with fewer blocks – as in *Meade* (submitted)'s parametrization of this region in his block model for the entire India–Asia collision zone. For our purposes, we are interested in representing the mapped geology as well as possible. Where we leave out faults, it is because the availability of geodetic data precludes being able to distinguish between our "preferred" model (fig. 4-7) and a more "realistic" one (as in the case of the faults southwest of the Lanping-Simao fold belt) or because adding more block boundaries significantly degraded the fit between model and observation (as in the case of the multiple strands of the southern Xiaojiang fault system).

Several features of this model are worth emphasizing. First, a comparison between the modeled slip rates on block bounding faults and the geologic slip rate determinations (fig. 4-8) shows broad agreement, with some notable exceptions. As discussed, due to the distribution of geodetic data, we have to represent the multiple faults southwest of the Lanping-Simao fold belt by only two boundaries, corresponding to the Nantinghe and Dien Bien Phu faults. The modeled slip rate for the Dien Bien Phu fault agrees well with the estimates of *Zuchiewicza et al.* (2004), and demon-

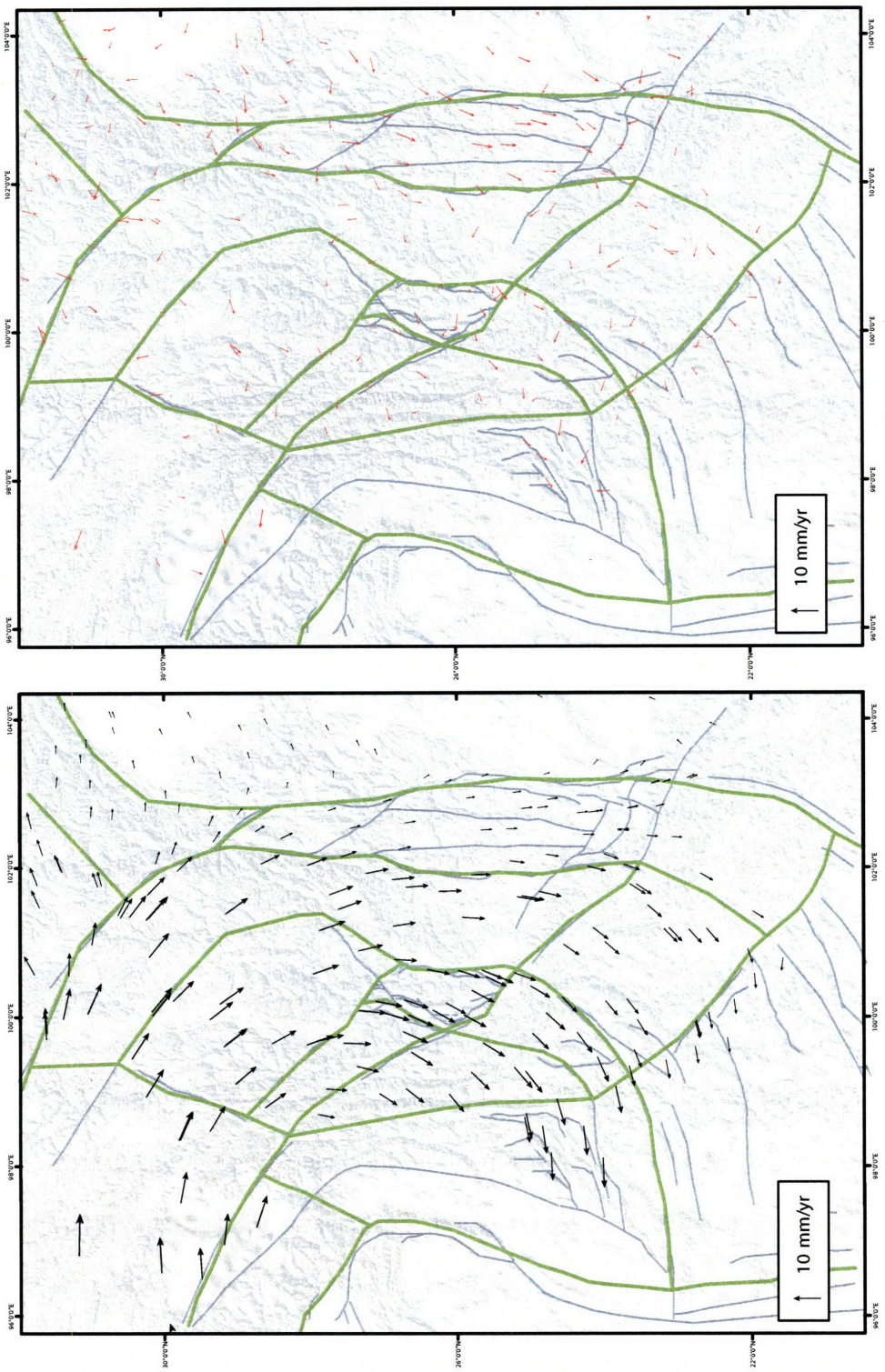

Figure 4-7: Full block model of geodetic velocities, block boundaries in green. Left: Model velocities. Right: Residual velocities, note coherent southward directed velocities in between the two block boundaries representing the multiple splays of the Xiaojiang fault system. Note also the presence of block boundaries where no faults are mapped.

strates the importance of faults and shear zones to the west in accommodating the relative motion of the crust east of the syntaxis and South China. On the other hand, these faults are collectively represented in the block model by the Nantinghe fault alone, and the modeled slip rate on this boundary is considerably greater than that estimated by *Lacassin et al.* (1998). In the model, the boundary corresponding to the Sagaing fault slips at 59.8±3.3 mm/yr, considerably faster than the 18±6 mm/yr determined by *Bertrand and Rangin* (2003). This is because a significant portion of the relative motion between India and Indochina is accommodated by oblique reverse faults in the Indo-Burman ranges (*Satyabala* (2003)), and we do not have geodetic data that would allow us to represent these boundaries separately.

Second, we find that the Xiaojiang fault system is poorly represented in the model, south of where the Xianshuihe fault splays into the Anninghe and Shimian faults. This is shown by both the poor match between modeled and geologic slip rates, and the large, coherent residuals within the two modeled strands of the fault. Most of the relative motion between the crust west of the Xiaojiang fault system and South China is accommodated in the model by slip on the western side of the fault system, which is contrary to all other slip rate estimates, where the easternmost strand is the most active and fastest slipping.

Third, the model demonstrates the importance of extension in this region. Fault-normal slip is inferred on most faults south of a latitude more or less parallel with the position of the eastern Himalayan syntaxis. Most prominently, the Chenghai fault is modeled as accommodating 6.8±1.4 mm/yr of fault-normal slip. Some of this motion may be accommodated on faults west of the Chenghai fault (fig. 4-4), but the significant extension in this area is consistent with abundant geologic evidence for extensional basin formation and the preponderance of normal fault focal mechanism solutions in this area. The modeled slip rate on the Red River fault is much lower than the modeled fault-normal slip on the Chenghai fault, and most of this motion is

therefore not transferred to right lateral slip on that fault, consistent with *Schoenbohm et al.* (2006)'s interpretation that slow right lateral slip on the Red River fault is not presently related to extension in the Dali region.

Finally, modeled slip rates for block boundaries defined in the absence of mapped geologic faults demonstrate that significant strain-rates are accommodated in these regions without obvious through-going faults (fig. 4-8). The boundary west of the Nu (Salween) River connecting normal faults of the Tengchong region with the Jiali fault accommodates 5.2±1 mm/yr of right-lateral slip. Although most published maps show a right lateral fault in the extremely straight Nu River valley, there is no geomorphic or seismic evidence for an active fault in this area. Right lateral shear may be either distributed in a broad zone or be accommodated on an unknown fault or set of faults west of the Nu river. The block boundary linking the northeastern tip of the Lijiang fault with the southeastern tip of the Litang fault accommodates 2.7±1 mm/yr of left-lateral slip. There is no mapped fault in this area, but the relocated earthquakes of *Yang et al.* (2005) seem to define a zone of deformation that may connect these faults. We model three block boundaries crossing the Lanping-Simao fold belt, each of which accommodates significant left-lateral motion. In fact, the modeled slip rates on these boundaries are considerably faster than either the modeled or geologically estimated slip rates on other, more prominent faults. We address the question of how to reconcile the apparently fast slip rates on these boundaries with the geology of these areas in the next section.

4.6 Geologic record of distributed deformation

Meade (submitted) has modeled the geodetic velocities in this area using a block geometry that involves only three major boundaries in this region, the first corresponding to the Xianshuihe, Xiaojiang and Dien Bien Phu faults, the second linking

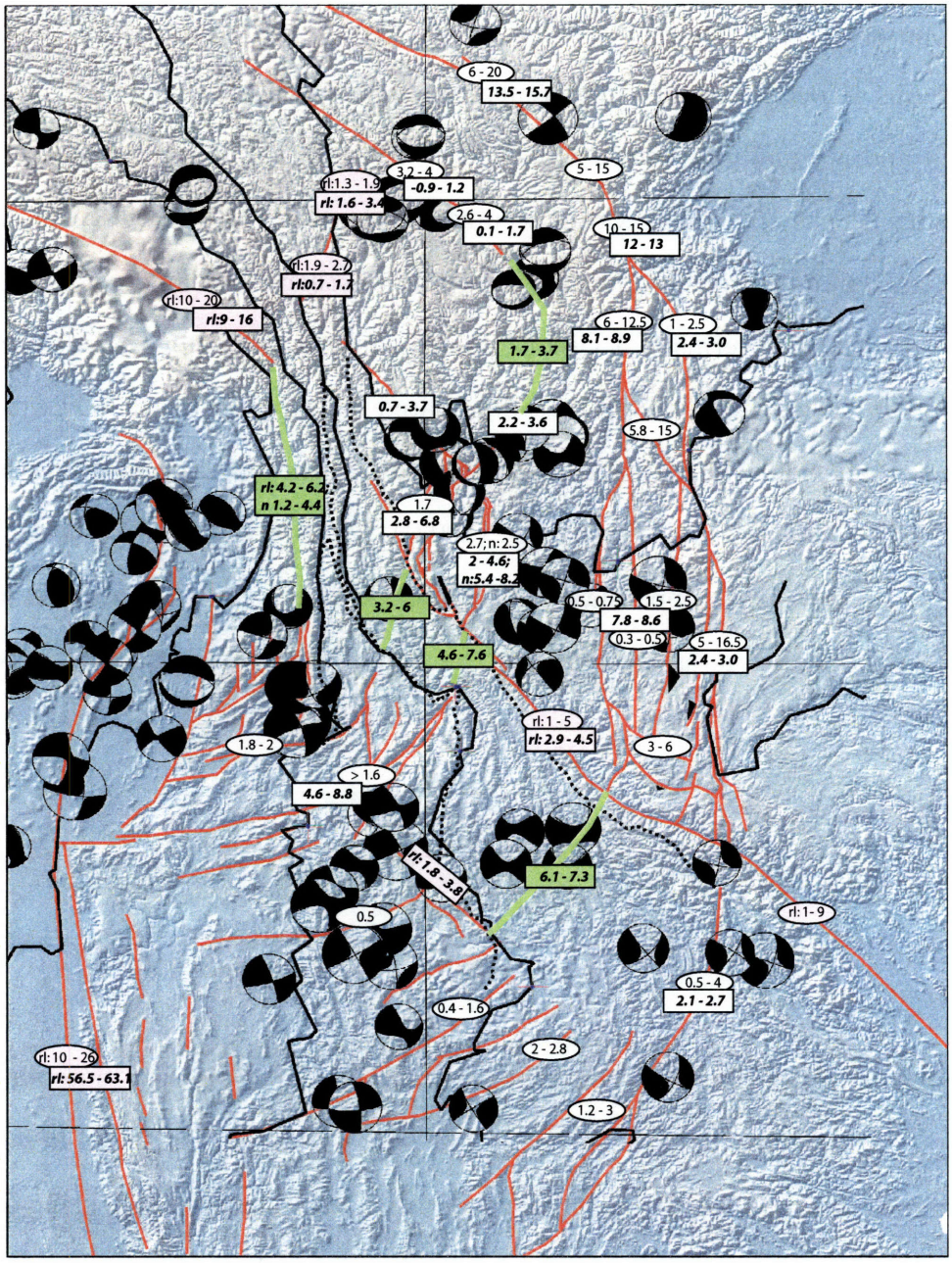

Figure 4-8: geologic slip rates compared to modeled slip-rates. Modeled slip-rates are shown in boxes, geologic slip-rates in ellipses. White boxes or ellipses show left-lateral slip-rates, pink boxes are right-lateral, extensional slip prefixed by "n:". Thick green lines show where block boundaries pass through areas where no active faults are mapped.

the Nantinghe and Chenghai faults and extending north to connect with the Xianshuihe fault and the third corresponding to the Sagaing and Jiali faults. Geodetic velocities are well explained by such a model, thus demonstrating that the apparent continuous velocity field need not reflect distributed deformation (eg. *Zhang et al.* (2004)) and is equally or better explained by the rotation of a very small number of deforming blocks and elastic strain accumulation at their boundaries. This work has considerable implications for debates regarding whether Eurasian crustal deformation is best described in terms of a viscous fluid model (eg. *England and Molnar* (1990); *England and Houseman* (1988)) or is dominated by the plate tectonic-like motions of a small number of rigid crustal blocks bounded by lithosphere penetrating strike-slip faults (eg. *Replumaz and Tapponnier* (2003)). At the very least, *Meade* (submitted)'s work shows that apparently continuous geodetic velocity fields cannot simply be taken at face value as representing the accumulation of permanent, distributed strain.

Our block modeling efforts, on the other hand, are an attempt to represent mapped geology as closely as possible. That is, the success of a block model description is determined, for us, not only by fitting geodetic velocities but also capturing important characteristics of the mapped geology. As described above, we find that in many places, our "preferred" model fits geodetic velocities, predicts reasonable slip-rates and uses a block geometry that is consistent with the distribution of mapped faults. In other places, however, this is not the case; in this section, we describe the geology of two areas that most obviously show important differences between the block model description and the geologic record.

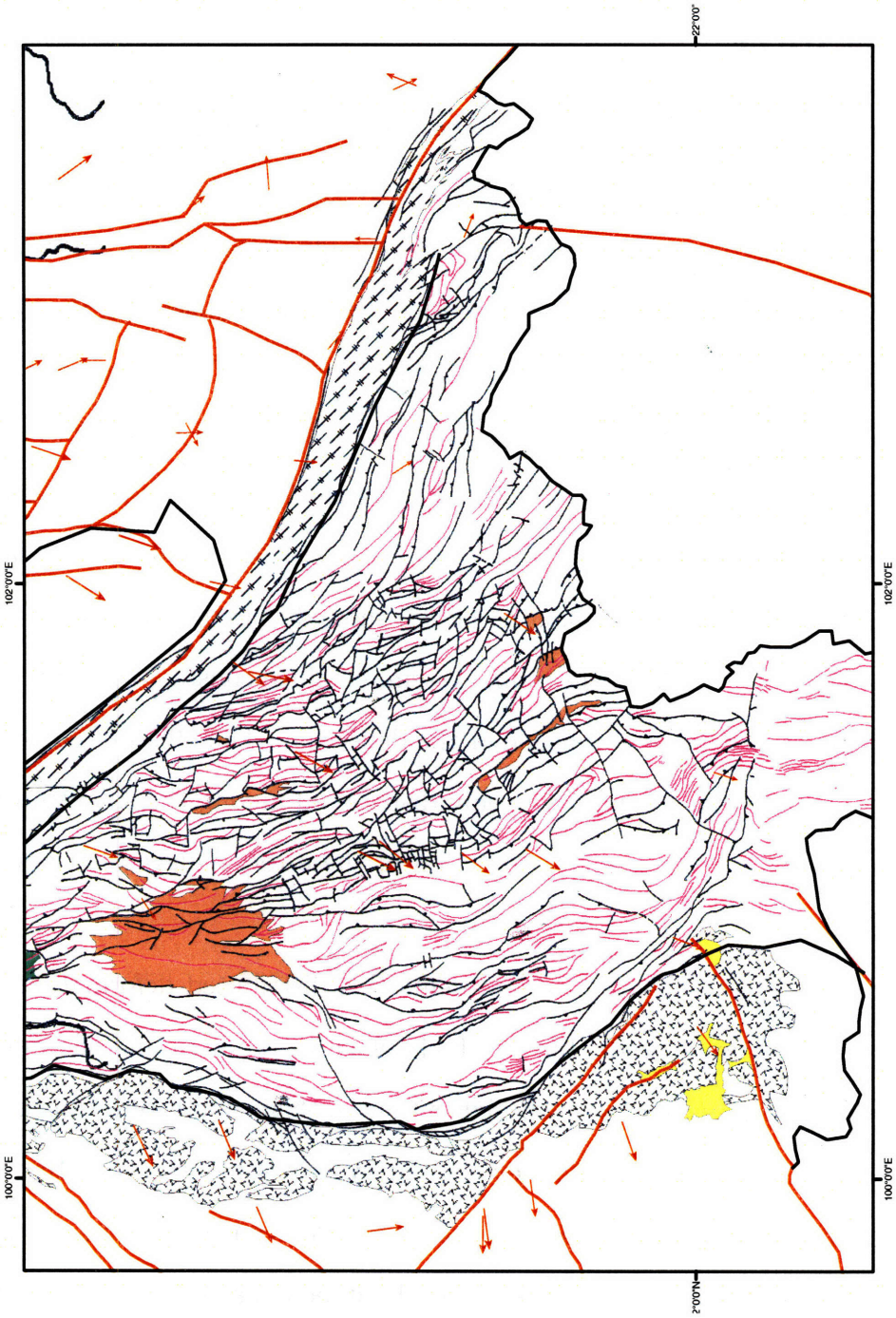

Figure 4-9: Map of the southern part of the Lanping-Simao fold belt. Active faults north and south of the belt are shown as red lines; geodetic velocities as red arrows. Thin purple lines and black lines show mapped fold axes and faults within the Lanping-Simao belt compiled from 1:200000 scale geological maps (*BGMR Yunnan* (1990); *Burchfiel et al.* (In prep.)).

4.6.1 Xiaojiang fault system and deformation south of the Red River

From where the Xianshuihe fault splits into two splays at the Anninghe and Shimian faults south to the Red river, strain becomes progressively less localized and is distributed among numerous splays of the Xiaojiang fault system (fig. 4-9). Where the splays of the Xiaojiang fault system intersect, they are numbered in the dozens, but none of them offset the contact between mylonitic rocks of the Ailaoshan shear zone and young sediments north of the shear zone (*Schoenbohm et al.* (2006)). Although not obviously affected by individual splays of the Xiaojiang fault system, the Ailaoshan rocks are deflected into a broad bend consistent with distributed left-lateral shear in a >125km wide zone. *Wang et al.* (1998) showed that the cumulative offsets of the various strands of the Xiaojiang fault system remained constant at about 60km, which is also the approximate amplitude of the deflection. The 60km of cumulative offset was not found to be completely evenly distributed among the splays north of the Ailaoshan rocks, but the smooth deflection of these rocks suggests very evenly distributed strain.

Our block model geometry poorly represents this distributed deformation. The block model involves two strands, but residual velocities are high and the modeled slip rate on the western strand is much higher than geologic slip rate estimates. On the other hand, we find that adding a block boundary corresponding to the Red River fault joining the southern ends of these two strands significantly degrades the model fit. West of the western fault, we require a block boundary that slips at a right lateral rate of 3.7±1.6 mm/yr, consistent with geologic slip rate estimates for the fault in this area (fig. 4-8 and table 4.4.2). The modeled slip rates on the Red River fault – slow but measurable west of the Xiaojiang fault, possibly inactive in the region of the Xiaojiang splays – is broadly consistent with the mapping and interpretations of *Schoenbohm et al.* (2006).

Similarly, there is no obvious correspondence between block boundaries and the geologic record of deformation south of the Ailaoshan rocks. In the block model, two boundaries cross the Lanping-Simao fold belt in the region shown in figure 4-9. The more easterly boundary corresponds to the Dien Bien Phu fault, and the modeled slip rates of 2.4±0.3 mm/yr are consistent with the geologic slip rates determined by *Zuchiewicza et al.* (2004). The other model boundary slips left-laterally at 6.7±0.6 mm/yr. The location of the boundary is close to the locations of four significant (magnitudes 6 - 7) earthquakes with left-lateral focal mechanisms, but there is no single, prominent through-going fault that might accommodate this deformation. In figure 4-9, we show mapped faults and folds in the Lanping-Simao fold belt from a compilation of 1:200000 geologic survey maps (*BGMR Yunnan* (1990); *Burchfiel et al.* (In prep.)). Folds and generally north-south striking reverse faults are Eocene to mid-Miocene compressional structures that were probably broadly contemporaneous with motion on the transpressional left-lateral Ailaoshan shear zone (*Wang and Burchfiel* (1997); *Schoenbohm et al.* (2005); *Leloup et al.* (1995)). Beyond these early structures, the map reveals a large number of east to east-northeast striking faults that offset the early structures, but which individually lack much along-strike continuity or appreciable separation. We suspect that these late structures accommodate the significant active left-lateral shear in this area. Strain in this area is thus more poorly localized than even in the southern part of the Xiaojiang fault system.

4.6.2 Deformation of the northern Lanping-Simao fold belt

The deformation of the northern part of the Lanping-Simao fold belt (fig. 4-10) shows many of the same characteristics as described in the previous section. In the block model, we require two boundaries that cross the Lanping-Simao fold belt in the northern part of the belt. One boundary connects the left-normal Jianchuan fault with the Wanding fault and another connects the Nantinghe and Chenghai faults.

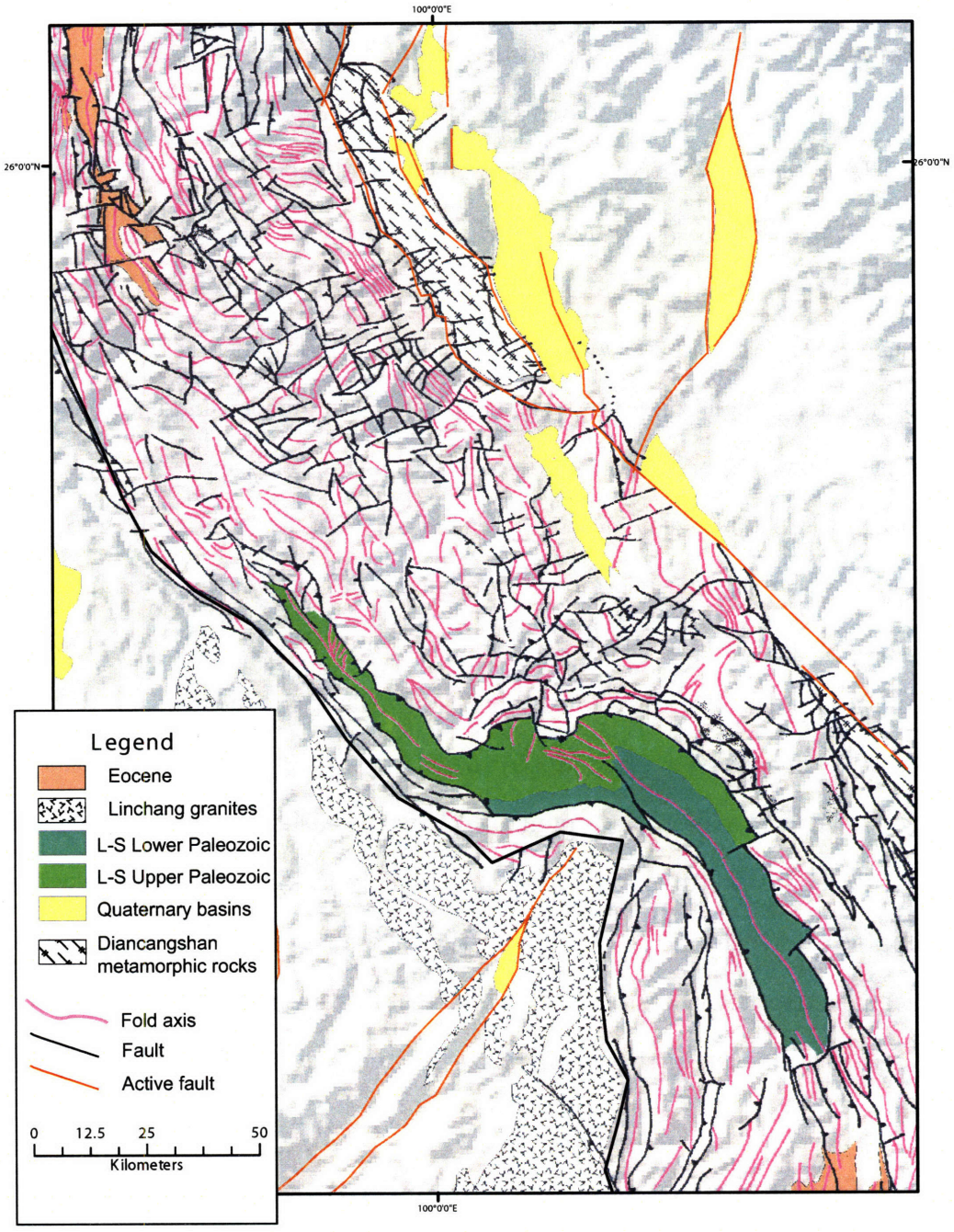

Figure 4-10: Map of the northern part of the Lanping-Simao fold belt. Active faults cannot be traced through the belt, but deform the boundaries of the belt. Fold axes and faults are compiled from mapped structures shown in 1:200000 scale geology maps *BGMR Yunnan* (1990); *Burchfiel et al.* (In prep.)

These accommodate 4.6±1.4 mm/yr and 6.1±1.5 mm/yr of left-lateral slip. The left-normal Jianchuan and Chenghai faults do not cross the boundary between South China rocks and rocks of Lanping-Simao. Similarly, left-lateral faults southwest of Lanping-Simao cannot be traced into Lanping-Simao proper. Slip propagates past the tip line of these faults, however, and deforms the boundary separating Lanping-Simao from Lingchang rocks to the southwest, most prominently northeast of the tip line of the Nantinghe fault. Paleozoic rocks that form the basement to the terrestrial Mesozoic-Cenozoic sediments of the Lanping-Simao belt are also seen to be deflected along with the boundary. As in the southern part of the Lanping-Simao fold belt described in the previous section, early formed folds and faults are folded, rotated and offset by small, discontinuous strike-slip faults. In short, there is abundant evidence that strain is propagated through this area, but it is diffuse, distributed and poorly localized.

4.7 Discussion

In this paper, we have considered both geologic and geodetic perspectives on the active tectonics of eastern Tibet and southwestern China in order to better characterize the active tectonics, as well as to gain insight into the nature of crustal deformation generally. In this section, we (1) assess the insights provided by block models of geodetic data and compare geodetic and geologic perspectives of the active deformation; (2) discuss implications for our understanding of the modes and mechanisms of crustal deformation; and (3) summarize the tectonic implications of the geologic and geodetic data in this area.

Geology, geodesy, and modeling We modeled the geodetic data in this area in terms of rotations of a finite number of fault-bounded blocks and strain accumulation at the block boundaries predicted by a simple model of interseismic strain accumu-

lation. The geodetic data are not particularly well fit by a simple model that only involves the rotation of a single crustal block bounded to the east by the Xianshuihe and related faults. Alternate model geometries can be found that adequately fit the geodetic data, using one or two additional block boundaries (*Meade* (submitted)). For our purposes, however, we attempted to represent the known geology in as detailed a manner as possible. The resulting model geometry explains the geodetic velocities and predicts slip rates on the block boundaries that are consistent with at least the better constrained geologic slip rates. This gives us some confidence that the geodetically constrained slip rates provide meaningful insight into the long term geologic slip rates for faults where independent geologically determined slip rates are poorly known. Many of the places where the modeled slip rates are obviously wrong are simple and expected consequences of having sparse data – for example, the modeled rate on the Sagaing fault is too high, because we do not have the data to resolve the contribution of oblique slip faults in the Indo-Burman ranges.

The block model description of deformation is considerably less satisfying where strain is poorly localized. In the southern part of the Xiaojiang fault system, complex partitioning of strain, rotation of small crustal fragments and interseismic strain accumulation are all potential contributors to the poor fit between model and observation. A related, but distinct question is how best to model broad zones of distributed strain, such as is observed in the Lanping-Simao fold belt. In this paper, we defined four block boundaries crossing the Lanping-Simao fold belt and found that this model geometry fits the observed geodetic data well. Accepting that the model description is an idealization, the block modeling approach proves very useful in quantifying the strain accumulation in these broad zones of diffuse deformation. Further work needs to be done to see how sensitive the model rates are to alternate model descriptions – possibly including more boundaries, different locking depths, or more complicated rheologies. Assessing how reliable these slip rates are is a challenge however, because

it is not clear how to determine meaningful long-term geologic rates in a place like the Lanping-Simao fold belt.

Crustal deformation Geodetic data have been used to weigh in on debates regarding the appropriate conceptualization of crustal deformation in Tibet and surrounding areas. *Zhang et al.* (2004) argued that the apparently continuous nature of the measured geodetic velocity field suggested diffuse, continuous deformation on the plateau. *Holt et al.* (2000) incorporated geodetic measurements in a viscous fluid model of Eurasian deformation. *Wallace et al.* (2004); *Shen et al.* (2001) and others have used geodetic data to infer relatively slow slip rates on major Tibetan faults. On the other hand, the same geodetic observations can be at least as well-explained in terms of a deforming block model (*Meade* (submitted)). In the area described in this paper, there are places where deformation is accommodated along a few, discrete, prominent faults, but elsewhere, the deformation is essentially totally diffuse. It is perhaps worth emphasizing that this is information known from the geology, not from modeling the geodetic data. Given that strain is localized in places but not in others, the relevant question to ask is what are the possible controls on strain localization. Clearly, the Lanping-Simao fold belt is associated with diffuse, poorly localized deformation. We note that the Lanping-Simao fold belt is dominated by poorly indurated terrestrial sediments and the tight, upright fold style that dominates the early deformation in the belt implies the presence of weak, shallow detachments. It is possible that poorly localized deformation observed here is an entirely upper crustal phenomena, and that the characteristics of the deformation at the surface tell us little about the middle or lower crust, let alone the mantle lithosphere.

The tectonics of the eastern Himalayan syntaxial region This review and compilation of the geologic and geodetic data on the active deformation in the eastern syntaxial region re-emphasizes the original interpretations put forward by *Wang and*

Burchfiel (1997) and *Wang et al.* (1998) from syntheses of geologic data and by *Holt et al.* (1991) from syntheses of limited fault slip data and seismicity catalogues. The modern tectonic regime in this area is dominated by the clockwise rotation of crustal material bounded by the Xianshuihe and Xiaojiang faults about the eastern Himalayan syntaxis. The geodetic and geologic data compiled here largely confirm these descriptions, with some distinctions. Although the Xianshuihe and related faults are the most important faults in the region, left lateral slip on these faults is not completely transferred to the Dien Bien Phu fault. Geodetic data are consistent with the low slip rates on this fault found by *Zuchiewicza et al.* (2004). Left-lateral slip, and consequently, rotation, are progressively relayed to structures west of the main bounding faults starting where the Xianshuihe first splays into the Anninghe and Shimian faults. This progressive relay into internal structures is accompanied by a significant component of east-west extension. With the exception of the Tengchong region, the importance of extension in the active tectonic regime has been under-emphasized, and normal faults are commonly interpreted as merely the second order results of extensional step-overs, pull-aparts and releasing bends on strike-slip faults. In this regard, it is worth mentioning the almost complete lack of slip-rate estimates for fault normal motion in this area. Despite the common occurrence of normal fault mechanisms in the seismic record, normal faulting may represent the largest source of poorly characterized, let alone quantified seismic risk in this area.

Acknowledgements

We thank Brendan Meade for providing us with his block modeling code, as well as for advice, encouragement and considerable insight. Lori Eich provided considerable assistance in using the block modeling code. The first author acknowledges support from Les Fonds Pour la Recherce en Sciences et Technologies (Québec) during the

course of graduate studies at MIT. This research was supported by NSF awards EAR 0003571 and EAR 8904096.

References

Akciz, S. O. (2004), Structural and geochronological constraints on the ductile deformation observed along the Gaoligong Shan and Chong Shan shear zones, Yunnan (China), Ph.D. thesis, MIT.

Allen, C. R., K. Sieh, A. Gillespie, Y. Han, B. Zhang, and C. Zhu (1984), Red River and associated faults, Yunnan province, China: Quaternary geology, slip rates, and seismic hazard, *Geological Society of America Bulletin*, *95*(6), 686–700.

Allen, C. R., Z. Luo, H. Qian, X. Wen, H. Zhou, and W. Huang (1991), Field study of a highly active fault zone: the Xianshuihe fault of southwest China, *Geological Society of America Bulletin*, *103*, 1178–1199.

Armijo, R., P. Tapponnier, and T. Han (1989), Late Cenozoic right-lateral strike-slip faulting in southern Tibet, *Journal of Geophysical Research*, *94*, 2787–2838.

Avouac, J.-P., and P. Tapponnier (1993), Kinematic model of active deformation in central Asia, *Geophysical Research Letters*, *20*, 895–898.

Bertrand, G., and C. Rangin (2003), Tectonics of the western margin of the Shan plateau (central myanmar): implication for the India-Indochina oblique convergence since the Oligocene, *Journal of Asian Earth Sciences*, *21*(10), 1139–1157, doi:10.1016/S1367-9120(02)00183-9.

BGMR Yunnan (1990), *Yunnan Bureau of Geology and Mineral Resources*, 1:200000 Regional Map Series, various sheets.

Burchfiel, B. C. (2004), 2003 Presidential address: New technology, new geological challenges, *GSA Today*, *14*, 4–9.

Burchfiel, B. C., and E. Wang (2003), Northwest-trending, middle Cenozoic, left-lateral faults in southern Yunnan, China, and their tectonic significance, *Journal of Structural Geology*, *25*, 781–792, doi:10.1016/S0191-8141(02)00065-2.

Burchfiel, B. C., Z. Chen, et al. (In prep.), Tectonostratigraphic map of eastern Tibet and Yunnan province, map and accompanying notes in preparation.

Burchfiel, B. C., C. Studnicki-Gizbert, J. Geissman, Z. Chen, L. Chen, and S. Akciz (submitted), How much strain can continental crust accommodate without developing obvious through-going faults?, submitted to *GSA Special Paper*.

Chen, Q., J. T. Freymueller, Q. Wang, Z. Yang, C. Xu, and J. Liu (2004), A deforming block model for the present-day tectonics of Tibet, *Journal of Geophysical Research*, *109*, B01,403+, doi:10.1029/2002JB002151.

Chen, Z., B. C. Burchfiel, Y. Liu, R. W. King, L. H. Royden, W. Tang, E. Wang, J. Zhao, and X. Zhang (2000), Global positioning system measurements from eastern Tibet and their implications for India/Eurasia intercontinental deformation, *Journal of Geophysical Research*, *105*(B7), 16,215–16,228.

Chevalier, M. L., F. J. Ryerson, P. Tapponnier, R. C. Finkel, J. Van Der Woerd, L. Haibing, and L. Qing (2005), Slip-rate measurements on the Karakorum fault may imply secular variations in fault motion, *Science*, *307*(5708), 411–414, doi: 10.1126/science.1105466.

Cong, D. C., and K. Feigl (1999), Geodetic measurement of horizontal strain across the Red River fault near Thac Ba, Vietnam, 1963-1994, *Journal of Geodesy*, *73*(6), 298–310, doi:10.1007/s001900050247.

England, P., and P. Molnar (1990), Right-lateral shear and rotation as the explanation for strike-slip faulting in eastern Tibet, *Nature*, *344*, 140–142.

England, P. C., and G. A. Houseman (1988), The mechanics of the Tibetan plateau, *Philosophical Transactions of the Royal Society of London A*, *326*, 301–320.

Guo, S., H. Xiang, X. Xu, W. Zhang, R. Zhou, and X. Dong (2000), Longlin-Lancang fault zone in southwest Yunnan, China – a newly-generated rupture zone in continental crust, *Chinese Science Bulletin*, *45*, 376–379.

Hallet, B., and P. Molnar (2001), Distorted drainage basins as markers of crustal strain east of the Himalaya, *Journal of Geophysical Research*, *106*(B7), 13,697–13,710.

He, H., and E. Tsukuda (2003), Recent progresses of active fault research in China, *Journal of Geography (Tokyo Geog. Soc.)*, *112*, 489–520.

Holt, W. E., J. F. Ni, T. C. Wallace, and A. J. Haines (1991), The active tectonics of the eastern Himalayan syntaxis and surrounding regions, *Journal of Geophysical Research*, *96*(B9), 14,595–14,632.

Holt, W. E., N. Chamot-Rooke, X. L. Pichon, A. J. Haines, B. Shen-Tu, and J. Ren (2000), Velocity field in Asia inferred from Quaternary fault slip rates and global positioning system observations, *Journal of Geophysical Research*, *105*(B8), 19,185–19,210.

King, R., F. Shen, B. Burchfiel, L. Royden, E. Wang, Z. Chen, Y. Liu, X. Zhang, J. Zhao, and Y. Li (1997), Geodetic measurement of crustal motion in southwest China, *Geology*, *32*, 809–812.

Kostrov, V. (1974), Seismic moment and energy of earthquakes, and seismic flow of rock, *Physics of the Solid Earth*, *1*, 13–21.

Lacassin, R., A. Replumaz, and H. P. Leloup (1998), Hairpin loops and slip-sense inversion on southeast Asian strike-slip faults, *Geology*, *26*, 703–706.

Lee, H. Y., S. L. Chung, J. R. Wang, D. J. Wen, C. H. Lo, and T. F. Yang (2003), Miocene Jiali faulting and its implications for Tibetan tectonic evolution, *Earth and Planetary Science Letters*, *205*, 185–194, doi:10.1016/S0012-821X(02)01040-3.

Leloup, P. H., R. Lacassin, P. Tapponnier, U. Scharer, D. Zhong, X. Liu, L. Zhang, S. Ji, and P. T. Trinh (1995), The Ailao Shan-Red River shear zone (Yunnan, China), Tertiary transform boundary of Indochina, *Tectonophysics*, *251*(1-4), 3–84, doi:10.1016/0040-1951(95)00070-4.

Leloup, P. H., N. Arnaud, R. Lacassin, J. R. Kienast, T. M. Harrison, T. T. P. Trong, A. Replumaz, and P. Tapponnier (2001), New constraints on the structure, thermochronology, and timing of the Ailao Shan-Red River shear zone, SE Asia, *Journal of Geophysical Research*, *106*(B4), 6683–6732.

Meade, B. (submitted), Present-day kinematics of the India-Asia collision zone, submitted to *Geology*, 2006.

Meade, B. J., and B. H. Hager (2005), Block models of crustal motion in southern California constrained by GPS measurements, *Journal of Geophysical Research*, *110*, B03,403+, doi:10.1029/2004JB003209.

Molnar, P., and Q. Deng (1984), Faulting associated with large earthquakes and the average rate of deformation in central and eastern Asia, *Journal of Geophysical Research*, *89*(B7), 6203–6208.

Molnar, P., and P. Tapponnier (1978), Active tectonics of Tibet, *Journal of Geophysical Research*, *83*(B11).

Okada, Y. (1985), Surface defomation due to shear and tensile faults in a half-space, *Bulletin of the Seismological Society of America*, *75*, 1135–1154.

Papadimitriou, E., X. Wen, V. Karakostaas, and X. Jin (2004), Earthquake triggering along the Xianshuihe fault zone of western Sichuan, China, *Pure and Applied Geophysics*, *161*, 1683–1707, doi:10.1007/s00024-003-2471-4.

Replumaz, A., and P. Tapponnier (2003), Reconstruction of the deformed collision zone between India and Asia by backward motion of lithospheric blocks, *Journal of Geophysical Research*, *108*(B6), 2285+, doi:10.1029/2001JB000661.

Replumaz, A., R. Lacassin, P. Tapponnier, and P. H. Leloup (2001), Large river offsets and Plio-Quaternary dextral slip rate on the Red River fault (Yunnan, China), *Journal of Geophysical Research*, *106*(B1), 819–836.

Satyabala, S. P. (2003), Oblique plate convergence in the Indo-Burma (Myanmar) subduction region, *Pure and Applied Geophysics*, *160*, 1611–1650.

Savage, J. C., and R. O. Burford (1973), Geodetic determination of relative plate motion in central California, *Journal of Geophysical Research*, *78*, 832–845.

Schoenbohm, L. M., C. B. Burchfiel, C. Liangzhong, and Y. Jiyun (2005), Exhumation of the Ailao Shan shear zone recorded by Cenozoic sedimentary rocks, Yunnan Province, China, *Tectonics*, *24*, TC6015+, doi:10.1029/2005TC001803.

Schoenbohm, L. M., C. B. Burchfiel, L. Chen, and J. Yin (2006), Miocene to present activity along the Red River fault, China, in the context of continental extrusion, upper-crustal rotation, and lower-crustal flow., *Geological Society of America Bulletin*, doi:10.1130/B25816.1.

Shen, Z.-K., M. Wang, Y. Li, D. D. Jackson, A. Yin, D. Dong, and P. Fang (2001), Crustal deformation along the Altyn Tagh fault system, western China, from GPS, *Journal of Geophysical Research*, *106*(B12), 30,607–30,622.

Shen, Z.-K., J. LÃ, M. Wang, and R. BÃrgmann (2005), Contemporary crustal deformation around the southeast borderland of the Tibetan Plateau, *Journal of Geophysical Research*, *110*, B11,409+, doi:10.1029/2004JB003421.

Sun, Y., S. Kuleli, F. D. Morgan, W. Rodi, and N. Toksoz (2004), Location robustness of earthquakes in Sichuan province, *Seismological Research Letters*, *75*, 54–62.

Tapponnier, P., and P. Molnar (1976), Slip-line theory and large-scale continental tectonics, *Nature*, *264*, 319–324.

Tapponnier, P., G. Peltzer, R. Armijo, and P. Cobbold (1982), Propagating extrusion tectonics in asia; new insights from simple experiments with plasticine, *Geology*, *10*(12), 611–616.

Tapponnier, P., G. Pelzer, and R. Armijo (1986), On the mechanics of the collision between India and Asia, in *Collision Tectonics*, *Geological Society of London Special Publication*, vol. 19, edited by M. P. Coward and A. C. Ries, The Geological Society, London.

Wallace, K., G. Yin, and R. Bilham (2004), Inescapable slow slip on the Altyn Tagh fault, *Geophysical Research Letters*, *31*, L09,613+, doi:10.1029/2004GL019724.

Wang, E., and B. Burchfiel (1997), Interpretation of Cenozoic tectonics in the right-lateral accomodation zone between the Ailao Shan shear zone and the eastern Himalayan syntaxis, *International Geology Review*, *39*, 191–219.

Wang, E., and B. C. Burchfiel (2000), Late Cenozoic to holocene deformation in southwestern Sichuan and adjacent Yunnan, China, and its role in formation of the southeastern part of the Tibetan plateau, *Geological Society of America Bulletin*, *112*, 413–423.

Wang, E., B. Burchfiel, L. Royden, L. Chen, J. Chen, W. Li, and Z. Chen (1998), *Late Cenozoic Xianshuihe-Xiaojiang, Red River, and Dali Fault Systems of Southwestern Sichuan and Central Yunnan, China*, *GSA Special Paper*, vol. 327, Geological Society of America.

Wang, S., G. Li, Q. Zhang, and C. Lan (2000), Engineering geological study of the active tectonic region for hydropower development on the Jinsha river, upstream of the Yangtze river, *Acta Geologica Sinica*, *74*, 353–361.

Weldon, R., K. Sieh, C. Zhu, Y. Han, J. Yang, and S. Robinson (), Slip rate and recurrence interval of earthquakes on the Hong He (Red River) fault, Yunnan, PRC.

Xu, X., X. Wen, R. Zheng, W. Ma, F. Song, and G. Yu (2003), Pattern of latest tectonic motion and its dynamics for active blocks in Sichuan-Yunnan region, China, *Science in China Series D*, *46*, 210–226.

Yang, Z. X., F. Waldhauser, Y. T. Chen, and P. G. Richards (2005), Double-difference relocation of earthquakes in central-western China, 1992 - 1999, *Journal of Seismology*, *9*, 241–264.

Zhang, P.-Z., Z. Shen, M. Wang, W. Gan, R. Bürgmann, P. Molnar, Q. Wang, Z. Niu, J. Sun, J. Wu, S. Hanrong, and Y. Xinzhao (2004), Continuous deformation of the Tibetan plateau from global positioning system data, *Geology*, *32*, 809–812.

Zhou, R.-J., G.-X. Chen, Y. Li, Z.-H. Zhou, Y. Gong, Y.-L. He, and X.-G. Li (2005), Research on active faults in Litang–Batang region, western Sichuan province, and the seismogenic structures of the 1989 Batang M6.7 earthquake swarm, *Dizhen Dizhi (Seismol. Geol.)*, *27*, 31–43.

Zuchiewicza, W., N. Q. Cuong, A. Bluszczc, and M. Michalik (2004), Quaternary sediments in the Dien Bien Phu fault zone, NW Vietnam: a record of young tectonic porcesses in the light of OSL-SAR dating results, *Geomorphology*, *60*, 269–302.

Chapter 5

Extension, erosion and localized exhumation of the Yulong mountains antiform, Yunnan, China

Christopher Studnicki-Gizbert
Yizhao Wang
B. C. Burchfiel
Liangzhong Chen

Abstract

The Yulong Xueshan (Jade Dragon Snow Mountains) range are an isolated range of anomalously high and steep mountains bisected by the Jinsha (Yangzi) river in western Yunnan province, south and east of Tibet. The range is defined by a closed network of active transtensional faults, the most recent major rupture of which was a M 7.0 quake in 1997. Some of the deepest structural and stratigraphic levels of the Yangzi platform and Three Rivers foldbelts are exposed in the footwalls of these faults and in the nearly 4km deep gorge cut by the Jinsha river through this range. Within the bounding faults, hillslopes are steep and characterised by frequent large magnitude landslides. The Jinsha river itself becomes extremely narrow and anomalously steep within the range, suggesting adjustment to anomalously high rates of surface uplift. We argue that the high, steep topography, exposure of deep structural levels and high rock uplift rates of the Yulong mountains are the result of the interaction of vigorous erosion processes that balance rock uplift rates, a closed network of normal faults that accommodate differential rock uplift rates, and weak middle crust that flows in response to topographically imposed pressure gradients. In this range, high erosion rates are responsible for sustained rapid rock uplift that continues to the present.

5.1 Introduction

The Yulong Xueshan ("Jade Dragon Snow Mountain") are a small isolated mountain range east of Tibet and north of the eastern Himalayan syntaxis. In an area characterized by high plateau like uplands and deep river gorges carved out by some of the largest rivers in Asia, the Yulong mountains stand out. Whereas the average elevation of the surrounding low-relief uplands is around 3600m, the summits of these mountains reach 5500m and are glaciated. Interestingly, the range is bisected by the Jinsha (Yangzi) river, which carves out one of the most spectacular canyons on Earth. From the bottom of the canyon at about 1600m, elevations reach 5500m over less than five kilometers. The range is also notable in that these physiographic anomalies are highly localized: the entire range is less than 40 km north to south and 20 km wide at its widest. The boundaries of the range are very clear, as the range is entirely bounded by a system of active normal and left-lateral transtensional faults, the most recent major rupture of which was a M 7.0 quake in 1997(*He et al.* (2001); *Akamatsu et al.*

(1998)). Moreover, some of the deepest structural levels of the region are exposed in the core of the range. In this paper, we describe geomorphic and geologic evidence for anomalously high rates of erosion and rock uplift within the range-bounding faults that account for the anomalous and localized exhumation. The coincidence of deep river incision with high elevations and active faults suggest a link between surface processes and tectonics, and we explore possible explanations that link extensional tectonics, rapid rock uplift rates and high erosion rates. In particular, we argue that although uplift in the foot walls of the range-bounding normal faults initiated uplift, and accommodate the localized anomalous high rock uplift rates in the range, high rates of erosion prevent the range from reaching static equilibrium elevations, and thus sustain rapid rock uplift rates that continue to the present.

5.2 Geologic Setting

The Yulong mountains lie near the intersection of several major geologic provinces (figure 5.2) whose boundaries are still somewhat imprecisely located, and this region is some times referred to as the Yunling Collage (*Wang et al.*, 1998; *Hughes et al.*, 2002). To the north are the Three Rivers fold belt and Yidun arc, which extend from the Tibetan Plateau. The Lanping-Simao and South China fold belts comprise geologic units to the southeast, southwest and east. Much of the juxtaposition of these units is thought to have occurred in Mesozoic time (*Metcalfe* (1998); *Sengor and Natalin* (1996)), but a considerable amount of subsequent deformation has modified and obscured the original relationships. Late deformation, poor access, poor exposure and limited study are responsible for the large uncertainties and differences between various interpretations and syntheses of the regional geology.

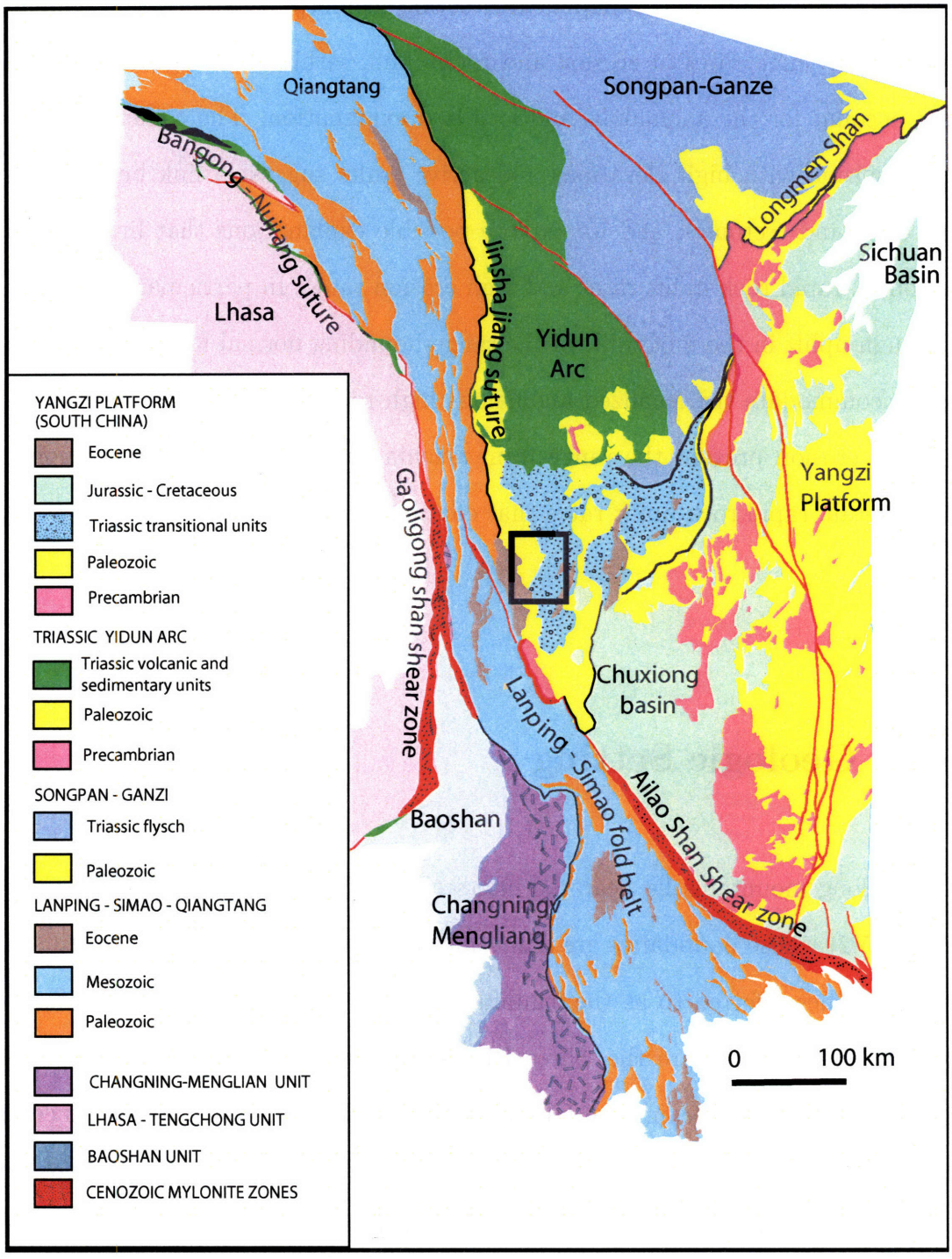

Figure 5-1: Main geologic provinces of Eastern Tibet and Southwest China. Box shows location of study area, and location of figure 5.2.2.

5.2.1 Cenozoic tectonic evolution

Early Cenozoic tectonics includes folding, shortening and rotation of the Lanping-Simao belt, limited shortening in Yangzi rocks, significant strike-slip and transpression on at least three major faults (and perhaps other, less-prominent faults), and rotation and shear of rocks within the Three Rivers zone. Limited crustal shortening accompanied extensive strike-slip accommodated rotation, translation and shear of deforming crustal blocks bounded by the major Gaoligong Shan, Chong Shan and Ailao Shan structures (*Geissman et al.* (submitted); *Akciz* (2004); *Wang and Burchfiel* (1997); *Leloup et al.* (1995, 2001)). Most of the translation, rotation and shear deformation is limited to Lanping-Simao rocks, west of the Jianchuan basin and Jinshajiang suture. In the vicinity of the Yulong mountains, evidence for upper crustal shortening is limited to tilting of poorly exposed early Tertiary rocks of the Jianchuan basin and to minor faults with 100s of meters of throw in the Lijiang area.

Low-relief topographic surfaces are widely developed over both metamorphic rocks associated with the major early faults and the deforming blocks that they bounded (*Clark et al.* (2005, in review); *Wang et al.* (1998)). In Yunnan province, Pliocene sediments are commonly found overlying these surfaces (*Schoenbohm* (2004); *Wang et al.* (1998)), which are typically found at high elevations. Epeirogenic uplift and subsequent incision of the landscape from late Miocene (*Clark et al.* (2005) to early Pliocene (*Schoenbohm et al.* (in press)) time has been interpreted as being the result of channel flows of lower or middle crustal material that thickened the crust with little or no contribution from upper-crustal shortening (*Clark* (2003); *Clark and Royden* (2000); *Royden et al.* (1997)).

5.2.2 Neotectonics

The active tectonics of eastern Tibet are characterized to first order by the clockwise rotation of crustal material about the eastern Himalayan syntaxis (*Wang et al.*

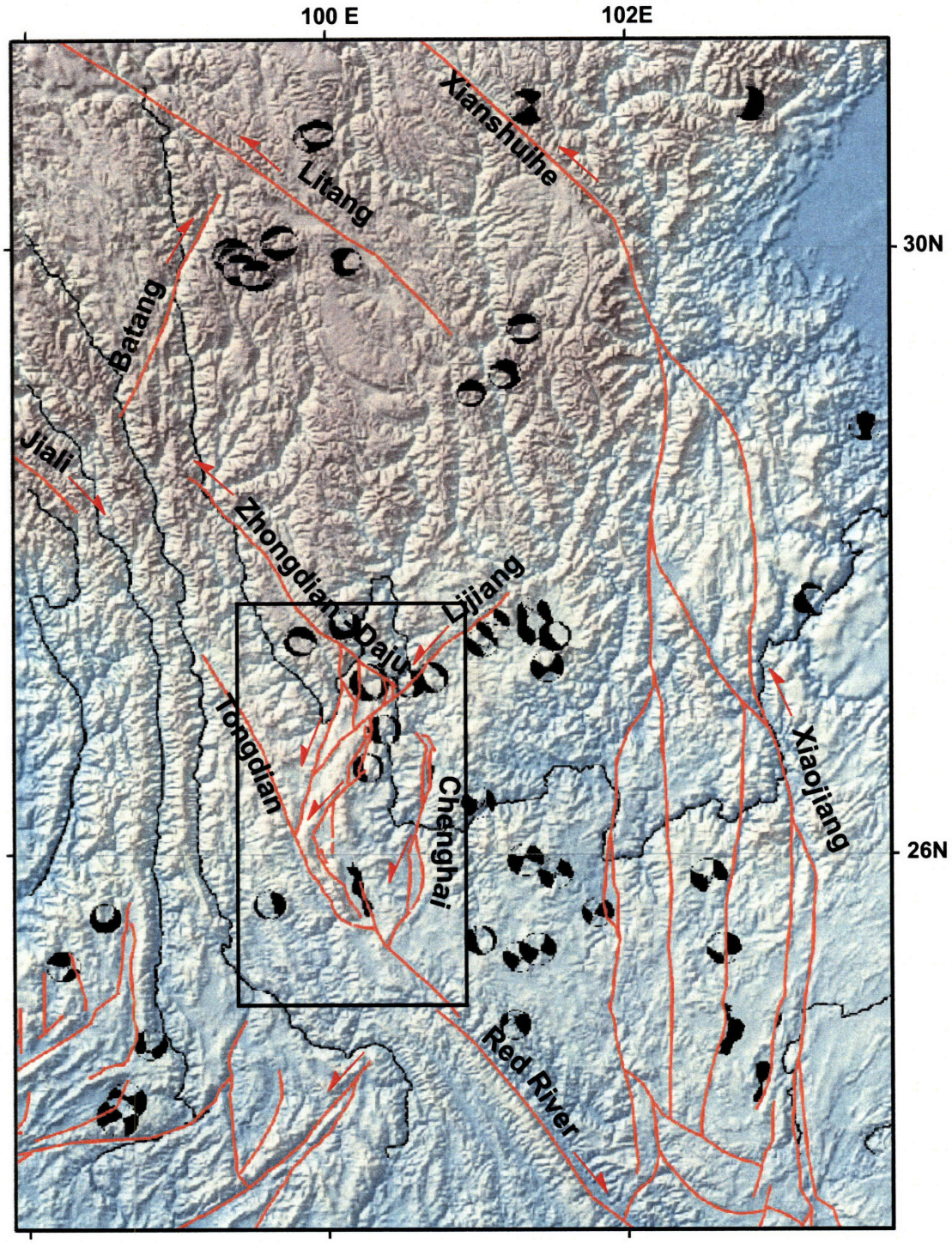

Figure 5-2: Young and active faults of Yunnan. The left-lateral Xianshuihe and Xiaojiang faults bound a broad region that (1) rotates clockwise about the eastern Himalayan syntaxis and (2) extends in east-west direction. Earthquake locations are drawn from the Harvard CMT catalogue, fault locations are compiled from our own mapping, Chinese regional geological survey maps and *Wang et al.* (1998). The box shows the location of fig.5-3; the Yulong mountains are located at the prominent bend of Dali-Jianchuan-Lijiang fault system in the center of the box.

(1998)). The arcuate left-lateral Xianshuihe and Xiaojiang faults bound this rotating region (the Chuan Dian fragment, e.g. *Wang et al.* (1998); *Yoshioka et al.* (2003); *Tamai et al.* (2004)) to the northeast and east from the eastern Tibetan plateau to the Red River fault. These first-order kinematics are well-established from mapping of active faults (*Wang et al.* (1998)), modelling of combined seismic strain release, fault slip-rates and geodetic velocities (*Holt et al.* (2000)), and geodetic data (*Chen et al.* (2000); *King et al.* (1997); *Zhang et al.* (2004); *Shen et al.* (2005)). Both geological and geodetic data show additional second-order complexities to this simple picture. Within the clockwise rotating region, smaller, differentially rotating blocks are bounded by the Dali - Jianchuan-Lijiang (DJL) fault system and the Chenghai, Tongdian, Zhongdian, Batang and Litang faults (fig. 5.2.2). The combined geodetic velocity field of *Chen et al.* (2000); *Zhang et al.* (2004) show an east-west component of extension and differential block rotation associated with these faults. The Yulong mountains are found near the northern margin of the DJL fault system, a corridor of transtensional faults characterized by north-south trending, east-west extending Quaternary extensional basins (c.f. section 5.2.2, fig. 5-3) linked by left-lateral northeast trending strike-slip or oblique strike-slip faults. The region is seismically very active, with a particular concentration of both major and minor earthquakes spatially associated with the Yulong mountains. Harvard CMT solutions show that all major (M > 5) events are extensional, with a very small strike-slip component. Most notable were the 1997 M 7 and M 6 (aftershock) quakes that ruptured the oblique-normal Daju fault that defines the eastern boundary of the Yulong mountains (*He et al.* (2001); *Akamatsu et al.* (1998)).

Quaternary extensional basins

The Chenghai fault and the transtensional Dali-Jianchuan-Lijiang (DJL) fault system are associated with numerous fault-bounded Quaternary basins, including the

Zhongdian, Daju, Lashi, Lijiang, Heqing, Baihanchang, Jianchuan, Madeng, Sanying and Dali basins (fig. 5-3). These basins are bounded by obvious normal and strike-slip faults and represent the main geomorphic expression of extension in this area. Consistent stream offsets, disruption of terra rossa colluvial cover and scarps cutting alluvial fan surfaces and soils attest to the young and active nature of the bounding structures. Apart from basin formation, active normal slip on the Chenghai fault is expressed by the development of a distinct alluviated reach of the Jinsha river upstream and in the hangingwall of the Chenghai fault. Notably, we found no field or remote sensing evidence to suggest significant flexural uplift of the footwalls of the Chenghai or DJL faults.

Wang et al. (1998) summarize existing age control for these basins, which are primarily based on fossils and a few C^{14} dates. The oldest ages (2.4 Ma) cited are associated with the Lijiang basin, but these are based on the correlation with the presumed age of earliest glaciation in eastern Tibet (*Zheng et al.* (2002); *Shi* (2002)). In the course of the present study, we mapped Quaternary basins associated with the Jianchuan, Lijiang and Daju faults. We opportunistically collected carbon bearing samples from these basins (the Daju, Lashi and Lijiang basins, fig. 5-3) for C^{14} and palynological dating. All samples collected were found to be too old for C^{14} age determination ($>$ 40ka). Palynological assemblages did not provide tight age constraints, with assemblages consistent with latest Pliocene or Quaternary time.

At present, the upper crustal tectonics of this region are dominated by extension and strike-slip faulting. There is neither geological, seismological nor geodetic evidence of upper crustal shortening in this area. Nevertheless, thick continental crust and consequent high elevations are present in this area, and have led to dramatic incision into the high landscape by the major rivers draining the Tibetan plateau and Yunnan highlands. If the crust underlying this region is currently being thickened, and elevations rising, then this thickening must be confined to the middle or lower

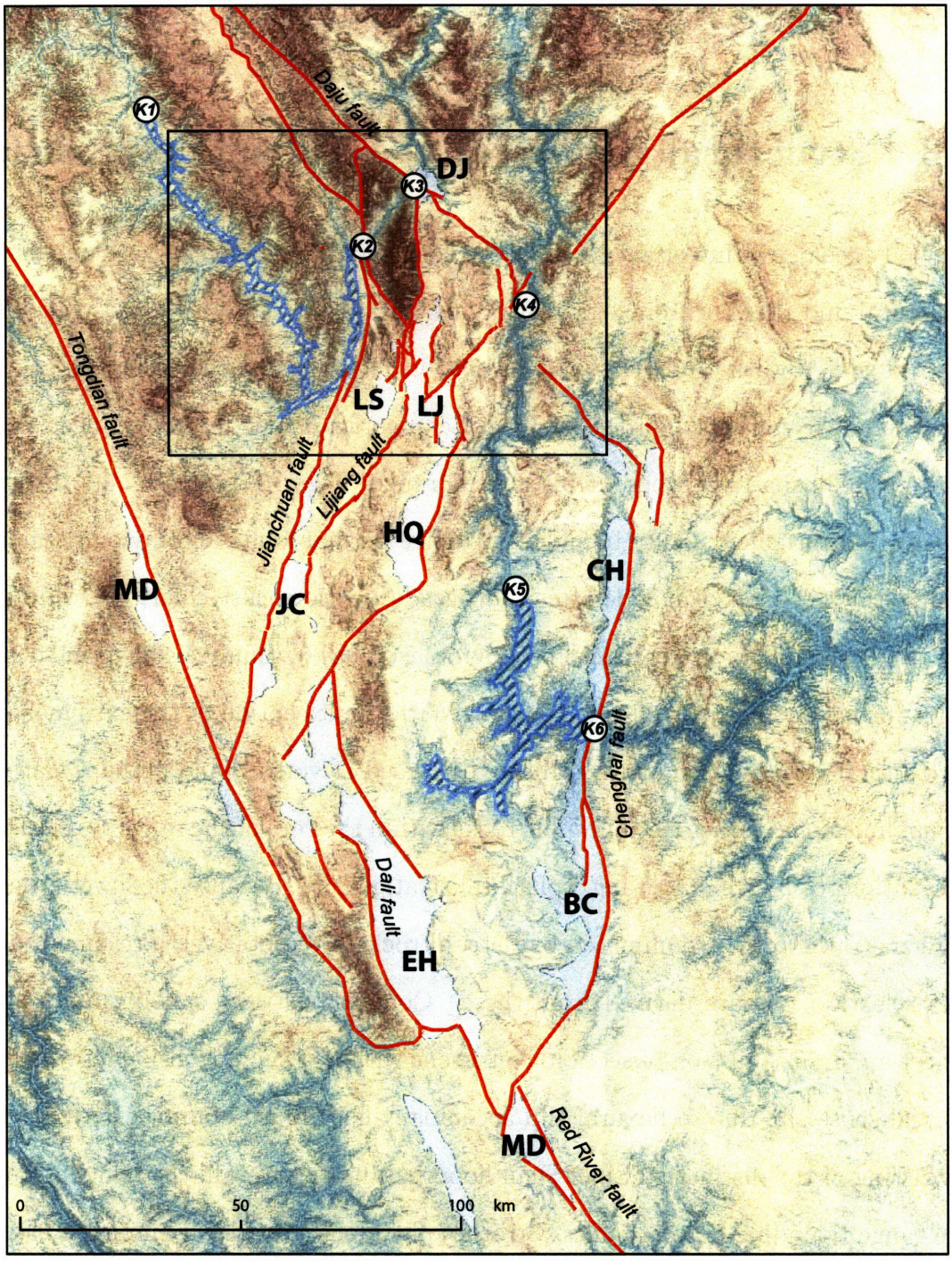

Figure 5-3: Quaternary basins associated with the active transtensional Jianchuan-Lijiang-Zhongdian fault system. DJ: the Daju basin; LS: Lashi basin; LJ: Lijiang basin; HQ: Heqing basin; JC: Jianchuan basin; CH: Chenghai basin; MD: Madeng basin; EH: Erhai basin; BC: Baihanchang basin, MI: Midu basin. Hatch marks show the alluviated reaches of the Jinsha river. Knickpoints on the Jinsha river are marked and numbered, see also figs. 5-7 and 5.4.1. Box shows the location of fig. 5-7

crust.

5.3 Structural geology of the Yulong culmination

Previous geological investigation of the Yulong mountains include a reconnaissance structural and thermochronological study by *Lacassin et al.* (1996) and regional geological survey work (*BGMR Yunnan* (1990)). These have focussed on the good exposure and easy access afforded by Tiger Leap gorge, a roughly 3.5 km deep canyon cut by the Jinsha river where it bisects the range. Tiger Leap gorge cuts through a broadly antiformal structure bounded by active normal faults and mylonitic marbles with a thick section of polydeformed low-grade pelitic rocks (chlorite-sericite phyllite, with a strongly retrogressed porphyroblast phase), thinly bedded and cleaved meta-turbidites and quartzites in its core. With the exception of the extremely pure mylonitic marbles, which are most likely deformed Devonian (and perhaps Carboniferous) limestones, other metamorphic rocks within the core of the range resist obvious correlation to the regional Yangzi platform stratigraphy. Because the lower Paleozoic Yangzi stratigraphy is dominated by detrital rocks, we tentatively presume that the meta-clastic rocks are derived from these. Contacts between missing units always reflect apparent omission of section, consistent with a strong extensional overprint or normal-sense slip due to flexural slip accompanying upward doming. Permian rocks consisting of the distinctive Emei Shan flood basalts crop out in the hanging walls of the range bounding normal faults. Stratigraphy alone provides a minimum estimate of the amount of differential exhumation between the core of the range and rocks exposed outside the range: the Permian basalts exposed on the northern, eastern and western margin are unmetamorphosed and do not bear penetrative fabrics, whereas rocks in the interior of the range are all foliated and bear chlorite, sericite, chloritoid and locally biotite.

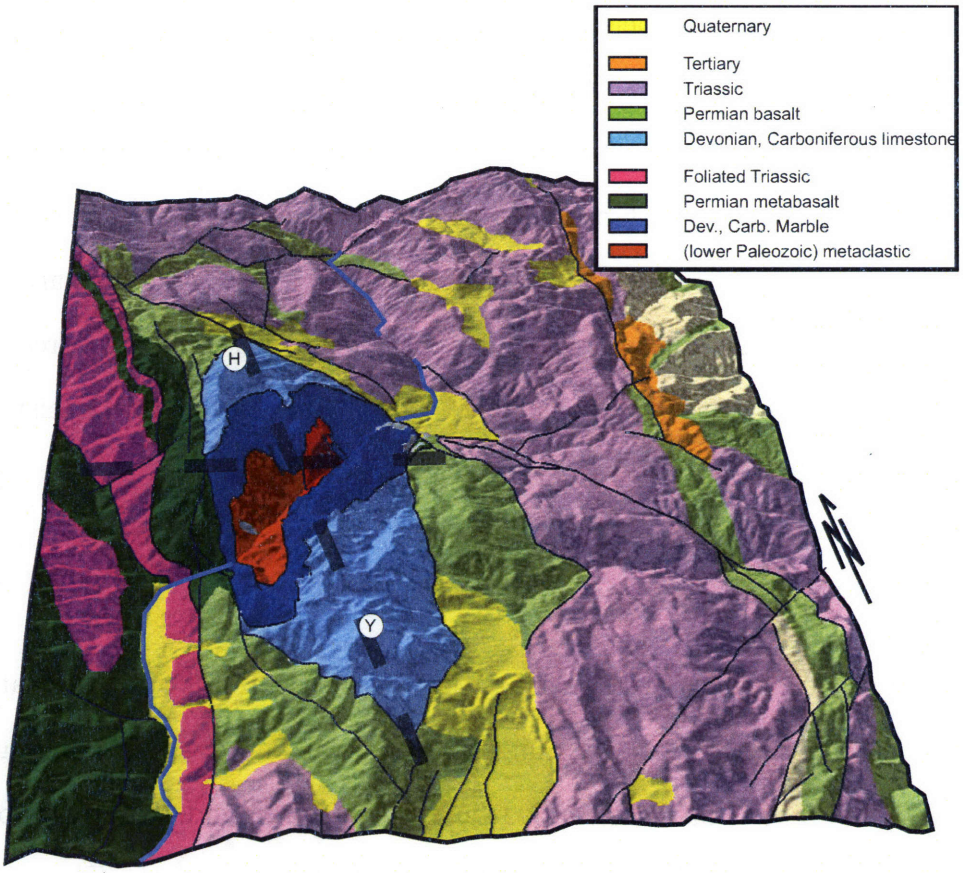

Figure 5-4: Oblique view of a geological map of the Yulong mountains, draped over a digital elevation model. Thick dashed lines show the locations of the cross-sections of fig. 5-5. More saturated colors indicate foliated chlorite bearing rocks, pale colors indicate uncleaved, unmetamorphosed rocks. The distinctive Permian Emei Shan basalts (light green) are used as a marker for estimating the amount of uplift and exhumation since the late Pliocene, see text for discussion. Circled letters show the location of the highest peaks of the north (Haba) and south (Yulong) parts of the range.

5.3.1 Early fabrics

All rocks exposed in the gorge show abundant evidence for multiple deformations. The most obvious deformation, and the one most responsible for the gross geometry of the range is an antiformal upright folding of the units within the bounding normal faults. This deformation is superimposed upon an early deformational history characterized by early metamorphism and transposition, subsequent recumbent folding and the development of a very strong stretching lineation. We have been able to correlate most of the fabrics and fabric relations with fabrics in variably metamorphosed rocks to the west of the range (cf. chapter 3). There, these structures are unconformably overlain by unmetamorphosed and weakly deformed Tertiary terrestrial sediments, which requires that most of the fabric development and metamorphism in the Yulong mountains had occurred by earliest Tertiary time.

5.3.2 Late antiformal refolding

The broadly antiformal structure of the range is the result of a single late, upright fold that we interpret as due to doming in the footwall of the range-bounding normal faults (figs. 5-4, 5-5). This fold trends nearly north-south, and, where it is bisected by the Tiger Leap gorge, plunges shallowly ($\sim$10 deg) to the south. The overall structure, however, is doubly-plunging: the fold plunges to the north at the northern end of the range, where Permian basalts are juxtaposed with weakly foliated carbonates across a northward dipping normal fault. The doubly-plunging geometry of the late antiform produces an overall domal geometry to the range, which we, contrary to *Lacassin et al.* (1996), do not interpret as a fold interference geometry. Unlike earlier fabrics and structures, this deformation is local to the Yulong mountains: it is expressed only within the young and active faults bounding the range and cannot be correlated to any regionally developed deformation. Rather, the non-cylindricity of the range's antiformal geometry reflects north-south variations in the amplitude of the antiform,

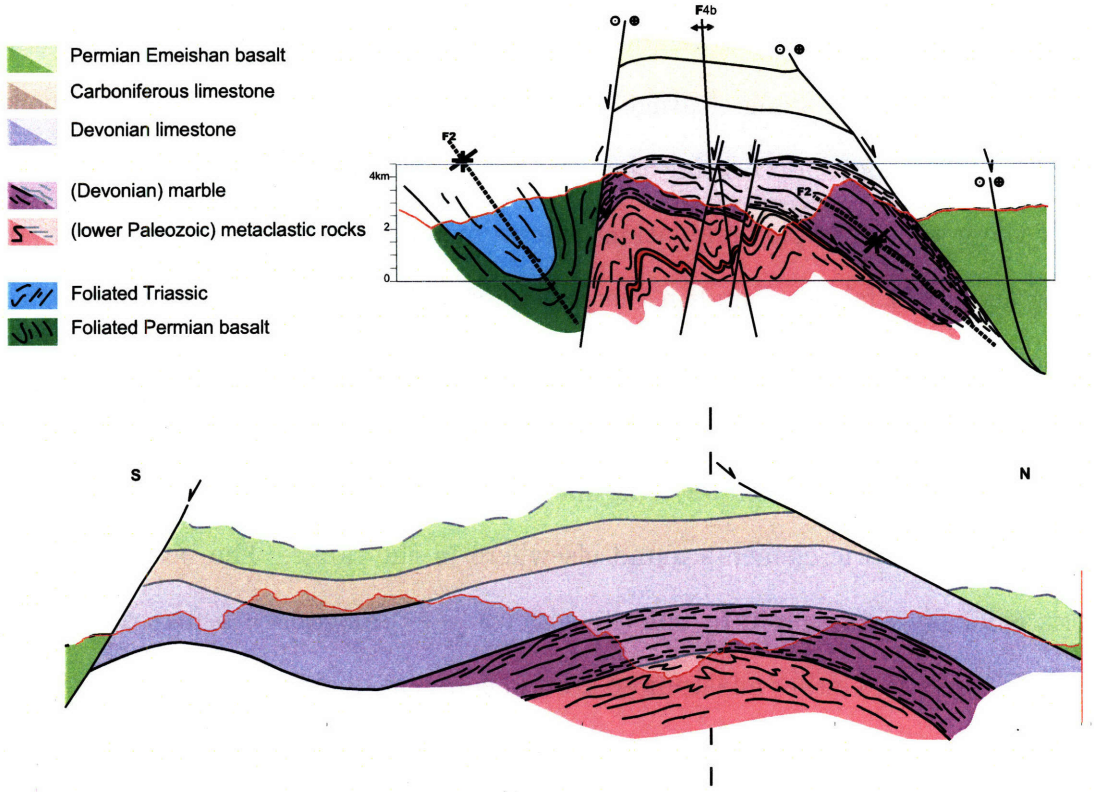

Figure 5-5: Geological cross-sections through the Yulong mountains, no vertical exaggeration. Darker, paler and greyscale fill is used to show regions where the cross-section is well constrained by our own mapping, where the cross-section is inferred, and where units project above the topographic surface.

where the greatest amplitude is coincident with the extreme incision of the Tiger Leap gorge. The localization of this deformation is accommodated by normal slip on the bounding active faults, particularly on the eastern boundary of the range.

5.3.3 Marble fabrics

Near the margins of the range, marble fabrics are parallel to the bounding young and active normal faults, whereas in the core of the range, marble fabrics are folded about a map-scale recumbent fold that deforms an early transposition foliation. Spectacular sections of marble mylonite are exposed on both the western and eastern margins of

Tiger Leap gorge. These rocks are extremely pure calcite marble, except for phlogopite and sericite along cleavage partings in the rock. Planar fabric is intense, and lineations are ubiquitous and well developed. Linear fabric elements consist of crenulations of phologopite along cleavage partings and the stretching and/or alignment of oxides and phlogopite decorating these partings. In exposures on the western margin of the gorge, multiple crenulation generations are observed, and are likely to be analogous to old fabrics found in the polydeformed metaclastic rocks in the core of the range. To the east, in the immediate foot walls of active normal faults, however, the marbles are characterized by particularly intense mylonites and ubiquitous, spectacular mineral (trails of oxides) and down-dip stretching lineations that are oblique to early linear fabric elements found elsewhere in the range. The intense mylonitic fabric is locally overprinted by chlorite-sericite (+/- phlogopite) brittle-ductile shear zones. These zones either anastomose around coherent, meter-scale lenses of mylonite or form fabric-parallel zones. Numerous kinematic indicators are apparent in these zones (fig. 5-6). Where the brittle-ductile zones define meter-scale lenses of coherent marble, these are typically asymmetric, whose asymmetry define normal-sense, top to the east (i.e. normal-sense) slip. Within east-dipping, fabric parallel zones, C/S fabrics, shear bands, σ and δ winged inclusions (of white calcite within a dark chloritic groundmass), domino structures and asymmetric folds all indicate top to the east (normal sense) slip (*Hanmer and Passchier* (1991)). Farther to the east, marbles become intensely fractured, and steep east-dipping fracture sets dominate. These then transition into zones of breccia and fault gouge incorporating mafic material presumably derived from the Permian basalts exposed to the east. The zone of breccia and fault gouge is coincident with the trace of the main bounding fault, an active normal or oblique normal fault that is defined by the obvious and spectacular facetted range front. We interpret the transition from ductile, to brittle-ductile, to brittle structures in the foot wall of the active normal fault as reflecting exhumation

of ductilely deformed rocks and progressive overprinting of ductile fabrics by brittle structures in an extensional setting.

5.3.4 Active, brittle normal faulting

The Yulong mountains are entirely contained within a network of predominantly normal faults that define a rhomb-shaped region of high elevation and extremely rugged topography (fig. 5-7). These faults are geomorphically well-expressed by steep, facetted scarps and are easily traced both in the field and on digital elevation models and satellite imagery. The range-bounding faults are not perfectly symmetric. The western boundary is defined by a set of very steep cliff faces and subvertical scarps. The trends of these fault traces do not appear to be deflected by the topography (particularly the nearly 3 kilometers of relief associated with Tiger Leap gorge), and are therefore likely to be subvertical. At the south end of the range, the main western fault strikes northwest, and is marked by high cliffs of Devonian limestone. The fault then swings to a north-south strike in the center of the range. North of the gorge, this fault connects with an array of steep and low angle normal faults on the north side of Haba peak (fig. 5-7).

The eastern boundary is marked by an obvious, east dipping fault that is the northward continuation of active faults defining the western boundary of the Quaternary Lijiang basin. South of the outlet of Tiger Leap gorge, this boundary (the Xueshan fault) strikes north-south. Clear evidence of active normal faulting is seen from the (oblique normal) offset of glacial moraines, and by scarps cut on landslide debris and colluvial material. At the outlet of Tiger Leap gorge the eastern bounding fault assumes a northwest strike and is known as the Daju fault. The Daju fault is moderately NE dipping (40–50°), and the fault surface is sub-parallel to, if slightly steeper than, the NE-dipping mylonitic and brittle-ductile shear zones in its footwall described above. To the north, this fault is connected with the western boundary fault

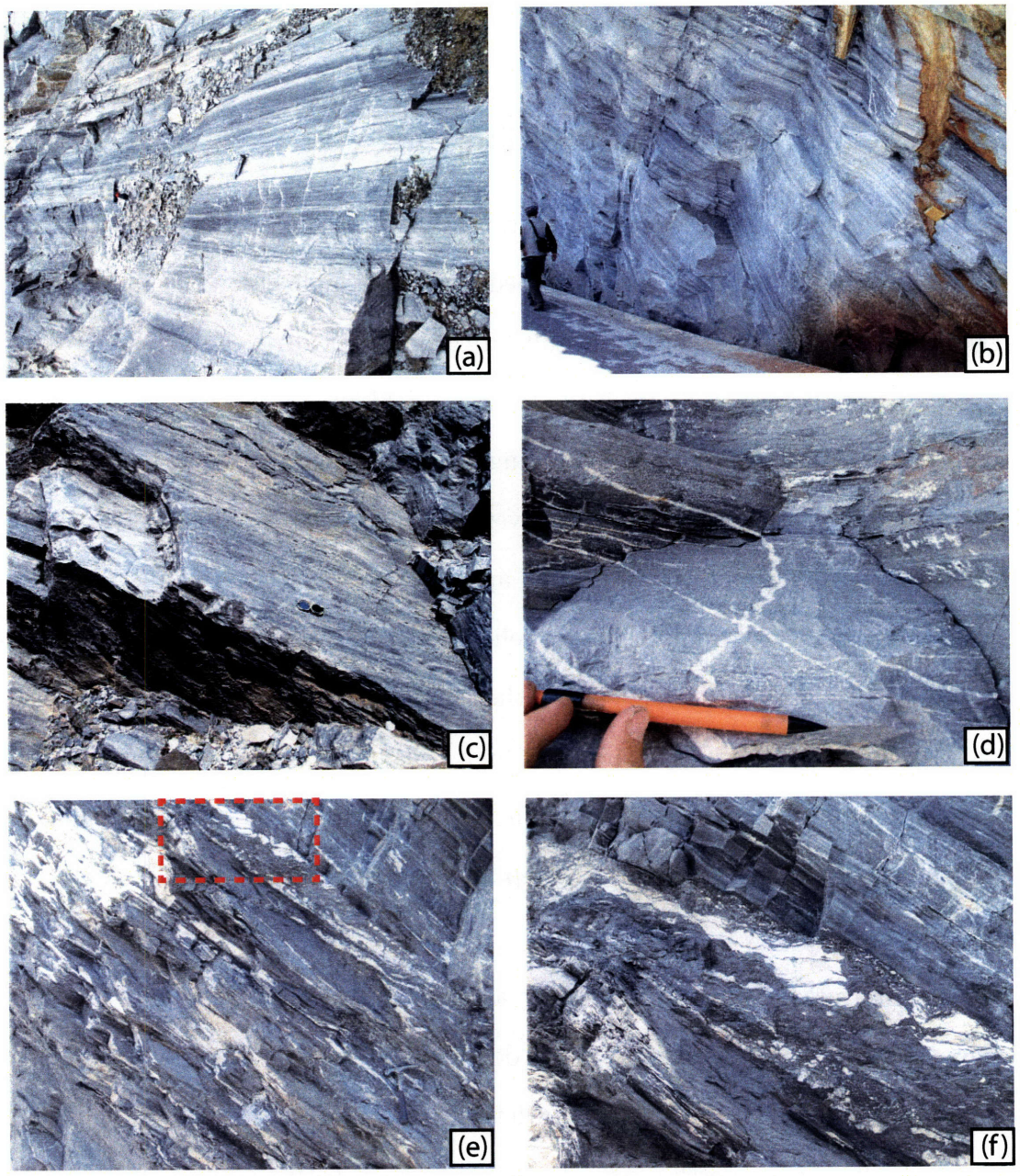

Figure 5-6: Mesoscale fabrics in mylonitic marbles. (a) Steeply dipping mylonitic marbles from the west side of Tiger Leap gorge; (b) Down-dip lineated mylonitic marbles from the east side of Tiger Leap gorge; (c) View of down-dip lineation in eastern marbles; (d) Shear sense indicators I: progressive deformation and rotation of vein sets; (e) Brittle- ductile shear zones sub-parallel to mylonite fabric; (f) Detail of (e); C/S fabrics, rotated boudinaged calcite veins and shear bands all indicate top to the right (east) shear sense.

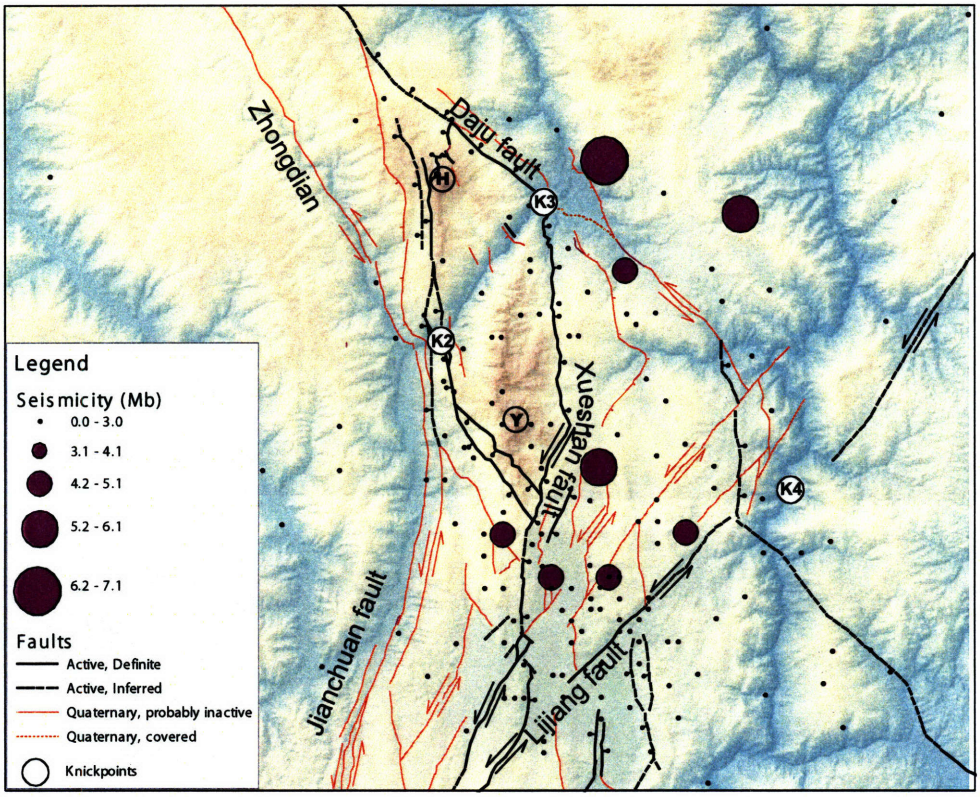

Figure 5-7: Map of Quaternary faults in the vicinity of the Yulong mountains. Knickpoints are labeled so as to correspond with figure 5.4.1. Earthquake locations are drawn from the catalogues of *Sun et al.* (2004). The letters H and Y in triangles show the locations of Haba and Yulong mountains, the main peaks north and south of Tiger Leap gorge.

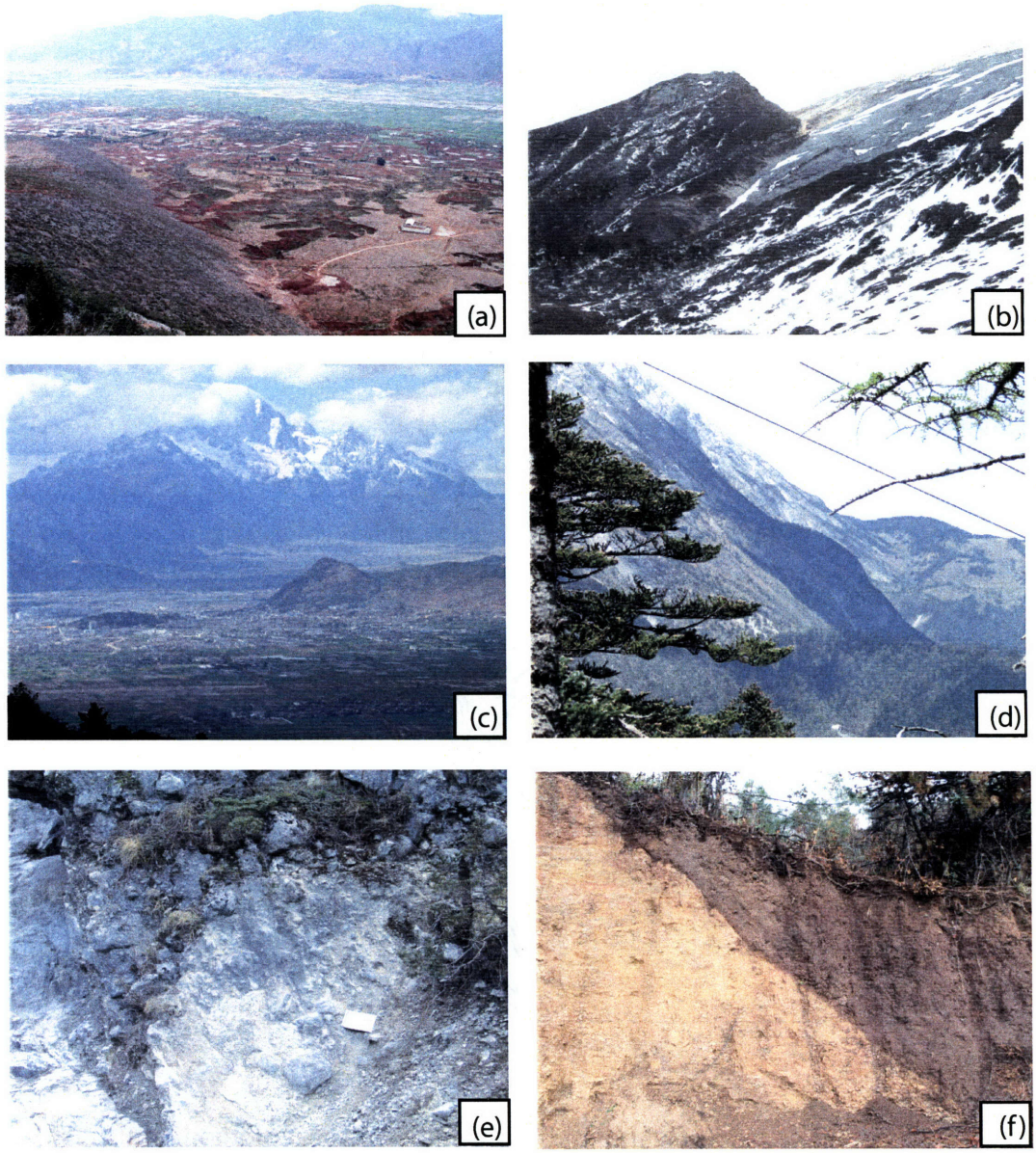

Figure 5-8: Photographs of active faults. (a) Erosion of terra rossa soils due to tilting of the footwall of a small normal fault in the Lijiang basin. (b) Moderate-angle (30°) normal fault on the northern margin of the Yulong mountains (Haba Xueshan). Dark rocks are Permian Emei Shan basalts, light rocks are Devonian limestone. (c) View of the Quaternary Lijiang basin with the Yulong mountains in the background. Elevation difference between the main peak of the Yulong Xueshan and the basin floor is approximately 3.5km. (d) Main eastern flank fault (Xueshan fault) surface juxtaposes Permian Emei Shan with Devonian limestone. (e) Fault scarp cutting alluvium along the trace of the fault pictured in (d). (f) Fault scarp placing colluvial soils over carbonate fault gouge (Xueshan fault).

on the north side of Haba mountain. The Daju fault probably eventually connects with the active trace of the left-lateral Zhongdian fault to the northwest, though the precise trace of the connection is difficult to unequivocally discern on remote sensing images and inaccessible in the field. The eastern range-bounding faults are not only more shallow than the western bounding faults, but they are also more obviously active. The largest (M >6) historical earthquakes are also appear to be associated with these faults.

5.3.5 Summary of structural evidence for active extensional exhumation

Early fabrics borne by polydeformed rocks in the core of the Yulong mountains are refolded into a upright, doubly-plunging antiform bounded by active normal faults. The late folding, and the overprinting of early fabrics at the margins of the range reflect extensional exhumation of these rocks accommodated by the range-bounding normal faults. The onset of extension in this area is likely to have occurred in the late Pliocene, based on the age of the oldest sediments found in the extensional basin associated with the network of extensional and transtensional faults of which the Yulong mountains range-bounding faults are a part. Extension in this area is on-going and the range-bounding faults are active and so the exposure of some of the deepest structural and stratigraphic levels of the region in the core of the Yulong mountains reflects recent exhumation accommodated by young and active extension.

5.4 Geomorphology of the Yulong mountains: anomalous elevation, relief, and erosion rates

Exposure of deeper structural levels in the Yulong mountains testifies to localized exhumation of rocks within its bounding fault circuit. The geomorphology of the range within the bounding faults reflects anomalous rates of both rock uplift and erosional denudation, and provides hints as to the mechanism producing these fault-localized anomalies. In this section, we describe evidence for anomalous mean and maximum elevations, relief, and erosion rates. We use the geomorphic and stratigraphical relationships to make estimates of the timing, magnitude and rates of rock uplift and exhumation. In the remainder of the paper, we use these relationships to test possible models that might account for the highly localized and ongoing deformation of the Yulong mountains.

5.4.1 Geomorphic metrics of high erosion rates

Within the Yulong mountains, we observe a preponderance of maximally steepened hillslopes, resulting in the dominance of mass-wasting as the principal process of hillslope erosion, and implies that the overall landscape lowering rate is set by the rate of the extreme incision of the Jinsha river where it bisects the range. The abrupt steepening and narrowing of the Jinsha river as it crosses the range faults implies increased stream power and thus incision rate. Finally, the extensive glaciation of the higher elevations, found within the bounding faults but outside the drainage basin of the Jinsha river, provide another possible contribution to high erosion rates both through the direct action of valley glaciers and, indirectly as glacial retreat leaves behind oversteepened hillslopes in cirque and glacial valley walls. Together, these suggest that this landscape is experiencing high erosion rates. The exposure of particularly deep structural levels within the range is the expected result of the localized rapid erosion

rates being balanced and sustained by protracted high rock uplift rates. Localization of high rock uplift and erosion rates, and consequent exhumation is accommodated by the range-bounding normal faults, and thus we interpret that rocks of the Yu-long mountains have been extruded by foot wall uplift along kinematic normal faults. This interpretation is strongly suggested by the observation that all indicators of high uplift rates (exposure level, high elevations, high erosion rates) are exactly localized by active faults whose kinematics require relative uplift of the range. In the sections that follow, we detail the geomorphic observations that lead us to this conclusion.

Hillslope processes

Intuitively, steeper, more rugged terrain often suggests higher rates of uplift and denudation (eg. *Wobus et al.* (2003)) since steeper hillslopes should lead to higher hillslope erosion rates. For certain hillslope erosion processes, it is, in fact, appropriate to model erosion rate as a slope-dependent diffusive process (*Burbank and Anderson* (2001); *Rosenbloom and Anderson* (1994)). Many quantitative models of the interaction of tectonics and surface processes thus assume a form of the diffusion equation to model erosion (eg. *Koons* (1989); *Beaumont et al.* (1992)). However, beyond a certain steepness, hillslope angles can no longer be assumed to track either uplift or erosion rates. At some point, the inherent limit of the strength of bedrock is such that diffusive hillslope erosion processes give way to mass-wasting (*Schmidt and Montgomery* (1995)). Average erosion rates may still track uplift rates, but hillslope steepness ceases to be an indicator of the vigor of tectonic or erosive processes (*Burbank et al.* (1996)).

If the landscape consists of maximally steepened hillslopes, the overall landscape lowering rate will then be controlled by the processes that set the erosion rates at the bases of hillslopes. In the Tiger Leap gorge, this is just the incision rate of the Jinsha river. Elsewhere in the range, debris flow channels and alpine glaciers are the relevant

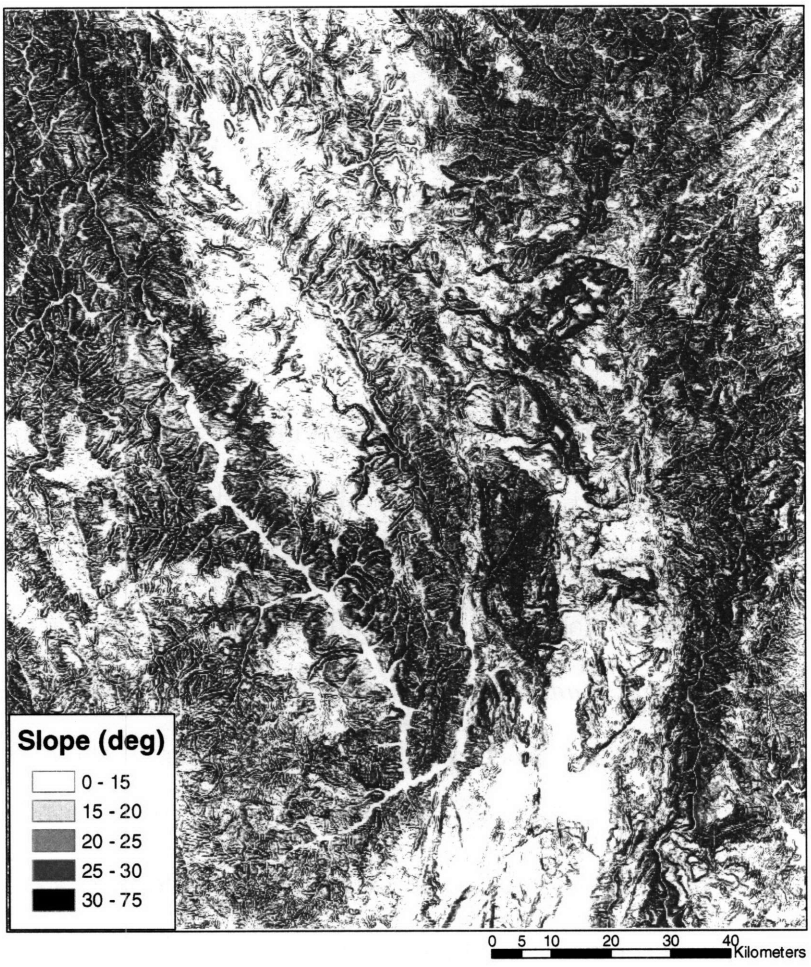

Figure 5-9: Slope map of the region, with steeper slopes shaded darker. Note how the Yulong mountains stand out as a rhomb-shaped area of high slopes. Also prominent are the low slopes in the alluviated reach of the Jinsha river upstream of the Yulong mountains and the low slopes of Quaternary basins south of the range.

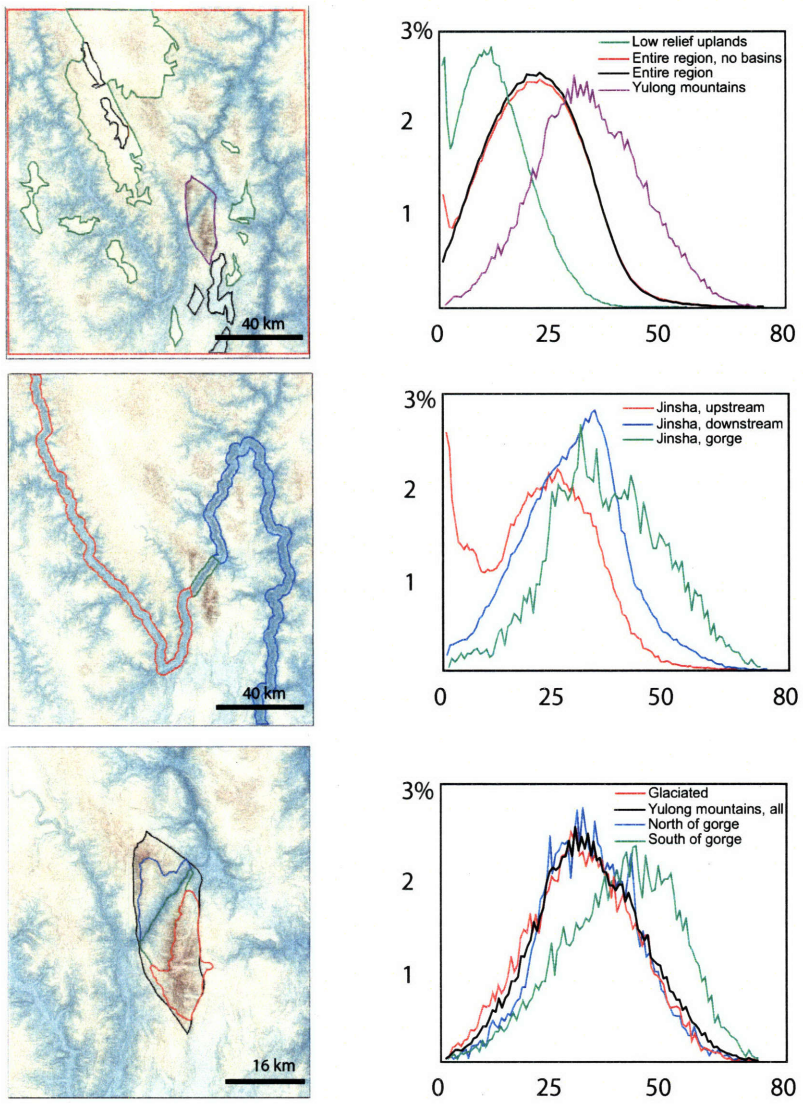

Figure 5-10: Top: PDFs of slope for Low relief uplands, entire region, entire region excluding Quaternary basins and Yulong mountains. Boundaries of these zones outlined on the DEM. Middle frame: PDFs of slope for Jinsha river valley upstream of the Yulong mountains, Jinsha river valley downstream of the Yulong mountains, Tiger Leap gorge and corresponding map of boundaries. Bottom: curves for entire Yulong mountains, glaciated areas of the Yulong mountains and northern gorge slopes are basically indistinguishable, the rightmost curve (green) is for southern gorge slopes. All slopes in degrees.

processes. Bearing this in mind, we compared the average slopes and distribution of slope angles for several zones within the region of interest. We find that, consistent with qualitative field observations of frequent, ubiquitous, large landslides, the Yulong mountains are indeed characterized by threshold hillslopes, even outside the drainage area of the Jinsha river. Moreover, although very steep topography, presumably reflecting maximally steepened hillslopes, is characteristic of the Jinsha river valley and its deeply incised tributaries even outside the range, the area defined by active normal faults bounding the Yulong mountains still stands out on maps of local slope (figure 5-10).

Following (*Burbank et al.* (1996)), we generated maps of local slope from 90m resolution digital elevation models by calculating the steepest gradient between all neigbouring pixels (fig. 5-10). Low slope areas include the floors of Quaternary basins and high, plateau uplands, which may form part of a regionally recognized, pre-incisional low relief paleolandscape (*Clark et al.* (2005); *Clark* (2003); *Schoenbohm et al.* (2004b); *Clark et al.* (in review); *Wang et al.* (1998)). The deeply incised Jinsha river and its tributaries are responsible for most of the steep parts of the landscape. Despite the tendency for slopes to saturate to rock-strength limited maximal slopes, however, the Yulong mountains stand out as a rhomb-shaped region of uniformly steep slopes. Unlike other steep parts of this region, here the range bounding faults sharply define a near uniformly steep part of the landscape. Figure 5-10 shows the distribution of slopes for various parts of the landscape. We extracted probability density curves for the calculated slopes and elevations for the following areas: (1) low relief uplands; (2, 3, 4) 2km wide swaths about the Jinsha river upstream, downstream and within Tiger Leap gorge; (5) the Yulong mountains as a whole; (6, 7) the parts of the Yulong mountains within the drainage area of Tiger Leap gorge north and south of the river; (8) the glacially dominated zones in the southern part of the range; (9) the region as a whole; (10) the region as a whole, excluding the floors of Quaternary

Zone	**Elevation**		**Slope**	
	Mean	1σ	Mean	1σ
(1) Low relief uplands	3595	345	12.7	7.9
(2) Jinsha upstream	2167	285	21.8	12.4
(3) Jinsha gorge	2486	494	37.4	13.2
(4) Jinsha downstream	1954	368	29.8	11.7
(5) Yulong, whole	3652	839	34.1	12.3
(6) Gorge slopes, north	3077	752	34.2	11.1
(7) Gorge slopes, south	3341	841	41.3	13.0
(8) Yulong, glacial	4149	585	32.3	12.2
(9) Entire region	3020	627	21.9	11.1
(10) All, no basins, no Yulong mnts.	3014	618	22.1	10.7

Table 5.1: Elevation and slope statistics for selected zones in the Yulong mountains and surrounding regions. See text for discussion.

basins. Table 1 lists the mean and standard deviation of slopes and elevations for these areas.

Zone 1: Low relief uplands Low relief uplands are ubiquitous in much of eastern Tibet and Yunnan province at the headwaters of tributaries to the major rivers draining the eastern margin of the plateau. Zone 1 consists of a few representative instances of these uplands. Average elevations are quite high, $\sim$ 500m higher than the $\sim$3000m regional average and $\sim$ 1000 – 1500m higher than the bottoms of steep valleys incised into them. Average slopes are fairly low: $\sim$ 13 °compared to $\sim$ 30°and 22°for river valleys and the region as a whole, respectively. These uplands are characterized by low gradient, meandering, commonly alluviated stream and river courses, relatively subdued topography, and the development of thick regolith and soil mantles (figure 5-11a). Where the surface is underlain by the relatively shallow dipping Tertiary Jianchuan basin rocks, the deep valleys produced by younger river incision separate striking flat-topped summits. Elsewhere, total relief on the subdued uplands is on the order of a few hundreds of meters, with wide valleys separating subdued hills and isolated, more rugged peaks.

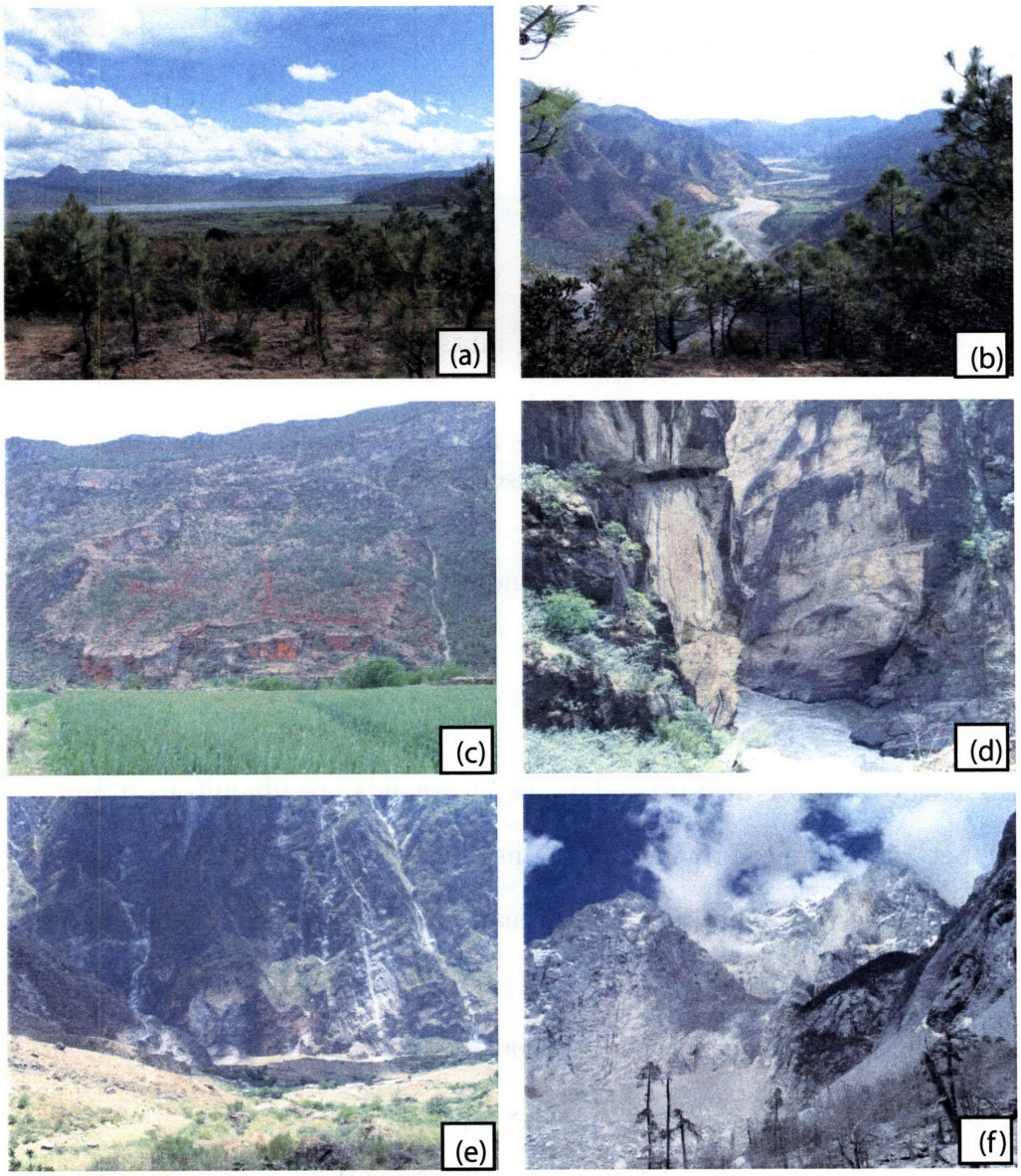

Figure 5-11: Photographs of the geomorphology of the Yulong mountains and surrounding regions. (a) Low-relief uplands, characterized by deep, red terra rosa soils where developed over carbonate rocks; (b) Jinsha river valley upstream of the Yulong mountains; (c) Thick terra rosa weathering cap developed on old landslide scar; (d) Tiger Leap gorge, inner gorge; (e) Vertical walls of the south side of Tiger Leap gorge, view is down slope from the north side of the gorge: this slope follows the projected contact between marbles and underlying meta-clastics, a weak interface prone to large landslides. (f) Cirque headwalls in the southern Yulong mountains. Note fresh looking rock from large landslide that occurred a day before this picture was taken.

These plateau like uplands have been interpreted as a regional low-relief paleo-landscape that existed prior to epeirogenic uplift and subsequent incision (*Clark et al.* (in review); *Clark* (2003); *Schoenbohm et al.* (2004a)). South and southeast of the Yulong mountains, Pliocene coal-bearing lacustrine and low-gradient fluvial sediments have been mapped on remnants of this low-relief paleolandscape (*Schoenbohm et al.* (2004a); *Wang et al.* (1998); *BGMR Yunnan* (1990)). These sediments, and late Miocene dates from low temperature thermochronometers (*Clark et al.* (2005)) provide rough constraints on the subsequent incision into the paleo-landscape by the Jinsha river and its tributaries. The age of establishment of this landscape is much more difficult to determine, since the history of the relief structure of the pre-incisional landscape is probably variable from place to place (*Clark et al.* (in review)). The topography in this region might have been rather subdued since Mesozoic time, since Tertiary-aged deformation was relatively minor, localized and did not involve significant amounts of exhumation (cf. chapters 2 and 3).

The presence of a low relief paleo-landscape has been used as a datum to infer both the amount and mechanism of Cenozoic crustal thickening at the sub-continental scale — i.e. all of Yunnan and eastern Tibet (*Clark et al.* (in review); *Clark* (2003)). At such large scales, the difference in elevation between the highest areas in the eastern Tibetan plateau and the lowest areas (the coast) is considerably greater than the hundreds of meters of relief characteristic of individual remnants of the paleo-landscape (eg. Table 5.4.1, cf. *Clark et al.* (in review)), and thus it provides a useful datum to measure Cenozoic crustal thickening. In the immediate vicinity of the Yulong mountains, low relief parts of the landscape are not useful in this regard. Instead, note the plateau like uplands only in order to provide a point of comparison to the more rugged parts of the landscape. Moreover, in figure 5-10, we do not attempt to exhaustively map out all possible locations of these plateau-like uplands, and instead identify just a few representative regions. More locally, our field work

and mapping has identified a series of relatively flat erosion surfaces in the immediate hanging wall of the normal faults bounding the Yulong mountains on their eastern and southern margins. These are cut on the Permian Emei Shan basalts, and it is possible that these may be relicts of the original landscape prior to uplift and erosion of the Yulong mountains. It is not possible to unequivocally correlate these small, locally preserved erosion surfaces with the putative regionally extensive low relief paleo-landscape. Rather, we argue that these small erosion surfaces suggest that the Permian basalts are the relevant datum for estimating the amount of rock eroded off the top of the Yulong mountains since rapid uplift and erosion began (cf. section 5.5).

Zones 2, 3, 4: The Jinsha river The incision of the Jinsha river and its tributaries is responsible for most of the steepest and most rugged parts of the landscape. Dramatic gorges and deep valleys create hundreds to thousands of meters of local relief. Hillslopes above the river courses are steep, show evidence of vigourous mass-wasting, and expose tall cliffs of bed rock. Zones 2, 3 and 4 consist of 2km wide swaths centered on the Jinsha river. Unsurprisingly, mean elevations are lowest of any zone, and average slope angles are considerably higher than the unincised plateau-like uplands. Distinct differences are notable in the slope statistics for the Jinsha river valley upstream, within and downstream of the Yulong mountains and are confirmed by field observations.

Upstream of the Yulong mountains (zone 2), the Jinsha river valley, although still defined by tall hillslopes, is relatively wide and open (figure 5-11b). Exposed bedrock and tall cliffs are exposed on some hillsides, but, in general, the river valley is characterized by thick red soils and dense vegetation. Tributary valleys to the Jinsha are wide and filled with thick alluvial fans that tend to deflect the trunk stream. Evidence for recent landslides is lacking, although evidence for older landslide events

is locally present. Interestingly, where old landslides involved carbonate rocks, the debris of these events are covered by thick *terra rosa* soil accumulations (figure 5-11c). We interpret the landscape upstream of the Yulong mountains as having been formed by the incision of the Jinsha river followed by a deceleration of the river incision rate. The Jinsha river in this area is heavily alluviated, probably in response to the anomalous uplift of the Yulong mountains downstream, and so cannot continue to incise. The pace of hillslope erosion must therefore have slackened considerably, and the current erosional regime is one of relatively slow lowering, infrequent mass-wasting and general widening and broadening of the river valley.

Downstream of the Yulong mountains (zone 4), the Jinsha river valley is rather typical of the deep gorges incised by large rivers into the eastern margin of the Tibetan plateau. Local relief is on the order of a kilometer or more, steep bedrock cliffs are ubiquitous, as are landslide scars and debris. Average slopes are around 30 degrees, and the distribution of slope angles (cf. figure 5-10) is very similar to the distribution of threshold hillslopes reported from the Nanga Parbat region by *Burbank et al.* (1996). At a local scale, the underlying bedrock lithology exerts a strong control on average slopes, with massive, thickly bedded carbonate rocks generally supporting steeper hillslopes. The generally steep slopes and apparent control of average slopes by lithology might suggest that hillslopes adjacent to the Jinsha river have achieved approximately maximal values, and that the generally steep character of the landscape is no longer sensitive to uplift rate, but is, rather, controlled by the mechanical strength of the underlying rock (*Schmidt and Montgomery* (1995); *Burbank et al.* (1996)). Nevertheless, the DEM swath taken from within the Yulong mountains (zone 3) does reveal differences within the inferred high uplift zone: average slopes are considerably greater within the Yulong mountains, and approach 40°. It appears that although rock strength may well be the principal control of average hillslope angles in these terrains, there is still some sensitivity to uplift rate, such that, contrary to

expectations, the Yulong mountains still stand out even compared to the extremely steep and rugged topography created by the Jinsha river along much of its course.

Zones 6, 7: Tiger Leap gorge Beyond just the 2km swath extracted along the Jinsha for the purposes of comparison with upstream and downstream reaches, we analyzed the slopes for the drainage area of the Jinsha river within the Yulong mountains, north and south of Tiger Leap gorge. This river gorge is one of the more spectacular topographic features anywhere. The Jinsha river sets the lower elevation of hillslopes on either side, which rise from elevations of around 1700m to >5000m summits over distances of 5km on the south side and 10 km on the north side. In places an inner gorge of near vertical walls rises about 300m above the river level (figure 5-11d). Above this, on the north side, hillslopes remain extremely steep and seem to be controlled by the contact between marbles and the underlying metaclastic rocks which generally dips toward the river. On the south side, there is no obviously steeper inner gorge and a series of near vertical walls (figure 5-11 e) rise directly from the river to high alpine peaks, interrupted only by rockfall gullies. All channels and gullies within this drainage area are dominated by debris flows or landslides.

The north side of the gorge is less steep than the south side, and its average slope appears to be set by large (~10s of km^2 in area) landslides that apparently exploit the south-dipping structural grain, particulary the contact between marbles and structurally lower metasediments (figure 5-11e). A road has been constructed on the north side of the gorge, but the frequency of landslides is such that it apparently requires regular blasting and digging out. During our fieldwork in the area, small scale rockfall was a regular occurrence. Landslide debris in the river channel creates rapids, but the comparative paucity of debris in the channels compared to landslide scars on the adjoining slopes is testimony to the apparent ease at which the Jinsha is able to evacuate the debris and restore its channel. The largest landslides must

completely damn the river – at least for a short time; the only preserved evidence from such an event is a 250m thick deposit of landslide debris preserved at the outlet of the gorge.

Zone 8: Glacially dominated zones in the southern part of the range As table 5.4.1 and figure 5-10 show, even outside the drainage area of the Jinsha river gorge, average slopes and elevations remain very high. Average slopes for the southern part of the Yulong mountains outside the drainage area of the Jinsha river are nearly as steep as within Tiger Leap gorge, though average elevations are markedly higher. Within the drainage area of the Jinsha river, the river sets the lower boundary condition to threshold hillslopes and the overall landscape lowering rate is set by the fluvial incision rate. Outside of the Jinsha's drainage area, base level is set by the elevation of the landscape in the hangingwall of the bounding faults. Operative erosional processes include channelized debris flows, land-sliding and glacial erosion. Average slopes in this area are steep, and result from (1) the steep, facetted escarpments associated with the bounding normal faults; (2) the cliff-forming nature of the lithology (massive, thickly bedded Devonian limestones); and (3) oversteepened glacial forms such as steep valley walls, cirque headwalls, sharp ridges and horns (figure 5-11f). In the present inter-glacial climate, these are the locii of particularly frequent, large landslides (e.g. figure 5-11c). The overall steepness of this region leads us to presume that landscape lowering rates are also anomalously high in this region and should tend to match the rate of rock uplift relative to adjacent depositional basins.

Extreme incision of Tiger Leap Gorge

The dramatic Tiger Leap gorge is obvious testimony to the extreme incision of the Jinsha river. From the bottom of the gorge at around 1780m (head of the gorge) to 1550m (south of the gorge), elevations rise to peaks in excess of 5000m over distances

of between 5km (south of the gorge) to 10km (north of the gorge). This represents some of the steepest topography in the world, and is in the same league as the Indus gorge at Nanga Parbat ($\sim$ 7km over $\sim$ 25km), the Tsangpo gorge at Namjabarwa ($\sim$ 4km - 6km over $\sim$ 20 - 30 km), the Colca canyon in Peru, and the steepest and narrowest parts of the Yalong and Dadu river gorges that incise into the Eastern Tibetan margin.

In the discussion that follows, we compare the Tiger Leap gorge reach of the river with reaches upstream and downstream of the gorge. In particular, we make frequent references to the following four sections of a 750km long profile of the Jinsha river (figure 5.4.1): (1) the farthest upstream reach consists of a deeply incised mixed bedrock – alluvium section. We refer to this as the upstream bedrock section. Although bedrock is probably not exposed at the bed, alluvial cover is sufficiently thin and ephemeral that the river is able to incise into its bed. Such rivers are common in rapidly incising areas such as Taiwan and the eastern margin of the Tibetan plateau (eg. *Whipple* (2004)). (2) For 130km upstream of the gorge, the Jinsha flows over a fully alluviated bed, and occupies a relatively wide floodplain. We refer to this section as the alluviated reach of the Jinsha. (3) Within the Yulong mountains, the steep and narrow bedrock section within Tiger Leap gorge is referred to as the gorge reach.(4) Once out of the gorge, the Jinsha is very much like the upstream bedrock reach: a deeply incised, steep, mixed bedrock and alluvium river whose bed is presumably exposed often enough to permit bedrock incision on geologic timescales. We refer to this as the lower bedrock section, with the same caveats as section (1).

The character of the Jinsha river changes dramatically as it passes over faults bounding the western margin of the range. These faults mark the transition from the upstream alluviated reach (reach 2) to the Tiger-Leap gorge steep bedrock reach (reach 3). Along the alluviated reach, the Jinsha river occupies a relatively wide valley of high hillslopes (figure 5.4.1a). These hillslopes are commonly covered by dense

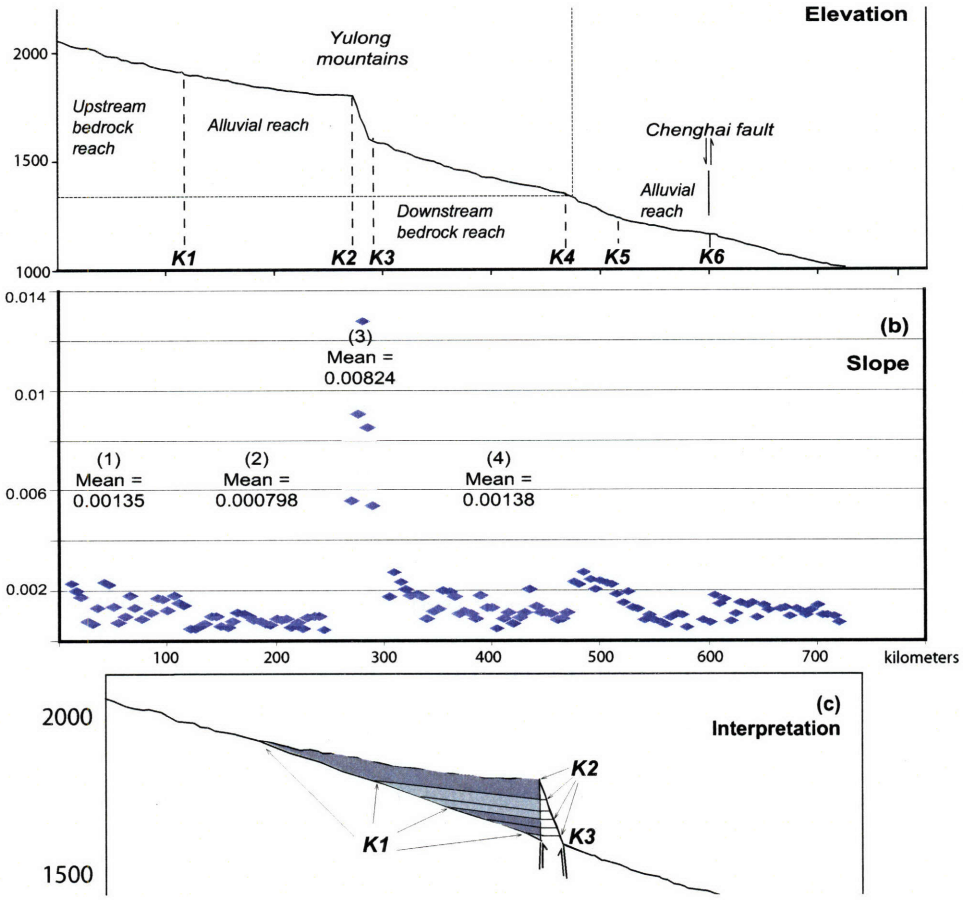

Figure 5-12: (a) Long profile of the Jinsha extracted from 90m DEM, with data artefacts smoothed from the profile. Knickpoints are labeled and correspond to locations on the maps of figures 5-3 and 5-7. (b) Slope vs. downstream distance of the Jinsha river calculated from a moving average of the smoothed profile. The four reaches discussed in the text are labelled, with the mean slope for each reach. Two other breaks are apparent beyond the first four: these are due to the effects of the west-dipping Chenghai normal fault. (c) Interpretation of the evolution of the Jinsha river profile from an initially graded bedrock channel.

vegetation and meters of red soils. There is evidence for landslides, but the debris and scars from these events are themselves typically covered with a thick regolith cover. Here, the Jinsha river is commonly deflected by alluvial fans filling the tributary valleys and prograding into the river. At low water, large (10s of meters width) sandy bars transported by the Jinsha are exposed and the river meanders through these (figure 5.4.1b). We could not directly determine the thickness of sediment underlying the river bed, but we note that the apparent alluvial character of the main trunk extends for about 160 kilometers distance upstream from the mouth of the gorge. Above this (reach 1), the river occupies a far steeper, narrower valley characterized by common landslide scars and loses its alluviated character. We assume that that the alluviated reach is the product of sedimentation over an intially graded bedrock or mixed reach similar to the present upstream reach. Since there is a negligible difference in the upstream drainage area along the profile, we expect that the slope of the pre-existing, adjusted bedrock or mixed alluvial-bedrock reach to have been essentially constant. We can then use the difference in slopes between the alluviated (mean 0.08%) and steeper upstream reaches (mean 0.15%) and the length of the alluviated reach (160km) to estimate that on the order of 240m of sediment underlie the Jinsha river immediately before entering the Tiger Leap gorge (fig. 5.4.1c).

As the river crosses the western bounding faults of the Yulong mountains, it dramatically steepens and narrows: between the western and eastern bounding faults the river drops 200m over 15km with an average grade of 1.3% and narrows from average widths of 250 - 350 meters to widths of 20 - 40m, and is occasionally even narrower. The relatively broad open valley upstream becomes a spectacular canyon of steep bedrock walls . For the most part, the river appears to flow over bedrock, but is punctuated with common rapids related to large blocks (up to 10s of meters) derived from mass wasting of the gorge walls (figure 5.4.1c). The river is in contact with near vertical bedrock walls for most of its length. Relatively low water allowed

Figure 5-13: Photographs of the Jinsha river: (a) Wide, alluviated reach of the Jinsha upstream of the Yulong mountains; (b) Sandy barforms in the alluviated reach; (c) Large boulders in the narrow gorge reach; (d) Orientation of foliation planes on the north bank of the river facilitate plucking, note also evidence for impacts by transported cobbles on the foliation plane; (e) Large potholes on the opposite bank; (f) View of the river downstream of the Yulong mountains.

us to observe evidence of multiple bedrock erosion mechanisms, especially plucking of jointed bedrock, fracturing of bedrock by the impacts of large blocks and large potholes and fluted surfaces testifying to abrasion (figure 5.4.1d, e). At the outlet of the gorge, the fabric and jointing in the marbles is oriented such that abrasion, fluting and potholing are mostly restricted to the southeast bank; whereas plucking and fracturing mechanisms dominate the opposite bank. Here, at least the last 150 m of downcutting incised nearly vertically, suggesting that rather distinct erosion mechanisms kept pace with one another.

Once out of the Tiger Leap gorge, the Jinsha river crosses the active Daju fault and cuts through the Quaternary Daju basin and a variety of bedrock lithologies. The river's grade abruptly relaxes, but remains steep in comparison to the alluviated reaches upstream of the Yulong mountains. Until the river begins to be influenced by subsidence west of the Chenghai fault, it is associated with the cutting of steep, deep valleys and relatively steep grades typical of the large rivers incising the eastern Tibetan margin (*Ouimet and Whipple* (2004); *Kirby et al.* (2003)).

We note that the two most obvious characteristics of the river as it passes through the fault-bounded gorge are its abrupt narrowing and steepening. Understood in the context of the commonly invoked stream-power model of bedrock erosion, these lead to an abrupt increase in the river's ability to both transport material and erode the bed. Stream power based models of bedrock incision typically cast erosion as a power law function of upstream drainage (as a proxy for discharge) and channel gradient and, in a generic form, are often expressed as

$$E = KA^m|S|^n \tag{5.1}$$

where A is the upstream drainage area, S is the channel gradient. K is a dimensional coefficient, and is influenced by climate parameters, erosion thresholds, channel width, sediment flux, among others (*Whipple and Tucker* (1999); *Whipple*

(2004); *Whipple et al.* (1999b); *Burbank and Anderson* (2001)). Channel width is generally not explicitly specified as an independent parameter. Instead, it is generally assumed that, just as discharge tends to scale with upstream drainage area, a similar empirical scaling relationship can be invoked for channel width:

$$W = k_w A^b \tag{5.2}$$

Such a scaling relationship has been shown to be robust for (gravel-bedded) alluvial rivers, and for at least some bedrock rivers (*Whipple* (2004); *Snyder et al.* (2003); *Montgomery and Gran* (2001)). However, there are also cases where bedrock rivers are observed to narrow significantly in higher uplift areas, suggesting that channel width provides another degree of freedom in the ways a channel can adjust to tectonic forcing (*Finnegan et al.* (2005); *Lavé and Avouac* (2001)), and neglecting this possibility can lead to a significant underestimate of channel erosivity (*Finnegan et al.* (2005). Since the Jinsha river drains a large part of eastern Tibet, for the reaches that we are interested in, changes in drainage area are negligible, and we concentrate on the predicted effects of variations in slope and width. The river narrows abruptly at the entrance of the gorge, and even comparing just actively incising reaches (1,3 and 4), the gorge reach is anomalously narrow. Therefore, in the discussion that follows, we follow *Whipple and Tucker* (1999)'s derivation of the generic bedrock erosion law, but leave width as an independent parameter. If, in terms of the shear stress at the bed, erosion is given by

$$E = k_b \tau_b^a \tag{5.3}$$

then the generic erosion law, stripped of the assumption of width-drainage area scaling, becomes

$$E = K^* A^{m*} S^n \frac{1}{W^{2a/3}} \tag{5.4}$$

where a is the exponent that relates erosion and shear stress. Values of a depend on dominant process, and probably fall in the range of $1 < a < 3.5$ (*Whipple et al.* (1999a); *Whipple and Tucker* (1999)). The parameters K^* and m^* are not the same as in the first equation, where they partly reflect the drainage area-width scaling. If width is considered independently, $n* = 2a/3$, and

$$E \propto (\frac{S}{W})^{2a/3} = (\frac{S}{W})^{n^*} \tag{5.5}$$

We expect that a halving of width should have the same effect as a doubling of slope, all other things being equal. However, although we can safely discount variations in upstream drainage area (and therefore discharge), we cannot assume that K is the same for all reaches of interest. A number of attempts have been made to estimate, K, the erosivity parameter (eg. *Stock and Montgomery* (1999); *Snyder et al.* (2000); *Kirby and Whipple* (2001)) and a wide range of values have been cited. In the generic stream power equation (1), at least some of the variation in erosivity is due to the channel width / drainage area scaling. Apart from that, K also depends on lithology, the distribution of precipitation in a drainage basin, the thickness and distribution of alluvial cover on the bed, the sediment flux, and the effect of debris flows. Comparing the gorge with the upstream and downstream bedrock reaches, we submit that neither lithology, precipitation or sediment flux are much different. Although we observed large landslide derived blocks in some places in the channel, if anything, there is less alluvial material armoring the channel in the gorge than the other bedrock reaches. Neglecting possible variation in K is therefore likely a conservative assumption. Comparing the gorge reach to either the upstream or downstream bedrock reaches (1 and 4), we note that the area between the bounding

faults is characterized by a six-fold increase in slope and a narrowing by a factor of 2 to 4. For a conservative range of n^* from 2/3 to 4/3, this suggests that the incision rate of the Jinsha river in Tiger Leap gorge may be between 5 and 70 times that of the other two bedrock reaches. Neglecting the possible effect of narrowing in the gorge, just the increase in slope suggests a factor of 3 to 10 increase in incision rate relative to the other deeply incised bedrock reaches.

The lack of pronounced knickpoints within the gorge suggests that the Jinsha river has adjusted to the increased uplift rate within the fault-bounded Yulong mountains. That is, we believe that the river's abrupt steepening and narrowing, exactly coincident with the range bounding faults represents the channel's adjustment so as to balance uplift and incision. Moreover, the exact co-location of knickpoints defining the steepened reach with the range-bounding faults indicates that high uplift rates continue in present day, since if uplift were to cease or slow, knickpoints would quickly migrate upstream. Taken at face value, the inferred greater than 5 times greater incision rate within the gorge compared to other deeply incised reaches of the Jinsha river implies correspondingly greater uplift rates within the range. Recent thermochronologic (*Clark et al.* (2005); *Kirby et al.* (2002)), cosmogenic (*Ouimet et al.* (2005); *Schoenbohm* (2004)) and geologic (*Schoenbohm et al.* (2004a)) studies have suggested incision rates of major rivers incising the eastern Tibetan plateau margin of between 0.25 and 1 mm/yr. Lacking direct data for the Jinsha river reaches, these studies merely provide a ballpark for making a reasonable and conservative estimate at the incision rate of the deeply incised bedrock reaches (1 and 4) of the Jinsha river of about 0.25 mm/yr. From this we submit the testable prediction that incision (and presumably therefore uplift) rates within the Yulong mountains are most likely on the order of 1 to 5 mm/yr, and may be even higher.

Summary of geomorphic evidence for anomalous rock uplift rates in the Yulong mountains

The Yulong mountains are an area of high, glaciated elevations, anomalously high local relief, and steep, threshold slopes. Within this region, hillslope processes are dominated by landsliding at many scales and average hillslope angles appear to reflect the maximum slope angles set by inherent rock strength. We therefore infer that the range is characterized by threshold hillslopes, and that the overall rate of landscape lowering is thus set by the process that sets the lower elevation of the hillslopes. In the part of the range that is within the drainage area of the Jinsha river, the river's incision into bedrock is just that process. Assessment of the change in inferred erosivity of the river as a function of its gradient and width implies a large increase in the incision rate of the Yulong mountains reach of the Jinsha river. Since the anomalous steepness and narrowness of the Jinsha is probably the result of the river's adjustment to higher rates of rock uplift, we assume that the high incision rate implies a similarly high rock uplift rate.

Threshold hillslopes suggest that we can infer high uplift rates everywhere within the drainage area of the Jinsha, which represents about 2/3 of the area contained within the active range bounding faults. Elsewhere in the Yulong mountains, we suspect that a variety of hillslope, fluvial and glacial processes also balance high uplift rates. The difference is that base level is either set by the elevation of tributaries to the Jinsha or by the elevation of (relatively) subsiding ground in the immediate hangingwalls of active normal faults. Threshold hillslopes are observed everywhere within the range; outside the immediate drainage area of the Jinsha river (i.e. Tiger Leap gorge) average elevations are higher, but slopes are as steep. In short, all geomorphic indicators of high rates of erosion – and therefore uplift, if the landscape is in approximate steady-state – suggest that the Yulong mountains are a region of anomalously high rates of uplift. We emphasize that all these geomorphic anomalies are exactly

demarcated by the basin bounding faults. Steep slopes are exactly coincident with the region within the bounding faults, and knickpoints on the Jinsha bounding the anomalously steep and narrow reach of the river within the range are located on the active faults.

5.5 Estimates of total erosion and exhumation rates

From several perspectives, both the geology and geomorphology of the Yulong mountains are distinct from its surroundings, the demarcation is always abrupt and always coincides exactly with the position of active faults. The mapped geology reflects anomalous exhumation within the bounding faults, and the geomorphology suggests that this is a result of a history of anomalous rock uplift rates balanced by erosion processes. In this section, we estimate the total amount of material removed by erosion and/or normal faulting from the core of the range and the likely exhumation rates. Unfortunately, the chlorite grade metaclastic and marble lithologies exposed in the core of the range do not lend themselves to low temperature thermochronometric methods, so instead we exploit the Permian Emei Shan basalts, one of the most distinctive parts of the Paleozoic Yangzi Platform stratigraphy as a marker unit in a structural reconstruction (fig. 5-5). These basalts form a large igneous province (LIP) and consist of a thick section of continental and marine basalts that is exposed in much of southwestern Sichuan and western Yunnan provinces (*Thompson et al.* (2001)). In the Lijiang area, the Emei Shan basalts are over 2km thick, though poor exposure and Mesozoic deformation makes these estimates somewhat imprecise. Around the Yulong mountains, Permian Emei Shan rocks are found almost everywhere in the hanging wall of the range bounding faults. At the northern margin of the range, Emei Shan basalts are juxtaposed against sheared Devonian limestones across a low angle domal normal fault. Along the east and south margins of the

range, in the hanging walls of moderately dipping normal faults, high flat topped surfaces are cut on the basalts and are covered by a thin colluvial cover. The western margin is more complicated, and low grade and cleaved Permian basalts west of the bounding faults are tightly and recumbently folded with lower Paleozoic and lower Triassic units.

Using the Emei Shan basalts as a datum, we use structural cross-sections (fig. 5-5) in order to estimate the amount of erosional and tectonic unroofing that accompanied uplift and erosion of rocks within the Yulong mountains since the late Pliocene. Projecting the base of the Permian basalts from the hanging wall of low angle normal faults from the northern margin of the range, cross-sections suggest a minimum of 6 km of rock were removed from rocks at the crest of the antiformal dome. This estimate does not take into account attenuation of units along extensional shear zones at the contacts between the Permian and Devonian limestones, or along foliation parallel zones below this contact. Alternatively, using the measured thicknesses cited by regional surveys (*BGMR Yunnan* (1990)), the removal of the Silurian to Carboniferous section represents perhaps 7 km of stratigraphic relief between rocks in the middle of Tiger Leap gorge and the Permian basalts. These estimates, together with our admittedly poor age constraints for the onset of extensional faulting ($\sim$ 2.5 Ma) suggest average unroofing rates in the neighborhood of 3 mm/yr. Although these estimates are subject to large uncertainties, this is consistent with our estimates of 1 to 5 mm/yr based on the anomalous steepness of the Tiger Leap Gorge reach of the Jinsha river (section 5.4.1).

5.6 A conceptual model for the Yulong mountains: the role of vigorous erosion, weak middle or lower crust, and normal faults.

The exposure of deep structural levels in the core of the normal-fault bounded antiformal dome is a fairly common structural association in extensional terrains. What is unique about the Yulong mountains culmination is that it is an active system, and thus this system presents an opportunity to understand a possible set of processes that can produce this geometry. With this in mind, it is impossible not to be struck by the exact coincidence of the Jinsha river and the crest of the dome, and pose the question as to whether it is possible that surface processes could have played a role in focussing deformation.

The crests of anticlines – particularly transverse anticlines – are commonly coincident with large rivers in many orogens (*Simpson* (2004a)), an association described by *Oberlander* (1985) as an "apparent stream preference" for antiformal culminations. These kinds of observations, and the possibly similar associations of fast and young exhumation spatially co-located with major rivers at the eastern and western Himalayan syntaxes (*Zeitler et al.* (2001b)) have motivated suggestions that erosion can actually cause localized deformation. A brief review of some of these proposals follows, in order to highlight whether or not these models might explain our observations in the Yulong mountains.

(*Simpson* (2004a,b,c)) described a series of numerical simulations of river incision in thin-skinned fold and thrust belts that predict that erosion – specifically river incision – can focus deformation and significantly modify structural geometries, creating doubly plunging anticlinal culminations centered on river valleys. River incision strongly affects deformation in these models because in the compressional setting of the models, stresses are close to the yield stresses of the rocks and the relatively small

perturbations in normal stresses due to erosional unloading can amplify deformation at a small scale (i.e. the scale of individual folds). *Finlayson et al.* (2002) noted the spatial coincidence of high erosion rates with structural culminations and young metamorphic massifs in the Himalaya, and anomalously high exhumation rates in the Nanga Parbat and Namche Barwa massifs have been explained as the result of focussed deformation driven by surface processes by *Koons et al.* (2002); *Zeitler et al.* (2001a,b). Their model is somewhat different: high erosion rates allow fast advection of hot and weak crustal material, weakening the upper crust and thus focussing deformation. Furthermore, they suggest that rapid advection leads to high topography and relief, which lead to fast erosion rates and thus possible feedbacks between erosion and focussed deformation. Beyond their argument that rapid advection of crustal material effectively weakens crustal rocks, their model is similar to *Simpson* (2004a) in that the mechanism whereby erosional unloading leads to localized advection of crust acts by decreasing vertical stresses that normally inhibit deformation in an area actively deforming in compression (*Koons et al.* (2002)).

These models cannot be applied to the Yulong mountains, because in an extensional setting erosional unloading ought to inhibit deformation, not focus it. Alternatively, the classic treatment of rift flank uplift in extensional environments models uplift as the response to unloading of a flexing elastic beam (eg. *Weissel and Karner* (1989)). Unloading of the crust can occur in two ways: extensional faults thin crust in the hanging walls of the normal faults or erosion can remove material. Thin crust adjacent to the faults is manifest as extensional basins, but we note that there are no deep or wide Quaternary basins adjacent to the Yulong mountains, which might otherwise provide a mechanism for the uplift of the mountains adjacent to them. Indeed, we have found no evidence for any measurable rift-flank uplift adjacent to the Quaternary basins associated with extensional faulting south of the Yulong mountains (fig. 5-3).

Erosion in the center of the range might provoke a measurable response, if the effective elastic thickness was small enough, otherwise uplift due to buoyant restoring forces is spread out over a large area, and the amount of uplift at any one point is very small. Alternatively, it is possible that the closed circuit of normal faults that bound the range allows the Yulong mountains to respond to erosional unloading as an independent block. If the middle crust underlying the block is weak, erosional unloading will lead to uplift of the block as the weak middle crust flows in response to the imposed pressure gradient underneath the block. In this case, however, uplift will always be less than the (crustal) isostatic response to unloading, which is given by:

$$w = \frac{\rho_u}{\rho_l} q_e$$

where w is the uplift, ρ_u and ρ_l are the densities of the rigid upper layer and fluid lower layer, respectively, and q_e is the unloading in terms of meters of uniform removal of material from the top. At most, if $\rho_u = \rho_l$, then the uplift response is equal to the amount of material removed from the top. If material is not removed uniformly – as in the excavation of a deep valley in the middle of a rigid block that is free to rise independently of its surroundings – the heights of peaks may rise even as average elevations remain constant. However, the Yulong mountains are not only characterized by high relief and maximum elevations, but anomalously high mean elevations. In figure 5-14a, we show the elevations of this part of the eastern Tibetan plateau margin smoothed by averaging over a 20km radius moving window, a distance over which elevations would be compensated even for very low effective elastic thicknesses. In figure 5-14b we show the deviation from the actual topography from the smoothed and averaged elevations. Although Tiger Leap gorge is an anomalously low area, the mountains as a whole are, on average, $\sim$ 640m higher than their surroundings (the elevations of which are biased upwards, since

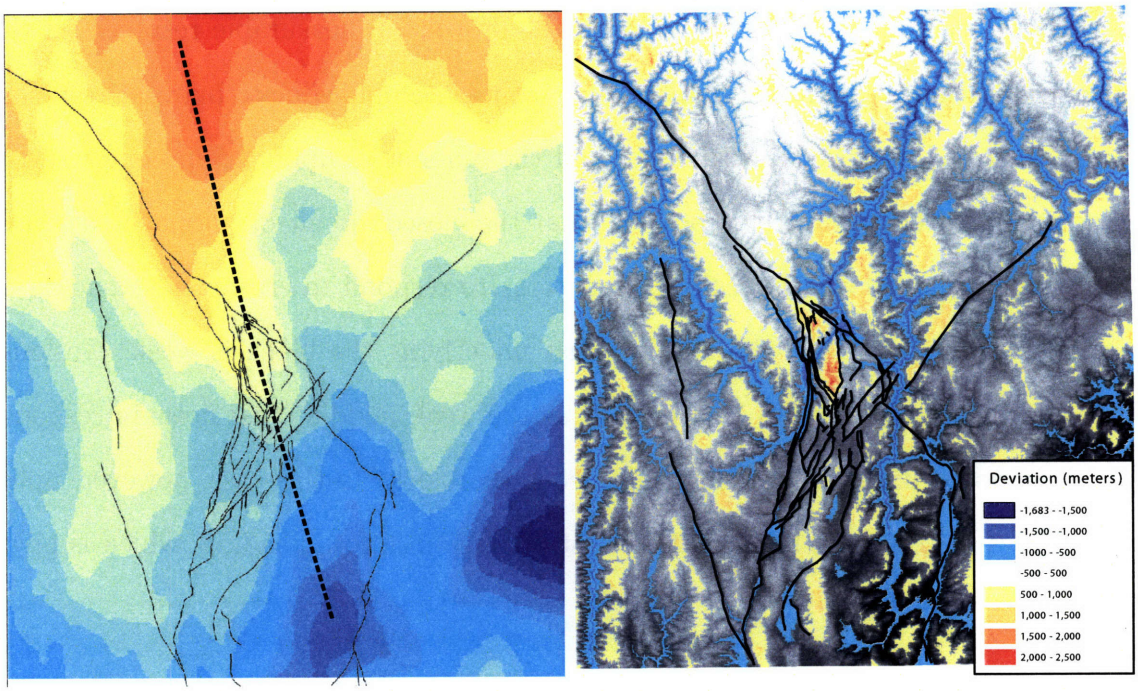

Figure 5-14: Left: Elevations smoothed by averaging over a 20km radius moving window. Right: Deviation of elevations from smoothed and averaged elevations superimposed over a grayscale image of the DEM. Areas in grayscale are within 500m of the smoothed and averaged elevations.

we do not exclude the Yulong mountains when calculating the smoothed elevations). Whether the problem is cast in terms of the unloading of an elastic plate or a rigid, independent block, the anomalously high elevations within the Yulong mountains cannot be produced merely by buoyancy forces. Anomalously high elevations can result if the upper part of the crust is heavier than the lower, inviscid layer, as in *Martinez et al.* (2001)'s model for core complexes offshore of Papua-New Guinea, but there is no reason to believe that this is the case here.

Models of flexure or crustal isostasy describe the static balance between elastic forces, the load, and the response of the substratum to deflection. When such a static balance obtains, uplift rates should be zero. However, a key feature of the Yulong Mountains are the anomalous uplift rates we infer from geomorphic evidence. It thus appears as though, if anything, the Yulong mountains are lower than their ultimate

static equilibrium elevation. So long as erosion rates balance rock uplift rates in the range, the range will never reach its equilibrium elevation.

The localization of anomalous uplift rates and high elevations requires that the range is underlain by material sufficiently weak enough to flow to accommodate the rise of the range block. In any case, the presence of a weak inviscid layer underlying the brittle upper crust is implicit in the thin elastic plate or independent, rigid block models alluded to above. The model of the range acting as a rigid, independent block is closely analogous to the reactive salt diapirs well known in salt tectonics (*Jackson and Vendeville* (1994); *Jackson et al.* (1994, 1995)), which are primarily driven by pressure differentials, including those caused by surface unloading, and only weakly controlled by density differences between salt and overburden. Surface unloading creates a pressure differential that drives flow – which in turn can flex plates or cause fault-bounded blocks to rise. However, surface unloading is not the only possible source of pressure differentials. In salt systems, for instance, regional dip of passive margin sediments is enough to drive salt towards the shelf edge and is a first order control on how high salt diapirs can rise. Similarly, the large-scale morphology of the eastern Tibetan plateau might have formed by topography driven channel flow in the middle or lower crust (*Clark and Royden* (2000)). The Yulong mountains lie south and east of high topography of the eastern Tibetan plateau, so the source of the additional pressure required to explain either the present anomalously high elevations or the even higher equilibrium elevation may be the topographic head caused by high elevations "up-stream" of the Yulong mountains. In this way, the Yulong mountains may represent an imperfect "tectonic barometer", imperfect because erosion processes do not permit the range to reach its equilibrium height (fig. 5-15).

It is worth recapitulating the main assumptions and consequences of this conceptual model of the mechanisms driving uplift and exhumation in the Yulong mountains. Surface processes explain the exhumation of deep structural levels in the range, the

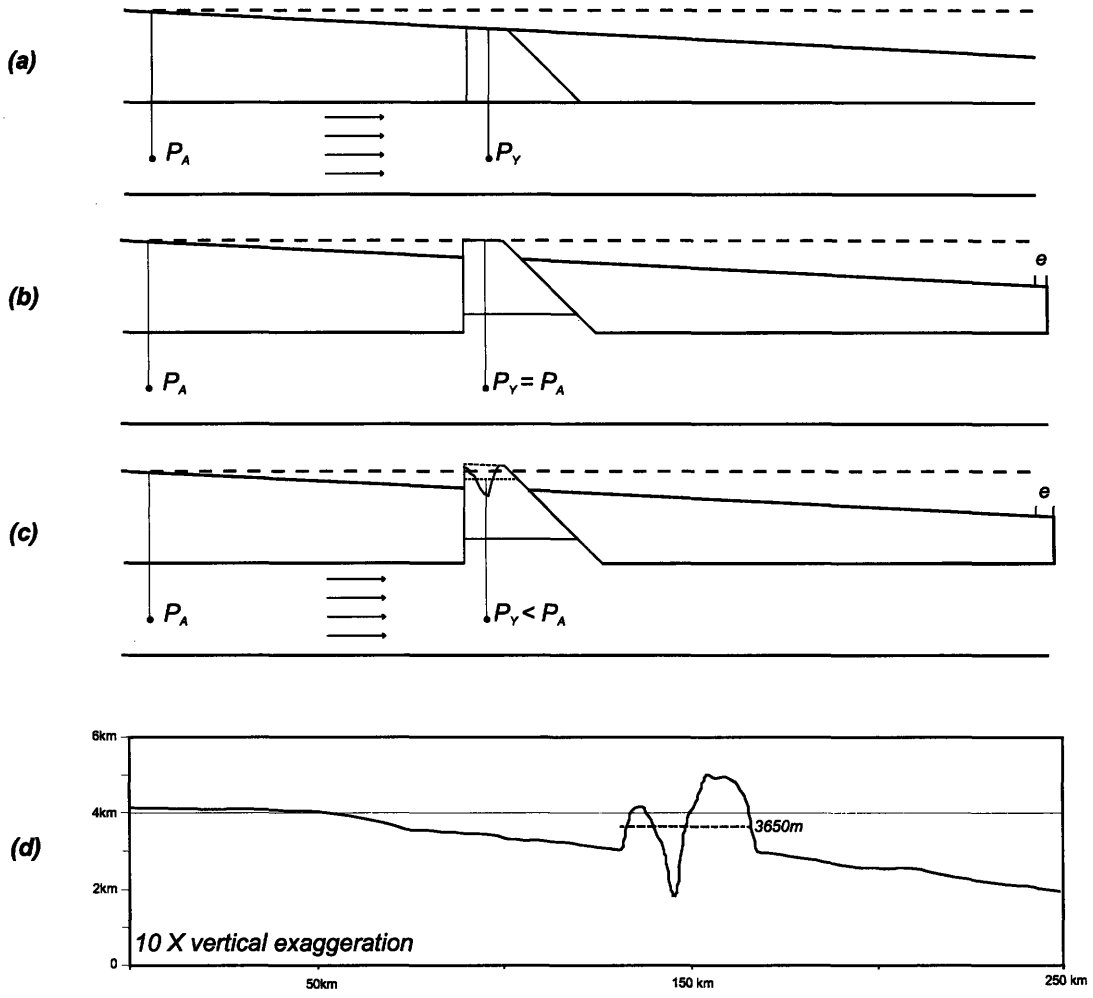

Figure 5-15: Cartoon model of the Yulong mountains as a reactive diapir. In panel (a), pressure differentials exist in a fluid channel due to the regional topographic slope. In panel (b), extension of the brittle, upper layer allows the block to rise independently, up to a maximum elevation where $P_Y = P_A$. If erosion rates balance uplift rates, the average elevation of the block will always be short of the equilibrium elevation, and continued uplift and exhumation occurs. Note, however, that extension of the upper layer is required to accommodate continued uplift, unless the bounding faults are completely vertical. Bottom panel (d) shows a N-S profile of the actual regional topography (see figure 5-14 for profile location). The average 3650m elevation of the Yulong mountains is shown as a dashed line.

result of erosion rates balancing rock uplift rates for a sustained period of time. In short, the role of surface processes is just to maintain uplift rates. Vigorous erosion processes by themselves, however are not sufficient to drive the system. Deep exposure levels and high uplift rates do not occur along the entire length of the Jinsha river, but rather only where the river intersects the transtensional faults of the Jianchuan-Lijiang-Zhongdian fault system. That is, a closed network of normal faults that accommodates uplift and permits the range to respond independently of its surroundings are a first order necessary condition for the model to work.

A second necessary condition is that the region as a whole has been subject to uplift and river incision that predates the specific, anomalous uplift rates in the Yulong mountains. The characteristics of the Jinsha river profile that lead us to infer high relative rock uplift rates within the range are an oversteepened reach defined by knickpoints co-located with the active bounding faults, and a long, alluviated reach upstream of the range. These characteristics are the expected products of the perturbation of a river profile adjusted to the regional rock uplift rates. Regional uplift and consequent development of the kind of steep river gorge characteristic of the eastern Tibetan plateau margin is a necessary condition because steep topography is needed to produce rapid erosion in competent rocks. Moreover, if the river were not deeply entrenched, it is possible that localized uplift along its course would have simply caused it to be diverted around the uplift, essentially eliminating erosion from the top of the uplift zone (eg. *Humphrey and Konrad* (2000)). Without erosion, uplift would end once mean elevations had attained the equilibrium elevations that satisfy static force balances. In short, *persistant*, localized extrusion between the range-bounding normal faults must be a response to erosion.

Finally, we need to appeal to weak middle or lower crust underlying the range, without which no localized uplift rates nor anomalously high elevations are possible. The inference of high equilibrium elevations furthermore requires that weak middle

or lower crustal material is continuing to flow into the region from the high Tibetan plateau. This explanation of the high uplift rates and elevations of the Yulong mountains leads us to consider the perhaps surprising possibility that the continental crust of the eastern margin of the Tibetan plateau continues to thicken, even as the upper crust is in extension.

Ackowledgments

We thank Kelin Whipple and Ben Crosby for valuable discussion and for suggesting many improvements to the manuscript. Lindsay Schoenbohm and Marin Clark sparked the interest of the first author in the Yulong mountains and pointed out the possibility of dynamical interactions between surface processes and tectonics in this area. The first author was supported by the Fonds Pour la Recherche en Sciences et Technologies (Québec) graduate student grant. Research for this study was funded by NSF Continental Dynamics grants EAR 0003571 and EAR 8904096.

References

Akamatsu, J., H. Morikawa, N. Nishimura, K. Onoue, M. Nakamura, N. Seto, M. Komazawa, L. Jiang, K. Li, Q. Luo, and Y. Wang (1998), Bedrock structure in Lijiang basin and its seismic effects, in *Effects of Surface Geology on Seismic Motion*, edited by K. Irikura, K. Kudo, H. Okada, and T. Sasatani, pp. 725–732.

Akciz, S. O. (2004), Structural and geochronological constraints on the ductile deformation observed along the Gaoligong Shan and Chong Shan shear zones, Yunnan (China), Ph.D. thesis, MIT.

Beaumont, C., P. Fullsack, and J. Hamilton (1992), Erosional control of active compressional orogens, in *Thrust Tectonics*, edited by K. McClay, pp. 1–18, Chapman & Hall, London.

BGMR Yunnan (1990), *Yunnan Bureau of Geology and Mineral Resources*, 1:200000 Regional Map Series, various sheets.

Burbank, D., and R. Anderson (2001), *Tectonic geomorphology*, Blackwell Science, Malden, Mass.

Burbank, D., J. Leland, E. Fielding, R. S. Anderson, N. Brozovic, M. R. Reid, and C. Duncan (1996), Bedrock incision, rock uplift and threshold hillslopes in the northwestern Himalayas, *Nature*, *379*, 505–510.

Chen, Z., B. C. Burchfiel, Y. Liu, R. W. King, L. H. Royden, W. Tang, E. Wang, J. Zhao, and X. Zhang (2000), Global positioning system measurements from eastern Tibet and their implications for India/Eurasia intercontinental deformation, *Journal of Geophysical Research*, *105*(B7), 16,215–16,228.

Clark, M. K. (2003), Late Cenozoic uplift of southeastern Tibet, Ph.D. thesis, MIT.

Clark, M. K., and L. H. Royden (2000), Topographic ooze: building the eastern margin of Tibet by lower crustal flow, *Geology*, *28*, 703–706.

Clark, M. K., M. A. House, L. H. Royden, K. X. Whipple, B. C. Burchfiel, X. Zhang, and W. Tang (2005), Late Cenozoic uplift of southeastern Tibet, *Geology*, *33*(6), 525–528.

Clark, M. K., L. H. Royden, K. X. Whipple, B. C. Burchfiel, X. Zhang, and W. Tang (in review), Deformation of a regional low-relief relict lanscape (erosion surface) in eastern Tibet, *Journal of Geophysical Research - Earth Surface*.

Finlayson, D., D. Montgomery, and B. Hallet (2002), Spatial coincidence of rapid inferred erosion with young metamorphic massifs in the Himalayas, *Geology*, *30*, 219–222.

Finnegan, N., G. Roe, D. Montgomery, and B. Hallet (2005), Controls on the channel width of rivers: Implications for modeling fluvial incision of bedrock, *Geology*, *33*, 229–232, doi:10.1130/G21171.1.

Geissman, J., B. C. Burchfiel, C. Studnicki-Gizbert, S. Akciz, and L. Chen (submitted), Complexities in the early Cenozoic extrusion of crustal fragments around the eastern Himalayan syntaxis, *Geosphere*.

Hanmer, S., and C. W. Passchier (1991), *Shear sense indicators: a review*, Paper 90 - 17, Geological Survery of Canada.

He, H., T. Oguchi, R. Zhou, J. Zhang, and S. Qiao (2001), Damage and seismic intensity of the 1996 Lijiang earthquake, China: A GIS analysis, *Tech. rep.*, Center for Spatial Information Science, University of Tokyo, Tokyo, Japan.

Holt, W. E., N. Chamot-Rooke, X. L. Pichon, A. J. Haines, B. Shen-Tu, and J. Ren (2000), Velocity field in Asia inferred from Quaternary fault slip rates and global positioning system observations, *Journal of Geophysical Research*, *105*(B8), 19,185–19,210.

Hughes, N., S. Peng, and H. Luo (2002), Kunmingaspis (Trilobita) putatively from the Yunling Collage and the Cambrian history of the Eastern Himalayan syntaxial region, *Journal of Paleontology*, *76*(4), 709–717.

Humphrey, N., and S. Konrad (2000), River incision or diversion in response to bedrock uplift, *Geology*, *28*, 43–46, doi:10.1130/0091-7613(2000)28¡43:RIODIR¿2.0.CO;2.

Jackson, M. P. A., and B. C. Vendeville (1994), Regional extension as a geologic trigger for diapirism, *Geological Society of America Bulletin*, *106*, 57–73.

Jackson, M. P. A., B. C. Vendeville, and D. D. Schultz-Ela (1994), Structural dynamics of salt systems, *Annual Reviews of Earth and Planetary Sciences*, *22*, 93–117, doi:10.1146/annurev.ea.22.050194.000521.

Jackson, M. P. A., D. G. Roberts, and S. Snelson (Eds.) (1995), *Salt tectonics, a global perspective*, AAPG Memoir 65, American Association of Petroleum Geologists.

King, R., F. Shen, B. Burchfiel, L. Royden, E. Wang, Z. Chen, Y. Liu, X. Zhang, J. Zhao, and Y. Li (1997), Geodetic measurement of crustal motion in southwest China, *Geology*, *32*, 809–812.

Kirby, E., and K. Whipple (2001), Quantifying differential rock-uplift rates via stream profile analysis, *Geology*, *29*, 415–418, doi:10.1130/0091-7613(2001)029¡0415:QDRURV¿2.0.CO.

Kirby, E., P. W. Reiners, M. A. Krol, K. X. Whipple, K. V. Hodges, K. A. Farley, W. Tang, and Z. Chen (2002), Late Cenozoic evolution of the eastern margin of the Tibetan plateau: Inferences from 40Ar/39Ar and (U-Th)/He thermochronology, *Tectonics*, *21*(1), 1001+, doi:doi:10.1029/2000TC001246.

Kirby, E., K. X. Whipple, W. Tang, and Z. Chen (2003), Distribution of active rock uplift along the eastern margin of the Tibetan Plateau: Inferences from bedrock channel longitudinal profiles, *Journal of Geophysical Research*, *108*(B4), 2217+, doi:10.1029/2001JB000861.

Koons, P. (1989), The topographic evolution of collisional mountain belts: a numerical look at the Southern Alps, N.Z., *American Journal of Science*, *289*, 1041–1069.

Koons, P. O., P. K. Zeitler, C. P. Chamberlain, D. Craw, and A. S. Meltzer (2002), Mechanical links between erosion and metamorphism in Nanga Parbat, Pakistan Himalaya, *American Journal of Science*, *302*, 749–773.

Lacassin, R., U. SchÃrer, P. H. Leloup, N. Arnaud, P. Tapponier, X. Liu, and L. Zhang (1996), Tertiary deformation and metamorphism SE of Tibet: The folded Tiger-leap decollement of NW Yunnan, China, *Tectonics*, *15*(3), 605–622.

Lavé, J., and J. P. Avouac (2001), Fluvial incision and tectonic uplift across the Himalayas of central Nepal, *Journal of Geophysical Research*, *106*(B11), 26,561–26,592.

Leloup, P. H., R. Lacassin, P. Tapponnier, U. Scharer, D. Zhong, X. Liu, L. Zhang, S. Ji, and P. T. Trinh (1995), The Ailao Shan-Red River shear zone (Yunnan, China), Tertiary transform boundary of Indochina, *Tectonophysics*, *251*(1-4), 3–84, doi:10.1016/0040-1951(95)00070-4.

Leloup, P. H., N. Arnaud, R. Lacassin, J. R. Kienast, T. M. Harrison, T. T. P. Trong, A. Replumaz, and P. Tapponnier (2001), New constraints on the structure, thermochronology, and timing of the Ailao Shan-Red River shear zone, SE Asia, *Journal of Geophysical Research*, *106*(B4), 6683–6732.

Martinez, F., A. M. Goodliffe, and B. Taylor (2001), Metamorphic core complex formation by density inversion and lower-crust extrusion, *Nature*, *411*(6840), 930–934, doi:10.1038/35082042.

Metcalfe, I. (1998), Palaeozoic and Mesozoic geological evolution of the SE Asian region: multidisciplinary constraints and implications for biogeography, in *Biogeography and Geological Evolution of SE Asia*, edited by R. Hall and J. Holloway, pp. 25–41, Backhuys Publishers, Leiden , the Netherlands.

Montgomery, D. R., and K. B. Gran (2001), Downstream variations in the width of bedrock channels, *Water Resources Research*, *37*(6), 1841–1846.

Oberlander, T. M. (1985), Origin of drainage transverse to structures in orogens, in *Tectonic Geomorphology*, edited by M. Morisawa and J. T. Hack, pp. 155–182, Allen & Unwin, New York.

Ouimet, W., K. Whipple, L. Royden, and D. Granger (2005), Long transient response times of rivers in eastern Tibet to regional plateau uplift: The effect of mega-landslides, *Geophysical Research Abstracts*, *7*, 05,743+.

Ouimet, W. B., and K. X. Whipple (2004), Mega-landslides in eastern Tibet: Implications for landscape and river profile evolution, and the interpretation of tectonics from topography, *AGU Fall Meeting Abstracts*, pp. #H44A–04.

Rosenbloom, N. A., and R. S. Anderson (1994), Hillslope and channel evolution in a marine terraced landscape, Santa Cruz, California, *Journal of Geophysical Research*, *99*(B7), 14,013–14,030.

Royden, L. H., B. C. Burchfiel, R. W. King, E. Wang, Z. Chen, F. Shen, and Y. Liu (1997), Surface deformation and lower crustal flow in eastern Tibet, *Science*, *276*(5313), 788–790, doi:10.1126/science.276.5313.788.

Schmidt, K. M., and D. R. Montgomery (1995), Limits to relief, *Science*, *270*(5236), 617–620.

Schoenbohm, L. (2004), Cenozoic tectonic and geomorphic evolution of the Red River region, Yunnan province, China, Ph.D. thesis, MIT.

Schoenbohm, L., K. Whipple, B. Burchfiel, and L. Chen (2004a), Geomorphic constraints on surface uplift, exhumation, and plateau growth in the Red River region, Yunnan Province, China, *Geological Society of America Bulletin*, *116*, 895–909, doi:10.1130/B25364.1.

Schoenbohm, L., K. Whipple, C. B. Burchfiel, and L. Chen (2004b), Geomorphic constraints on surface uplift, exhumation, and plateau growth in the Red River region, Yunnan Province, China, *Geological Society of America Bulletin*, *116*, 895–909, doi:10.1130/B25364.1.

Schoenbohm, L., B. C. Burchfiel, and L. Chen (in press), Propagation of surface uplift, lower crustal flow, and Cenozoic tectonics of the southeast margin of the Tibetan plateau, *Geology*.

Sengor, A. M. C., and B. A. Natalin (1996), Paleotectonics of Asia: fragments of a synthesis, in *The Tectonic Evolution of Asia*, edited by A. Yin and M. Harrison, pp. 486–641, Cambridge University Press.

Shen, Z.-K., J. LÃ, M. Wang, and R. BÃrgmann (2005), Contemporary crustal deformation around the southeast borderland of the Tibetan Plateau, *Journal of Geophysical Research*, *110*, B11,409+, doi:10.1029/2004JB003421.

Shi, Y. (2002), Characteristics of late Quaternary monsoonal glaciation on the Tibetan Plateau and in East Asia, *Quaternary International*, *97*, 79–91, doi:10.1016/S1040-6182(02)00053-8.

Simpson, G. (2004a), Role of river incision in enhancing deformation, *Geology*, *32*, 341–344.

Simpson, G. (2004b), Dynamic interactions between erosion, deposition, and three-dimensional deformation in compressional fold belt settings, *Journal of Geophysical Research*, *109*, F03,007+, doi:10.1029/2003JF000111.

Simpson, G. (2004c), A dynamic model to investigate coupling between erosion, deposition, and three-dimensional (thin-plate) deformation, *Journal of Geophysical Research*, *109*, F02,006+, doi:10.1029/2003JF000078.

Snyder, N., K. Whipple, G. Tucker, and D. Merritts (2000), Landscape response to tectonic forcing: Digital elevation model analysis of stream profiles in the Mendocino triple junction region, northern California, *Geological Society of America Bulletin*, *112*, 1250–1263.

Snyder, N., K. Whipple, G. Tucker, and D. Merritts (2003), Channel response to tectonic forcing: field analysis of stream morphology and hydrology in the mendochino triple junction region, northern california, *Geomorphology*, *53*, 97–127.

Stock, J. D., and D. R. Montgomery (1999), Geologic constraints on bedrock river incision using the stream power law, *Journal of Geophysical Research*, *104*(B3), 4983–4994.

Sun, Y., S. Kuleli, F. D. Morgan, W. Rodi, and N. Toksoz (2004), Location robustness of earthquakes in Sichuan province, *Seismological Research Letters*, *75*, 54–62.

Tamai, M., Y. Liu, L. Z. Lu, M. Yokoyama, N. Halim, H. Zaman, and Y.-i. Otofuji (2004), Palaeomagnetic evidence for southward displacement of the Chuan Dian fragment of the Yangtze Block, *Geophysical Journal International*, *158*, 297–309.

Thompson, G. M., J. R. Ali, X. Song, and D. W. Jolley (2001), Emeishan basalts, SW China: reappraisal of the formation's type area stratigraphy and a discussion of its significance as a large igneous province, *Journal of the Geological Society*, *158*, 593–599.

Wang, E., and B. Burchfiel (1997), Interpretation of Cenozoic tectonics in the right-lateral accomodation zone between the Ailao Shan shear zone and the eastern Himalayan syntaxis, *International Geology Review*, *39*, 191–219.

Wang, E., B. Burchfiel, L. Royden, L. Chen, J. Chen, W. Li, and Z. Chen (1998), *Late Cenozoic Xianshuihe-Xiaojiang, Red River, and Dali Fault Systems of Southwestern Sichuan and Central Yunnan, China*, *GSA Special Paper*, vol. 327, Geological Society of America.

Weissel, J., and G. Karner (1989), Flexural uplift of rift flanks due to mechanical unloading of the lithosphere during extension., *Journal of Geophysical Research*, *94*(B10), 13,919–13,950.

Whipple, K. (2004), Bedrock rivers and the geomorphology of active orogens, *Annual Review of Earth and Planetary Sciences*, *32*, 151–185, doi: 10.1146/annurev.earth.32.101802.120356.

Whipple, K., G. Hancock, and R. Anderson (1999a), River incision into bedrock: Mechanics and relative efficacy of plucking, abrasion, and cavitation., *Geological Society of America Bulletin*, *112*, 490–503.

Whipple, K., E. Kirby, and S. Brocklehurst (1999b), Geomorphic limits to climate-induced increases in topographic relief, *Nature*, *401*, 39–43.

Whipple, K. X., and G. E. Tucker (1999), Dynamics of the stream-power river incision model: Implications for height limits of mountain ranges, landscape response timescales, and research needs, *Journal of Geophysical Research*, *104*(B8), 17,661–17,674.

Wobus, C., K. Hodges, and K. Whipple (2003), Has focused denudation sustained active thrusting at the Himalayan topographic front?, *Geology*, *31*, 861–864, doi: 10.1130/G19730.1.

Yoshioka, S., Y. Liu, K. Sato, H. Inokuchi, L. Su, H. Zaman, and Y. Otofuji (2003), Paleomagnetic evidence for post-Cretaceous internal deformation of the Chuan Dian Fragment in the Yangtze block: a consequence of indentation of India into Asia, *Tectonophysics*, *376*(1-2), 61–74.

Zeitler, P. K., P. O. Koons, M. P. Bishop, P. C. Chamberlain, D. Craw, M. A. Edwards, S. Hamidullah, Q. M. Jan, A. M. Khan, , W. S. F. Kidd, R. L. Mackie, A. S. Meltzer, S. K. Park, A. Pecher, M. A. Poage, G. Sarker, D. A. Schneider, L. Seeber, and J. F. Shroder (2001a), Crustal reworking at Nanga Parbat, Pakistan: Metamorphic consequences of thermal-mechanical coupling facilitated by erosion, *Tectonics*, *20*(5), 712–728.

Zeitler, P. K., A. S. Meltzer, P. O. Koons, D. Craw, B. Hallet, C. P. Chamberlain, W. S. F. Kidd, S. K. Park, L. Seeber, M. Bishop, and J. Shroder (2001b), Erosion, Himalayan geodynamics, and the geomorphology of metamorphism, *GSA Today*, *11*, 4–9, doi:10.1130/1052-5173(2001)011¡0004:EHGATG¿2.0.CO;2.

Zhang, P.-Z., Z. Shen, M. Wang, W. Gan, R. Bürgmann, P. Molnar, Q. Wang, Z. Niu, J. Sun, J. Wu, S. Hanrong, and Y. Xinzhao (2004), Continuous deformation of the Tibetan plateau from global positioning system data, *Geology*, *32*, 809–812.

Zheng, B., Q. Xu, and Y. Shen (2002), The relationship between climate change and Quaternary glacial cycles on the Qinghai-Tibetan Plateau: review and speculation, *Quaternary International*, *97-98*, 93–101, doi:10.1016/S1040-6182(02)00054-X.

Chapter 6

Synthesis

This dissertation comprises investigations into a seemingly wildy disparate series of of problems from interpreting ductile fabrics to active tectonics, sedimentology and geomorphology and even brief excursions into geodesy, seismology and geodynamics. What unifies the various chapters of the thesis is the overarching motivation to attempt to understand the tectonic evolution of the world's premier natural laboratory for studying continental deformation. There is an obvious benefit for attempting to bring as many different perspectives and even disciplines to bear on a problem, as they are commonly complimentary and where there are apparent contradictions, there is the potential for insight. At times, however, the need to exhaustively document a large body of disparate data and observations may admittedly sometimes make it hard to "see the forest for the trees." In this section, I try to step back a little and summarize the main contributions of this thesis to Tibetan tectonics specifically, as well as to continental tectonics generally.

6.1 The importance of pre-Cenozoic deformation in the Tibetan orogen

Even before the collision of India with the Eurasian continent occurred in the early Cenozoic (*Rowley* (1996)), the southern margin of Eurasia was an active margin and the site of a number of terrane accretion events. As a result, the Eurasian crust is collage of distinct geological terranes separated by sutures of mainly Mesozoic age. This pre-Indian collision accretionary history is well-known (*Sengor and Natalin* (1996); *Sengor et al.* (1984); *Metcalfe* (1998)), as are the possible consequences for the Cenozoic evolution of Tibet – either in terms of localizing major strike-slip faults along old sutures boundaries (eg. *Sengor et al.* (1984) or in terms of weakening the Eurasian crust (eg. *Kerr* (2004)). Work by *Kapp et al.* (2005) and colleagues has also suggested the possibility that considerable crustal thickening may have preceded the India-Asia collision.

In the thesis, both the Gonjo Basin and First Bend chapters directly address the issue of the pre-Cenozoic history of Tibet. In the First Bend area, I document a rich and complicated set of fabric generations that are the direct product of the extensive Mesozoic deformation in this area. Surprisingly enough, apart from the recent work of *Reid et al.* (2005) or perhaps *Yan et al.* (2003), there is no mention or acknowledgment of the multiple generations of fabrics in metamorphic rocks exposed in eastern Tibet or southwestern China. The work of *Lacassin et al.* (1996) in the Yulong mountains presents an interpretation of the geology of the Yulong mountains that proposes multiple generations of deformation, but fails to recognize more than a single foliation generation. What is striking is that these multiple generations of fabrics are not just confined to the Yulong mountains, but are exposed in all foliated rocks east of the Jinsha suture, as demonstrated both in Chapter 3, by the work of *Reid et al.* (2005) to the north. The obvious question raised is whether there are additional unrecognized

and unreported complexities and complications in other exposures of metamorphic rocks in this part of the world, most notably in the Diancang Shan and Ailao Shan rocks, interpreted by *Leloup et al.* (1995) and his colleagues as the products of one generation of simple shear deformation.

Near the Gonjo basin, evidence is described for the existence of at least two pre-Cenozoic episodes of shortening, one of which post-dated deposition of Triassic strata. This presents a major problem for attempts to quantify Cenozoic shortening and thus its possible contribution to crustal thickening in this area. Structures affecting Gonjo basin rocks are clearly Cenozoic in age, but most of the rocks in this region are Triassic or older in age. These rocks have potentially suffered both Mesozoic and early Cenozoic shortening, and the lack of cross-cutting relations, re-folded folds or overprinting of fabrics rules out obvious ways of disentangling the two post-Triassic episodes of deformation (fig. 1-2). This raises questions about whether retrodeformed cross-sections published for nearby regions (eg. *Spurlin et al.* (2005)) are capable of quantifying Cenozoic shortening, or whether these estimates should be considered maxima.

6.2 Limited upper crustal shortening in the early stages of continental collision

Perhaps the defining characteristic of Tibet is that it is underlain by extremely thick continental crust, and so a first order question is how and when the crust was thickened. Chapter 2 of the dissertation investigates the possibility of an upper crustal record of crustal thickening processes during the early stages of India-Asia collision recorded by sedimentary rocks and structures of the Gonjo basin. Rocks of the Gonjo basin are folded into a broad syncline, and basin bounding reverse faults are demonstrated to have little throw associated with them. That is, rocks of the basin itself

have suffered little shortening. The basin, however, is underlain by crust that exceeds 65km in thickness, which therefore raises the question of how this thickening was accomplished.

Alternative models of the evolution of the eastern margin of the plateau have suggested that much of the crustal thickening of the eastern margin of the Tibetan plateau as well as into southwestern China occurred without upper crustal shortening (*Clark and Royden* (2000); *Royden et al.* (1997)). Exposures of Cenozoic continental sedimentary rocks associated with compressional structures analogous to those exposed in the Gonjo basin are widely distributed from the latitude of the Gonjo basin south into southwest China. Unequivocally Cenozoic structures are generally parallel to the trends of fold axes and faults that do not directly affect Cenozoic rocks, but the strikes of faults and folds are strongly oblique to the gradient of surface elevations and crustal thickness. That is, although the Cenozoic basins of the eastern margin of the plateau do not completely constrain the amount of Cenozoic shortening, just the spatial pattern alone of that deformation is not obviously and straightforwardly related to variations in crustal thickness of the eastern plateau.

6.3 Recognizing the importance of extensional tectonics in the active deformation of eastern Tibet and southwest China

To a first order, active tectonism in eastern Tibet is characterized by clockwise rotation of a crustal fragment bounded by the left-lateral Ganzi, Xianshuihe, Xiaojiang, Dien Bien Phu and related faults about the eastern Himalayan syntaxis. This first order picture is well-established from modelling of seismic moment release (*Holt et al.* (2000, 1991), geologic mapping *Wang et al.* (1998); *Wang and Burchfiel* (2000) and

geodetic data (*Shen et al.* (2005); *Chen et al.* (2000); *King et al.* (1997); *Zhang et al.* (2004)). Beyond this simple picture are additional complexities: within the larger rotating blocks are smaller, differentially rotating fragments (*Wang et al.* (1998)); normal faulting and extensional strain is at least as important as strike-slip faulting in many places. East-west extension is a clear and robust feature of the geodetic velocity field and is reflected in the patterns of seismic moment release, but most geologic work in this area has failed to recognize the importance of extension. The compilation of geologically inferred slip-rates includes almost no determinations of extensional slip rate. An important consequence of this is that a major source of seismic risk has been almost completely neglected.

6.4 Assessing end-member descriptions of continental tectonics in eastern Tibet

Models for the growth and evolution of Tibet are rather varied, and the subject of considerable debate. This debate is often characterized in terms of two end-member member conceptions of how continental crust deforms in general, underscoring again the pre-eminent place of the India-Asia collision in continental tectonics. The first model emphasizes the apparent weakness of the Eurasian continent and suggests that the deformation of Eurasia – and by implication, continental crust generally – is best described as diffuse and continuous (eg. *England and Houseman* (1988)). The second characterizes the deformation of Eurasia in terms of the plate tectonics-like motion of a few rigid blocks bounded by narrow, lithospheric penetrating faults (eg. *Tapponnier et al.* (1982); *Replumaz and Tapponnier* (2003)). Apparently smoothly-varying geodetic velocities in the central Tibetan plateau have been interpreted as requiring continuous and "fluid-like" deformation of the upper crust (*Zhang et al.* (2004)), but most of the apparent smoothness of geodetic velocity gradients can be ascribed to

interseismic locking of faults. Recent work by *Meade* (submitted) has shown that the same data which have been interpreted as reflecting continuous deformation are better described by a model consisting of a small number of fault-bounded elastic blocks.

In chapter 4, it is shown that geodetic velocities can be readily fit by block modeling, but important characteristics of the mapped geology remain unexplained. In particular, there are places where upper crustal deformation is poorly localized and diffuse and sometimes not associated with obvious faults at all. In the end, geodetic velocities cannot be taken at face value as implying continuous, "fluid-like" deformation, but it is also true that, in places, a rigid block description of continental deformation fails to capture important features of the geology. An outstanding question for future work is what, then, controls strain localization and the mode of continental deformation.

6.5 Extension and efficient erosion as necessary conditions for the development of isolated structural and metamorphic culminations

Considerable recent attention has been paid to areas where anomalously deep exhumation is in some sense driven by erosional processes (eg. *Zeitler et al.* (2001)), and the Yulong mountains represent an area where similar processes might be taking place. Although the rocks of the Yulong mountains have not been exhumed from as great depths as in Nanga Parbat or Namchebarwa, the well-constrained active deformation and better accessibility of the Yulong mountains make this range a better field site for assessing how upper crustal deformation and erosional processes interact to produce a localized zone of anomalous exhumation. In the Yulong mountains, exten-

sion characterizes the deformational regime, and the kinematics of normal faults are shown in chapter 5 to be a necessary – though not sufficient – condition for localized exhumation. Similarly, vigorous erosion processes by themselves are not sufficient to drive the system. Deep exposure levels and high uplift rates do not occur along the entire length of the Jinsha river, but rather only where the river intersects the transtensional faults of the Jianchuan-Lijiang-Zhongdian fault system. That is, a closed network of normal faults that accommodates uplift and permits the range to respond independently of its surroundings.

Although river incision alone is not sufficient to produce localized exhumation, regional uplift and consequent development of the kind of steep river gorge characteristic of the eastern Tibetan plateau margin is a necessary condition because steep topography is needed to produce rapid erosion in competent rocks. Moreover, if the river were not deeply entrenched, it is possible that localized uplift along its course would have simply caused it to be diverted around the uplift, essentially eliminating erosion from the top of the uplift zone (eg. *Humphrey and Konrad* (2000)). Without erosion, uplift would end once mean elevations had attained the equilibrium elevations that satisfy static force balances. In short, *persistant*, localized extrusion between the range-bounding normal faults must be a response to erosion.

References

Chen, Z., B. C. Burchfiel, Y. Liu, R. W. King, L. H. Royden, W. Tang, E. Wang, J. Zhao, and X. Zhang (2000), Global positioning system measurements from eastern Tibet and their implications for India/Eurasia intercontinental deformation, *Journal of Geophysical Research*, *105*(B7), 16,215–16,228.

Clark, M. K., and L. H. Royden (2000), Topographic ooze: building the eastern margin of Tibet by lower crustal flow, *Geology*, *28*, 703–706.

England, P. C., and G. A. Houseman (1988), The mechanics of the Tibetan plateau, *Philosophical Transactions of the Royal Society of London A*, *326*, 301–320.

Holt, W. E., J. F. Ni, T. C. Wallace, and A. J. Haines (1991), The active tectonics of the eastern Himalayan syntaxis and surrounding regions, *Journal of Geophysical Research*, *96*(B9), 14,595–14,632.

Holt, W. E., N. Chamot-Rooke, X. L. Pichon, A. J. Haines, B. Shen-Tu, and J. Ren (2000), Velocity field in Asia inferred from Quaternary fault slip rates and global positioning system observations, *Journal of Geophysical Research*, *105*(B8), 19,185–19,210.

Humphrey, N., and S. Konrad (2000), River incision or diversion in response to bedrock uplift, *Geology*, *28*, 43–46, doi:10.1130/0091-7613(2000)28¡43:RIODIR¿2.0.CO;2.

Kapp, P., A. Yin, M. T. Harrison, and L. Ding (2005), Cretaceous–Tertiary shortening, basin development, and volcanism in central Tibet, *Geological Society of America Bulletin*, *117*(7-8), 865–878, doi:10.1130/B25595.1.

Kerr, R. A. (2004), GEOPHYSICS: Hammered by India, puttylike Tibet shows limits of plate tectonics, *Science*, *305*(5681), 161a+, doi:10.1126/science.305.5681.161a.

King, R., F. Shen, B. Burchfiel, L. Royden, E. Wang, Z. Chen, Y. Liu, X. Zhang, J. Zhao, and Y. Li (1997), Geodetic measurement of crustal motion in southwest China, *Geology*, *32*, 809–812.

Lacassin, R., U. SchÃrer, P. H. Leloup, N. Arnaud, P. Tapponier, X. Liu, and L. Zhang (1996), Tertiary deformation and metamorphism SE of Tibet: The folded Tigerleap decollement of NW Yunnan, China, *Tectonics*, *15*(3), 605–622.

Leloup, P. H., R. Lacassin, P. Tapponnier, U. Scharer, D. Zhong, X. Liu, L. Zhang, S. Ji, and P. T. Trinh (1995), The Ailao Shan-Red River shear zone (Yunnan, China), Tertiary transform boundary of Indochina, *Tectonophysics*, *251*(1-4), 3–84, doi:10.1016/0040-1951(95)00070-4.

Meade, B. (submitted), Present-day kinematics of the India-Asia collision zone, submitted to *Geology*, 2006.

Metcalfe, I. (1998), Palaeozoic and Mesozoic geological evolution of the SE Asian region: multidisciplinary constraints and implications for biogeography, in *Biogeography and Geological Evolution of SE Asia*, edited by R. Hall and J. Holloway, pp. 25–41, Backhuys Publishers, Leiden , the Netherlands.

Reid, A., C. Wilson, and S. Liu (2005), Structural evidence for the Permian-Triassic tectonic evolution of the Yidun Arc, eastern Tibet, *Journal of Structural Geology*, *27*, 119–137, doi:10.1016/j.jsg.2004.06.011.

Replumaz, A., and P. Tapponnier (2003), Reconstruction of the deformed collision zone between India and Asia by backward motion of lithospheric blocks, *Journal of Geophysical Research*, *108*(B6), 2285+, doi:10.1029/2001JB000661.

Rowley, D. B. (1996), Age of initiation of collision between India and Asia: A review of stratigraphic data, *Earth and Planetary Science Letters*, *145*(1-4), 1–13, doi: 10.1016/S0012-821X(96)00201-4.

Royden, L. H., B. C. Burchfiel, R. W. King, E. Wang, Z. Chen, F. Shen, and Y. Liu (1997), Surface deformation and lower crustal flow in eastern Tibet, *Science*, *276*(5313), 788–790, doi:10.1126/science.276.5313.788.

Sengor, A. M. C., and B. A. Natalin (1996), Paleotectonics of Asia: fragments of a synthesis, in *The Tectonic Evolution of Asia*, edited by A. Yin and M. Harrison, pp. 486–641, Cambridge University Press.

Sengor, A. M. C., D. Altiner, A. Cin, T. Ustaomer, and K. J. Hsu (1984), Origin and assembly of the Tethyside orogenic collage at the expense of Gondwanaland, in *Gondwana and Tethys*, edited by M. G. Audley-Charles and A. Hallam, pp. 119–182, Oxford University Press, Oxford, UK.

Shen, Z.-K., J. LÃ, M. Wang, and R. BÃrgmann (2005), Contemporary crustal deformation around the southeast borderland of the Tibetan Plateau, *Journal of Geophysical Research*, *110*, B11,409+, doi:10.1029/2004JB003421.

Spurlin, M., A. Yin, B. Horton, J. Zhou, and J. Wang (2005), Structural evolution of the Yushu–Nanqian region and its relationship to syncollisional igneous activity, east-central Tibet, *Geological Society of America Bulletin*, *117*(9-10), 1293–1317.

Tapponnier, P., G. Peltzer, R. Armijo, and P. Cobbold (1982), Propagating extrusion tectonics in asia; new insights from simple experiments with plasticine, *Geology*, *10*(12), 611–616.

Wang, E., and C. C. Burchfiel (2000), Late Cenozoic to Holocene deformation in southwestern Sichuan and adjacent Yunnan, China, and its role in formation of the southeastern part of the Tibetan Plateau, *Geological Society of America Bulletin*, *112*, 413–423.

Wang, E., B. Burchfiel, L. Royden, L. Chen, J. Chen, W. Li, and Z. Chen (1998), *Late Cenozoic Xianshuihe-Xiaojiang, Red River, and Dali Fault Systems of Southwestern Sichuan and Central Yunnan, China*, *GSA Special Paper*, vol. 327, Geological Society of America.

Yan, D., M. Zhou, H. Song, and Z. Fu (2003), Structural style and tectonic significance of the Jianglang dome in the eastern margin of the Tibetan plateau, China, *Journal of Structural Geology*, *25*, 765–779.

Zeitler, P. K., A. S. Meltzer, P. O. Koons, D. Craw, B. Hallet, C. P. Chamberlain, W. S. F. Kidd, S. K. Park, L. Seeber, M. Bishop, and J. Shroder (2001), Erosion, Himalayan geodynamics, and the geomorphology of metamorphism, *GSA Today*, *11*, 4–9, doi:10.1130/1052-5173(2001)011¡0004:EHGATG¿2.0.CO;2.

Zhang, P.-Z., Z. Shen, M. Wang, W. Gan, R. Bürgmann, P. Molnar, Q. Wang, Z. Niu, J. Sun, J. Wu, S. Hanrong, and Y. Xinzhao (2004), Continuous deformation of the Tibetan plateau from global positioning system data, *Geology*, *32*, 809–812.